SYNTHESIS AND REACTIVITY OF TRANSITION METAL-GROUP 13 COMPLEXES

A thesis submitted in partial fulfilment of the requirements for the degree of Doctor of Philosophy

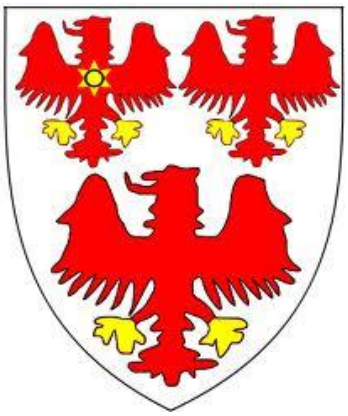

Ian Martin Riddlestone

The Queen's College, Oxford

April 2013

DOCTOR OF PHILOSOPHY SCHOOL OF CHEMISTRY

DECLARATION OF AUTHORSHIP

Name: IAN MARTIN RIDDLESTONE **Candidate number: 929356**

College: THE QUEEN'S COLLEGE **Supervisor: PROF. SIMON ALDRIDGE**

Title of thesis:
SYNTHESIS AND REACTIVITY OF TRANSITION METAL-GROUP 13 COMPLEXES

Word count: ~50,000

Please tick to confirm the following:

I have read and understood the University's disciplinary regulations concerning conduct in examinations and, in particular, the regulations on plagiarism (*Essential Information for Students. The Proctors' and Assessor's Memorandum*, Section 9.6; also available at www.admin.ox.ac.uk/proctors/info/pam/section9.shtml). ☐

I have read and understood the Education Committee's information and guidance on academic good practice and plagiarism at www.admin.ox.ac.uk/edc/goodpractice. ☐

The thesis I am submitting is entirely my own work except where otherwise indicated. ☐

It has not been submitted, either partially or in full, for another Honour School or qualification of this University (except where the Special Regulations for the subject permit this), or for a qualification at any other institution. ☐

I have clearly indicated the presence of all material I have quoted from other sources, including any diagrams, charts, tables or graphs. ☐

I have clearly indicated the presence of all paraphrased material with appropriate references. ☐

I have acknowledged appropriately any assistance I have received in addition to that provided by my supervisor. ☐

I have not copied from the work of any other candidate. ☐

I have not used the services of any agency providing specimen, model or ghostwritten work in the preparation of this thesis. (See: http://www.admin.ox.ac.uk/statutes/352-051a.shtml#_Toc28142348.) ☐

I agree to retain an electronic copy of this work until the publication of my final examination result, except where submission in hand-written format is permitted. ☐

I agree to make any such electronic copy available to the examiners should it be necessary to confirm my word count or to check for plagiarism. ☐

Candidate's signature: …….. Date: ……..

This thesis is dedicated to my fiancée Amy

Abstract

The synthesis and reactivity of a number of mixed transition metal-aluminium and σ-alane complexes are detailed in this thesis.

Chapter III reports on the formation and structural characterisation of *N,N'*-chelated aluminium dihalide precursors featuring amidinate and guanidinate substituents. These precursors of the type $RC(R'N)_2AlX_2$ (R = $^{i}Pr_2N$ or Ph; R' = Cy or ^{i}Pr or Dipp; X = hal), readily react with $Na[CpFe(CO)_2]$ *via* salt elimination to form the corresponding mixed iron-aluminium complexes $CpFe(CO)_2[(X)Al(NR')_2CR]$ which have been characterised both spectroscopically and by X-ray diffraction. The reactivity of the novel mixed aluminium-iron complexes towards halide abstraction agents has been investigated and a propensity for augmented coordination at the aluminium centre observed. Furthermore, complementary syntheses of the methyl substituted complex $CpFe(CO)_2[(Me)Al(NCy)_2CN^{i}Pr_2]$ have been developed. This can be achieved either *via* the reaction between the related chloride complex and MeLi, or from the reaction between $^{i}Pr_2C(CyN)_2Al(Me)Cl$ and $Na[CpFe(CO)_2]$.

The research detailed in Chapter IV builds on the previous chapter and is focussed on the use of more sterically demanding substituents at both aluminium and transition metal, as well as more electron rich transition metal fragments. The transition metal anions $Na[Cp^*Fe(CO)_2]$ and $Na[Cp^{Si}Fe(CO)(PPh_3)]$ react with the aluminium precursors forming related mixed iron-aluminium complexes which have been structurally characterised. The $Dipp_2NacNacAlCl_2$ precursor has been shown to undergo reaction with both $Na[CpFe(CO)_2]$ and $Na[Cp^*Fe(CO)_2]$. The halide abstraction chemistry of the latter utilising both Lewis acid and salt metathesis based abstraction approaches has been investigated. The dehydrohalogenation chemistry of the $Dipp_2NacNacAlCl_2$ precursor was investigated and the ligand activated products of reactions with both alkyl lithium and alkyl potassium reagents characterised.

Chapter V reports the extension of salt metathesis for the formation of an Al-H-Mn interaction, and the product has been fully characterised. In addition, the coordination of Al-H bonds from a number of alane precursors to *in situ* generated 16-electron fragments has allowed the structural characterisation of a number of novel σ-alane complexes. The incorporation of the transition metal fragments $[Cp'Mn(CO)_2]$ and $[W(CO)_5]$ permit comparison to archetypal borane and silane σ-complexes. Quantum chemical calculations suggest that the alane ligand has a binding energy close to that of dihydrogen but significantly less than that of CO, consistent with a predominant σ-donor role of the Al-H bond. The formation and structural characterisation of the κ^2-complexes $(OC)_4M[\kappa^2\text{-}H_2AlDipp_2NacNac]$ (M = Cr, Mo or W) define an unprecedented binding motif for the alane ligand. In the cases of chromium and molybdenum the κ^2-complexes can be prepared either photolytically or *via* alkene displacement from the corresponding $(OC)_4M(cod)$ reagent. In the case of tungsten the alkene displacement route yields the desired product, but only under more forcing conditions. Spectroscopic characterisation of the related κ^1-complex $(OC)_5Cr[\kappa^1\text{-}H_2AlDipp_2NacNac]$, which readily forms the κ^2-complex in solution without photolysis, has enabled the kinetics of chelate ring closure to be investigated. This analysis further characterises the formation of the unprecedented κ^2-binding motif for the alane ligand.

Acknowledgements

First and foremost I would like to thank my supervisor Prof. Simon Aldridge for all his encouragement, enthusiasm, advice, wisdom and support throughout my DPhil. I would also like to thank my BP CASE Award supervisor Dr. Russell Taylor for all his support, ideas, help and enthusiasm.

I am very grateful to all members of the Aldridge group, both past and present, for making my DPhil a truly memorable experience. In particular I would like to thank Dr. Juan Urbano, Dr. Dave Addy, Mr. Nicholas Phillips and Mr. Michael Kelly for their initial supervision, help throughout my DPhil and for making the lab a great place to work. I am particularly grateful to my two Part II students Miss Sian Edmonds and Mr Paul Kaufman for their exceptional hard work which has contributed to some of the discussion in this thesis. I am hugely grateful to Dr Joshua Bates for his work not only on DFT calculations but also for his advice and support.

Thank you to Mr. Michael Kelly, Dr. Dragoslav Vidovic, Mr. Nicholas Phillips and Dr. Amber Thompson for helping me with crystallography, and to the EPSRC Mass Spectrometry Service for running samples.

I would like to acknowledge to Dr. Nick Rees for his help running NMR experiments.

Thank you to BP and EPSRC for funding the research.

I would like to thank my fiancée Amy for her unconditional love and support. Your belief in me has made the more difficult times easier, and for that I am forever grateful.

To my family, Mum, Dad, Claire and Granny I would like to say thank you. You have supported and guided me through life with love and encouragement, and for that I am sincerely grateful. I would also like to thank Amy's family, in particular John and Marilyn, for their encouragement, support and advice.

Notes

The following abbreviations are used in the text:

Ar = Aryl

Ar^f = $C_6H_3(CF_3)_2$-3,5

br = broad

^{i}Bu = $-CH_2CH(CH_3)_2$

^{n}Bu = $-CH_2CH_2CH_2CH_3$

^{t}Bu = $-C(CH_3)_3$

calc = calculated

cat = 1,2-$O_2C_6H_4$

cdt = *cyclo*dodecatriene

coe = *cyclo*octene

cod = 1,5-*cyclo*octadiene

Cp = *cyclo*pentadienyl, η^5-C_5H_5

Cp' = methyl*cyclo*pentadienyl, η^5-C_5H_4Me

Cp* = pentamethyl*cyclo*pentadienyl, η^5-C_5Me_5

Cy = *cyclo*hexyl

δ = NMR chemical shift

d = doublet, days

dcpe = 1,2-*bis*(di*cyclo*hexylphosphino)ethane

DFT = Density Functional Theory

Dipp = 2,6-di*iso*propylphenyl

dmpe = 1,2-*bis*(dimethylphosphino)ethane

dvds = 1,3-divinyl-1,1,3,3-tetramethyldisiloxane

EI = electron ionisation

ES = electrospray

FT = Fourier transform

h = hours

I^{t}Bu = 1,3-di-*tert*-butyl imidazolin-2-ylidene

IMe = 1,3-dimethyl imidazolin-2-ylidene

IMes = 1,3-dimesityl imidazolin-2-ylidene

IR = infrared

J = coupling constant

LDA = lithium di*iso*propylamide

λ = wavelength

m = multiplet, medium

Me = $-CH_3$

Mes = -2,4,6-$Me_3C_6H_2$

min. = minutes

μ = bridged

MS = mass spectrometry

ν = stretching frequency

NMR = nuclear magnetic resonance

obs = observed

Ph = $-C_6H_5$

pin = 1,2-$O_2C_2Me_4$

ppm = parts per million

^{i}Pr = $-CH(CH_3)_2$

q = quartet

ref = reference

RT = room temperature

s = singlet

sept = septet

sh = shoulder

SIMes = 1,3-dimesityl imidazolylidene

st = strong

t = triplet

THF = tetrahydrofuran

TMEDA = *N*,*N*,*N*',*N*'-tetramethylethylenediamine

TMPDA = *N*,*N*,*N*',*N*'-tetramethyl-1,3-propanediamine

VT-NMR = variable temperature nuclear magnetic resonance

w = weak

1 Torr = 1 mmHg = 133.3 Pa

Contents

Appendices

1 Introduction

1.1 Introduction

Perhaps the greatest current challenge facing the scientific community is the replacement of depleted fossil fuel reserves to sustain the chemical industry and support the production of food, fuel and medicines. There are a number of approaches to dealing with this challenge, but all involve the development of sustainable chemical resources and the more efficient use of both new and current feedstocks. Consequently, research into both of these areas, the replacement of the current chemical infrastructure, and reliance on raw materials sourced from the petrochemical industry has received much attention. The ability to carry out both novel and existing chemical transformations more efficiently, both in terms of atom and energy efficiency, has highlighted the importance of catalytic chemical transformations.

The field of homogenous catalysis is dominated by transition metals, particularly the late and precious metals, which have suitable M^n and M^{n+2} redox couples to allow for the two electron processes of oxidative addition and reductive elimination. However, main group chemistry has been resurgent in recent years with the emergence and utilisation of highly reactive systems, *e.g.* carbenoids, and 'frustrated Lewis pairs' as new paradigms in small molecule activation. Both of these discoveries have led to renewed interest in group 13 chemistry, focused on the accessibility of the potentially ambiphilic +1 oxidation state, and the Lewis acid properties of the elements in the traditional +3 oxidation state.

Of the group 13 elements aluminium is a desirable choice for catalytic chemistry as it is non-toxic and the cheapest of the group 13 metals. Aluminium is the most abundant metal in the Earth's crust (8.3% by weight) and, on either its own or alloyed with other

metals, forms materials that have a number of applications ranging from heat exchangers to aircraft parts to corrosion resistant building parts and tools. The various solid state forms of aluminium oxide (alumina, Al_2O_3) are widely used as catalysts and catalyst supports, ion exchangers, and more recently Al_2O_3 fibres have been converted into textile forms.[1] In the solid state the differing forms of alumina feature aluminium in coordination environments exceeding the standard valency of three (*e.g.* octahedral and tetrahedral). The tendency of aluminium to adopt higher coordination numbers, of four, five or six, means that the formation of oligomeric and polymeric structures is common (*e.g.* as in Al_2O_3, α–AlH_3).

Within synthetic and organometallic chemistry the most commonly used aluminium compounds are $LiAlH_4$, a hydride source for the reduction of organic and organometallic compounds, and $AlCl_3$, a strong Lewis acid catalyst for Friedel-Crafts type chemistry. Aluminium chloride is produced on a vast scale and is one of the cheapest metal halides available at £43.50 per kg, providing a cheap and readily available route into aluminium organometallic chemistry (*cf.* $RuCl_3 \cdot xH_2O$ £32,400 per kg and $PdCl_2$ £71,400 per kg).[2] The high Lewis acidity of aluminium compounds, the least electronegative element in group 13, and the cheap nature of starting materials makes organometallic and coordination chemistry of aluminium an important research area.

1.2 Frustrated Lewis Pair Chemistry

Since the classification of electron pair donors as bases and electron pair acceptors as acids by Lewis in 1923, Lewis acid and base chemistry has provided a fundamental explanation of reactivity in both main group and transition metal chemistry.[3] Strategies for preventing the formation of Lewis acid/base adducts have been reported a number of times in the literature,[4,5] however, it was not until recently that sterically bulky systems, in which sterics preclude adduct formation, were shown to induce the facile activation of small molecules.

In 2006 Stephan and co-workers reported the reversible activation of dihydrogen by a main group system, derived from a Lewis acid/base pair in which sterics preclude adduct formation (Scheme 1.1).[6]

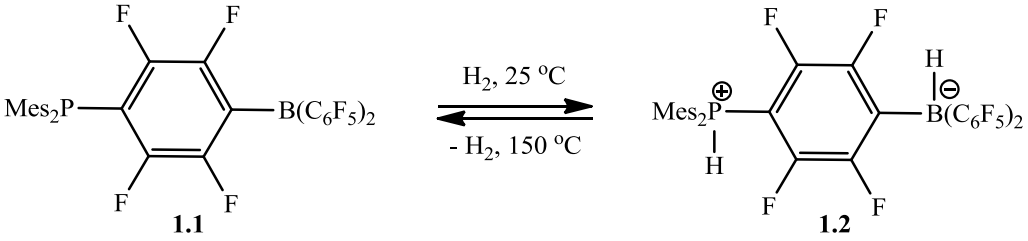

Scheme 1.1: *A phosphine-borane derived frustrated Lewis pair (FLP) system for reversible dihydrogen activation.*

The phosphine-borane **1.1** in Scheme 1.1 heterolytically cleaves dihydrogen with the phosphine accepting a proton and the borane a hydride, thereby forming the corresponding phosphonium-borate **1.2**. The reactivity of **1.1** towards dihydrogen is attributed to the inability of the Lewis acid and base to mutually quench through adduct formation. The term frustrated Lewis pair (FLP) was introduced to describe such systems, and since this landmark discovery a number of other FLP systems have been shown to heterolytically cleave dihydrogen.[7,8] Moreover, FLP systems have been shown to act as hydrogenation catalysts, predominantly reducing enamines and imines, with the reduction taking place under very mild conditions and low pressures of hydrogen.[9-12] FLP systems of this type provide an alternative to established transition metal systems, and demonstrate that under the right conditions main group mediated catalysis can begin to compete with transition metal systems.

The number of Lewis acid/base combinations that meet the criteria to be classified as 'frustrated' has been steadily increasing, with reports of alkyl boranes,[13] aluminium

halides[14] and borenium ions[15] as Lewis acid components, and carbenes[16] and amines[17] as Lewis bases. Unsurprisingly, the scope of small molecules activated by FLP systems has also increased significantly with reports of CO_2 activation[14,18] as well as π-systems of unsaturated carbon-carbon bonds (alkene,[19,20] alkyne[21] and dienes,[22]) highlighting the growing versatility of FLP systems.

The activation of a range of small molecules and the catalytic hydrogenation of certain substrates by FLP systems has thus been demonstrated in the literature. However, the incorporation of FLP based small molecule activation as part of a catalytic transition metal system remains rare.[23,24] The ability of FLPs to activate small molecules, particularly dihydrogen, makes them a potentially powerful addition to transition metal mediated catalysis. Moreover, the incorporation of a pendant FLP moiety to such a catalyst could allow the incorporation of the products of small molecule activation in a catalytic cycle performed by the transition metal. Consequently, the formation and study of transition metal complexes containing Lewis acidic group 13 ligands, and their hydrides, represents a potential step towards the incorporation of FLPs into transition metal systems.

1.3 Transition Metal Complexes of Group 13 Elements

The synthesis of compounds containing two-centre two-electron M-E bonds (M = transition metal, E = group 13 element) has received much recent attention, not least due to the implication of boryl complexes (L_nMBX_2) in the functionalisation of saturated and unsaturated hydrocarbons.[25,26] The importance of hydroboration in organic synthesis has seen the development of reagents to facilitate the catalytic hydroboration of substrates with regioselective (Markownikoff versus anti-Markownikoff) control over the addition process.[27-29] Boryl ligands are proposed as intermediates in these transformations and, as a result, boryl complexes have gone from being regarded as mere structural novelties to key

components in catalysis. The growing precedent in the literature for boryl complexes has led to a range of synthetic approaches being developed for the formation M-B two-centre two-electron bonds. These approaches usually involve salt metathesis between a haloborane and a transition metal anion, or oxidative addition of a B-H, B-B or B-X bond at a late transition metal centre.[30-33] More recently salt metathesis in the reverse sense utilising a lithium boryl reagent and transition metal electrophiles has been reported for the preparation of early transition metal and *f*-block boryl complexes.[34-38]

By contrast, the synthesis of M-E bonds (where M = transition metal and E = Al, Ga, In or Tl) represents an area in which there has been significantly less activity. There have been a number of recent reviews of complexes containing M-E bonds (where E = Ga, In or Tl).[39-41] However, structurally characterised M-Al two-centre two-electron bonds remain comparatively rare. In part this reflects the additional synthetic challenges associated with the heavier congeners of group 13, with aggregation involving higher coordination numbers typically being favoured, and simple well defined monomeric precursors of the EX_2 ligand being less readily accessible.[42] Synthetic approaches to the formation of M-Al bonds, unlike the formation of M-B bonds, are far more limited with salt metathesis chemistry most prevalent and oxidative addition of Al-X bonds (where X = H, hal or alkyl) remaining unknown.

1.3.1 Types of M-Al Bonding Interactions

The fundamental properties of aluminium and the ability to form complexes featuring aluminium in either the +1 or +3 oxidation state mean that different types of two-centre two-electron bonding interactions between aluminium and transition metals are conceivable. The nature of the bonding in such systems is largely dependent upon the

specific aluminium and transition metal components involved. There are three broad classifications of M-Al two-centre two-electron interactions (Figure 1.1).

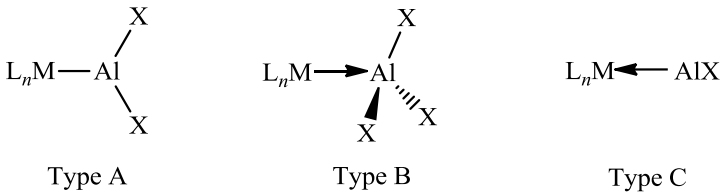

Figure 1.1: *Types of M-Al Bond*

Complex type A represents the aluminium analogue of a boryl compound, *viz.* an alanyl complex. The alanyl ligand (formally $[AlX_2]^-$) contains aluminium in the formal +3 oxidation state and the transition metal aluminium bond is essentially a metal-metal sigma bond. Complexes of this type have been formed *via* salt metathesis between transition metal anions and aluminium halides, or through alkane elimination reactions involving aluminium alkyls and transition metal hydrides. Complex type B involves the formation of a dative bond between a low valent electron rich transition metal fragment and a Lewis acidic aluminium(III) centre. This type of interaction is analogous to the formation of classical Lewis adducts where the Lewis base is a transition metal fragment. Consequently, the bonding interaction differs from that of type A and can be described as a donor-acceptor complex in which the aluminium is the acceptor component and the transition metal the donor. Complex type C is also a donor-acceptor complex, however, unlike A or B, it contains aluminium in the +1 oxidation state acting as the donor. In the +1 oxidation state and in the singlet form, aluminium can be described as amphoteric acting as a strong σ-donor, but is also able to accept electron density back into the formally vacant *p*-orbital. Complexes of this type have been formed through the coordination chemistry of an isolable

aluminium(I) species to a transition metal fragment or through the *in situ* formation of an aluminium(I) centre within the coordination sphere of a transition metal through double salt elimination reactions.

1.3.2 Transition Metal Alanyl Complexes

The use of transition metal anions to perform salt elimination reactions with aluminium halides represents a logical extension of the established chemistry with the other group 13 elements for the formation of M-E bonds (M = transition metal; E = group 13 element).[39] In 1994 Fischer and Priermeier used salt elimination reactions to such effect and spectroscopically characterised mixed metal iron-aluminium compounds (Scheme 1.2).

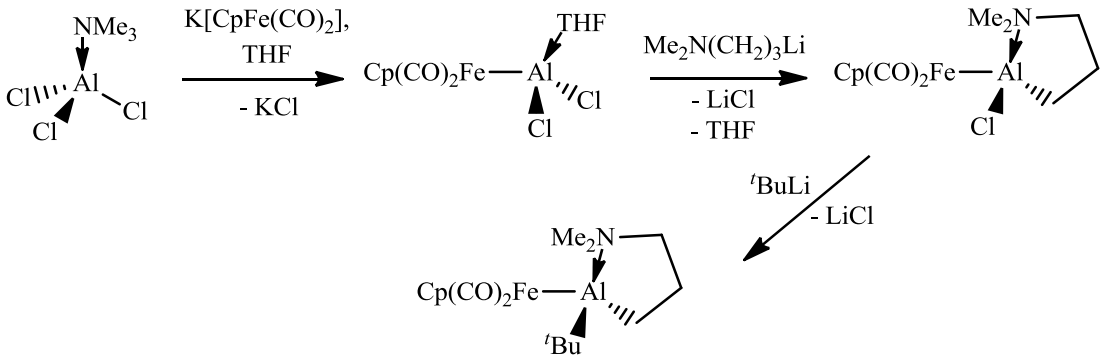

Scheme 1.2: *Salt elimination to form Fe-Al complexes*

The related complex $Cp(CO)_2FeAl[(CH_2)_3NMe_2](^tBu)$ (**1.3**) was characterised by single crystal X-ray diffraction confirming the presence of an iron-aluminium σ-bond.[43] Subsequently, Braunschweig and co-workers isolated the related intramolecularly stabilised mixed metal complex $Cp(CO)_2Fe[Al(Cl)Ar]$ (where Ar = 2-[(dimethylamino)methyl]phenyl) (**1.4**) from the reaction of $ArAlCl_2$ and $Na[CpFe(CO)_2]$ (Scheme 1.3). It was shown that the reaction of $ArAlCl_2$ with two equivalents of

Na[CpFe(CO)$_2$] leads to the formation of [Cp(CO)$_2$Fe]$_2$AlAr (**1.5**) (Scheme 1.3) which was characterised by single crystal X-ray diffraction. In the solid state the aluminium centre has a distorted tetrahedral geometry with the tethered NMe_2 functionality remaining bound, even with two [CpFe(CO)$_2$] moieties coordinated.[44] The formation of [Cp(CO)$_2$Fe]$_2$AlAr shows that terminal Al-X bonds at a mixed metal aluminium-iron complex remain reactive not only towards alkyllithium reagents, but also toward transition metal anions.

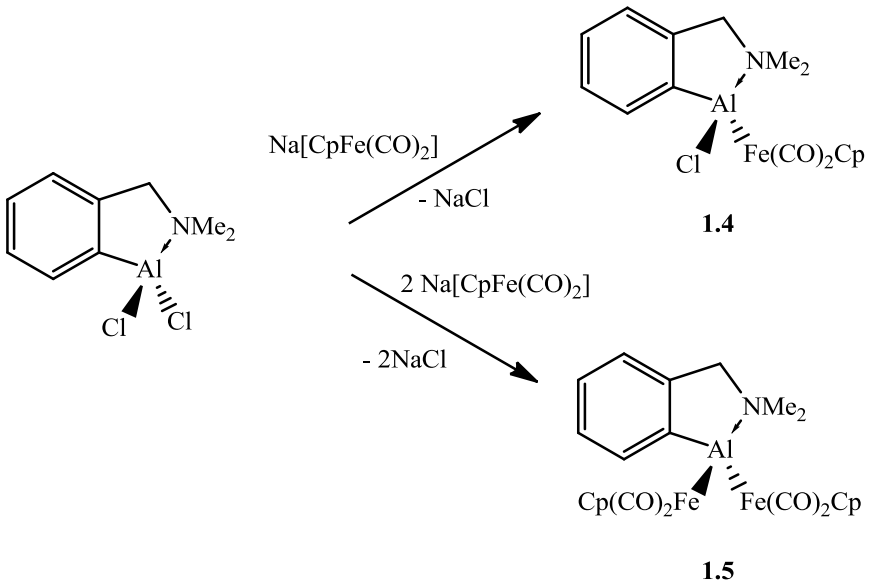

Scheme 1.3: *Reactivity of ArAlCl$_2$ towards Na[CpFe(CO)$_2$] (Ar = 2-[(dimethylamino)methyl]phenyl)*

The use of tethered intramolecular donor groups, such as the pendant NMe_2 functionality, reduces the propensity for aluminium compounds to oligomerise by providing an additional donor, thereby enabling the isolation of discrete monomeric complexes. However, the potential for metal-metal multiple bonding resulting from π back-bonding from a transition metal to the vacant *p*-orbital on aluminium, can only be investigated in a three coordinate alanyl complex, and so the pendant amino functionality has to be removed. To disfavour

oligomerisation in a three coordinate aluminium complex, the ligand system and substituents chosen must be sufficiently sterically demanding.

In 1997 Nöth and co workers characterised the first three coordinate alanyl complex as the product from the reaction between the very bulky *bis*-amide precursor $(tmp)_2AlBr$ (tmpH = 2,2,6,6-tetramethylpiperidine) and $Na[CpFe(CO)_2]$ (Scheme 1.4).

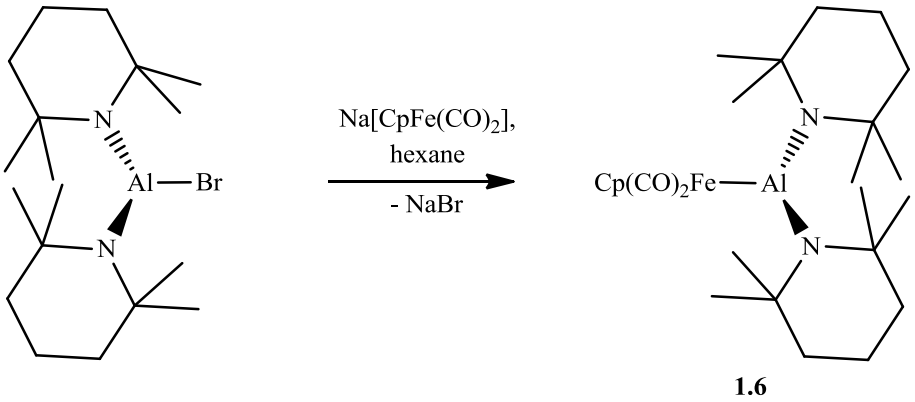

1.6

Scheme 1.4: *Formation of $Cp(CO)_2Fe$-$Al(tmp)_2$ (**1.6**)*

Structural characterisation by single crystal X-ray diffraction confirmed that the aluminium centre in $CpFe(CO)_2[Al(tmp)_2]$ (**1.6**) is indeed three coordinate, providing insight into the extent of π back-bonding to the formally vacant aluminium *p*-orbital through the Fe-Al bond distance. The iron-aluminium bond distance is shorter in **1.6** than those observed in the four coordinate systems previously discussed (2.450(1) Å for **1.6** *cf.* 2.456(1) and 2.468(1), 2.496(1) Å for **1.3** and **1.5** respectively).[43,44] However, comparison of the covalent radii (Al 1.25 Å and Fe 1.26 Å)[45] indicates a more significant shortening of the iron-aluminium bond would be expected if significant double bond character was present. Related theoretical studies into the extent of π back-bonding present in carbene complexes of the $[CpFe(CO)_2]$ fragment showed the transition metal based orbital with most effective overlap for π back-bonding lies parallel with the Cp ring.[46] Consequently, maximum π

back-bonding would be present when a torsion angle of Cp centroid-Fe-Al-N of 0 or 180° was observed (*cf.* observed Cp centroid-Fe-Al-N torsion angles of 53.2 and 54.4°). Therefore, only a small contribution to the short iron-aluminium bond distance in $CpFe(CO)_2[Al(tmp)_2]$ can be attributed to π back-bonding.[47]

The aforementioned transition metal alanyl complexes feature alkyl or aryl substituents equipped with secondary donors or a very bulky *bis*-amide ancillary ligand framework. Closely related *N,N'*-chelating ligands, such as amidinates and guanidinates (Figure 1.2), have been shown to complex and stabilise a multitude of elements from across the Periodic Table in low oxidation states and coordination numbers.[48-53] Such mono-anionic *N,N'*-chelating ligands are an ideal ancillary framework for the formation of M-Al two-centre two-electron bonds, and potentially low valent mixed metal complexes.

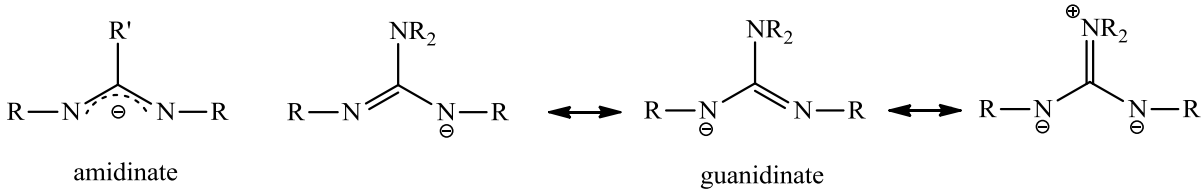

Figure 1.2: *Resonance forms of amidinate and guanidinate ligands*

Complexes of the type $\{R'C(RN)_2\}AlX_2$ (where R' = alkyl, aryl or amide; R = alkyl or aryl; X = halide or alkyl) have received significant attention in the literature as precursors to highly Lewis acidic cationic catalysts for olefin polymerisation.[51,52,54,55] The ability of suitable aluminium *N,N'*-chelated species to undergo salt elimination chemistry, in common with other group 13 elements, was shown by Jones, Aldridge and co-workers in 2006.[56] This work led to the structural characterisation of the novel dihalo precursors $\{^tBuC(CyN)_2\}ECl_2$ (where E = Al **1.7** or Ga **1.8**) as well as $\{^tBuC(CyN)_2\}InBr_2$ (**1.9**). Subsequent reactions between **1.7**-**1.9** and $Na[CpFe(CO)_2]$ yielded the corresponding

complexes $CpFe(CO)_2[(Cl)E(NCy)_2C^tBu]$ (where E = Al **1.10** or Ga **1.11**) and $CpFe(CO)_2[(Br)In(NCy)_2C^tBu]$ (**1.12**) (Scheme 1.5) which were also characterised by single crystal X-ray diffraction.

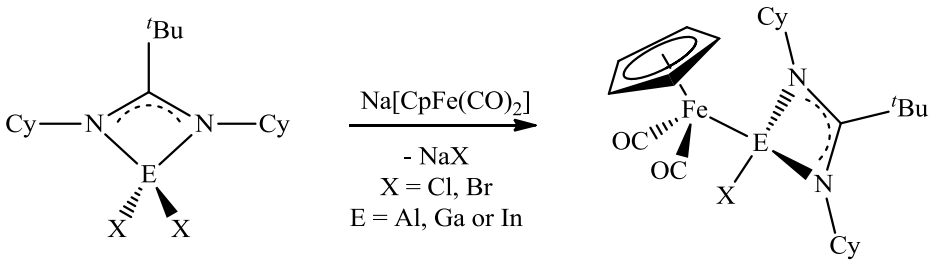

Scheme 1.5: *Formation of $CpFe(CO)_2[(X)E(NCy)_2C^tBu]$*

Halide abstraction reactions between **1.10**-**1.12** and $Na[BAr^f_4]$ to yield the corresponding three coordinate cationic complexes were also attempted. Whilst the diethyl ether stabilised gallium cation $CpFe(CO)_2[(Et_2O)Ga(NCy)_2C^tBu][BAr^f_4]$ (**1.13**) was characterised, in the case of aluminium no reaction was observed, and this was attributed to the strength of the aluminium-chloride bond.[56]

The use of salt elimination chemistry for the formation of M-Al bonds has been shown to be effective for the formation of transition metal alanyl complexes. However, in 1998 Bergman and co-workers demonstrated that alkane elimination can also be used in a manner analogous to other group 13 elements as an alternative synthetic route for the formation of transition metal alanyl complexes.[57-59] Reaction between $Cp^*Ir(H)_2(PMe_3)$ (**1.14**) and Et_3Al results in the elimination of two equivalents of ethane and formation of the dimeric species $[Cp^*(PMe_3)IrAlEt]_2$ (**1.15**) which was characterised by single crystal X-ray diffraction (Scheme 1.6).[57]

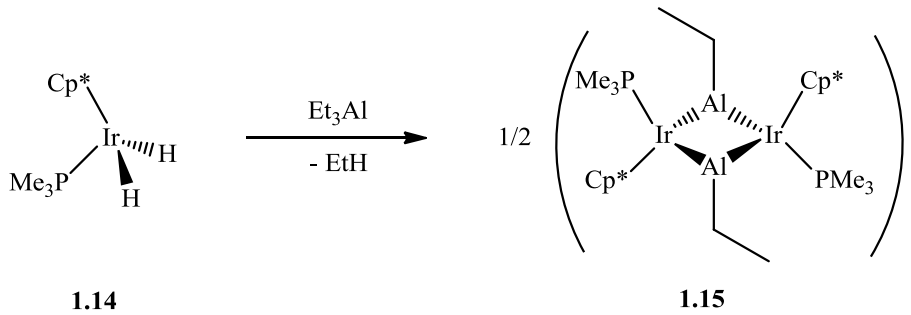

1.14 **1.15**

Scheme 1.6: *Reaction of Cp*Ir(H)$_2$PMe$_3$ (**1.14**) with Et$_3$Al*

Although the formation of two M-Al two-centre two-electron bonds to a single aluminium centre has been characterised previously (**1.5**), structural characterisation of a three coordinate aluminium centre, without additional intramolecular donor stabilisation, and without the use of highly sterically demanding ligands is quite remarkable. The solid state structure closely resembles that of the related species [Cp*Co(C_2H_4)AlEt]$_2$ (**1.16**), isolated in low yield (less than 2%) from the reaction of Cp*Co(C_2H_4)$_2$ (**1.17**) with Et_2AlH *via* the elimination of two equivalents of ethane; the major product of this reaction is the *cis*-dimetallated olefin product (Cp*CoH)$_2$-μ-{η^2:η^2-*cis*-[(C_2H_5)$_2$AlCHCHAl(C_2H_5)$_2$]} (**1.18**).[60] Whilst alkane elimination is an attractive method for the formation of M-Al two-centre two-electron bonds, the dearth of examples of the formation of discrete molecular complexes in the literature implies that this is not a suitable generic synthetic strategy to these types of complexes, and is perhaps more likely to result in cluster formation.

1.3.3 Transition Metal Donor Aluminium Acceptor Complexes

The formation of simple Lewis acid/base donor acceptor complexes has been extensively researched and is a fundamental concept in inorganic chemistry. A vast number of Lewis base adducts of alanes have been characterised in which the Lewis base plays a fundamental role in stabilising the electropositive aluminium centre, providing both steric

and electronic protection against oligomerisation. Such classic two-centre two-electron dative bonds between Lewis bases and alanes typically feature *p*-block donors (such as P, N or O). However, low valent electron rich transition metals under appropriate conditions can form metal only Lewis adducts. Complexes of this type (type B, Figure 1.1) feature a two-centre two-electron dative bond and represent some of the first transition metal aluminium bonds to be discussed in the literature.

In 1979 Burlitch, Hughes and co-workers reported their findings on the coordination of transition metal carbonylate anions to EPh_3 (E = Al, Ga or In). Weakly coordinating cations were used to promote anion/cation dissociation, and coordination of the former to EPh_3. The interaction of the carbonylate anions $[CpFe(CO)_2]^-$, $[CpW(CO)_3]^-$, $[Co(CO)_4]^-$ and $[Mn(CO)_5]^-$ with $AlPh_3$ were investigated primarily through IR spectroscopy. The complexes formed in the cases of cobalt and manganese proved difficult to isolate, but the reactivity with the corresponding iron and tungsten anions was more definitive. In the case of $[CpFe(CO)_2]^-$ a direct iron-aluminium bond is formed and the product $[NEt_4][CpFe(CO)_2AlPh_3]$ (**1.19**) was structurally characterised. The analogous reaction with $[CpW(CO)_3]^-$ (**1.20**) results in the formation of an *iso*-carbonyl bridged species as characterised by IR spectroscopy.[61] This presumably results from the hard Lewis acid nature and oxophilicity of the aluminium centre, and the greater steric crowding of the metal centre in **1.20**, indicating that the nature of the transition metal component is important in transition metal-aluminium bond formation. Mayer and co-workers further developed this approach with the isolation and structural characterisation of the neutral transition metal-aluminium bonded species $CpRh(PMe_3)_2(Al_2Me_4Cl_2)$ (**1.21**) (Scheme 1.7).[62]

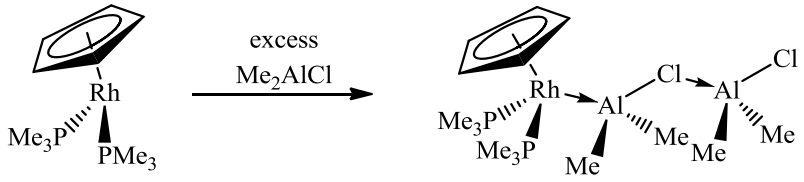

Scheme 1.7: *Formation of $CpRh(PMe_3)_2(Al_2Me_4Cl_2)$(**1.21**)*

The solid state structure of **1.21** contains a Rh-Al bond distance of 2.458(1) Å, compared to 2.510(2) Å in **1.19**,[61] a shortening which is all the more marked when the difference in the respective covalent radii is considered (Δr = 0.10 Å).[63] An alternative bonding description of **1.21** can be considered in which $[CpRh(PMe_3)_2AlMe_2]^+$ is coordinated by $[Cl_2AlMe_2]^-$ (Figure 1.3).

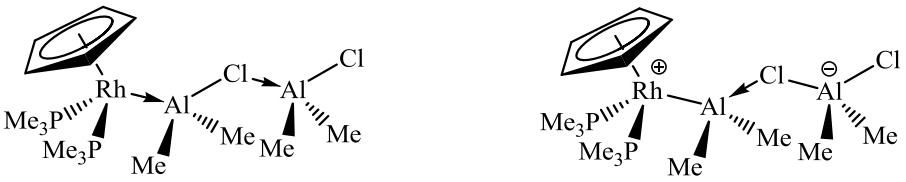

Figure 1.3: *Potential bonding descriptions for **1.21***

The geometric parameters of **1.21** in which the bridging chloride lies closer to the $ClAlMe_2$ moiety than $CpRh(PMe_3)_2AlMe_2$, and the distortion of the rhodium bound aluminium geometry towards planar implies that a significant contribution to bonding arises from this second limiting description.[62] More recently Bergman and co-workers used the related iridium(III) species $Cp^*Ir(PMe_3)(H)_2$ (**1.14**) to isolate and structurally characterise the adduct $Cp^*Ir(PMe_3)(H)_2AlPh_3$ (**1.22**) (Scheme 1.8).[57]

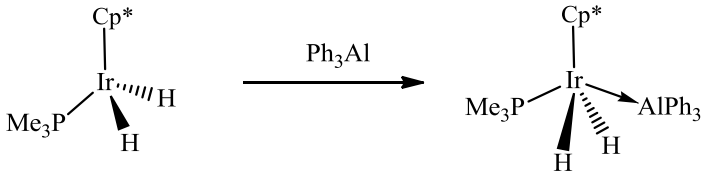

1.14 **1.22**

Scheme 1.8: *Reaction between **1.14** and $AlPh_3$*

The solid state structure of **1.22** shows the Ir-Al bond distance to be 2.864(2) Å, notably longer than the Rh-Al distance of 2.458(1) Å observed in **1.21**.[62] The formation of a donor-acceptor complex featuring transition metal hydrides and an aluminium aryl is quite remarkable and in the solid state the formation of an iridium-aluminium bond rather than two 3-centre-2-electron Ir-H-Al interactions is implied. The formation and stability of the adduct **1.22** with respect to aryl elimination (*i.e.* Ph-H) is attributed to the strength of the sp^2-carbon-aluminium bond. This is of contrast to alkyl sp^3-carbon-aluminium bonds which, in the case of $AlEt_3$, go on to eliminate an equivalent of the corresponding alkane resulting in the formation of a direct iridium-aluminium σ-bond and the dimeric complex $[Cp^*(PMe_3)IrAlEt]_2$ (**1.15**) (section 1.3.2).[57]

The ability of platinum(0) and palladium(0) complexes of the type $(R_3P)_2M$ (R = Cy; M = Pd or Pt) to act as transition metal bases is well documented for transition metal boryl and borylene systems.[64-66] The reactivity of platinum(0) complexes towards aluminium trihalides has also received recent attention. In 2007 Braunschweig and co-workers structurally characterised an $AlCl_3$ adduct of platinum $(Cy_3P)_2PtAlCl_3$ (**1.23**), and spectroscopically characterised the $AlBr_3$ and AlI_3 analogues.[67] Investigations by the same group into the effect of substituting phosphines for carbenes in these systems led to the structural characterisation of complexes of the type $L(Cy_3P)PtAlCl_3$ (where L = I^tBu **1.24** or SIMes **1.25**) and the homoleptic system $(SIMes)_2PtAlCl_3$ (**1.26**) (Scheme 1.9).[67,68]

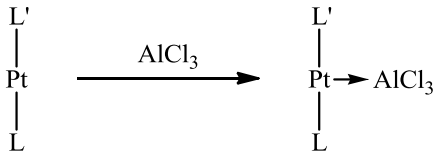

where L = PCy_3; L' = I^{t}Bu, SIMes
or L = L' = SIMes, PCy_3

Scheme 1.9: *Formation of (L)(L')PtAlCl$_3$ adducts*

The effect of the N-heterocyclic carbene (NHC) on the platinum Lewis base can be examined by complex formation with $AlCl_3$ and subsequent structural and spectroscopic characterisation, as well as through quantum chemical calculations. DFT studies predict the strongest Pt-Al bond for the heteroleptic phosphine/NHC systems as a combined result of steric and electronic factors. Although substitution of a phosphine by the NHC results in a more electron rich complex, the NHC is significantly more sterically demanding. The result is a staggered conformation in $(SIMes)_2Pt$ (**1.27**), blocking the coordination sites at the platinum centre. In order to accommodate the $AlCl_3$ Lewis acid, a more eclipsed geometry is required, which is less favourable and higher in energy. The heteroleptic complex is more basic than the homoleptic $(Cy_3P)_2Pt$ (**1.28**), as a result of the superior electron donating properties of the NHC, and does not have as large a preparation or reorganisation energy associated with complex formation with $AlCl_3$ as **1.27**. The greater affinity of the heteroleptic complex has been proven experimentally by the transfer of $AlCl_3$ from the homoleptic complexes $(Cy_3P)_2PtAlCl_3$ (**1.23**) and $(SIMes)_2PtAlCl_3$ (**1.26**) to the stronger Lewis base $(Cy_3P)Pt(I^tBu)$.[68]

A more recent study using the related homoleptic and heteroleptic complexes, $(^iPr_3P)_2Pt$ (**1.29**) and $(^iPr_3P)Pt(IMes)$ (**1.30**), led to the structural characterisation of the adducts $(^iPr_3P)_2PtAlX_3$ (X = Cl **1.31** or Br **1.32**) and $(^iPr_3P)(IMes)PtAlX_3$ (X = Cl **1.33** or Br **1.34**), which closely resemble the previously discussed systems **1.23**-**1.26**. However,

computational analysis on the effect of replacing a $^{i}Pr_3P$ ligand with IMes contrasts with the findings in the Cy_3P case, and does not indicate that the phosphine is a weaker electron donor. Replacement of chloride for bromide on the aluminium does, however, decrease the Lewis acidity of the aluminium fragment.[69]

The concept of metal-only Lewis pairs has been expanded to include not only platinum(0) complexes with aluminium trihalides but also a palladium analogue. The synthesis of $(Cy_3P)Pd(I^{t}Bu)$ (**1.35**), unlike the platinum analogue, cannot be achieved *via* ligand substitution from the $Pd(PCy_3)_2$ complex. It requires stepwise ligand addition to $(\eta^5\text{-}C_5H_5)Pd(\eta^3\text{-}1\text{-}PhC_3H_4)$ and subsequent reductive elimination of an isomeric mixture of $C_{14}H_{14}$ hydrocarbon products. The aluminium chloride adduct $(Cy_3P)(I^{t}Bu)PdAlCl_3$ (**1.36**) is formed in a stoichiometric reaction between the heteroleptic palladium complex and aluminium chloride and bears close structural resemblance to the platinum analogue **1.24**.[70]

The aforementioned examples of metal-only Lewis pairs feature unsupported M→Al interactions, and involve electron rich late transition metal centres. To expand the scope and range of M→Al interactions a stabilising 'tethering' approach can be employed, analogous to the well documented metallaboratranes.[71-73] This approach effectively incorporates the aluminium centre into the ligand, thereby forcing a close approach of the transition metal and the aluminium centres. This has enabled successful characterisation of related Au→Ga, Pd→In and Au→In interactions.[74] Extension of this approach to the formation of metallalumatranes through the use of the $N(o\text{-}NHCH_2P^{i}Pr_2\text{-}C_6H_4)_3$ framework has led to the isolation and characterisation of nickel(0), cobalt(0) and iron(0) complexes (**1.37**-**1.39** respectively) (Scheme 1.10).

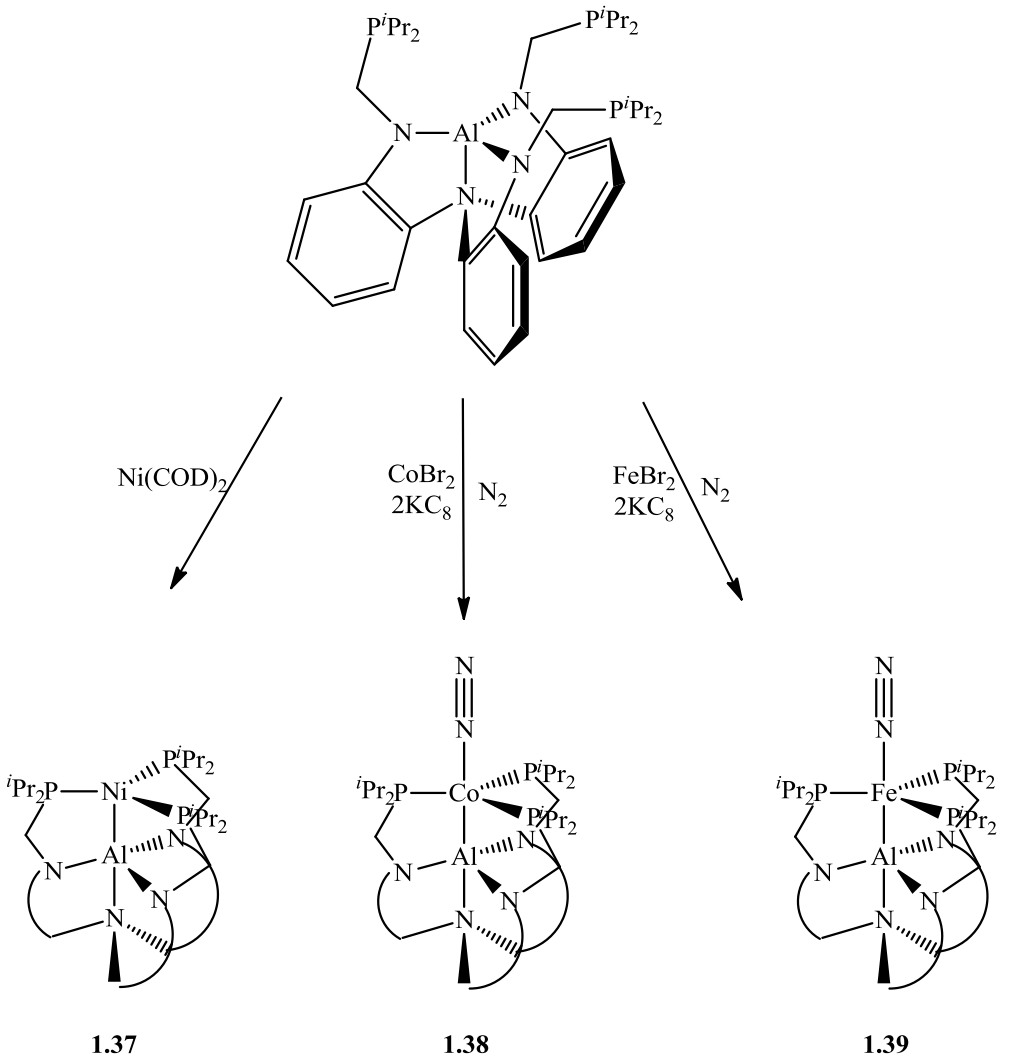

Scheme 1.10: *Formation of metallalumatrane complexes **1.37**-**1.39***

While the design of the ligand framework holds the transition metal and aluminium centres in close proximity, the extent of bonding that exists between them is not obvious. The ratios of the M-Al bond lengths to the respective covalent radii are close to unity in **1.37**-**1.39**, providing some evidence for metal-metal bonding. The study of the M-Al interaction in metallalumatrane complexes is somewhat more challenging than that of unsupported M-Al interactions due to the less well defined nature of the metal-metal interaction.[75]

1.3.4 Aluminium Donor Transition Metal Acceptor Complexes

The formation of aluminium donor transition metal acceptor complexes (Type C, Figure 1.1) requires the aluminium centre to be in the +1 oxidation state rather than the more typical +3. There has been renewed interest in main group chemistry and much of this is attributable to the realisation that heavier main group elements can be stabilised in unusual oxidation states, coordination number and in some cases possessing unusual bond orders.[42] The isolation and coordination chemistry of aluminium(I) complexes featuring a dative bond from an aluminium lone pair to a transition metal centre has been widely researched, and is well documented in the literature. Much of the early aluminium(I) and low valent aluminium chemistry was pioneered by Schnöckel and co-workers who developed coordination complexes featuring aluminium(I) ligands as well as aluminium metalloid clusters. The chemistry of metalloid clusters of aluminium and gallium has recently been reviewed and the chemistry of aluminium(I) complexes has also been extensively reviewed.[40,76-79]

1.3.4.1 Isolable Aluminium(I) Precursors

The formation of stable aluminium(I) complexes can be achieved through two routes: (i) reaction of an anionic substituent with an aluminium(I) species; or (ii) through the reduction of an aluminium(III) precursor with an alkali metal. Sources of aluminium(I) precursors are fairly limited given the propensity for disproportionation to metallic aluminium and the corresponding aluminium(III) complex. Whilst aluminium(I) hydrides have only been isolated in argon matrices at very low temperatures, metastable aluminium(I) halides have been utilised as synthetic precursors to aluminium(I) chemistry. These are formed either by comproportionation reactions of AlX_3 and molten aluminium metal or by reaction of HX with molten aluminium at high temperatures (800-1000 °C). A synthetically useful

precursor can be obtained by co-condensation with donor solvents resulting in the formation of metastable solutions of AlX (X = Cl, Br or I) in diethyl ether, THF or triethylamine.[42,79] Despite the potential for salt metathesis chemistry to generate organometallic aluminium(I) complexes from these metastable solutions, few are stable and those that are, exist predominantly as tetramers.[80-84] The first structurally characterised and most widely studied AlR complex is $[Cp^*Al]_4$, synthesised *via* the reaction of a metastable diethyl ether/toluene solution of AlCl with Cp^*_2Mg. The structure of $[Cp^*Al]_4$ (Figure 1.4) contains a tetrahedron of aluminium atoms with each in a tetrahedral environment featuring bonds to three other aluminium atoms, and a Cp* substituent coordinated *via* an η^5-binding motif.[85]

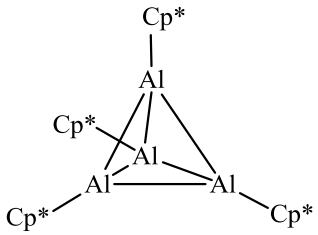

Figure 1.4: *Structure of the $[Cp^*Al]_4$ tetramer*

In solution, however, the tetramer exists in equilibrium with monomeric Cp*Al and, as a result, the coordination chemistry of Cp*Al has been widely investigated, and a range of transition metal complexes structurally characterised.[78] The $[Cp^*Al]_4$ tetramer can also be formed through the reduction of $[Cp^*AlX(\mu\text{-}X)]_2$ (X = Cl, Br or I) with sodium/potassium alloy or potassium.[86] This approach of reducing a dihalo precursor to the corresponding aluminium(I) species represents a more general approach to the synthesis of aluminium(I) compounds.

The emergence and increasing presence of carbene complexes in the literature has generated much interest in the synthesis and properties of group 13 analogues of classical

N-heterocyclic carbenes. Whilst a number of carbene analogues exist for gallium,[87-91] indium[53,87,92] and thallium,[53,87,92-94] only two have been isolated in the case of aluminium. Both carbene analogues incorporate the very bulky β-diketiminate ($Dipp_2NacNac$) substituent with highly sterically demanding aryl groups (Figure 1.5).

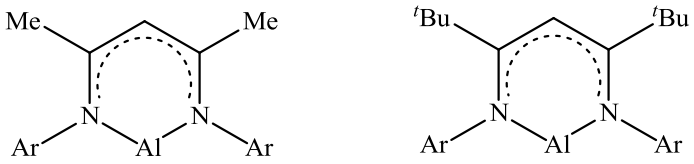

1.40 **1.41**

Ar = 2,6-di*iso*propylphenyl

Figure 1.5: *Structures of isolable monomeric N-heterocyclic aluminium(I) compounds*

Both of the N-heterocyclic aluminium(I) species **1.40** and **1.41** (Figure 1.5) were obtained through the reduction of the corresponding diiodide complexes with potassium metal.[95,96] As analogues of carbenes, **1.40** and **1.41** possess singlet lone pairs and are good σ-donors. Due to the formally vacant *p*-orbital and the electropositivity of aluminium there is also the potential for π-acceptor properties, potentially to a greater degree than for a classical carbene ligand due to poorer nitrogen-aluminium π-overlap. This ability is demonstrated in the Lewis acid/base adduct formed between **1.40** and the Lewis acid $B(C_6F_5)_3$. The solid state structure of the adduct $\{Dipp_2NacNacAl\}B(C_6F_5)_3$ (**1.42**) shows that the aluminium centre binds directly to the Lewis acidic boron, and additionally accepts electron density from one of the *ortho*-fluoro substituents of the C_6F_5 ring (Figure 1.6). The coordination of the *ortho*-fluoro substituent is strong enough to be observed in solution by ^{19}F NMR, highlighting the amphoteric nature of **1.40**.[97]

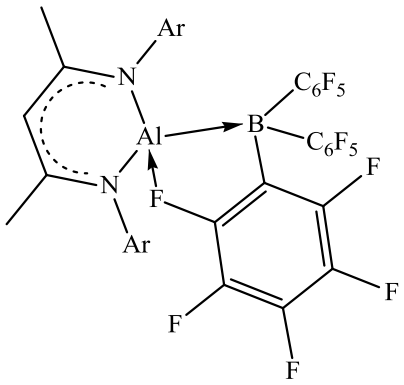

Figure 1.6: *Structure of the Lewis acid/base adduct **1.42***

1.3.4.2 Transition Metal Complexes of Cp*Al

Although 'free' monomeric aluminium(I) species are rare, related transition metal complexes give insight into the bonding and reactivity of such systems. The potential for amphoteric behaviour, *i.e.* σ-donation as well as π-acceptor properties, enables aluminium(I) ligands to be considered in a similar fashion to classical ligands such as CO and PR_3. As a consequence, the majority of complexes that have been structurally characterised are derived from low valent late transition metals.

Possibly the simplest synthetic approaches are ligand displacement reactions involving the addition of the Cp*Al moiety *e.g.* to bimetallic $[Co_2(CO)_8]$ to yield the related compound $[Co_2(CO)_6(\mu\text{-Cp*Al})_2]$ (**1.43**), in which the Cp*Al ligands have displaced two bridging carbonyl ligands.[98] The displacement of labile ligands by the Cp*Al moiety has been extended to include coordinated alkenes such as coe, cod and dvds. Schnöckel and co-workers showed that the reaction between the $[Cp*Al]_4$ tetramer and preformed $Cr(CO)_5(coe)$ at 60 °C in toluene leads to the formation of $Cp*AlCr(CO)_5$ (**1.44**).[99] Furthermore, the homoleptic complexes $M(AlCp*)_4$ (M = Ni **1.45**, Pd **1.46**) can be obtained through the use of carbonyl free starting materials (Scheme 1.11).[100]

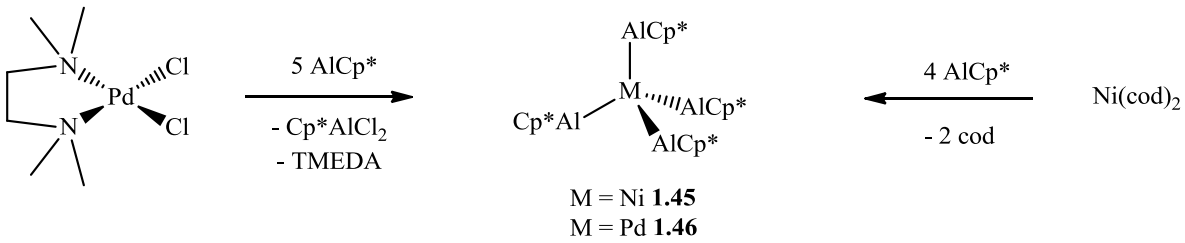

Scheme 1.11: *Formation of homoleptic AlCp* complexes **1.45** and **1.46***

Interestingly, in the case of palladium, the reaction requires an extra equivalent of Cp*Al in order to reductively eliminate Cp^*AlCl_2 and generate the homoleptic complex **1.46**, something which is not necessary in the formation of **1.45** (Scheme 1.11). The displacement of cod from the cationic complex $[Rh(\eta^2,\eta^2\text{-cod})_2][BAr^f{}_4]$ (**1.47**) was also used to generate the heteroleptic complex $[Rh(\eta^2,\eta^2\text{-cod})(AlCp^*)_3][BAr^f{}_4]$ (**1.48**). The stronger σ-donor properties of the Cp*Al ligand make the rhodium more electron rich and increased back-bonding to the remaining cod ligand prevents further substitution to the homoleptic complex.[101] The formation of homoleptic compounds can be extended through the use of multinuclear precursors such as $Pd_2(dvds)_3$ (**1.49**), which upon reaction with excess $[Cp^*Al]_4$ yields the cluster compound $Pd_3(AlCp^*)_2(\mu_2\text{-}AlCp^*)_2(\mu_3\text{-}AlCp^*)_2$ (**1.50**).[102]

The platinum(II) species (dcpe)Pt(H)($CH_2{}^tBu$) (**1.51**) (dcpe = 1,2-*bis*(di*cyclo*hexylphosphino)ethane) when warmed to 45-80 °C reductively eliminates neopentane yielding the highly reactive platinum(0) species [(dcpe)Pt], which has been shown to readily activate C-H bonds.[103] Warming a solution of **1.51** in the presence of Cp*Al allows the reactive [(dcpe)Pt] fragment to be trapped as (dcpe)Pt$(AlCp^*)_2$ (**1.52**).[104] The addition of the Cp*Al moiety to the bi- and tri-metallic complexes $(Cp^*Ru)_2(\mu_2\text{-H})_4$ (**1.53**) and $(Cp^*Ru)_3(\mu_2\text{-H})_3(\mu_3\text{-H})_2$ (**1.54**) leads to cluster formation. The corresponding polyhydride clusters $[Cp^*Ru(\mu_2\text{-H})(H)(\mu_2\text{-}AlCp^*)]_2$ (**1.55**) and $(Cp^*Ru)_3(\mu_2\text{-H})_5(\mu_3\text{-}AlCp^*)$

(**1.56**) (Figure 1.7) can be formed, from which reductive elimination of neither Cp*H or dihydrogen is observed.

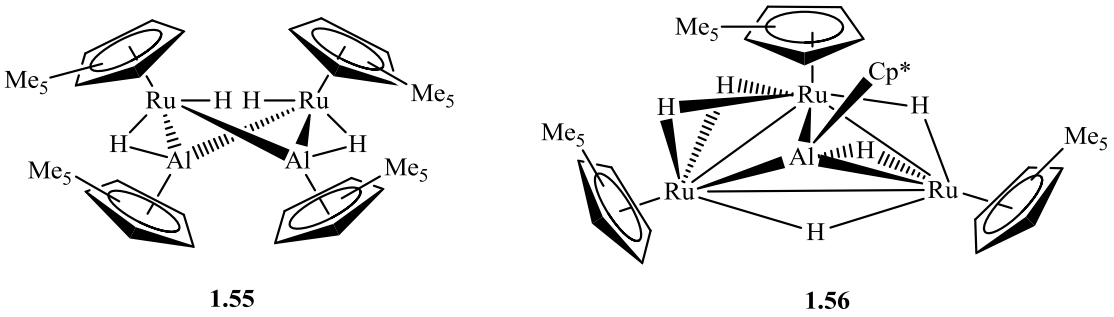

1.55 **1.56**

Figure 1.7: *Structures of **1.55** (left) and **1.56** (right)*

The triruthenium cluster **1.56** contains a triply bridging aluminium centre in which the Cp* ligand has altered its coordination mode from η^5- to η^1, thereby enabling the aluminium to bridge all of the ruthenium atoms in the cluster.[105] This change in coordination mode of the Cp* ligand means this penta-hydrido cluster closely resembles the tri-hydrido cluster $(Cp^*Ru)_3(\mu\text{-}H)_3(\mu_3\text{-}AlEt)$ (**1.57**) reported by Suzuki and co-workers.[106] However, the different syntheses applied to these clusters result in different levels of hydride inclusion. Whilst Cp*Al enables direct coordination of an aluminium(I) moiety to a polyhydride cluster, **1.57** is formed through deprotonation of the ruthenium complex by Et_3Al and the elimination of two equivalents of ethane, thereby reducing the number of hydride ligands incorporated.

The potential for the $[Cp^*Al]_4$ tetramer to act as a reducing agent was demonstrated by Schnöckel and co-workers who used it to reduce Cp_2Ni and form $(CpNi)_2(\mu\text{-}AlCp^*)_2$ (**1.58**), which is directly comparable to the corresponding carbonyl complex $[(CpNi)_2(\mu\text{-}CO)_2]$ (**1.59**) with Cp*Al ligands replacing carbonyls.[107] Whilst this landmark discovery identified the use of Cp*Al as an electron-rich carbenoid-like species, it remains one of few

examples in which an aluminium(I) precursor acts as the reducing agent. There has been much interest in performing redox chemistry in the opposite direction and the use of transition metal dianions for the reduction of aluminium(III) halides to aluminium(I) complexes *via* salt metathesis.

The reactions of transition metal dianions with aluminium(III) dihalide electrophiles provides an alternative approach for the synthesis of transition metal-aluminium bonds. Furthermore, this approach does not require the free aluminium(I) moiety to be stable, as it can be formed and stabilised in the coordination sphere of the transition metal. Thus, for example, a number of base stabilised aluminium(I) adducts have been reported. The first base stabilised aluminium(I) complexes were reported in 1996 by Fischer and co-workers who showed that the reaction between $K_2[Cr(CO)_5]$ and Cl_2AlR (R = Me, Et or Cl) followed by the addition of tmeda resulted in double salt elimination to generate complexes of the type $(CO)_5Cr[Al(R)(tmeda)]$ (R = Me **1.60**, Et **1.61** or Cl **1.62**).[108] Furthermore, the extension to the tungsten dianion $K_2[W(CO)_5]$ enabled the structural characterisation of the related complexes $(CO)_5W[Al(R)(L)]$, (L = tmeda and R = Et **1.63**; L = tmpda and R = Cl **1.64**, or ^{t}Bu **1.65**) (Scheme 1.12).[109,110]

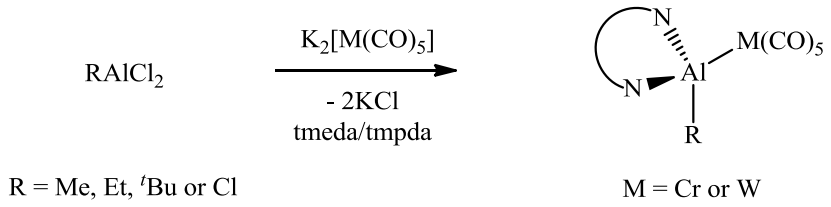

Scheme 1.12: *Generic scheme for the formation of base stabilised aluminium(I) complexes*

While the formation of base stabilised complexes through double salt elimination chemistry is an effective approach to otherwise inaccessible aluminium(I) complexes, it can also be applied to Cp^*AlCl_2, which upon reaction with $K_2[Fe(CO)_4]$ yields $(CO)_4Fe(AlCp^*)$ (**1.66**),

in which the aluminium centre is reduced to form the donor acceptor complex $Cp^*Al{\rightarrow}Fe(CO)_4$.[111] Despite the close relationship of this species to related coordination complexes formed from the $[Cp^*Al]_4$ tetramer, it remains the only example to have been synthesised *via* double salt elimination without additional base stabilisation.

1.3.4.3 Transition Metal Complexes of *N*-heterocycle Stabilised Aluminium(I)

The emergence of *N*-heterocyclic carbenes as a strong σ-donating and robust ligand class in a number of catalytic processes has sparked significant research into the group 13 and 14 analogues.[40] The *N*-heterocyclic aluminium(I) complex **1.40** reported by Roesky and co-workers, along with the related more bulky derivative reported by Cui and co-workers **1.41**, remain the only isolable monomeric aluminium analogues of *N*-heterocyclic carbenes.[95,96] Much work has been carried out investigating the reactivity of these carbene analogues towards main group compounds and this has been extensively reviewed;[78,112] however, there is much less literature surrounding the transition metal coordination chemistry of **1.40** and **1.41** and the formation of M←Al complexes supported by the β-diketiminate substituent.[113,114]

The strong σ-donor properties of **1.40** and **1.41** make ligand substitution reactions a straightforward approach to the formation of coordination complexes. The olefinic precursor $Pd_2(dvds)_3$ (**1.49**) undergoes ligand substitution and, depending on the reaction stoichiometry, yields either the monomeric species ($Dipp_2$NacNacAl)Pd(dvds) (**1.67**) or the dinuclear complex $\{Pd(dvds)\}_2$(μ-$Dipp_2$NacNacAl) (**1.68**) (Scheme 1.13).[113,114]

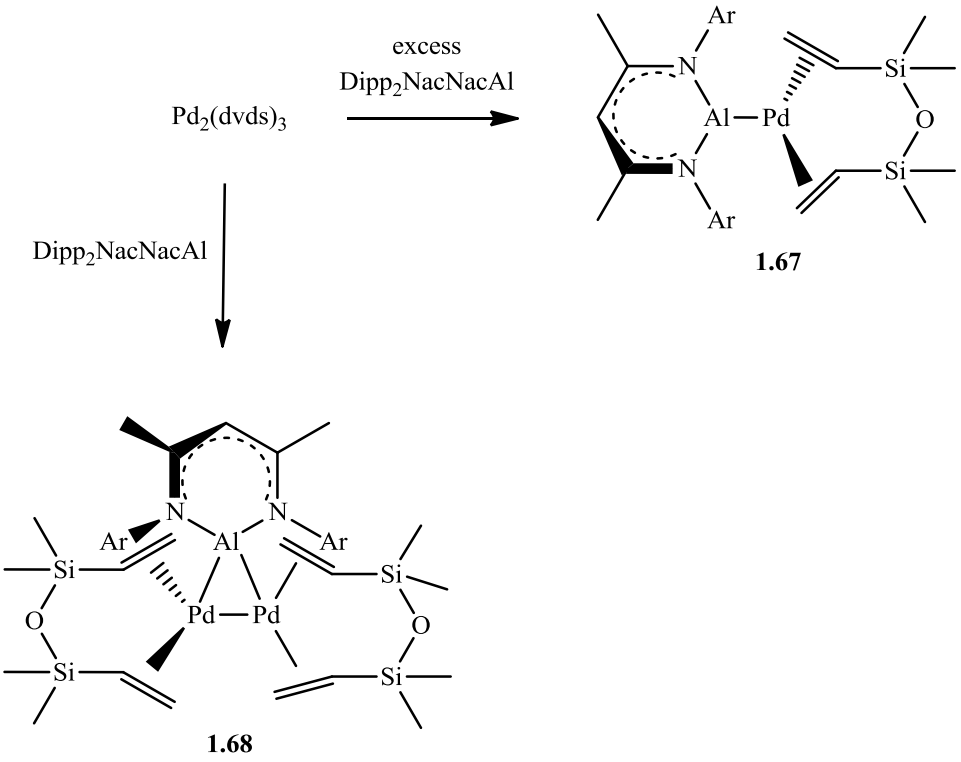

Scheme 1.13: *Reaction between **1.40** and **1.49***

Despite multiple literature references to the rich potential for developing the coordination chemistry of the carbene analogues **1.40** and **1.41**, transition metal complexes remain surprisingly few and far between.

1.4 Transition Metal Sigma (σ) Complexes

Bonds featuring a classical two-centre two-electron interaction between two atoms have a prominent role in chemistry from across the Periodic Table. The formation of non-classical three-centre two-electron bonds has much precedent in main group chemistry (for example B_2H_6) with bridged structures being relatively common.[115] However, the ability of transition metals to form complexes featuring non-classical three-centre two-electron bonds was realised relatively later in the groundbreaking discovery of Kubas' dihydrogen complex.[116] Transition metal sigma (σ) complexes are defined as those involving the coordination of a

bond X-Y to a transition metal through the electron density of the X-Y σ-bond. The σ-bond acts as a two electron donor into a vacant *d*-orbital of the transition metal, with the X-Y anti-bonding (σ*) orbital participating in back-bonding by accepting electron density from the filled transition metal π-bonding orbitals. This bonding description, illustrated in Figure 1.8 for E-H bonds, closely resembles the Dewar-Chatt-Duncanson model for olefin coordination.[117]

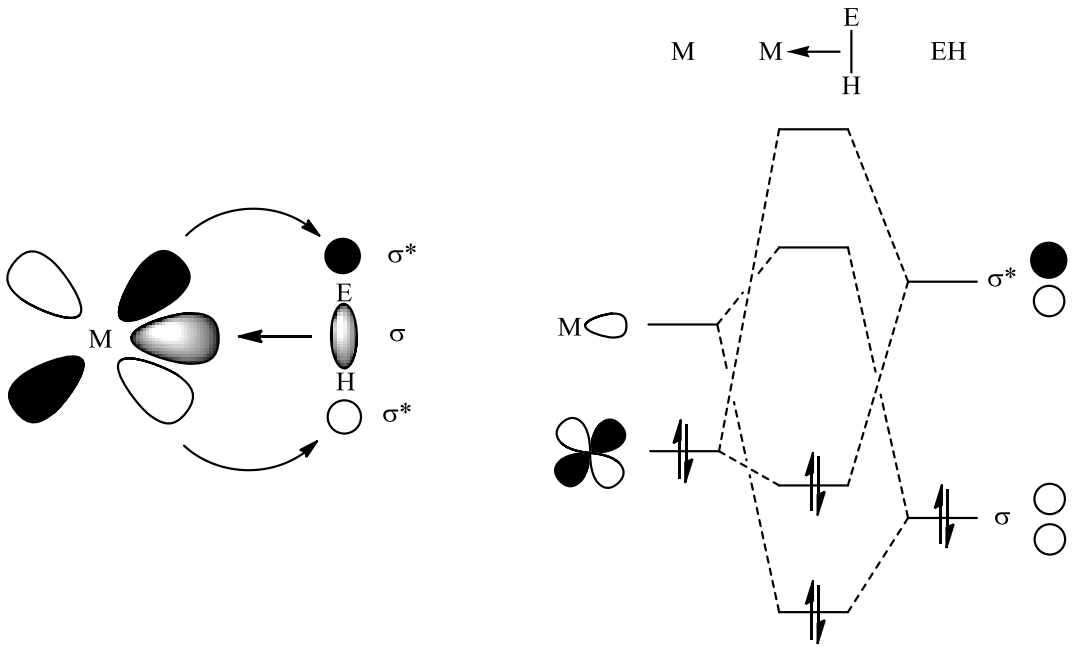

Figure 1.8: *Orbitals involved in the bonding of a transition metal σ-complex (left) and the corresponding molecular orbital energy level diagram (right)*[118]

The precise nature of the complex formed, and how far along the oxidative addition pathway the product is considered, largely depends upon the extent of back-bonding into the E-H σ*-orbital. Complexes in which the extent of back-bonding present is minimal contain E-H bonds which are very close to those reported in the free molecule. However, in complexes where back-bonding is significant (stretched σ-complexes) an elongated E-H

bond is observed, up to a point where full oxidative addition is considered to have taken place, and the E-H σ-bond has been cleaved (Figure 1.9).

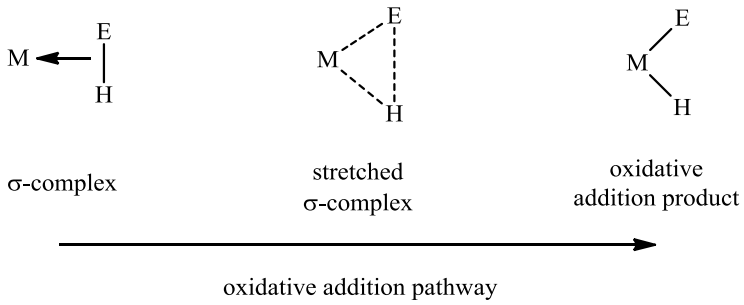

Figure 1.9: *Progressive elongation of the E-H bond as a function of oxidative addition*

Whilst the extent of back-bonding is clearly dependent upon the transition metal component, and its comparative electron richness, the energy of the E-H σ- and σ*-orbitals also have a key role in determining the energy match and effective orbital overlap with the *d*-orbitals involved in bonding.[115,118] Determination of the extent of oxidative addition is difficult and often depends upon the nature and identity of E. Whilst solid state techniques such as single crystal X-ray or neutron diffraction studies (for hydride location) can provide data in the solid state, NMR and IR spectroscopy, as well as theoretical studies are required to fully assess the bonding in any given complex.[117]

Transition metal σ-complexes represent important models for, and provide insights into, the process of oxidative addition of E-H bonds at transition metal centres. They can be thought of as an arrested state along the oxidative addition pathway and provide information about the parameters of what is a crucial and potentially rate determining step in a catalytic cycle.

1.4.1 Dihydrogen (H-H) σ-Complexes

The first σ-complex to be fully characterised was reported by Kubas *et. al.* in 1984 as the product of addition of dihydrogen to complexes of the type $(CO)_3W(PR_3)_2$ (R = ^{i}Pr **1.69** or Cy **1.70**) (Scheme 1.14).[116]

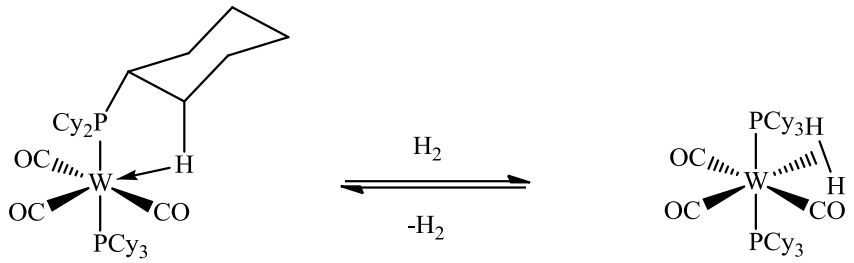

1.70 **1.71**

Scheme 1.14: *Formation of the first characterised dihydrogen complex*

Coordination of dihydrogen to **1.69** and **1.70** is both facile and reversible with dihydrogen being taken up at 1 atm pressure, and released on exposure to vacuum or an atmosphere not enriched with dihydrogen. Characterisation by both single crystal X-ray and neutron diffraction showed an H-H bond distance with only slight elongation compared to that of free H_2.[116] There are now many dihydrogen complexes present in the literature including *bis*(dihydrogen) species such as $Ru(H)_2(H_2)_2(PCy_3)_2$ (**1.72**), as well as the isoelectronic cationic analogues $[Rh(H)_2(H_2)_2(PCy_3)_2][BAr^f_4]$ (**1.73**) and $[Ir(H)_2(H_2)_2(PCy_3)_2][BAr^f_4]$ (**1.74**).[119-121] Whilst these species exist as dihydrogen complexes, rather than the dihydride product of oxidative addition, further studies on Kubas' system concluded that an equilibrium exists in solution between the dihydrogen complex and the dihydride product of oxidative addition. Through a combination of NMR and isotopic labelling studies it was shown that **1.71** actually exists in a 4:1 ratio of dihydrogen and dihydride complexes in solution at 298 K.[116,122,123]

The bonding model proposed for dihydrogen σ-complexes is closely related to that of the Dewar-Chatt-Duncanson model, as a result of the inherently non-polar nature of the H-H bond. Consequently, the related but cationic and therefore less electron rich analogues of **1.71** $[(CO)_3Mn(PCy_3)_2(H_2)]^+$ (**1.75**) and $[(CO)_3Re(PPh_3)_2(H_2)]^+$ (**1.76**) are best described as true dihydrogen complexes.[122,124] With a range of dihydrogen σ-complexes having been reported in the literature with differing degrees of H-H oxidative addition, a continuum can be used to describe and classify the electronic structure of these important complexes (Figure 1.10).[125]

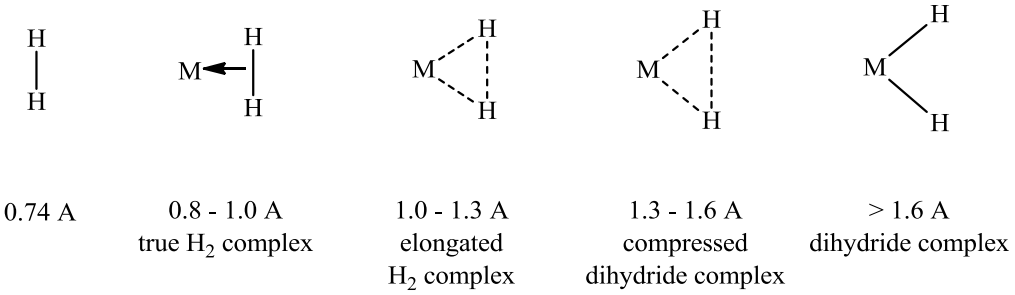

Figure 1.10: *Classifications of dihydrogen complexes*

The absence of any additional substituents, by the very nature of molecular dihydrogen, means the energy of the H-H σ- and σ*-orbitals cannot be manipulated. Consequently, the extent of oxidative addition is solely determined by the electron richness of the transition metal fragment, which in turn is a function of the metal and ancillary ligand set. The ability to 'tune' the E-H σ- and σ*-orbital energies (where E ≠ H) represents an additional consideration when comparing the extent of oxidative addition in other σ-complexes.

1.4.2 Silane (Si-H) σ-Complexes

The bonding interactions in transition metal dihydrogen complexes represent the most straightforward description of the contributing factors towards σ-complex formation, but with due consideration these can be developed to describe the bonding in E-H σ-complexes where E ≠ H. A closely related set of σ-complexes are those of silanes, R_3SiH, which represent the second most studied family of σ-complexes primarily due to their role as reaction intermediates in transition metal catalysed hydrosilylation reactions. Silane σ-complexes differ from dihydrogen complexes due to the asymmetry of the Si-H bond, reflecting not only the differing sizes of the R_3Si and H groups, but also the differing electronegativities which give rise to the polarity of the Si-H bond.[126] Consequently, additional factors need to be considered when describing and investigating the bonding in silane σ-complexes. Of particular importance is the ability of the substituents on the silicon to influence the position along the oxidative addition pathway through tuning the energy of the Si-H σ*-orbital. More electronegative substituents lower the energy of the Si-H σ*-orbital, making it more closely matched in energy to the transition metal *d*-orbitals and hence suitable for back-bonding, thereby promoting oxidative addition.

Although not described as a σ-complex at the time, the first structurally characterised compound featuring coordination to a metal by the electrons within a bonding σ-bond was the bimetallic species $(CO)_8Re_2(\kappa^2\text{-}H_2SiPh_2)$ (**1.77**) reported by Hoyano *et. al.* in 1969.[127] Since this landmark discovery many σ-silane complexes have been reported and the factors that affect their bonding extensively investigated.[128] There has been much effort invested in identifying the extent of oxidative addition observed in a number of σ-silane complexes, much of which has been conducted by employing the [Cp'Mn(CO)(L)] (L = CO or PR_3) fragment. Initial work by Schubert and co-workers used spectroscopic methods to investigate the bonding within complexes of the type $Cp(CO)_2Mn(H)SiR_3$.[129] The

complexes characterised by Schubert have since been re-investigated using a combination of single crystal neutron diffraction and Density Functional Theory (DFT) by McGrady and co-workers, to further probe the effect of electronegative silicon substituents on the oxidative addition of the Si-H bond (Figure 1.11).[130,131]

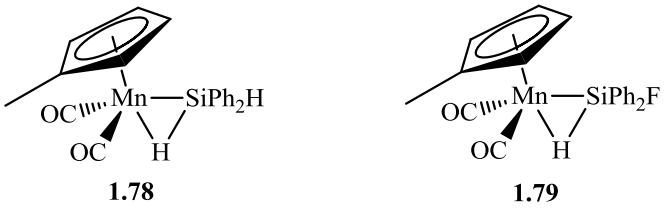

Figure 1.11: *σ-Silane complexes probing the effect of the electronegativities of substituents at silicon*

Comparison of both experimental data and quantum chemical calculations ultimately identified close similarities in the bonding between both Cp'Mn(CO)$_2$(κ^1-H$_2$SiPh$_2$) (**1.78**), Cp'Mn(CO)$_2$(κ^1-HSiPh$_2$F) (**1.79**) and the previously characterised chlorosilane complex Cp'Mn(CO)$_2$(κ^1-HSiCl$_3$) (**1.80**). The bonding in each can be described by considering an asymmetric oxidative addition process of the Si-H bond where the Mn-H bond is formed early, giving rise to minimal variation in both Mn-H bond length and strength of interaction regardless of the extent of oxidative addition observed. The Mn-Si interaction is more sensitive to the oxidative addition process, and hence the electronegativity of the substituents at the silicon, and is determined by the extent of Mn→σ*(X-Si-H) π back-donation observed [*e.g. d*(Mn-Si) = 2.391(12) Å for **1.78** and 2.254(1) Å for **1.80**]. Back-donation is increased by incorporation of a more electronegative substituent *trans* to the coordinated Si-H bond at the *hyper*coordinate silicon, and populates an orbital with both Si-H and Si-X antibonding character.[131] Consequently, the electronegativity of X directly influences the direct Mn-Si interaction, by altering the energy of the molecular orbital

which participates in π-back-bonding with the manganese fragment. The extent of oxidative addition observed in these complexes is thus varied.

1.4.3 Alkane (C-H) σ-Complexes

The selective functionalisation of alkane C-H bonds remains one of the most sought after catalytic transformations in organometallic chemistry, and as such the interaction of alkanes with coordinatively unsaturated transition metal complexes has received much attention in the literature. The first transition metal C-H σ-interactions were reported by Green and co-workers in the characterisation of (dmpe)$TiCl_3R$ (R = Me **1.81** or Et **1.82**) in which α- and β-C-H···Ti interactions were observed respectively, and in the case of **1.81** the hydrogen atoms unambiguously located by neutron diffraction.[132,133] Such intramolecular interactions have been termed 'agostic' and, whilst difficult to determine definitively, are relevant in C-H bond functionalisation steps and β-hydride elimination processes.[118] Agostic interactions are now well precedented in the literature with a number of examples including Kubas' **1.69** and **1.70** having been unambiguously characterised; moreover agostic interactions have even been implicated in mechanistic processes relevant to the stereochemical control in olefin polymerisations and migratory insertions.[134,135]

The formation and characterisation of intermolecular σ-alkane complexes, analogous to those of the aforementioned σ-silane complexes, remains much more challenging with no room-temperature stable σ-alkane complexes known. The major contributing factors to the limited number of σ-alkane complexes in comparison to σ-silane is the non-polar nature and the reduced polarisability of the C-H bond, in comparison to the Si-H bond, and the poorer σ-donor and π-acceptor properties of the C-H bond in comparison to its Si-H counterpart. Consequently, the Si-H···M interaction is more easily stabilised than that of C-H···M.[118]

Early work using matrix isolation techniques at 12 K showed evidence for σ-alkane complex formation through the use of infra-red and UV/visible spectroscopy.[136] It was not until Ball and co-workers showed detailed NMR studies of the alkane complexes formed *in situ* from the photolysis of $Cp'Re(CO)_2(PF_3)$ (**1.83**) in alkane solvents that σ-alkane complexes were characterised by NMR.[137] Furthermore, Brookhart and co-workers characterised a σ-methane complex at low temperature generated from the protonation of a rhodium methyl complex (Scheme 1.15).[138]

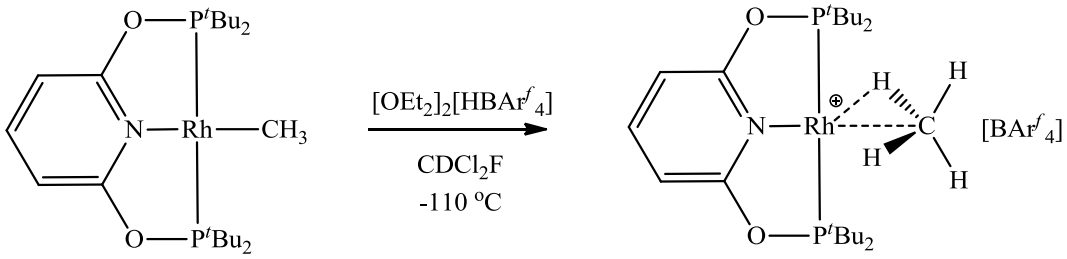

1.84 **1.85**

Scheme 1.15: *Formation of a Rh(I) σ-methane complex*

This species was characterised through a series of NMR and isotopic labelling experiments and was shown to be distinct from the Rh-CH_3 starting material and the related Ir(III)-(H)(CH_3) complex. It was also shown that the rhodium bound hydrogen atom is fluxional with a quintet observed in the ^{13}C NMR spectrum for the methane carbon atom. The σ-methane complex is only stable at low temperature, with facile extrusion of methane inevitably resulting in the formation of the $CDCl_2F$ solvated cation.[138]

Whilst a number of σ-alkane complexes have been characterised spectroscopically under specialised reaction conditions, the number of σ-alkane complexes structurally characterised by either single crystal X-ray or neutron diffraction are considerably fewer. Boyd and co-workers reported the crystal structure of an iron(II) porphyrin complex in which a heptane solvent molecule is coordinated to the iron centre. This coordination is

potentially aided by a host/guest interaction, and significant disorder in the heptane molecule prevented further analysis of the iron-alkane interaction.[139] In 2003 Meyer and co-workers reported the ability of an aryloxy substituted uranium(III) complex to coordinate alkanes, and structurally characterised the methyl*cyclo*hexane adduct.[140]

While both of the aforementioned systems feature the incorporation of a hydrocarbon solvent within the metal coordination sphere, Weller and co-workers reported an elegant alternative approach to obtain single crystals of a σ-alkane complex. Solid state hydrogenation of the cationic norbornadiene rhodium complex [(^{i}Bu$_2$PCH$_2$CH$_2$P^{i}Bu$_2$)Rh(η^2 η^2-C$_7$H$_8$)][BAr$^{f}_4$] (**1.86**) proceeds *via* sequential hydrogenation of the alkenes and before decomposition to the alkane extrusion product the corresponding norbornane σ-alkane complex (**1.87**) can be characterised (Scheme 1.16).[141]

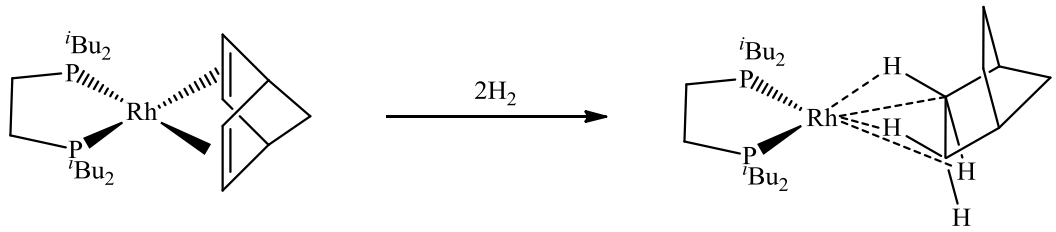

1.86 **1.87**

Scheme 1.16: *Solid state hydrogenation of **1.86** forming the σ-norbornane complex **1.87***

Although the norbornane fragment is disordered in the crystal structure the Rh-C distances observed are within the range reported for related agostic Rh-C interactions and the Rh-P distances in **1.87** are shorter than those in **1.86**, which is expected based on the respective *trans*-influences.[141] Structural characterisation of a σ-alkane complex analogous to other E-H σ-complexes highlights not only the challenges in direct C-H bond coordination processes but also the similarities in C-H···M interactions between intramolecular agostic and intermolecular σ-alkane complexes.

1.4.4 Borane (B-H) σ-Complexes

The long standing desire to use an organometallic system to selectively functionalise C-H bonds, and the inherent challenges related to this process, has seen a number of systems developed to model the C-H bond activation process (for example silanes and boranes). The isoelectronic relationship between CH_4 and BH_4^- has led to much interest in the formation of transition metal, lanthanide and actinide borohydride complexes featuring κ^1, κ^2 and κ^3 coordination modes (Figure 1.12).[142]

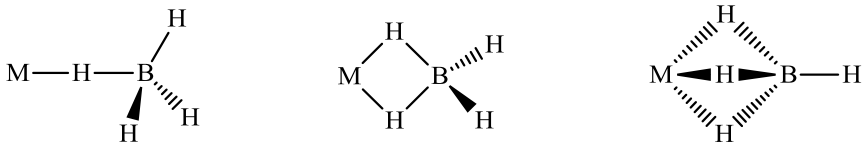

Figure 1.12: *Coordination modes of BH_4^- to a single transition metal centre*

Although isoelectronic with CH_4, the inherent negative charge possessed by the BH_4^- anion provides a significant electrostatic contribution to bonding. Consequently, the coordination chemistry of neutral boranes is seen as a better potential model for alkane coordination and has been the subject of significant interest in recent literature. Two clear classes of coordinated boranes have developed: those involving three-coordinate and four-coordinate boranes, respectively.

The formation of Lewis base adducts of BH_3 is well established, and being formally neutral, $L{\cdot}BH_3$ systems perhaps more closely resemble methane in certain bonding aspects than does the borohydride anion. Crucial in explaining the observed bonding in complexes of $L{\cdot}BH_3$ is the coordinative saturation of the boron centre, most importantly population of the vacant *p*-orbital on boron by the Lewis base (L). Consequently, the $L{\cdot}BH_3$ moiety is

unable to act as a π-acceptor (participate in back-bonding) as the B-H σ*-orbital is too high in energy to interact significantly with metal based *d*-orbitals (Figure 1.13).

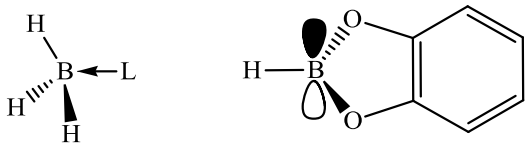

Figure 1.13: *Four- and three-coordinate boranes*

In contrast, three-coordinate boranes *e.g.* HBCat, still possess a formally vacant *p*-orbital at the boron centre, which is of suitable energy to interact with transition metal *d*-orbitals allowing for π-back-bonding.[143]

1.4.4.1 Four-Coordinate Borane σ-Complexes

The isoelectronic relationship between neutral $L{\cdot}BH_3$ adducts and methane means that they provide a model system for the study of C-H activation parameters. A number of σ-complexes of Lewis base borane adducts have been reported featuring a variety of bases. These complexes are all formed *via* the *in situ* generation of a 16-electron transition metal fragment following photolytic ejection of a CO ligand. The groups of Shimoi and Braunschweig have structurally characterised a number of σ-borane complexes of the type $(OC)_5M(\kappa^1\text{-}H_3B{\cdot}L)$ (M = Cr and L = NMe_3 **1.88**, PMe_3 **1.89**, PPh_3 **1.90** and IMe **1.91**; M = W = NMe_3 **1.92**, PMe_3 **1.93**, PPh_3 **1.94** and IMe **1.95** (Scheme 1.17).[143,144]

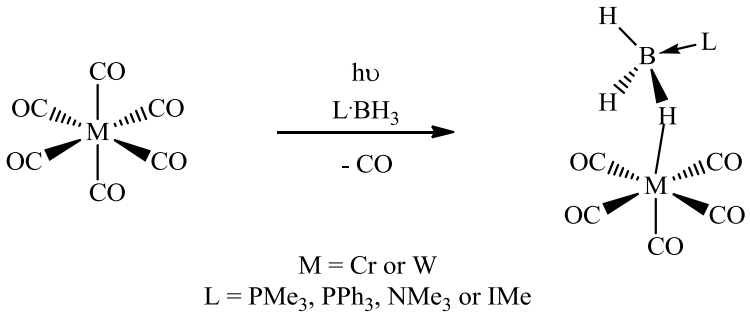

Scheme 1.17: *Formation of four-coordinate borane σ-complexes **1.88-1.95***

Structural characterisation of these κ^1-$H_3B{\cdot}L$ complexes by single crystal X-ray diffraction shows in each case that the borane exhibits a signifcantly more 'end on' binding motif than that seen in σ-silane and dihydrogen systems. This binding motif is consistent with the B-H σ-bond acting as a σ-donor with negligible π-acceptor capabilities. This distinguishes these B-H σ-complexes from the σ-complexes discussed in sections 1.4.1 and 1.4.2 in that the coordinated B-H bond shows very little activation, and the complex therefore represents minimal progression along the oxidative addition pathway. Rapid exchange of bridging and terminal B-H bonds typically results in a statistically averaged ^{1}H NMR chemical shift, between that expected for bridging M-H-B and terminal B-H bonds, and this fluxionality is unable to be frozen out even at low temperatures.

Direct bonding comparisons between $L{\cdot}BH_3$ complexes and the plethora of σ-silane complexes reported can be drawn from the complexes featuring the $[CpMn(CO)_2]$ fragment reported by the groups of both Shimoi and Braunschweig (Scheme 1.18).[144,145]

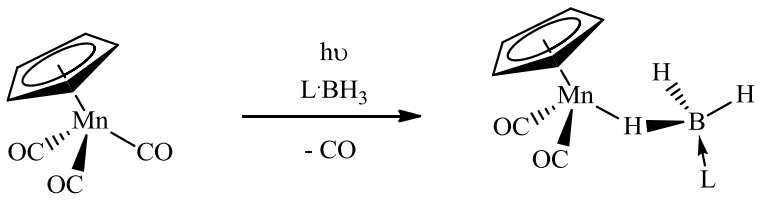

L = NMe_3 **1.96**, PMe_3 **1.97** or IMe **1.98**

Scheme 1.18: *Formation of $CpMn(CO)_2\{\kappa^1\text{-}H_3B{\cdot}L\}$*

Complexes **1.96**-**1.98** have been fully characterised, including in the solid state by single crystal X-ray diffraction. In each, the solid state structure is consistent with the coordinated B-H bond acting almost exclusively as a σ-donor with negligible π back-donation. This is demonstrated structurally by larger M-H-B angles than related M-H-Si angles, and by the orientation of the coordinated B-H bond, which deviates significantly from the close-to-horizontal orientation observed in σ-silane complexes due to back-bonding from the metal HOMO (Figure 1.14).

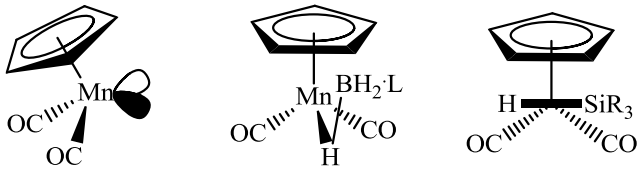

Figure 1.14: *(left) $[CpMn(CO)_2]$ HOMO, (centre) orientation of the B-H bond in $CpMn(CO)_2(\kappa^1\text{-}H_3B{\cdot}L)$, (right) orientation of the B-H bond in $CpMn(CO)_2(\kappa^1\text{-}HSiR_3)$*

This deviation attests to negligible π-contributions to the binding of the B-H bond, as the orbitals of the $[CpMn(CO)_2]$ fragment of suitable symmetry for π back-bonding are coplanar with the Cp ring. To optimise such an interaction the same orientation as that of the Si-H bond in σ-silane complexes would need to be adopted, and this is clearly not the case in **1.96**-**1.98**. As a consequence the IR stretching frequencies for the CO ligands in

1.96-**1.98** are lower than those of the $CpMn(CO)_3$ precursor, consistent with replacement of a σ-donor and good π-acceptor ligand (CO), with a σ-donor only ligand.[145] Negligible contributions from back-bonding also result in less stable complexes, as the σ-donation from the B-H bond is the only stabilising interaction and complex stability is essentially determined by the energy match between the B-H σ-bond and the LUMO of the transition metal fragment. The stronger the σ-donating properties of the Lewis base, L, the higher in energy the B-H σ-bond, and closer to that of the transition metal LUMO. The energy of the transition metal LUMO can be reduced, to more closely match that of the B-H σ-bond, through the use of ligands with electron withdrawing properties. As a result cationic metal centres have been investigated as these are likely to form more stable complexes, due to the lower energy of the LUMO.

In 2006 Shimoi and co-workers carried out a study using the electron rich, ruthenium precursors $CpRu(PMe_3)_2Cl$ (**1.99**) and $Cp^*Ru(PMe_3)_2Cl$ (**1.100**) fragments as sources of cationic transition metal centres *via* halide abstraction, to coordinate boranes of the type $Me_3E{\cdot}BH_3$ (E = P or N) (Scheme 1.19).

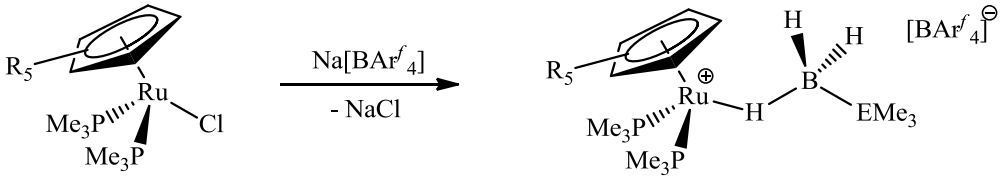

R = H (**1.99**)
R = Me (**1.100**)

R = H, E = N (**1.101**) or P (**1.102**);
R = Me, E = N (**1.103**) or P (**1.104**)

Scheme 1.19: *Formation of κ^1-$H_3B{\cdot}L$ complexes **1.101**-**1.104***

Complexes **1.101**-**1.104** show a more elongated B-H bond than the aforementioned neutral complexes, providing structural evidence for a stronger interaction, slightly more π back-bonding and a more stable complex.[146]

The coordination of amine boranes has received much attention due to their relevance to the catalytic dehydrocoupling of ammonia borane and related model systems. Ammonia borane is considered a potential hydrogen storage material due to its high weight percentage of hydrogen and the products of dehydrocoupling, BN based polymers have materials applications. These topics have been extensively reviewed in the literature.[147-149] Interest in transition metal catalysed oligo/polymerisation of ammonia/amine boranes has led to the characterisation of a number of borane complexes thought to be likely intermediates in this catalytic process. Weller and co-workers have investigated the dehydrogenation ability of the cationic rhodium(I) species $[(^{i}Bu_3P)_2Rh][BAr^{f}_4]$ (**1.105**) reporting a number of $H_3B{\cdot}NRMe_2$ (R = H or Me) κ^2-complexes, as well as the κ^2-complex $[(^{i}Bu_3P)_2Rh(\kappa^2\text{-}H_3B{\cdot}NMe_2BH_2{\cdot}NHMe_2)]^+$ (**1.106**) and the rhodium(III) analogue $[(^{i}Bu_3P)_2(H)_2Rh(\kappa^2\text{-}H_3B{\cdot}NMe_2BH_2{\cdot}NHMe_2)]^+$ (**1.107**).[150,151] The effect of the ancillary phosphine ligand on amine borane coordination was investigated through the preparation of the rhodium(I) species $[(^{i}Pr_3P)_2Rh]^+$ (**1.108**) and the corresponding rhodium(III) analogue $[(^{i}Pr_3P)_2Rh(H)_2]^+$ (**1.109**), and their subsequent reactivity with $H_3B{\cdot}NMe_3$ (Scheme 1.20).[152]

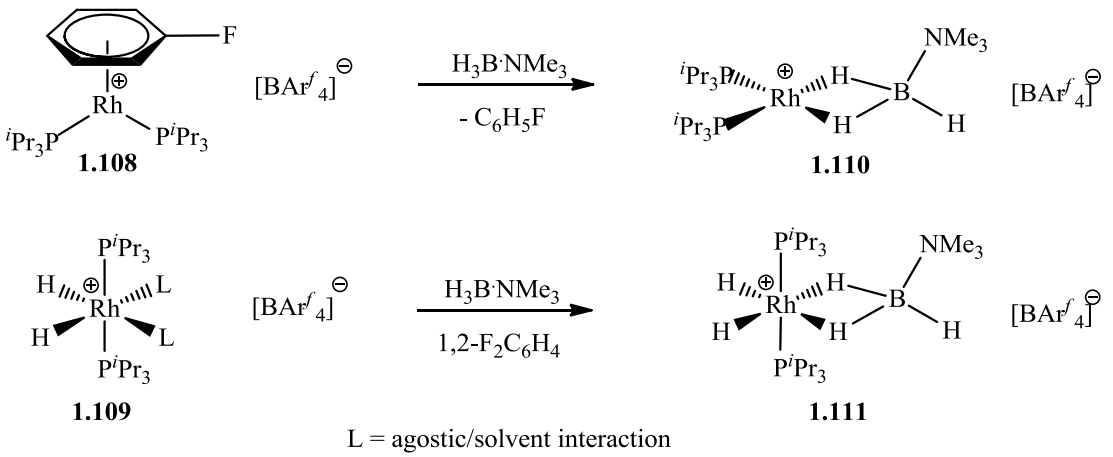

Scheme 1.20: *(top) Displacement of C_6H_5F by $H_3B{\cdot}NMe_3$ to form $[(^{i}Pr_3P)_2Rh\{\kappa^2\text{-}H_3B{\cdot}NMe_3\}][BAr^{f}_4]$ (**1.110**); (bottom) formation of $[(^{i}Pr_3P)_2Rh(H)_2\{\kappa^2\text{-}H_3B{\cdot}NMe_3\}][BAr^{f}_4]$ (**1.111**)*

Interestingly, the related reaction between [(^{i}Bu$_3$P)$_2$Rh][BAr$^{f}_4$] (**1.105**) and two equivalents of $H_3B{\cdot}NMe_2H$ results in initial formation of [(^{i}Bu$_3$P)$_2$Rh(κ^2-$H_3B{\cdot}NMe_2H$)][BAr$^{f}_4$] (**1.112**), which reacts further to yield the dihydride rhodium(III) species [(H)$_2$(^{i}Bu$_3$P)$_2$Rh{κ^2-$H_3B{\cdot}NMe_2H$}][BAr$^{f}_4$] (**1.113**).[150] This highlights the effects of the changes in ligand and substrate and the challenges presented in elucidating the mechanism of catalytic dehydrocoupling, for a given system.

1.4.4.2 Three Coordinate Borane σ-Complexes

Although not isoelectronic with methane, but related to Lewis base stabilised borane complexes, three-coordinate boranes and complexes thereof have shown increasing presence in the literature. With atom efficiency a growing focus for industrial processes in order to reduce both costs and emissions, catalytic processes are increasingly desirable. The importance of hydroboration in the synthesis of functionalised organic molecules has driven the emergence of organometallic complexes to perform this process catalytically. In transition metal catalysed hydroboration oxidative addition of the B-H bond must occur and this is a potentially rate limiting step within the catalytic cycle. It is through the mechanistic investigations of Hartwig and co-workers into their Cp_2TiMe_2 (**1.114**) catalyst for hydroboration that the first three-coordinate borane σ-complex was characterised.[153,154] Three-coordinate borane σ-complexes have played a fundamental role in developing understanding of the B-H oxidative addition process, which is crucial to the understanding and development of catalytic processes.

Hartwig and co-workers characterised the first *bis*-borane complex as the product of the reaction between **1.114** and three equivalents of HBCat or HBCat' (Cat = $O_2C_6H_4$, Cat' = $O_2C_6H_3$-4-Me) yielding the corresponding *bis*-borane complex $Cp_2Ti(\kappa^1$-HBCat$)_2$ (**1.115**), methane, and MeBCat (Scheme 1.21).

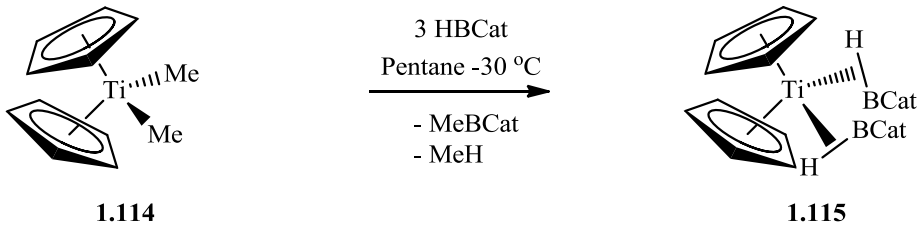

1.114 **1.115**

Scheme 1.21: *Reaction between **1.114** and three equivalents of HBCat forming **1.115***

These σ-borane complexes proved to be particularly thermally sensitive and decompose in many solvents, making full spectroscopic characterisation difficult. However, characterisation by NMR and infra-red spectroscopy indicated the presence of both Ti···B and Ti···H interactions, as well as incomplete cleavage of the B-H bond. The solid state structure showed the boron atom to be in a plane also containing both catechol oxygen atoms and the titanium centre, with the hydride sitting above this plane.[153] The related *mono*-borane complex $Cp_2Ti(PMe_3)(\kappa^1$-HBCat) (**1.116**) was prepared through a redistribution reaction between $Cp_2Ti(PMe_3)_2$ (**1.117**) and **1.115**; the solid state structure was determined of the fluorinated analogue $Cp_2Ti(PMe_3)(\kappa^1$-HBCat-3-F) (**1.116a**). The B-H bond in **1.116a** appears to be further along the oxidative addition pathway in comparison to the *bis*-borane analogue **1.115**, as reflected in the relative B-H and Ti-H bond lengths (*cf.* **1.116a** Ti-H 1.61(5) B-H 1.35(5); **1.115** Ti-H 1.74(4) B-H 1.25(3) Å). The greater extent of oxidative addition can be rationalised by the phosphine substituent giving rise to a more electron rich titanium centre, as well as slightly enhanced electrophilicity of the borane due to fluoride incorporation.[155]

With the formation of σ-borane complexes of three-coordinate boranes established, Hartwig and co-workers investigated the formation of complexes that would provide suitable comparison to the classical silane σ-complexes present in the literature.[131,156] The characterisation of a range of σ-complexes featuring the $[Cp'Mn(CO)_2]$ fragment enable

comparison to silane complexes, but also investigation into the effect of the borane ligand on the progression towards oxidative addition. The synthesis, properties and reactivity of a number of complexes were subsequently reported, including $Cp'Mn(CO)_2(\kappa^1\text{-HBCat})$ (**1.118**), $Cp'Mn(CO)_2(\kappa^1\text{-HBPin})$ (**1.119**) and $Cp'Mn(CO)_2(\kappa^1\text{-HBCy}_2)$ (**1.120**) (Figure 1.15).[156]

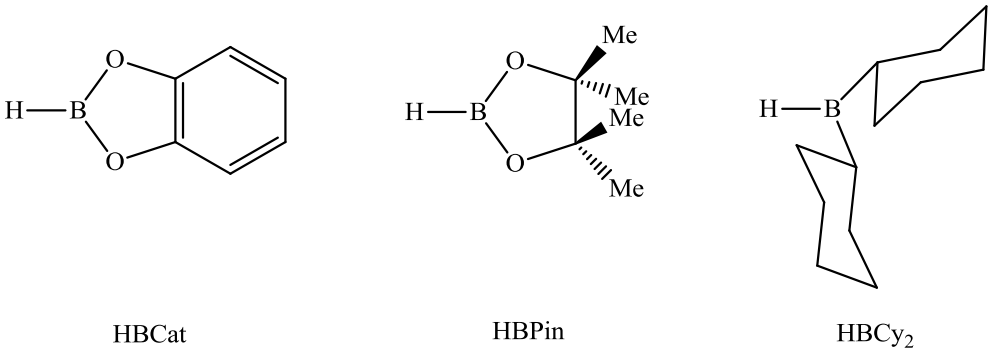

Figure 1.15: *Three-coordinate boranes (left) HBCat, (centre) HBPin and (right) $HBCy_2$*

The σ-complexes **1.118** and **1.119** can be formed through the photolytic reaction of the borane with $Cp'Mn(CO)_3$ with loss of CO. However, substantially increased yields are obtained by using the salt metathesis reaction between $K[Cp'Mn(CO)_2H]$ and the corresponding chloroborane. Photolytic reaction of $Cp'Mn(CO)_3$ with $HBCy_2$ did not proceed due to the dimeric nature of the parent borane (Scheme 1.22).

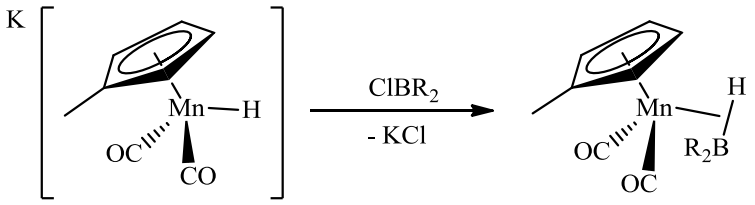

Scheme 1.22: *Salt metathesis formation of σ-borane complexes*

Comparison of the solid state structures of **1.118-1.120** shows that the centre of the B-H bond is equidistant from the manganese centre in all three complexes, indicating that the oxidative addition process is reflected in a 'pivoting' around this point which thereby determines the B-Mn and Mn-H distances. This pivoting is a function of the ancillary substituents of the borane (Figure 1.16).

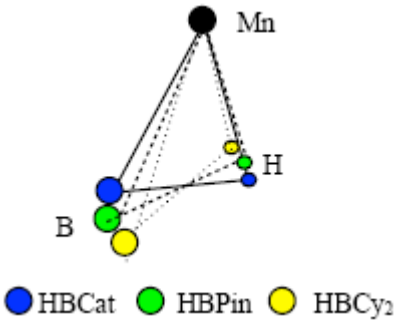

Figure 1.16: *Overlaid positions of Mn, B and H atoms from the crystal structures of* ***1.118-1.120***

The mode of coordination for the different boranes shown in Figure 1.16 shows that HBCat has the most 'side on' binding, bearing closest resemblance to that of dihydrogen, whereas $HBCy_2$ is bound significantly more 'end on' and more closely resembles the binding observed in Lewis base adducts of boranes $L{\cdot}BH_3$. The HBPin complex lies between those of HBCat and $HBCy_2$. The structural data shows that the π-acceptor capability of the boranes follows the order HBCat > HBPin > $HBCy_2$, and that the reverse trend exists for the σ-donating capability.[156] These trends can be rationalised on the basis of the electron richness of the ancillary ligand on boron. This determines how hydridic the B-H bond will be, and therefore the σ-donor strength of the borane. The most electron rich borane $HBCy_2$ binds significantly more 'end on' than the more electron-poor alkoxy and aryloxy boranes. As seen for other E-H σ-complexes, the incorporation of more electron withdrawing

substituents, *e.g.* alkoxy or aryloxy groups, makes the LUMO of the borane ligand a better energy match to the HOMO of the transition metal fragment, thereby, enhancing π back-bonding. Consequently, a shorter Mn-B interaction is observed for the catechol (aryloxy) borane than pinacol (alkoxy) borane, and di*cyclo*hexylborane has the longest Mn-B interaction.

The differences in σ-donor and π-acceptor capabilities are reported by the IR stretching frequencies of the CO ancillary ligands, giving insight into how electron rich the manganese centre is in each of the complexes. The experimentally observed stretching frequencies are consistent with the rationale for the solid state structures, with the value for the $HBCy_2$ complex (**1.120**) being lower than both HBPin (**1.119**) and HBCat (**1.118**) complexes (**1.120** 1967, 1901, **1.119** 1981, 1924 and **1.118** 1995, 1937 cm^{-1}), reflecting a more electron rich metal fragment resulting from a combination of stronger σ-donation and weaker π-acceptor properties for $HBCy_2$.[153]

Whilst significant differences between σ-silane and three-coordinate σ-borane complexes exist, most notably the formally vacant *p*-orbital on boron, similarities between the oxidative addition processes can be identified. The 'pivoting' of the E-H fragment (E = B or Si) in $[Cp'Mn(CO)_2]$ complexes to determine the extent of oxidative addition highlights these similarities, and can be used to develop a general understanding and insight into the fundamental principles controlling oxidative addition and reductive elimination processes of E-H bonds.

The coordination of three-coordinate boranes through two B-H bonds has been reported more recently with the first example reported by Sabo-Etienne and co-workers. This study focused on the reaction of $Ru(H_2)_2(H)_2(PCy_3)_2$ (**1.72**) with H_2BMes resulting in the displacement of dihydrogen to form the κ^2-complex $(Cy_3P)_2(H)_2Ru\{\kappa^2\text{-}H_2BMes\}$ (**1.121**) (Scheme 1.23).[157]

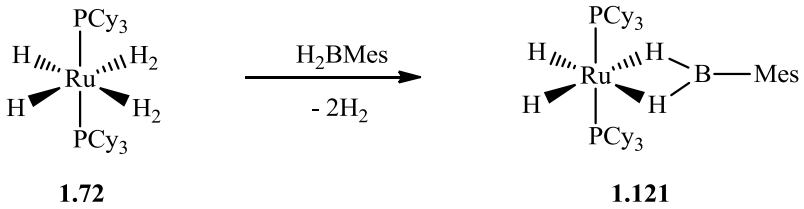

1.72 **1.121**

Scheme 1.23: *Displacement of dihydrogen from **1.72** by H_2BMes*

In the solid state the Ru-B distance of **1.121** is exceptionally short, due to the geminal B-H coordination mode. Theoretical calculations indicate population of the vacant *p*-orbital on boron through π back-donation from ruthenium in a manner which is not possible in κ^1-complexes.[157] Stradiotto and co-workers demonstrated the same coordination mode for H_2BMes using the 16-electron precursor Cp*Ru(Cl)(P^iPr_3) (**1.122**) and subsequent halide abstraction (Scheme 1.24).[158]

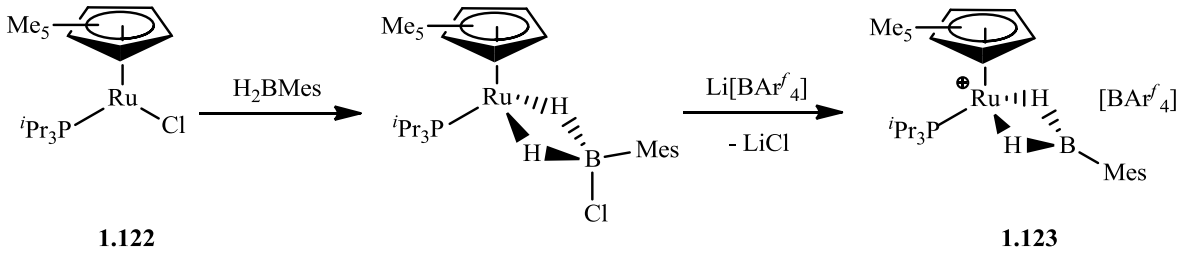

1.122 **1.123**

Scheme 1.24: *Formation of [Cp*Ru(P^iPr_3){κ^2-H_2BMes}][BAr^f_4] (**1.123**)*

Through halide abstraction Stradiotto and co-workers were able to isolate a cationic system featuring κ^2-coordination of H_2BMes resulting in the 18-electron ruthenium complex **1.123**. The Ru···B···C angle is almost linear and theoretical calculations also show population of the formally vacant *p*-orbital on boron as a result of π back-donation from ruthenium.[158] With much interest in the catalytic dehydrogenation of ammonia/amine boranes the

κ^2-binding motif represents an interesting potential intermediate in the catalytic cycle and the coordination chemistry of aminoboranes has subsequently received much attention.

1.4.4.3 Aminoborane σ-Complexes

The intrinsic electronegativity difference between boron and nitrogen results in B-H hydrogen atoms being hydridic, and N-H hydrogen atoms being protic. Molecules containing both protic and hydridic hydrogen atoms have received much attention with a view to applying such compounds to hydrogen storage.[148,149,159] Consequently, there has been much interest in developing catalysts for the efficient release of hydrogen from ammonia/amine boranes. The investigation of transition metal systems has featured highly in the literature however, a number of main group systems based on the Group 2, 3 and 13 metals have also been investigated by the groups of, Harder, Hill and Wright respectively.[160-165]

The first product of dehydrogenation of ammonia/amine boranes is an aminoborane of the type H_2BNRR'. Interest in these dehydrogenation processes results in part from the realisation that such compounds represent monomeric building blocks from which an interesting class of inorganic polymer can be formed.[166,167] Thus, for example, Manners and co-workers have reported the polymerisation of methylamineborane ($H_3B{\cdot}NMeH_2$) to give high molecular weight polyaminoboranes $[H_2BNMeH]_n$ by the use of ruthenium, rhodium and palladium catalysts.[168,169] Such compounds represent BN analogues of polypropylene and are thought to be formed by initial dehydrogenation of the amine borane $H_3B{\cdot}NMeH_2$ to give the aminoborane H_2BNMeH which then polymerises at the metal. The interaction of aminoboranes with catalytically relevant transition metal centres therefore represents an area of research relevant to both hydrogen storage chemistry, and to inorganic polymer formation.

A monomeric aminoborane is formally isoelectronic with an alkene, and therefore has the potential not only to bind through the B-H bonds, but also in an analogous manner to an alkene through the B-N π-system. Sabo-Etienne and co-workers used the $Ru(H_2)_2(H)_2(PCy_3)_2$ fragment to trap a number of aminoboranes resulting from dehydrogenation of the parent amine boranes as κ^2-complexes.[170] Most notably the solid state structure of $(Cy_3P)_2(H)_2Ru(\kappa^2\text{-}H_2BNH_2)$ (**1.124**) was determined and showed the aminoborane to bind through both B-H bonds. Calculations to determine the difference in energy between the *bis*(σ-BH) coordination and the classical 'side on' binding showed the *bis*(σ-BH) motif to be at least 14 kcal mol^{-1} more stable than binding through the B-N π-system.[170]

Aldridge and co-workers also observed the *bis*(σ-BH) binding motif for a number of aminoborane complexes involving carbene-stabilised rhodium and iridium cations (Scheme 1.25).[171-173]

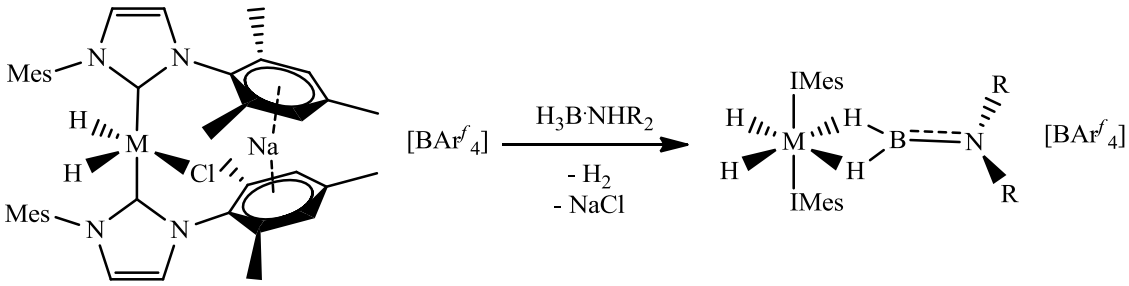

1.125

M = Rh and R = ^{i}Pr (**1.126**) or Cy (**1.127**)
M = Ir and R = ^{i}Pr (**1.128**) or Cy (**1.129**)

Scheme 1.25: *Dehydrogenation of $H_3B{\cdot}NHR_2$ and subsequent coordination of H_2BNR_2 at bis-carbene Rh and Ir centres*

Addition of amineborane triggers NaCl elimination from (**1.125**) and dehydrogenation of the amineborane to the corresponding (monomeric) aminoborane which is trapped as the

κ^2-complex allowing the *bis*(σ-BH) coordination mode also to be identified in these complexes.[171-173]

The groups of Weller and Sabo-Etienne have prepared the related and isoelectronic aminoborane complexes $Ru(H)_2(PCy_3)_2(\kappa^2\text{-}H_2BN^iPr_2)$ (**1.130**) and the cationic $[M(H)_2(PCy_3)_2\{\kappa^2\text{-}H_2BN^iPr_2\}]^+$ (M = Rh **1.131** or Ir **1.132**).[174] These complexes provide the ability to study the impact of the metal fragment on aminoborane complex formation. In all of these complexes the *bis*(σ-BH) coordination mode is observed. Furthermore, the extent of π back-bonding from metal based *d*-orbitals into the *p*-orbital on boron, which is part of the B-N π*-orbital that corresponds to the LUMO of the aminoborane ligand can also be investigated. The formally vacant *p*-orbital on boron is stabilised in aminoboranes by donation from the nitrogen lone pair, providing a higher energy B-N π*-orbital to accept electron density from the transition metal (Figure 1.17).

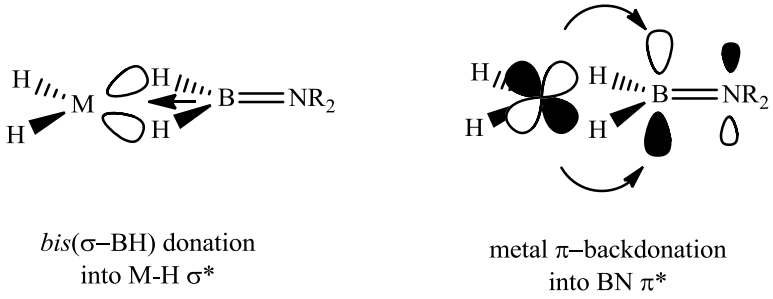

Figure 1.17: *σ- and π-bonding contributions in κ^2-aminoborane transition metal complexes*

The results of NBO analysis indicate the extent of π-back-donation into the B-N π*-orbital decreases in the following order Ru > Ir^+ > Rh^+. Greatest interaction is observed with the neutral Ru complex **1.130**, and this is rationalised on the basis that lower energy orbitals for the cationic fragments result in less effective overlap with the B-N π*-orbital. The greater radial extension of the 5*d*-orbitals in Ir^+ partially compensate for this and result in greater π back-donation than in Rh^+.[174]

The formation of the κ^2-complexes of aminoboranes is well precedented from the aforementioned literature, and these complexes have been formed through displacement of two labile dihydrogen ligands,[174] or through the generation and trapping of a 14-electron transition metal centre,[172,173] potentially favouring the κ^2-coordination mode which acts as a 4-electron donor to electronically satisfy the transition metal. Investigation of the 2-electron donor preference, *i.e.* either mono-BH σ-coordination or through the BN π-system, has been carried out by Aldridge and co-workers using the 16-electron fragment $[CpRu(PR_3)_2]^+$ (PR_3 = PPh_3 **1.133** or ½ dcpe **1.134**).[175] The resulting complexes of H_2BNCy_2 show the aminoborane acting as a 2-electron donor through the coordination of a single B-H σ-bond (Scheme 1.26).

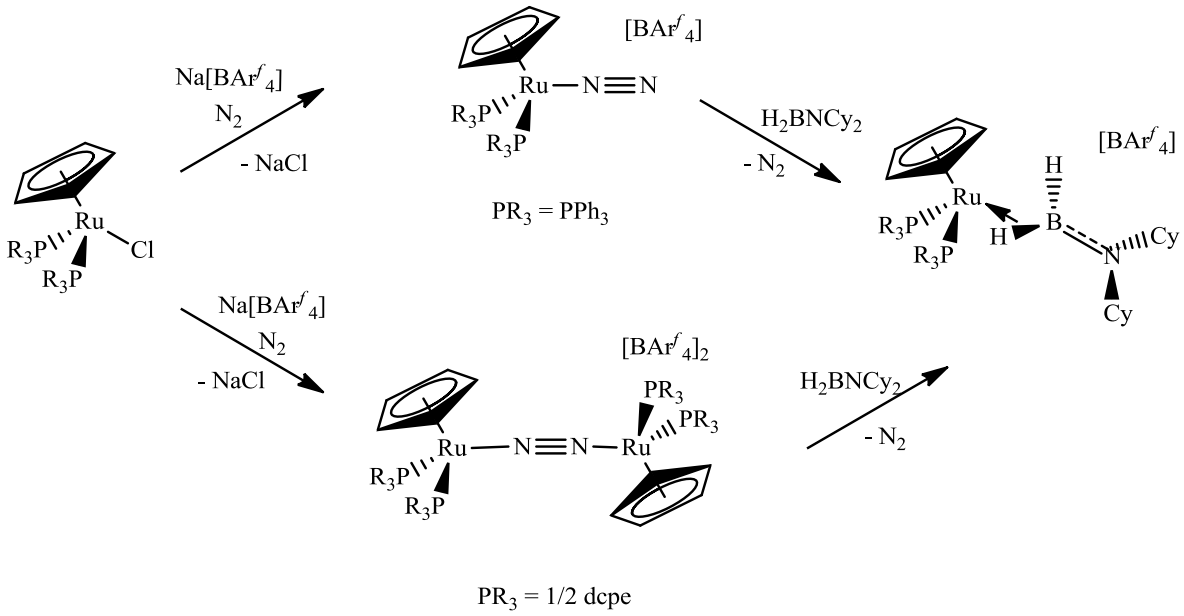

Scheme 1.26: *Formation of $[CpRu(PR_3)_2\{\kappa^1\text{-}H_2BNCy_2\}][BAr^f_4]$*

Whilst a number of fluxional processes exist in both $[CpRu(PPh_3)_2\{\kappa^1\text{-}H_2BNCy_2\}][BAr^f_4]$ (**1.135**) and $[CpRu(dcpe)_2\{\kappa^1\text{-}H_2BNCy_2\}][BAr^f_4]$ (**1.136**), it is clear that π back-donation provides a significant contribution to bonding as the more electron rich ruthenium complex

1.136 is notably more stable. This is also represented in the calculated binding energies of the aminoborane to both fragments, with **1.136** having a ligand association energy of -26 kcal mol^{-1} (*cf.* -15.2 kcal mol^{-1} for **1.135**).[175]

σ-Borane complexes represent a diverse field which has seen much interest for a number of reasons, from modelling alkane (most notably methane) activation, to potential hydrogen storage applications, as well as acting as potential intermediates in the formation of inorganic polymers. It is perhaps slightly surprising that the heavier congeners of group 13 have seen significantly less investigation into the formation of σ-complexes.

1.4.5 Alane (Al-H) σ-Complexes

In contrast to the large amount of literature pertaining to the coordination of the B-H bond to a transition metal centre, reports of Al-H bond coordination are comparatively sparse. A number of complexes featuring the coordination of the $[AlH_4]^-$ anion to early transition metal centres have been reported,[176-181] however, as in the case of the $[BH_4]^-$ anion complexes, the electrostatic contribution to bonding is significant. Neutral complexes featuring unsupported Al-H bond coordination, similar to those previously discussed for the B-H bond are notably few, and have seen sporadic reports in the literature.

Early work from Lobkovsky, Bulychev and co-workers investigated the effect of the Lewis base on the structural aggregation of complexes of the type $(Cp_2YCl)_2{\cdot}H_3Al{\cdot}L$ with the emphasis on reducing aggregation.[182] Use of diethyl ether yields the polymeric system $[(Cp_2YCl)_2H_3Al{\cdot}OEt_2]_n$ (**1.137**) but the stronger σ-donor NEt_3 yields the dimeric complex $[(Cp_2YCl)_2{\cdot}H_3Al{\cdot}NEt_3]_2$ (**1.138**) (Figure 1.18).

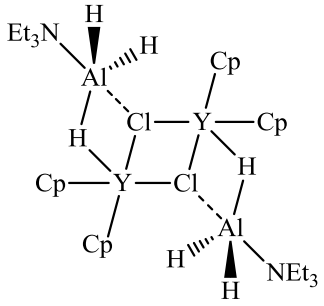

Figure 1.18: *Structure of the dimeric **1.138***

Structural characterisation of **1.138** reveals secondary interactions between the bridging chloride ligands and the aluminium centre, which provide an additional tether to stabilise the coordination of the Al-H bond to the yttrium centre.[182] The use of the more strongly σ-donating trialkyl amine reduced aggregation forming a dimeric species, rather than an oligo/polymeric species, thereby showing that molecular systems are accessible. Pörschke and co-workers used the strongly σ-donating quinuclidine adduct of dimethylalane (quin·$AlHMe_2$) to characterise the first unsupported Al-H σ-complex, utilising the nickel(0) metal centre in Ni(cdt) (**1.139**) to form {quin·$AlMe_2H$}Ni(cdt) (**1.140**) (Scheme 1.27).[183]

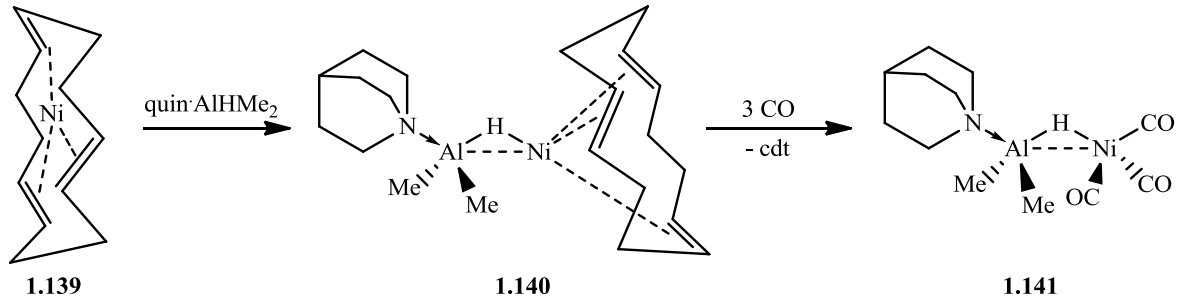

Scheme 1.27: *Formation of **1.140** and subsequent reaction with three equivalents of CO*

Remarkably, the Al-H-Ni interaction remains intact upon exposure of **1.140** to three equivalents of CO, resulting in the displacement of the cdt ligand affording {quin·$AlMe_2H$}$Ni(CO)_3$ (**1.141**).[183] The stability of the Al-H-Ni interaction, even in the

presence of CO, is attributable to the electron donating properties of quinuclidine and the methyl substituents at aluminium. These reduce the Lewis acidity and increase the σ-donor strength of the Al-H bond.

Through the investigation into metallocene-type Ziegler-Natta catalyst activation by Lewis acid activators, Arndt and co-workers have characterised Al-H σ-complexes that also feature a 'tether' which provides additional stability to the Al-H-M interaction (Figure 1.19).[184,185]

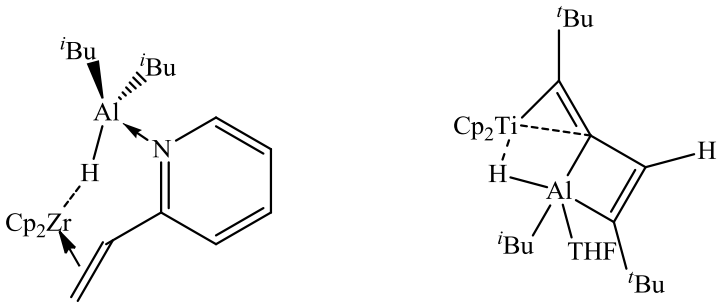

1.142 **1.143**

Figure 1.19: *Alane complexes featuring additional tethers*

The vinylpyridine linkage in **1.142** acts as a bridge between the $^{i}Bu_2AlH$ and zirconocene units tethering them together and providing stability in addition to the Al-H-Zr interaction.[185] The same can be said for **1.143** as the coordinated Al-H bond represents an intramolecular interaction.[184] Consequently, objective comparison of the Al-H-M bonding with classical σ-complexes is not possible, as the tether is likely to dominate both the geometry and bonding contribution within the complex.

An alternative method for the formation of Al-H σ-complexes is through C-H bond activation by transition metal aluminium(I) complexes forming an aluminium(III) complex, as a result of C-H addition across the M-Al bond. It is through the activation of benzene in

this manner that Fischer and co-workers characterised the nickel complex $(Cp^*Al)_3Ni\{HAlPh(\eta^2\text{-}C_5Me_5)\}$ (**1.144**) (Scheme 1.28).[186]

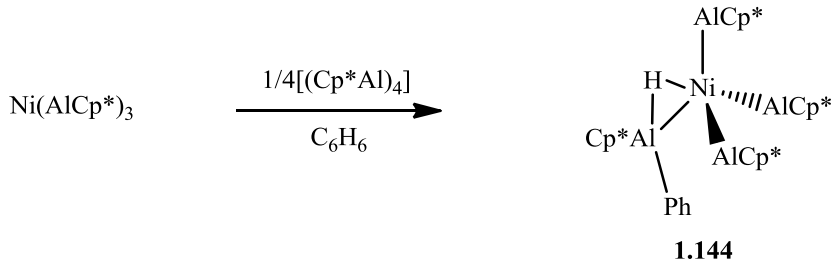

Scheme 1.28: *Benzene activation by $Ni(AlCp^*)_3$ forming **1.144***

The solid state structure of **1.144** shows that the Ni-Al bond distances reflect the oxidation state of the aluminium centre, and the complex can be considered a σ-complex featuring coordination of $(\eta^2\text{-}C_5Me_5)(Ph)AlH$ to $(Cp^*Al)_3Ni$ through the Al-H σ-bond. The activation of benzene is presumed to go through a low coordinate nickel complex $[Ni(AlCp^*)_n]$ ($n < 4$), followed by a subsequent rearrangement to form **1.144**.[186] The same group subsequently reported the formation of iron containing σ-alane complexes, again resulting from coordination of the Cp*Al moiety. It is thought that a low coordinate iron species $[Fe(AlCp^*)_n]$ ($n < 5$) is responsible for the intramolecular C-H activation which occurs in the reaction between $(\eta^6\text{-toluene})Fe(\eta^4\text{-1,3-butadiene})$ (**1.145**) and AlCp* resulting in the formation of two C-H activated isomers (**1.146** and **1.147**) (Scheme 1.29).[187]

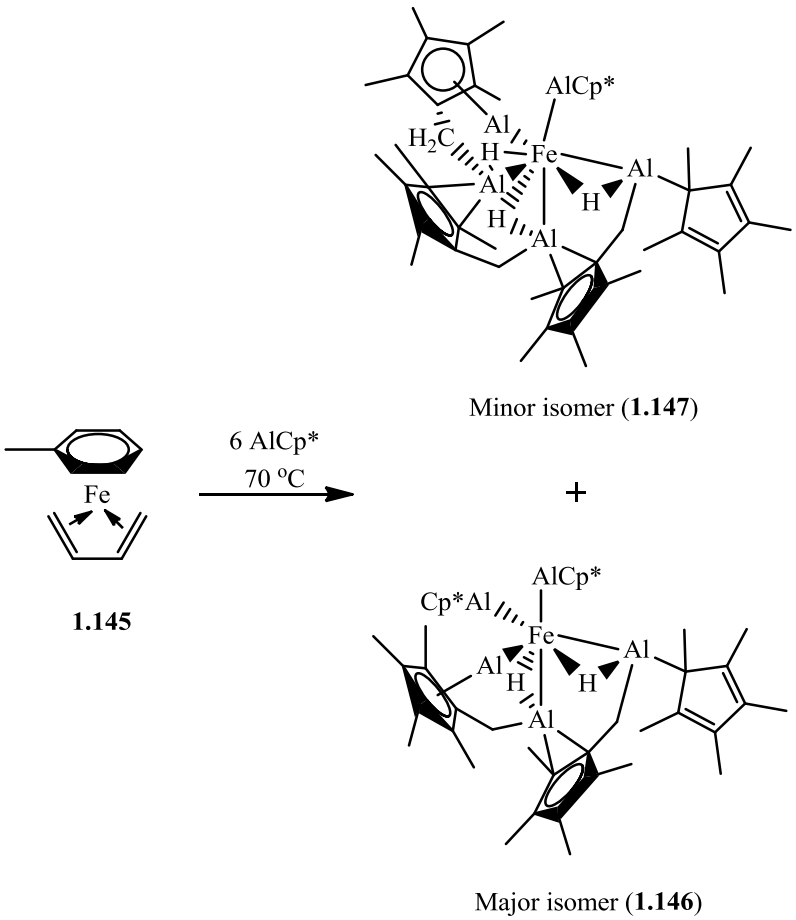

Scheme 1.29: *Reaction between **1.145** and AlCp**

The Cp* methyl groups are C-H activated resulting in the formation of aluminium(III) centres which have a hydride coordinated to the iron forming a σ-complex. The Fe-Al bond distances correlate with the aluminium oxidation state, with the Fe-Al^{III} bond distances being roughly 0.1 Å longer than Fe-Al^{I} linkages, reflecting the greater coordination number at aluminium and the differing electronic situation. The ruthenium analogue of the major isomer was also identified and structurally characterised.[187]

Whilst a number of M-H-Al interactions have been observed, unsupported M-H-Al interactions remain strikingly rare, particularly given the abundance of related B-H and Si-H σ-complexes. It is also noteworthy that despite reports of transition metal dopants catalysing dihydrogen cycling from aluminium hydrides,[188,189] studies of the reactivity

between transition metal aluminium complexes and dihydrogen, or transition metal hydrides are surprisingly few.

1.4.6 Gallane (Ga-H) σ-Complexes

Given the scarcity of σ-alane complexes, it is perhaps not surprising that the number of σ-gallane complexes is fewer still. This reflects the difference in reactivity and stability of Al-H and Ga-H bonds. Although very sensitive towards moisture, the Al-H bond is thermally robust in comparison to its gallium counterpart. Whilst $Me_3N{\cdot}AlH_3$ is stable at room temperature and can be purified through vacuum sublimation at slightly elevated temperatures (*ca.* 40 °C),[190] $Me_3N{\cdot}GaH_3$ begins to decompose above -30 °C and is best stored under vacuum at -78 °C.[191,192] Handling of free gallane itself requires specialist grease free glassware as well as low temperature storage under vacuum.[193] The extreme sensitivity of gallanes represents a significant challenge in the synthesis of σ-gallane complexes.

In 1991 the thermally robust quinuclidine adduct of gallane was reported and the following year the first σ-gallane complex was reported in the literature.[194,195] The σ-gallane complex of $[W(CO)_5]$ was formed through either direct photolysis of $W(CO)_6$ in the presence of $quin{\cdot}GaH_3$ or by the thermal displacement of THF from $W(CO)_5(THF)$ (Scheme 1.30).

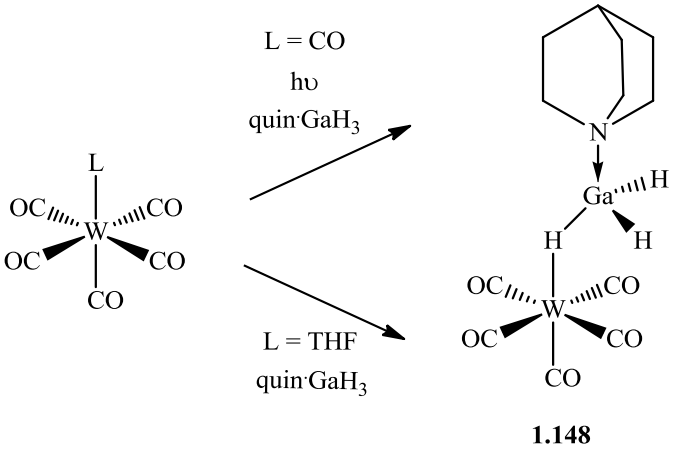

1.148

Scheme 1.30: *Routes to the formation of σ-gallane complexes*

Although structurally characterised, $(CO)_5W(\kappa^1\text{-}H_3Ga\cdot quin)$ (**1.148**) decomposes slowly at room temperature and more quickly upon heating to 70 °C.[195] More recently, the related complex $Cp^*Mn(CO)_2(\kappa^1\text{-}H_3Ga\cdot quin)$ (**1.149**) was reported, allowing geometrical parameters to be compared to classical silane and borane complexes.[196] In contrast to the complexes of the type $CpMn(CO)_2(\kappa^1\text{-}H_3B\cdot L)$ the Ga-H bond is bound significantly more 'side-on' and the metal-ligand interaction appears therefore to feature a greater contribution from π back-donation than that observed in the related $L\cdot BH_3$ complexes **1.96**-**1.98**. This is also implied from the comparative Mn-B and Mn-Ga distances, which in the case of gallium is within the range of that reported for Mn-Ga single bonds. It seems the gallane complex is further along the oxidative addition pathway than an analogous borane complex.

The thermal displacement of THF from $W(CO)_5(THF)$ by half an equivalent of $quin\cdot GaH_3$ results in the formation of the bridged complex $[(CO)_5W]_2(H_3Ga\cdot quin)$ (**1.150**) featuring κ^1-coordination of the $quin\cdot GaH_3$ to two $[W(CO)_5]$ fragments. Furthermore, **1.150** goes on to eliminate hydrogen when dissolved in THF to form a formal tungsten gallium double bond to one of the tungsten moieties (Scheme 1.31).[196]

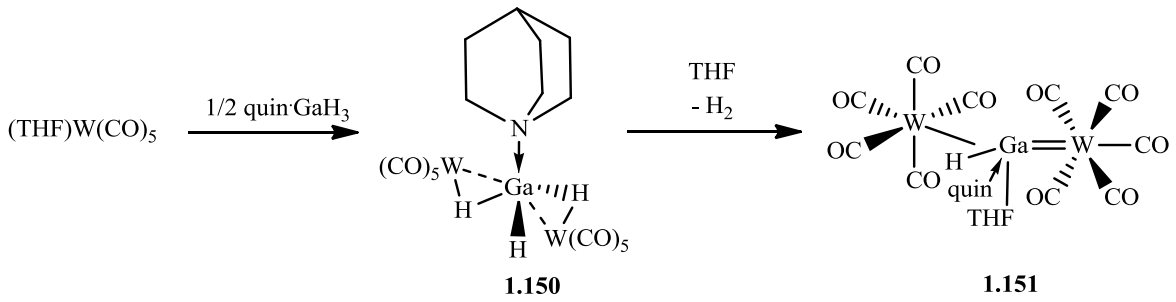

1.150 **1.151**

Scheme 1.31: *Formation and reactivity of a bis-gallane σ-complex*

The elimination of hydrogen results in a hydrogallylene complex in which the Ga-H bond is coordinated to a [$W(CO)_5$] fragment and the gallylene is stabilised by quinuclidine and THF.[196] There are few reports of spontaneous hydrogen elimination from borane, silane or alane σ-complexes and is further evidence of the potential challenges encountered when working with heavier main group element hydrides.[197] With only these preliminary reports of σ-gallane complexes available this remains an area ripe for further research. With the +1 oxidation state more readily accessible for gallium, the potential for novel and interesting chemistry initiated by the interaction of gallane complexes with transition metal complexes is an attractive combination of main group and transition metal chemistry.

1.5 Research Proposal

The ability of frustrated Lewis pair (FLP) systems to heterolytically cleave dihydrogen under mild conditions has revolutionised the scope of complexes used for small molecule activation. With greater understanding of how to identify, characterise and utilise such systems, the number of FLPs reported in the literature is rapidly increasing. Although FLPs have been shown to act as hydrogenation catalysts in their own right, the potential for cooperation between a main group FLP system and a transition metal catalyst represents an

attractive synergic approach to the incorporation of small molecule activation into transition metal mediated catalysis.

With a number of neutral aluminium complexes reported in the literature, and the successful formation of related cationic terminal borylene complexes, a highly Lewis acidic three-coordinate cationic aluminium-transition metal complex (**a**) (Figure 1.20) is an interesting synthetic target. The fundamental bonding within such a species (in particular the potential for multiple bond character in the transition metal-aluminium bond), and reactivity comparisons with existing borylene and silylene systems are also of interest.

Such a system, if sterically shrouded, may also provide a suitable Lewis acid for incorporation into a FLP (featuring a suitably sterically demanding basic component) which has potential in facilitating catalytic small molecule reduction as shown in Figure 1.20.

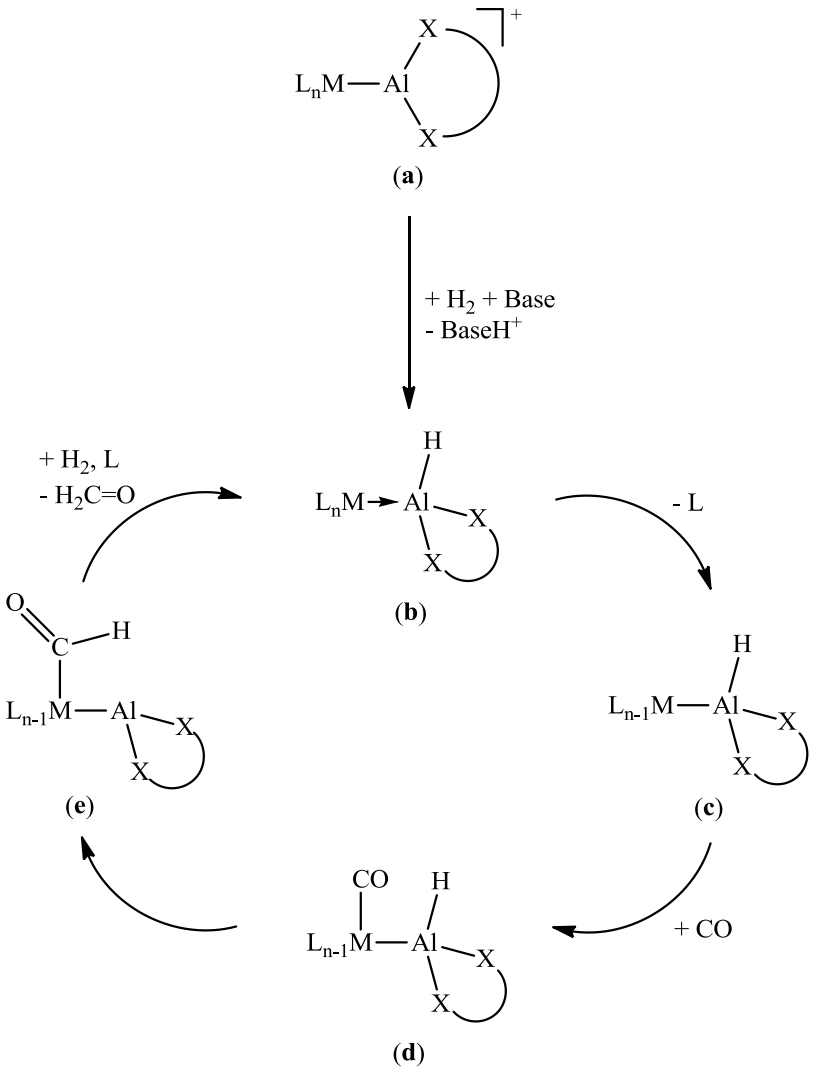

Figure 1.20: *Idealised catalytic CO reduction via FLP hydrogen activation*

FLP systems of this type could potentially be used for the heterolytic cleavage of dihydrogen forming the aluminium hydride Lewis acid/base adduct (**b**) (Figure 1.20). Loss of a labile ligand (L) from (**b**) would transiently generate the 16-electron complex (**c**) allowing coordination of a small molecule (*e.g.* CO) to the transition metal centre reforming an 18-electron system (**d**). Addition of dihydrogen (**d**) may effect hydride transfer to the CO generating a formyl species (**e**), which upon heterolytic cleavage of dihydrogen and coordination of L could regenerate the Lewis acid/base adduct (**b**) and an equivalent of formaldehyde.

Whilst highly idealised, Figure 1.20 shows the potential for the incorporation of the ability of FLP systems to activate small molecules into a transition metal mediated catalytic cycle. The transition metal fragment chosen, in addition to the ancillary ligand framework at aluminium are expected to be significant in determining not only the stability of the resulting complexes but also the synthetic approach(es) applicable to their synthesis.

1.6 References for Chapter I

1. N. N. Greenwood and A. Earnshaw, *Chemistry of the Elements*, Second Edition, Elsevier, 1997.
2. www.sigmaaldrich.com, Accessed 27/01/13, 2013.
3. G. N. Lewis, Chemical Catalogue Company New York, 1923.
4. H. C. Brown, H. I. Schlesinger and S. Z. Cardon, *J. Am. Chem. Soc.*, 1942, **64**, 325.
5. H. C. Brown and B. Kanner, *J. Am. Chem. Soc.*, 1966, **88**, 986.
6. G. C. Welch, R. R. S. Juan, J. D. Masuda and D. W. Stephan, *Science*, 2006, **314**, 1124.
7. D. W. Stephan and G. Erker, *Angew. Chem. Int. Ed.*, 2010, **49**, 46.
8. D. W. Stephan, *Org. Biomol. Chem.*, 2008, **6**, 1535.
9. P. Spies, S. Schwendemann, S. Lange, G. Kehr, R. Froehlich and G. Erker, *Angew. Chem. Int. Ed.*, 2008, **47**, 7543.
10. D. W. Stephan, S. Greenberg, T. W. Graham, P. Chase, J. J. Hastie, S. J. Geier, J. M. Farrell, C. C. Brown, Z. M. Heiden, G. C. Welch and M. Ullrich, *Inorg. Chem.*, 2011, **50**, 12338.
11. P. A. Chase, G. C. Welch, T. Jurca and D. W. Stephan, *Angew. Chem. Int. Ed.*, 2007, **46**, 8050.
12. S. Schwendemann, T. A. Tumay, K. V. Axenov, I. Peuser, G. Kehr, R. Froehlich and G. Erker, *Organometallics*, 2010, **29**, 1067.
13. A. J. M. Miller, J. A. Labinger and J. E. Bercaw, *J. Am. Chem. Soc.*, 2010, **132**, 3301.
14. G. Menard and D. W. Stephan, *J. Am. Chem. Soc.*, 2010, **132**, 1796.
15. J. M. Farrell, J. A. Hatnean and D. W. Stephan, *J. Am. Chem. Soc.*, 2012, **134**, 15728.

16. P. A. Chase, A. L. Gille, T. M. Gilbert and D. W. Stephan, *Dalton Trans.*, 2009, **35**, 7179.

17. S. J. Geier and D. W. Stephan, *J. Am. Chem. Soc.*, 2009, **131**, 3476.

18. A. E. Ashley, A. L. Thompson and D. O'Hare, *Angew. Chem. Int. Ed.*, 2009, **48**, 9839.

19. J. S. J. McCahill, G. C. Welch and D. W. Stephan, *Angew. Chem. Int. Ed.*, 2007, **46**, 4968.

20. C. M. Moemming, S. Froemel, G. Kehr, R. Froehlich, S. Grimme and G. Erker, *J. Am. Chem. Soc.*, 2009, **131**, 12280.

21. M. A. Dureen and D. W. Stephan, *J. Am. Chem. Soc.*, 2009, **131**, 8396.

22. M. Ullrich, K. S. H. Seto, A. J. Lough and D. W. Stephan, *Chem. Commun.*, 2009, **17**, 2335.

23. A. M. Chapman, M. F. Haddow and D. F. Wass, *J. Am. Chem. Soc.*, 2011, **133**, 8826.

24. A. M. Chapman, M. F. Haddow and D. F. Wass, *J. Am. Chem. Soc.*, 2011, **133**, 18463.

25. I. A. I. Mkhalid, J. H. Barnard, T. B. Marder, J. M. Murphy and J. F. Hartwig, *Chem. Rev.*, 2010, **110**, 890.

26. J. F. Hartwig, *Acc. Chem. Res.*, 2012, **45**, 864.

27. H. C. Brown and B. Singaram, *Pure Appl. Chem.*, 1987, **59**, 879.

28. K. Burgess and M. J. Ohlmeyer, *Chem. Rev.*, 1991, **91**, 1179.

29. I. Beletskaya and A. Pelter, *Tetrahedron*, 1997, **53**, 4957.

30. G. J. Irvine, M. J. G. Lesley, T. B. Marder, N. C. Norman, C. R. Rice, E. G. Robins, W. R. Roper, G. R. Whittell and L. J. Wright, *Chem. Rev.*, 1998, **98**, 2685.

31. D. L. Kays and S. Aldridge, *Contemporary Metal Boron Chemistry I: Borylenes, Boryls, Borane (Sigma)-Complexes, and Borohydrides*, 2008, **130**, 29.

32. L. Dang, Z. Lin and T. B. Marder, *Chem. Commun.*, 2009, **27**, 3987.

33. H. Braunschweig, R. D. Dewhurst and A. Schneider, *Chem. Rev.*, 2010, **110**, 3924.

34. Y. Segawa, M. Yamashita and K. Nozaki, *Science*, 2006, **314**, 113.

35. Y. Segawa, M. Yamashita and K. Nozaki, *Angew. Chem. Int. Ed.*, 2007, **46**, 6710.

36. T. Terabayashi, T. Kajiwara, M. Yamashita and K. Nozaki, *J. Am. Chem. Soc.*, 2009, **131**, 14162.

37. A. V. Protchenko, L. M. A. Saleh, D. Vidovic, D. Dange, C. Jones, P. Mountford and S. Aldridge, *Chem. Commun.*, 2010, **46**, 8546.

38. L. M. A. Saleh, K. H. Birjkumar, A. V. Protchenko, A. D. Schwarz, S. Aldridge, C. Jones, N. Kaltsoyannis and P. Mountford, *J. Am. Chem. Soc.*, 2011, **133**, 3836.

39. N. A. Compton, R. J. Errington and N. C. Norman, *Adv. Organomet. Chem.*, 1990, **31**, 91.

40. M. Asay, C. Jones and M. Driess, *Chem. Rev.*, 2011, **111**, 354.

41. S. Gonzalez-Gallardo, T. Bollermann, R. A. Fischer and R. Murugavel, *Chem. Rev*, 2012, **112**, 3136.

42. S. Aldridge and A. J. Downs, *The Group 13 Metals Aluminium, Gallium, Indium and Thallium.*, Wiley, 2011.

43. R. A. Fischer and T. Priermeier, *Organometallics*, 1994, **13**, 4306.

44. H. Braunschweig, J. Muller and B. Ganter, *Inorg. Chem.*, 1996, **35**, 7443.

45. J. E. Huheey, *Inorganic Chemistry*, 3rd Edition, Harper and Row: New York, 1983.

46. B. E. R. Schilling, R. Hoffmann and D. L. Lichtenberger, *J. Am. Chem. Soc.*, 1979, **101**, 585.

47. B. N. Anand, I. Krossing and H. Noth, *Inorg. Chem.*, 1997, **36**, 1979.

48. C. Jones, C. Schulten, R. P. Rose, A. Stasch, S. Aldridge, W. D. Woodul, K. S. Murray, B. Moubaraki, M. Brynda, G. La Macchia and L. Gagliardi, *Angew. Chem. Int. Ed.*, 2009, **48**, 7406.

49. C. Jones, L. Furness, S. Nembenna, R. P. Rose, S. Aldridge and A. Stasch, *Dalton Trans.*, 2010, **39**, 8788.

50. R. P. Rose, C. Jones, C. Schulten, S. Aldridge and A. Stasch, *Chem. Eur. J.*, 2008, **14**, 8477.

51. S. L. Aeilts, M. P. Coles, D. G. Swenson, R. F. Jordan and V. G. Young, *Organometallics*, 1998, **17**, 3265.

52. M. P. Coles, D. C. Swenson, R. F. Jordan and V. G. Young, *Organometallics*, 1997, **16**, 5183.

53. G. Jin, C. Jones, P. C. Junk, A. Stasch and W. D. Woodul, *New J. Chem.*, 2008, **32**, 835.

54. S. Dagorne, I. A. Guzei, M. P. Coles and R. F. Jordan, *J. Am. Chem. Soc.*, 2000, **122**, 274.

55. M. P. Coles and R. F. Jordan, *J. Am. Chem. Soc.*, 1997, **119**, 8125.

56. C. Jones, S. Aldridge, T. Gans-Eichler and A. Stasch, *Dalton Trans.*, 2006, **45**, 5357.

57. J. T. Golden, T. H. Peterson, P. L. Holland, R. G. Bergman and R. A. Andersen, *J. Am. Chem. Soc.*, 1998, **120**, 223.

58. D. L. Thorn, *J. Organomet. Chem.*, 1991, **405**, 161.

59. J. N. St. Denis, W. Butler, M. D. Glick and J. P. Oliver, *J. Organomet. Chem.*, 1977, **129**, 1.

60. J. J. Schneider, C. Kruger, M. Nolte, I. Abraham, T. S. Ertel and H. Bertagnolli, *Angew. Chem. Int. Ed.*, 1995, **33**, 2435.

61. J. M. Burlitch, M. E. Leonowicz, R. B. Petersen and R. E. Hughes, *Inorg. Chem.*, 1979, **18**, 1097.

62. J. M. Mayer and J. C. Calabrese, *Organometallics*, 1984, **3**, 1292.

63. B. Cordero, V. Gomez, A. E. Platero-Prats, M. Reves, J. Echeverria, E. Cremades, F. Barragan and S. Alvarez, *Dalton Trans.*, 2008, **3**, 2832.

64. H. Braunschweig, K. Radacki, D. Rais and G. R. Whittell, *Angew. Chem. Int. Ed.*, 2005, **44**, 1192.

65. H. Braunschweig, D. Rais and K. Uttinger, *Angew. Chem. Int. Ed.*, 2005, **44**, 3763.

66. H. Braunschweig, K. Radacki, D. Rais and F. Seeler, *Angew. Chem. Int. Ed.*, 2006, **45**, 1066.

67. H. Braunschweig, K. Gruss and K. Radacki, *Angew. Chem. Int. Ed.*, 2007, **46**, 7762.

68. J. Bauer, H. Braunschweig, P. Brenner, K. Kraft, K. Radacki and K. Schwab, *Chem. Eur. J.*, 2010, **16**, 11985.

69. J. Bauer, R. Bertermann, H. Braunschweig, K. Gruss, F. Hupp and T. Kramer, *Inorg. Chem.*, 2012, **51**, 5617.

70. J. Bauer, H. Braunschweig, A. Damme, K. Gruss and K. Radacki, *Chem. Commun.*, 2011, **47**, 12783.

71. A. F. Hill, G. R. Owen, A. J. P. White and D. J. Williams, *Angew. Chem. Int. Ed.*, 1999, **38**, 2759.

72. M. Sircoglou, S. Bontemps, G. Bouhadir, N. Saffon, K. Miqueu, W. Gu, M. Mercy, C.-H. Chen, B. M. Foxman, L. Maron, O. V. Ozerov and D. Bourissou, *J. Am. Chem. Soc.*, 2008, **130**, 16729.

73. S. Bontemps, G. Bouhadir, W. Gu, M. Mercy, C.-H. Chen, B. M. Foxman, L. Maron, O. V. Ozerov and D. Bourissou, *Angew. Chem. Int. Ed.*, 2008, **47**, 1481.

74. M. Sircoglou, M. Mercy, N. Saffon, Y. Coppel, G. Bouhadir, L. Maron and D. Bourissou, *Angew. Chem. Int. Ed.*, 2009, **48**, 3454.

75. P. A. Rudd, S. Liu, L. Gagliardi, V. G. Young, Jr. and C. C. Lu, *J. Am. Chem. Soc.*, 2011, **133**, 20724.

76. H. Schnockel, *Chem. Rev.*, 2010, **110**, 4125.

77. G. Linti and H. Schnockel, *Coord. Chem. Rev.*, 2000, **206**, 285.

78. H. W. Roesky and S. S. Kumar, *Chem. Commun.*, 2005, **32**, 4027.

79. C. Dohmeier, D. Loos and H. Schnockel, *Angew. Chem. Int. Ed.*, 1996, **35**, 129.

80. A. Purath, C. Dohmeier, A. Ecker, H. Schnockel, K. Amelunxen, T. Passler and N. Wiberg, *Organometallics*, 1998, **17**, 1894.

81. C. Schnitter, H. W. Roesky, C. Ropken, R. Herbst-Irmer, H. G. Schmidt and M. Noltemeyer, *Angew. Chem. Int. Ed.*, 1998, **37**, 1952.

82. H. Sitzmann, M. F. Lappert, C. Dohmeier, C. Uffing and H. Schnockel, *J. Organomet. Chem.*, 1998, **561**, 203.

83. E. P. Schram and N. Sudha, *Inorg. Chim. Acta*, 1991, **183**, 213.

84. A. Purath and H. Schnockel, *J. Organomet. Chem.*, 1999, **579**, 373.

85. C. Dohmeier, C. Robl, M. Tacke and H. Schnockel, *Angew. Chem. Int. Ed.*, 1991, **30**, 564.

86. S. Schulz, H. W. Roesky, H. J. Koch, G. M. Sheldrick, D. Stalke and A. Kuhn, *Angew. Chem. Int. Ed.*, 1993, **32**, 1729.

87. C. Jones, P. C. Junk, J. A. Platts and A. Stascht, *J. Am. Chem. Soc.*, 2006, **128**, 2206.

88. R. J. Baker, R. D. Farley, C. Jones, M. Kloth and D. M. Murphy, *J. Chem. Soc. Dalton Trans.*, 2002, **20**, 3844.

89. E. S. Schmidt, A. Jockisch and H. Schmidbaur, *J. Am. Chem. Soc.*, 1999, **121**, 9758.

90. E. S. Schmidt, A. Schier and H. Schmidbaur, *J. Chem. Soc. Dalton Trans.*, 2001, **5**, 505.

91. N. J. Hardman, B. E. Eichler and P. P. Power, *Chem. Commun.*, 2000, **20**, 1991.

92. M. S. Hill, P. B. Hitchcock and R. Pongtavornpinyo, *Dalton Trans.*, 2005, **2**, 273.

93. C. Jones, P. C. Junk, J. A. Platts, D. Rathmann and A. Stasch, *Dalton Trans.*, 2005, **15**, 2497.

94. Y. X. Cheng, P. B. Hitchcock, M. F. Lappert and M. S. Zhou, *Chem. Commun.*, 2005, **6**, 752.

95. C. M. Cui, H. W. Roesky, H. G. Schmidt, M. Noltemeyer, H. J. Hao and F. Cimpoesu, *Angew. Chem. Int. Ed.*, 2000, **39**, 1815.

96. X. Li, X. Cheng, H. Song and C. Cui, *Organometallics*, 2007, **26**, 1039.

97. Z. Yang, X. L. Ma, R. B. Oswald, H. W. Roesky, H. P. Zhu, C. Schulzke, K. Starke, M. Baldus, H. G. Schmidt and M. Noltemeyer, *Angew. Chem. Int. Ed.*, 2005, **44**, 7072.

98. C. Uffing, A. Ecker, R. Koppe and H. Schnockel, *Organometallics*, 1998, **17**, 2373.

99. Q. Yu, A. Purath, A. Donchev and H. Schnockel, *J. Organomet. Chem.*, 1999, **584**, 94.

100. B. Buchin, T. Steinke, C. Gemel, T. Cadenbach and R. A. Fischer, *Z. Anorg. Allg. Chem.*, 2005, **631**, 2756.

101. T. Cadenbach, C. Gemel, T. Bollermann and R. A. Fischer, *Inorg. Chem.*, 2009, **48**, 5021.

102. T. Steinke, C. Gemel, M. Winter and R. A. Fischer, *Chem. Eur. J.*, 2005, **11**, 1636.

103. M. Hackett, J. A. Ibers, P. Jernakoff and G. M. Whitesides, *J. Am. Chem. Soc.*, 1986, **108**, 8094.

104. D. Weiss, T. Steinke, M. Winter, R. A. Fischer, N. Frohlich, J. Uddin and G. Frenking, *Organometallics*, 2000, **19**, 4583.

105. T. Cadenbach, T. Bollermann, C. Gemel and R. A. Fischer, *Dalton Trans.*, 2009, **2**, 322.

106. M. Ohashi, K. Matsubara, T. Iizuka and H. Suzuki, *Angew. Chem. Int. Ed.*, 2003, **42**, 937.

107. C. Dohmeier, H. Krautscheid and H. Schnockel, *Angew. Chem. Int. Ed.*, 1995, **33**, 23.

108. M. M. Schulte, E. Herdtweck, G. RaudaschlSieber and R. A. Fischer, *Angew. Chem. Int. Ed.*, 1996, **35**, 424.

109. R. A. Fischer, M. M. Schulte, J. Weiss, L. Zsolnai, A. Jacobi, G. Huttner, G. Frenking, C. Boehme and S. F. Vyboishchikov, *J. Am. Chem. Soc.*, 1998, **120**, 1237.

110. H. Folsing, O. Segnitz, U. Bossek, K. Merz, M. Winter and R. A. Fischer, *J. Organomet. Chem.*, 2000, **606**, 132.

111. Weiss J, Stetzkamp D, Nuber B, Fischer R, Boehme C and F. G, *Angew. Chem. lnt. Ed.*, 1997, **36**, 70.

112. S. Nagendran and H. W. Roesky, *Organometallics*, 2008, **27**, 457.

113. A. Kempter, C. Gemel and R. A. Fischer, *Chem. Eur. J.*, 2007, **13**, 2990.

114. A. Kempter, C. Gemel and R. A. Fischer, *Chem. Commun.*, 2006, **14**, 1551.

115. R. H. Crabtree, *Angew. Chem. Int. Ed.*, 1993, **32**, 789.

116. G. J. Kubas, R. R. Ryan, B. I. Swanson, P. J. Vergamini and H. J. Wasserman, *J. Am. Chem. Soc.*, 1984, **106**, 451.

117. G. Alcaraz, M. Grellier and S. Sabo-Etienne, *Acc. Chem. Res.*, 2009, **42**, 1640.

118. G. S. McGrady and G. Guilera, *Chem. Soc. Rev.*, 2003, **32**, 383.

119. S. Sabo-Etienne and B. Chaudret, *Chem. Rev.*, 1998, **98**, 2077.

120. M. J. Ingleson, S. K. Brayshaw, M. F. Mahon, G. D. Ruggiero and A. S. Weller, *Inorg. Chem.*, 2005, **44**, 3162.

121. C. J. Stevens, R. Dallanegra, A. B. Chaplin, A. S. Weller, S. A. Macgregor, B. Ward, D. McKay, G. Alcaraz and S. Sabo-Etienne, *Chem. Eur. J.*, 2011, **17**, 3011.

122. G. J. Kubas, R. R. Ryan and D. A. Wrobleski, *J. Am. Chem. Soc.*, 1986, **108**, 1339.

123. G. J. Kubas, C. J. Unkefer, B. I. Swanson and E. Fukushima, *J. Am. Chem. Soc.*, 1986, **108**, 7000.

124. A. Toupadakis, G. J. Kubas, W. A. King, B. L. Scott and J. Huhmann-Vincent, *Organometallics*, 1998, **17**, 5315.

125. J. C. Green, M. L. H. Green and G. Parkin, *Chem. Commun.*, 2012, **48**, 11481.

126. G. Alcaraz and S. Sabo-Etienne, *Coord. Chem. Rev.*, 2008, **252**, 2395.

127. J. K. Hoyano, M. Elder and W. A. G. Graham, *J. Am. Chem. Soc.*, 1969, **91**, 4568.

128. J. Y. Corey and J. Braddock-Wilking, *Chem. Rev.*, 1999, **99**, 175.

129. U. Schubert, *Adv. Organomet. Chem.*, 1990, **30**, 151.

130. W. Scherer, G. Eickerling, M. Tafipolsky, G. S. McGrady, P. Sirsch and N. P. Chatterton, *Chem. Commun.*, 2006, **28**, 2986.

131. G. S. McGrady, P. Sirsch, N. P. Chatterton, A. Ostermann, C. Gatti, S. Altmannshofer, V. Herz, G. Eickerling and W. Scherer, *Inorg. Chem.*, 2009, **48**, 1588.

132. Z. Dawoodi, M. L. H. Green, V. S. B. Mtetwa, K. Prout, A. J. Schultz, J. M. Williams and T. F. Koetzle, *J. Chem. Soc. Dalton Trans.*, 1986, **8**, 1629.

133. A. J. Schultz, J. M. Williams, T. F. Koetzle, Z. Dawoodi, M. L. H. Green and K. Prout, *Acta Cryst. Section A*, 1984, **40**, C292.

134. H. J. Wasserman, G. J. Kubas and R. R. Ryan, *J. Am. Chem. Soc.*, 1986, **108**, 2294.

135. M. Brookhart, M. L. H. Green and G. Parkin, *Proc. Natl. Acad. Sci. U. S. A.*, 2007, **104**, 6908.

136. R. N. Perutz and J. J. Turner, *J. Am. Chem. Soc.*, 1975, **97**, 4791.

137. G. E. Ball, C. M. Brookes, A. J. Cowan, T. A. Darwish, M. W. George, H. K. Kawanami, P. Portius and J. P. Rourke, *Proc. Natl. Acad. Sci. U. S. A.*, 2007, **104**, 6927.

138. W. H. Bernskoetter, C. K. Schauer, K. I. Goldberg and M. Brookhart, *Science*, 2009, **326**, 5952.

139. D. R. Evans, T. Drovetskaya, R. Bau, C. A. Reed and P. D. W. Boyd, *J. Am. Chem. Soc.*, 1997, **119**, 3633.

140. I. Castro-Rodriguez, H. Nakai, P. Gantzel, L. N. Zakharov, A. L. Rheingold and K. Meyer, *J. Am. Chem. Soc.*, 2003, **125**, 15734.

141. S. D. Pike, A. L. Thompson, A. G. Algarra, D. C. Apperley, S. A. Macgregor and A. S. Weller, *Science*, 2012, **337**, 1648.

142. T. J. Marks and J. R. Kolb, *Chem. Rev.*, 1977, **77**, 263.

143. M. Shimoi, S. Nagai, M. Ichikawa, Y. Kawano, K. Katoh, M. Uruichi and H. Ogino, *J. Am. Chem. Soc.*, 1999, **121**, 11704.

144. P. Bissinger, H. Braunschweig, T. Kupfer and K. Radacki, *Organometallics*, 2010, **29**, 3987.

145. T. Kakizawa, Y. Kawano and M. Shimoi, *Organometallics*, 2001, **20**, 3211.

146. Y. Kawano, M. Hashiva and M. Shimoi, *Organometallics*, 2006, **25**, 4420.

147. T. B. Marder, *Angew. Chem. Int. Ed.*, 2007, **46**, 8116.

148. A. Staubitz, A. P. M. Robertson, M. E. Sloan and I. Manners, *Chem. Rev.*, 2010, **110**, 4023.

149. A. Staubitz, A. P. M. Robertson and I. Manners, *Chem. Rev.*, 2010, **110**, 4079.

150. T. M. Douglas, A. B. Chaplin and A. S. Weller, *J. Am. Chem. Soc.*, 2008, **130**, 14432.

151. T. M. Douglas, A. B. Chaplin, A. S. Weller, X. Yang and M. B. Hall, *J. Am. Chem. Soc.*, 2009, **131**, 15440.

152. A. B. Chaplin and A. S. Weller, *Inorg. Chem.*, 2010, **49**, 1111.

153. J. F. Hartwig, G. N. Muhoro, X. M. He, O. Eisenstein, R. Bosque and F. Maseras, *J. Am. Chem. Soc.*, 1996, **118**, 10936.

154. X. M. He and J. F. Hartwig, *J. Am. Chem. Soc.*, 1996, **118**, 1696.

155. C. N. Muhoro and J. F. Hartwig, *Angew. Chem. Int. Ed.*, 1997, **36**, 13.

156. S. Schlecht and J. F. Hartwig, *J. Am. Chem. Soc.*, 2000, **122**, 9435.

157. G. Alcaraz, E. Clot, U. Helmstedt, L. Vendier and S. Sabo-Etienne, *J. Am. Chem. Soc.*, 2007, **129**, 8704.

158. K. D. Hesp, F. O. Kannemann, M. A. Rankin, R. McDonald, M. J. Ferguson and M. Stradiotto, *Inorg. Chem.*, 2011, **50**, 2431.

159. G. Alcaraz and S. Sabo-Etienne, *Angew. Chem. Int. Ed.*, 2010, **49**, 7170.

160. J. Spielmann, M. Bolte and S. Harder, *Chem. Commun.*, 2009, **45**, 6934-6936.

161. J. Spielmann, G. Jansen, H. Bandmann and S. Harder, *Angew. Chem. Int. Ed.*, 2008, **47**, 6290.

162. M. S. Hill, G. Kociok-Koehn and T. P. Robinson, *Chem. Commun.*, 2010, **46**, 7587.

163. D. J. Liptrot, M. S. Hill, M. F. Mahon and D. J. MacDougall, *Chem. Eur. J.*, 2010, **16**, 8508.

164. H. J. Cowley, M. S. Holt, R. L. Melen, J. M. Rawson and D. S. Wright, *Chem. Commun.*, 2011, **47**, 2682.

165. M. M. Hansmann, R. L. Melen and D. S. Wright, *Chem. Sci.*, 2011, **2**, 1554.

166. C. W. Hamilton, R. T. Baker, A. Staubitz and I. Manners, *Chem. Soc. Rev.*, 2009, **38**, 279.

167. T. J. Clark, K. Lee and I. Manners, *Chem. Eur. J.*, 2006, **12**, 8634.

168. A. Staubitz, M. E. Sloan, A. P. M. Robertson, A. Friedrich, S. Schneider, P. J. Gates, J. S. A. D. Guenne and I. Manners, *J. Am. Chem. Soc.*, 2010, **132**, 13332.

169. A. Staubitz, A. P. Soto and I. Manners, *Angew. Chem. Int. Ed.*, 2008, **47**, 6212.

170. G. Alcaraz, L. Vendier, E. Clot and S. Sabo-Etienne, *Angew. Chem. Int. Ed.*, 2010, **49**, 918.

171. C. Y. Tang, A. L. Thompson and S. Aldridge, *J. Am. Chem. Soc.*, 2010, **132**, 10578.

172. C. Y. Tang, N. Phillips, J. I. Bates, A. L. Thompson, M. J. Gutmann and S. Aldridge, *Chem. Commun.*, 2012, **48**, 8096.

173. C. Y. Tang, A. L. Thompson and S. Aldridge, *Angew. Chem. Int. Ed.*, 2010, **49**, 921.

174. G. Alcaraz, A. B. Chaplin, C. J. Stevens, E. Clot, L. Vendier, A. S. Weller and S. Sabo-Etienne, *Organometallics*, 2010, **29**, 5591.

175. D. Vidovic, D. A. Addy, T. Kraemer, J. McGrady and S. Aldridge, *J. Am. Chem. Soc.*, 2011, **133**, 8494.

176. E. B. Lobkovskii, G. L. Soloveichik, A. I. Sisov, B. M. Bulychev, A. I. Gusev and N. I. Kirillova, *J. Organomet. Chem.*, 1984, **265**, 167.

177. V. K. Belskii, B. M. Bulychev, A. B. Erofeev and G. L. Soloveichik, *J. Organomet. Chem.*, 1984, **268**, 107.

178. V. K. Belsky, A. B. Erofeev, B. M. Bulychev and G. L. Soloveichik, *J. Organomet. Chem.*, 1984, **265**, 123.

179. K. Khan, C. L. Raston, J. E. McGrady, B. W. Skelton and A. H. White, *Organometallics*, 1997, **16**, 3252.

180. M. Plois, T. Wiegand and R. Wolf, *Organometallics*, 2012, **31**, 8469.

181. S. Aldridge and A. J. Downs, *Chem. Rev.*, 2001, **101**, 3305.

182. E. B. Lobkovsky, G. L. Soloveychik, B. M. Bulychev, A. B. Erofeev, A. I. Gusev and N. I. Kirillova, *J. Organomet. Chem.*, 1983, **254**, 167.

183. K. R. Porschke, W. Kleimann, Y. H. Tsay, C. Kruger and G. Wilke, *Chem. Ber.*, 1990, **123**, 1267.

184. V. V. Burlakov, K. Kaleta, T. Beweries, P. Arndt, W. Baumann, A. Spannenberg, V. B. Shur and U. Rosenthal, *Organometallics*, 2011, **30**, 1157.

185. P. Arndt, A. Spannenberg, W. Baumann, V. V. Burlakov, U. Rosenthal, S. Becke and T. Weiss, *Organometallics*, 2004, **23**, 4792.

186. T. Steinke, C. Gemel, M. Cokoja, M. Winter and R. A. Fischer, *Angew. Chem. Int. Ed.*, 2004, **43**, 2299.

187. T. Steinke, M. Cokoja, C. Gemel, A. Kempter, A. Krapp, G. Frenking, U. Zenneck and R. A. Fischer, *Angew. Chem. Int. Ed.*, 2005, **44**, 2943.

188. X. Liu, H. W. Langmi, S. D. Beattie, F. F. Azenwi, G. S. McGrady and C. M. Jensen, *J. Am. Chem. Soc.*, 2011, **133**, 15593.

189. B. Bogdanovic and M. Schwickardi, *J. Alloys Compd.*, 1997, **253**, 1.

190. J. K. Ruff and M. F. Hawthorne, *J. Am. Chem. Soc.*, 1960, **82**, 2141.

191. N. N. Greenwood, A. Storr and M. G. H. Wallbridge, *Inorg. Chem.*, 1963, **2**, 1036.

192. D. F. Shriver and R. W. Parry, *Inorg. Chem.*, 1963, **2**, 1039.

193. C. R. Pulham, A. J. Downs, M. J. Goode, D. W. H. Rankin and H. E. Robertson, *J. Am. Chem. Soc.*, 1991, **113**, 5149.

194. J. L. Atwood, S. G. Bott, F. M. Elms, C. Jones and C. L. Raston, *Inorg. Chem.*, 1991, **30**, 3482.

195. K. Ueno, T. Yamaguchi, K. Uchiyama and H. Ogino, *Organometallics*, 2002, **21**, 2347.

196. T. Muraoka and K. Ueno, *Coord. Chem. Rev.*, 2010, **254**, 1348.

197 G. Alcaraz, U. Helmstedt, E. Clot, L. Vendier and S. Sabo-Etienne, *J. Am. Chem. Soc.*, 2008, **130**, 12878.

2 Experimental Techniques

2.1 Manipulation of Air-Sensitive Compounds

The majority of compounds used during the research documented in this thesis were highly sensitive to both air and moisture. Consequently, inert atmosphere and high vacuum techniques were employed instead of traditional bench-top methods for the manipulation of these compounds.

2.1.1 Inert Atmosphere Techniques

The two most common types of inert atmosphere techniques involve the use of a Schlenk line or a glove box. These techniques allow the handling of air and moisture sensitive compounds by using either argon or nitrogen gas to achieve an inert atmosphere.[1,2]

Schlenk techniques are more suitable for the manipulation of solutions and reduce the risk of decomposition due to hydrolysis or oxidation.[3] The Schlenk line used consisted of a dual Pyrex manifold fitted with several ports for attaching apparatus (Figure 2.1). One manifold was connected to a source of purified argon allowing the attached apparatus to be filled with argon. The other manifold was connected to a vacuum pump, evacuated and maintained at *ca.* 10^{-2} Torr. The pressure within this manifold was monitored by the use of a Pirani pressure gauge. The two manifolds were connected *via* a ground glass two-way tap lubricated with high vacuum grease, which allowed attached glassware to contain either a positive pressure of argon or to be evacuated to pressures of *ca.* 10^{-2} Torr. To achieve a largely air and moisture free environment, a 'pump and purge' cycle, in which the glassware was evacuated to *ca.* 10^{-2} Torr and subsequently filled with argon, was repeated

three times. During the first cycle the glassware was heated strongly under vacuum with a Bunsen burner and allowed to cool to ambient temperature under vacuum before filling with argon and completing the 'pump and purge' cycles. The inert gas manifold was vented through a mercury bubbler to avoid excessive pressure and a liquid nitrogen cold trap was used to prevent solvent vapours and volatile reaction products from contaminating the pump. All ground glass joints were lubricated with high vacuum grease to provide an air-tight seal. Liquids were transferred between flasks using either cannulae or syringes, preventing exposure to the external atmosphere.

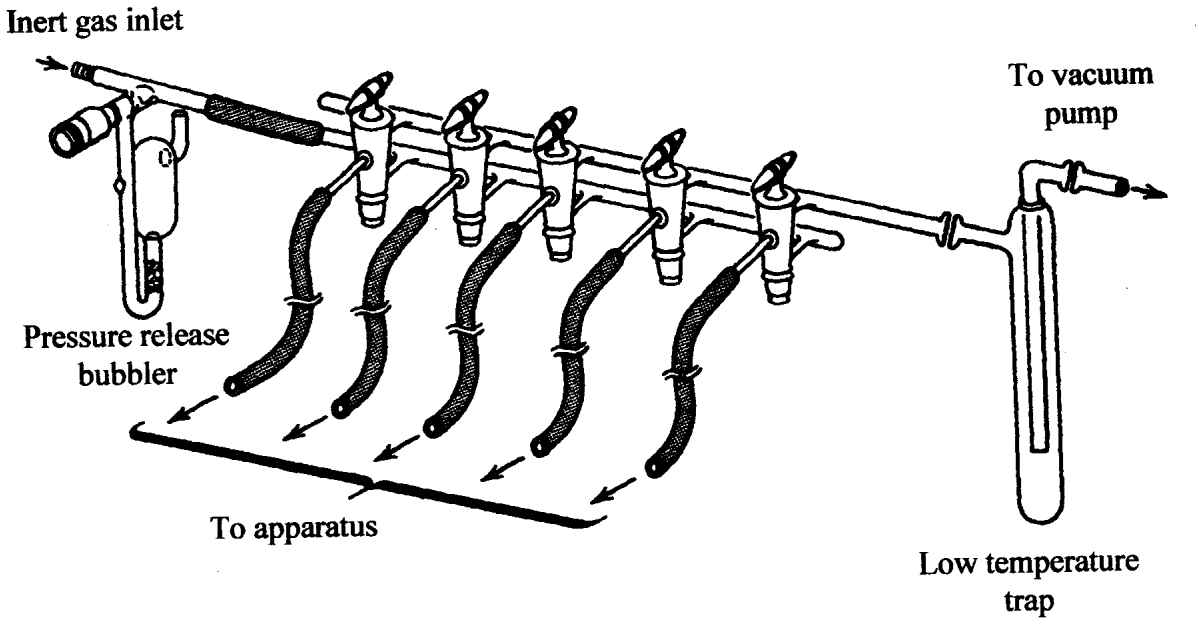

Figure 2.1: *A Schlenk line*

For the manipulation of air and moisture sensitive solids a Saffron Alpha glove box was used. It consisted of a sealed air-tight stainless steel container, fitted with a glass viewing window and was designed to allow the manipulation of compounds in an inert atmosphere. Neoprene gloves built into the sides allowed the required manipulations to be carried out

inside the box. The nitrogen atmosphere within the box was purified by scrubbing through activated copper metal and molecular sieves to remove oxygen and moisture respectively. The integrity of both the copper and molecular sieve scrubbers was maintained through a regular regeneration process. Compounds and apparatus were admitted to the box through a small antechamber using three 'pump and purge' cycles.

2.1.2 High Vacuum Techniques

A high vacuum line was used for the removal of trace solvent from compounds for which the vacuum attainable on a standard Schlenk line was insufficient.[1,2] The vacuum line consisted of a standard rotary pump, a mercury diffusion pump, a cold trap and a single manifold with J Young's greaseless taps. The combination of rotary and mercury diffusion pumps allowed pressures of ca. 10^{-4} Torr to be obtained. A Tesla coil, which produced a discharge at pressures between 1 and 10^{-3} Torr, was used to gauge the pressure in the line and check for leaks.

2.2 Spectroscopic and Characterisation Techniques

Due to the nature of the research reported in this thesis, a range of spectroscopic and characterisation techniques were used and are documented below.

2.2.1 NMR Spectroscopy

NMR spectra were measured on a Varian 'Mercury' 300 MHz or Varity Unity +500 spectrometer. Residual signals of deuterated solvents were used as references for ^{1}H and ^{13}C NMR measurements. ^{27}Al, ^{11}B, ^{19}F and ^{31}P were referenced against $[Al(H_2O)_6]^{3+}$, $Et_2O{\cdot}BF_3$, $CFCl_3$, and 85% aqueous H_3PO_4, respectively. Samples were prepared by

generating an inert atmosphere in a J Young's NMR tube using the 'pump and purge' method, followed by solution transfer by cannula.

2.2.2 Infrared Spectroscopy

Infrared spectra were measured as a solution in a compatible solvent, within a solution infrared cell. Spectra were recorded on a Nicolet 500 FT-IR spectrometer.

2.2.3 Mass Spectrometry

Samples for mass spectrometry were submitted to the EPSRC National Mass Spectrometry Service Centre, Swansea University if the compound was charge-neutral. Charged species were analysed by the author using a Bruker MicroTOF ESI mass spectrometer linked to a glove box via PEEK tubing.[4]

2.2.4 Single Crystal X-Ray Crystallography

Determination of single crystal X-ray structures were carried out by the author as well as Dr. Dragoslav Vidovic, Mr. Michael Kelly and Mr. Nicholas Philips of the Aldridge research group. Crystal data were collected on either a Bruker-Nonius KappaCCD diffractometer or Oxford Diffraction (Agilent) Supernova diffractometer at 150 K.[5] Data were reduced using DENZO/SCALEPACK[6] or CrysAlisPro. The structures were solved with SIR92[7] or SuperFlip[8] and refined with full-matrix least-squares within CRYSTALS[9, 10] or SHELX[11] as described in the CIFs in the appendix (CD).

2.2.5 Theoretical Calculations

Theoretical calculations were carried out by Dr. Joshua Bates using the Amsterdam Density Functional (ADF) Package Software 2012.[12-14] Calculations were performed using the Vosko-Wilk-Nusair local density approximation with exchange from Becke[15] and correlation corrections from Perdew.[16] Slater-type orbitals (STOs)[17] were used for the triple zeta basis set with an additional set of polarization functions (TZP). The large frozen core basis set approximation was applied with no molecular symmetry. The general level of numerical integration was 6. Frequency calculations were performed for freely optimized structures and no significant imaginary frequencies were observed for ground state structures. Estimates of binding energies were obtained following the strategy outlined by Baerends[18] using the counterpoise method[19] and were corrected for Basis Set Superposition Error (BSSE). Fragment analysis and use of the "REMOVEFRAGORBITALS" key were used to assess complex formation.

2.2.6 Photolysis Experiments

Photolysis experiments were carried out using a Spectral Energy mercury arc lamp (1 kW) with samples contained within either a quartz Schlenk vessel or a J Young's NMR tube. Low temperature photolysis experiments were carried out by Dr. George Whittell at the University of Bristol using a 400 W lamp and a quartz immersion well.

2.2.7 Elemental Analyses

Elemental analyses were performed by Dr. Stephen Boyer of the London Metropolitan University. Samples of all new compounds were submitted for microanalysis. In the incidents where measured values did not give satisfactory agreement it is thought that the

high level of air/moisture sensitivity was a factor. In some cases the presence of $[CpFe(CO)_2]_2$ or $[Cp^*Fe\ (CO)_2]_2$, even after repeated recrystallisation was a contributing factor. In all cases ^1H and ^{13}C NMR revealed samples to be >95 % pure.

2.3 Preparation and Purification of Starting Materials

A list of commercially available chemicals used along with their sources, quoted purity and purification methods is given in the appendix.

2.3.1 Synthesis of Starting Materials

Precursors that were not readily available from commercial sources were synthesised from the readily available reagents listed in the appendix.

Preparation of $^iPr_2NLi$ (LDA)

^{n}BuLi (40.0 cm^3, 1.6 M in hexanes, 64.0 mmol) was added dropwise to a stirred solution of di*iso*propylamine (10.0 cm^3, 71.4 mmol) in diethyl ether (30 cm^3) at -78 °C. After addition the reaction mixture was warmed to room temperature and stirred for 2.5 h. The solvent was removed *in vacuo* to yield a pyrophoric white powder which was used without further purification. Yield 7.83 g, 88%.

Preparation of PhLi

To a stirred solution of bromobenzene (4.0 cm^3, 38.0 mmol) in hexane (10 cm^3) was added ^{n}BuLi (23.8 cm^3, 1.6 M in hexanes, 38.0 mmol) and the reaction mixture warmed to 50 °C for 2.5 h leading to the formation of a white precipitate. The precipitate was isolated by filtration and washed with pentane (3 x 10 cm^3) and dried under vacuum yielding a pyrophoric white powder which was used without further purification. Yield 2.32 g, 71%.

Preparation of $^{i}Pr_2NC(^{i}PrN)_2AlCl_2$

The method employed for the formation of $^{i}Pr_2NC(^{i}PrN)_2AlCl_2$ followed that reported by Aeilts *et al*.[20] To a stirred solution of *N*,*N'*-di*iso*propylcarbodiimide (3.16 g, 25.0 mmol) in diethyl ether (30 cm^3) at 0 °C was added slowly a solution of $^{i}Pr_2NLi$ (2.68 g, 25.0 mmol) in diethyl ether (25 cm^3). The reaction mixture was stirred for 2 h whilst attaining room temperature and then added slowly to a solution of $AlCl_3$ (3.61 g, 27.0 mmol) also in diethyl ether (20 cm^3) at -78 °C. After stirring for 18 h while slowly attaining room temperature the solvent was removed *in vacuo* to yield a white solid. Extraction with toluene (3 x 25 cm^3) followed by concentration and cooling to -30 °C afforded pale yellow crystals of $^{i}Pr_2NC(^{i}PrN)_2AlCl_2$. Yield 5.30 g, 65%. Spectroscopic data matched those given in the literature.[20]

Preparation of Na[CpFe(CO)$_2$]

The method employed for the formation of $Na[CpFe(CO)_2]$ followed that reported by King *et al*.[21] Sodium metal (3.50 g, 152.0 mmol) was dissolved slowly in mercury forming a Na/Hg amalgam to which a solution of $[CpFe(CO)_2]_2$ (7.00 g, 19.8 mmol) in THF (30 cm^3) was then added. The reaction mixture was stirred for 36 h and then filtered, yielding a dark brown filtrate. The solvent was removed *in vacuo* to yield a dark yellow solid. This was triturated with hot toluene (50 °C, 2 x 15 cm^3) and hot hexane (50 °C, 1 x 15 cm^3) with the solvent being removed *in vacuo* after each addition. Subsequent washings with toluene (2 x 15 cm^3) and hexane (15 cm^3) yielded a dark yellow powder which was dried overnight *in vacuo* and used without further purification. Yield 6.85 g, 86%.

Prepearation of Na[BAr$^f_4$] (Ar^f = 3,5-(CF$_3$)$_2$C$_6$H$_3$)

The method employed for the formation of Na[BAr$^f_4$] followed that reported by Reger *et al*.[22] A 3-necked round-bottomed flask fitted with a reflux condenser and a dropping funnel was charged with activated magnesium turnings (1.58 g, 66 mmol) and diethyl ether (300 cm^3). 1-bromo-3,5-trifluoromethyl benzene (8.0 cm3, 46 mmol) was added dropwise over 2 h. $BF_3{\cdot}OEt_2$ (1.4 cm^3, 11 mmol) was then added *via* syringe, and the reaction mixture refluxed for 6 h, the reaction being monitored by *in situ* ^{11}B NMR spectroscopy. The reaction mixture was allowed to cool to room temperature and filtered into aqueous Na_2CO_3 and stirred vigorously. After separation of the organic fraction the aqueous fraction was washed with diethyl ether (3 x 40 cm^3), the organic fractions combined and the solvent removed *in vacuo* to yield a pale brown powder. Recrystallisation from a minimal amount of a 1:1:1 mixture of diethyl ether, THF and dichloromethane layered with hexane gave a white solid, which was dried *in vacuo* at 140 °C for *ca.* 60 h. Yield 6.72 g, 69%. Spectroscopic data matched those given in the literature.[22]

Preparation of [H(OEt$_2$)$_2$][BAr$^f_4$] (Ar^f = 3,5-(CF$_3$)$_2$C$_6$H$_3$)

The method employed for the formation of [H(OEt$_2$)$_2$][BAr$^f_4$] followed that reported by Brookhart *et al*.[23] To a stirred solution of Na[BAr$^f_4$] (1.00 g, 1.13 mmol) in diethyl ether (30 cm^3) at -30 °C was added HCl (3.0 cm^3, 2.0 M in diethyl ether, 6.0 mmol). The reaction mixture was stirred at -30 °C for 30 min, then filtered and concentrated (*ca.* 5 cm^3) and cooled to -78 °C. After standing for 1 h hexane was added slowly to precipitate the product which was isolated by filtration and dried *in vacuo*. Yield 4.54 g, 75%. Spectroscopic data matched those given in the literature.[23]

Preparation of (DippNH)$_2$CS

The method employed for the formation of (DippNH)$_2$CS followed that reported by Cowley and co-workers.[24] CS_2 (8.0 cm^3, 130.0 mmol) was added dropwise to a stirred solution of $DippNH_2$ (50.0 cm^3, 265.0 mmol) and NEt_3 (37.2 cm^3, 265.0 mmol) in water (100 cm^3). The reaction mixture was stirred for 1 h at room temperature and then heated to 90 °C for 14 h resulting in the formation of a yellow precipitate. Dichloromethane (40 cm^3) was then added and the organic fraction separated and dried over $MgSO_4$. Filtration followed by cooling of a concentrated dichloromethane solution to 0 °C yielded colourless crystals of (DippNH)$_2$CS. Yield 38.46 g, 75%. Spectroscopic data matched those given in the literature.[24]

Preparation of DippNCNDipp

The method employed for the formation of DippNCNDipp followed that reported by Cowley and co-workers.[24] A slurry of (DippNH)$_2$CS (3.16 g, 8.0 mmol), HgO (3.47 g, 16.0 mmol) and $MgSO_4$ (2.31 g, 19.2 mmol) in toluene (100 cm^3) was refluxed for 18 h. After cooling to room temperature the reaction mixture was filtered and the solvent was removed *in vacuo* to afford a pale oil. Trituration with hexane (2 x 100 cm^3), diethyl ether (2 x 100 cm^3) and dichloromethane (2 x 100 cm^3) followed by addition of diethyl ether (50 cm^3), filtration and removal of the solvent *in vacuo* yielded DippNCNDipp as a white powder. Yield 1.92 g, 67%. Spectroscopic data matched those given in the literature.[24]

Preparation of ^{i}Pr$_2$NC(DippN)(DippNH)

The method employed for the formation of ^{i}Pr$_2$NC(DippN)(DippNH) followed that reported by Jin *et al*.[25] To a stirred solution of DippNCNDipp (1.20 g, 3.3 mmol) in THF (45 cm^3) was added a solution of LDA (0.35 g, 3.3 mmol) in THF (30 cm^3) and the reaction mixture

refluxed for 18 h. After cooling to room temperature the solvent was removed *in vacuo* to yield a yellow solid which was dissolved in diethyl ether (20 cm^3) forming a yellow solution. Degassed water (20 cm^3) was added slowly and the reaction mixture stirred for 20 min. The aqueous fraction was extracted with dichloromethane (3 x 30 cm^3) and the organic fractions combined, dried over $MgSO_4$ and filtered before drying *in vacuo* to yield a yellow oil. The oil solidified on standing and recrystallisation from minimal hot hexane afforded colourless crystals of $^{i}Pr_2NC(DippN)(DippNH)$. Yield 0.80 g, 53%. Spectroscopic data matched those given in the literature.[25]

Preparation of $H_3Al{\cdot}NMe_3$

The method employed for the formation of $H_3Al{\cdot}NMe_3$ followed that reported by Ruff and Hawthorne.[26] A solution of $LiAlH_4$ (2.07 g, 54.0 mmol) in diethyl ether (45 cm^3) at -78 °C was added dropwise to a slurry of $[Me_3NH]Cl$ (4.58 g, 46.0 mmol) in diethyl ether (40 cm^3) also at -78 °C and the reaction mixture stirred for 18 h whilst slowly attaining room temperature. The solvent was removed *in vacuo* yielding a white solid which was purified by vacuum sublimation (*ca.* 10^{-2} mbar, 40 °C) yielding a white microcrystalline powder. Yield 3.96 g, 97%. Spectroscopic data matched those given in the literature.[26]

Preparation of $[\{^{i}Pr_2NC(DippN)_2Al(H)(\mu\text{-}H)\}_2]$

The method employed for the formation of $[\{^{i}Pr_2NC(DippN)_2Al(H)(\mu\text{-}H)\}_2]$ followed that reported by Bonyhady *et al.*[27] A solution of $H_3Al{\cdot}NMe_3$ (0.74 g, 8.3 mmol) in toluene (40 cm^3) was added to a stirred solution of $^{i}Pr_2NC(DippN)(DippNH)$ (3.80 g, 8.2 mmol) in toluene (50 cm^3) at room temperature and the reaction mixture stirred for 12 h. Filtration followed by concentration and cooling to -30 °C afforded colourless crystals of

[{$^{i}Pr_2NC(DippN)_2Al$ (H)(μ-H)}$_2$]. Yield 3.55 g, 88%. Spectroscopic data matched those given in the literature.[27]

Preparation of $^{i}Pr_2NC(DippN)_2AlI_2$

The method employed for the formation of $^{i}Pr_2NC(DippN)_2AlI_2$ followed that reported by Bonyhady *et al.*[27] A solution of I_2 (1.47 g, 5.8 mmol) in toluene (35 cm^3) was added slowly to a solution of [{$^{i}Pr_2NC(DippN)_2Al(H)(\mu\text{-}H)\}_2$] (2.86 g, 2.9 mmol) also in toluene (40 cm^3) at -30 °C. The reaction mixture was maintained at -30 °C for 10 min and then warmed to room temperature and filtered. The concentrated filtrate was stored at -30 °C affording colourless crystals of $^{i}Pr_2NC(DippN)_2AlI_2$. Yield 2.62 g, 61%. Spectroscopic data matched those given in the literature.[27]

Preparation of $[Cp^*Fe(CO)_2]_2$

The method employed for the formation of $[Cp^*Fe(CO)_2]_2$ followed that reported by King *et al.*[21] Cp^*H (5.5 cm^3, 35.1 mmol) was added to a solution of $Fe(CO)_5$ (9.8 cm^3, 74.6 mmol) in xylene (50 cm^3) and the reaction mixture refluxed for 24 h. After this period the reaction mixture was cooled to room temperature before the addition of more $Fe(CO)_5$ (7.0 cm^3, 53.3 mmol). The reaction mixture was then refluxed for a further 24 h. The crude product was washed with hexane (1 x 40 cm^3, 2 x 20 cm^3) and extracted with CH_2Cl_2 (3 x 300 cm^3). Cooling of a concentrated CH_2Cl_2 solution to -30 °C yielded purple crystals of $[Cp^*Fe(CO)_2]_2$. Yield 4.27 g, 49%. Purity was verified by IR (CH_2Cl_2 solution) 1922, 1748 cm^{-1} (ν_{CO}, terminal and bridging).

*Preparation of Na[Cp*Fe(CO)$_2$]*

The method employed for the formation of Na[Cp*Fe(CO)$_2$] followed that reported by King *et al*.[21] Sodium metal (1.20 g, 52.0 mmol) was dissolved slowly in mercury forming a Na/Hg amalgam to which a solution of [Cp*Fe(CO)$_2$]$_2$ (4.26 g, 8.6 mmol) in THF (150 cm^3) was added. The reaction mixture was stirred for 72 h and then filtered, yielding a purple filtrate. The solvent was removed *in vacuo* to yield an orange solid. This was triturated with hot toluene (70 °C, 2 x 20 cm^3) and hot hexane (70 °C, 1 x 20 cm^3) with the solvent being removed *in vacuo* after each addition. Subsequent washings with toluene (2 x 20 cm^3) and hexane (20 cm^3) yielded a dark yellow powder which was dried overnight *in vacuo* and used without further purification. Yield 4.19 g, 96%.

Preparation of B(C$_6$F$_5$)$_3$

The method employed for the formation of B(C$_6$F$_5$)$_3$ followed minor modification from that reported by Wang *et al*.[28] To a stirred solution of BrC$_6$F$_5$ (12.35 g, 50.0 mmol) in pentane (200 cm^3) at -78 °C was added dropwise ^{n}BuLi (31.0 cm^3, 1.6 M in hexanes, 50.0 mmol) and the reaction mixture stirred at -78 °C for 1 h (great care was taken to ensure that the reaction mixture was maintained below -50 °C at all times as C$_6$F$_5$Li is explosive at higher temperatures). BCl$_3$ (16.7 cm^3, 1.0 M in heptane, 16.7 mmol) was then added quickly and the reaction mixture stirred at -78 °C for a further 3 h before being allowed to attain room temperature slowly whilst stirring for a further 12 h. The reaction mixture was filtered, and the filtrate concentrated and cooled to -30 °C yielding a white precipitate of B(C$_6$F$_5$)$_3$. Yield 3.97 g, 47%. Spectroscopic data matched those given in the literature.[28]

Preparation of $CpFe(CO)_2(SiMe_3)$

The method employed for the formation of $CpFe(CO)_2(SiMe_3)$ followed that reported by King and Pannell.[21] To a stirred solution of Me_3SiCl (1.56 g, 14.4 mmol) in THF (20 cm^3) at -30 °C was added slowly a solution of $Na[CpFe(CO)_2]$ (1.84 g, 9.2 mmol) also in THF (40 cm^3). The reaction mixture was stirred for 18 h whilst attaining room temperature and the solvent removed *in vacuo* to yield a brown solid. Extraction with pentane (3 x 15 cm^3) followed by the removal of solvent *in vacuo* yielded a brown solid. $CpFe(CO)_2(SiMe_3)$ was purified by vacuum sublimation (*ca.* 10^{-2} mbar, 50 °C) yielding a waxy orange solid. Yield 1.33 g, 58%. Spectroscopic data matched those given in the literature.[21]

Preparation of $CpFe(CO)(PPh_3)(SiMe_3)$

The method employed for the formation of $CpFe(CO)(PPh_3)(SiMe_3)$ followed that reported by King and Pannell.[21] A solution of $CpFe(CO)(SiMe_3)$ (0.30 g, 1.2 mmol) and PPh_3 (0.31 g, 1.2 mmol) in hexane (40 cm^3) was subjected to UV irradiation at room temperature for 3.5 h. The reaction mixture was filtered and the solvent removed *in vacuo* yielding an orange solid which was recrystallised by cooling a dichloromethane/hexane mixture to -30 °C. Yield 0.26 g, 45%. Spectroscopic data matched those given in the literature.[21]

Preparation of $^{i}Pr_2NNa$ (NaDA)

The method employed for the formation of NaDA followed that reported by Munguia *et al.*[29] To a stirred solution of $^{i}Pr_2NH$ (1.1 cm^3, 8.0 mmol) in hexane (20 cm^3) at room temperature was added dropwise $^{n}BuLi$ (5.0 cm^3, 1.6 M in hexane, 8.0 mmol). After stirring for 1 h the reaction mixture was transferred onto a slurry of $NaO^{t}Bu$ (0.69 g, 7.2 mmol) also in hexane (10 cm^3) at room temperature and stirred for a further 12 h. The precipitate of

NaDA was isolated by filtration and washed with hexane (3 x 10 cm^3) and dried *in vacuo* and used without further purification. Yield 0.70 g, 79%.

Preparation of Na[Cp^{Si}Fe(CO)(PPh_3)] (Cp^{Si} = η^5-$C_5H_4SiMe_3$)

The method employed for the formation of Na[Cp^{Si}Fe(CO)(PPh_3)] followed minor modification from that reported by Munguia *et al*.[29] To a rapidly stirred suspension of NaDA (0.20 g, 1.6 mmol) in hexane (35 cm^3) at room temperature was added a solution of CpFe(CO)(PPh_3)($SiMe_3$) (0.77 g, 1.6 mmol) also in hexane (150 cm^3) and the reaction mixture stirred for 6 h. The resulting solution of Na[Cp^{Si}Fe(CO)(PPh_3)] was used *in situ* assuming quantitative conversion.

Preparation of $Dipp_2$NacNacH

The method employed for the formation of $Dipp_2$NacNacH followed that reported by Stender *et al*.[30] 12 M HCl (5 cm^3) was added to a solution of $DippNH_2$ (19.1 g, 107.7 mmol) and 2,4-pentanedione (4.45 g, 44.4 mmol) in ethanol (250 cm^3) and the reaction mixture refluxed for 3 d. After cooling to room temperature the solvent was removed *in vacuo* yielding a pale pink solid to which hexane (350 cm^3) was added and the resulting slurry refluxed for 1 h. After cooling to room temperature, the precipitate was isolated by filtration and dried *in vacuo* yielding a white powder. The solid hydrochloride salt was then treated with a saturated aqueous solution of Na_2CO_3 (200 cm^3) and dichloromethane (300 cm^3) and stirred for 30 min. The aqueous layer was extracted with dichloromethane (3 x 70 cm^3) and the organic fractions combined and dried over $MgSO_4$. Filtration and the removal of the solvent *in vacuo* yielded a white solid which was washed with cold (0 °C) methanol to remove traces of $DippNH_2$ and subsequently dried *in vacuo*. Yield 12.82 g, 66%. Spectroscopic data matched those given in the literature.[30]

Preparation of $Dipp_2NacNacLi{\cdot}OEt_2$

The method employed for the formation of $Dipp_2NacNacLi{\cdot}OEt_2$ followed that reported by Stender *et al*.[30] To a stirred solution of $Dipp_2NacNacH$ (8.64 g, 20.6 mmol) in diethyl ether (80 cm^3) at 0 °C was added dropwise ^{n}BuLi (12.9 cm^3, 1.6 M in hexane, 20.9 mmol) and the reaction mixture stirred for 12 h whilst attaining room temperature. Concentration and subsequent cooling of the reaction mixture to -30 °C yielded colourless crystals of $Dipp_2NacNacLi{\cdot}OEt_2$. Yield 7.20 g, 70%. Spectroscopic data matched those given in the literature.[30]

Preparation of $Dipp_2NacNacAlCl_2$

The method employed for the formation of $Dipp_2NacNacAlCl_2$ followed that reported by Stender *et al*.[31] A solution of $Dipp_2NacNacLi{\cdot}OEt_2$ (1.50 g, 3.0 mmol) in toluene (20 cm^3) was added dropwise to a slurry of $AlCl_3$ (0.41 g, 3.1 mmol) in toluene (30 cm^3) at 0 °C. After stirring for 12 h whilst attaining room temperature the reaction mixture was filtered and the filtrate concentrated and cooled to –30 °C affording colourless crystals of $Dipp_2NacNacAlCl_2$. Yield 0.91 g, 59%. Spectroscopic data matched those given in the literature.[31]

Preparation of $[Et_3Si][B(C_6F_5)_4]$

The method employed for the formation of $[Et_3Si][B(C_6F_5)_4]$ followed that reported by Lambert *et al*.[32] A solution of $[Ph_3C][B(C_6F_5)_4]$ in Et_3SiH (5 cm^3) was subjected to sonic agitation for 18 h. Filtration and removal of the solvent *in vacuo* yielded a white solid which was used without further purification with quantitative yield assumed.

Preparation of $Dipp_2$NacNacAl(Cl)(Me)

The method employed for the formation of $Dipp_2$NacNacAl(Cl)(Me) followed that reported by Zhu *et al*.[33] To a solution of $Dipp_2$NacNacLi·OEt_2 (0.99 g, 2.0 mmol) in toluene (25 cm^3) at -78°C was added dropwise $MeAlCl_2$ (2.0 cm^3, 1.0 M in hexane, 2.0 mmol). After stirring for 12 h whilst slowly attaining room temperature the reaction mixture was filtered and the solvent removed *in vacuo* to yield a white solid which was washed with hexane (2 x 10 cm^3) and dried *in vacuo*. Yield 0.41 g, 40%. Spectroscopic data matched those given in the literature.[33]

Preparation of $(Me_3Si)_2CHBr$

^{n}BuLi (148.0 cm^3, 1.6 M in hexane, 237.0 mmol) was added dropwise over 3 h to a solution of bromoform (29.90 g, 118.0 mmol) and Me_3SiCl (25.80 g, 237.0 mmol) in THF (200 cm^3) at -90 °C. The temperature of the solution was monitored during the addition to ensure that it remained close to -90 °C throughout the course of addition; it was then stirred for 18 h and allowed to attain room temperature slowly. The reaction mixture was filtered and the precipitate washed with light petroleum ether, combined with the filtrate and concentrated. The organic solution was washed with water (2 x 30 cm^3) and brine (3 x 50 cm^3) and dried over $MgSO_4$. Filtration followed by removal of the solvent *in vacuo* afforded a yellow oil which was purified by low pressure distillation and collected as a single colourless fraction distilling at 25 °C at 10^{-2} Torr. Yield 19.14 g, 68%. Purity was verified by ^{1}H NMR spectroscopy.

Preparation of $Li[CH(SiMe_3)_2]$

^{n}BuLi (8.3 cm^3, 1.6 M in hexane, 13.2 mmol) was added dropwise to a solution of $(Me_3Si)_2CHBr$ (3.150 g, 13.2 mmol) in diethyl ether (80 cm^3) -78 °C. After addition the

reaction mixture was maintained at -78 °C for 2 h and then warmed to room temperature. The solvent was removed *in vacuo* to yield a white solid which upon gentle warming under vacuum melted and further evaporation yielded a highly pyrophoric fine white powder which was used without further purification. Yield 1.88 g, 86%.

Preparation of K[CH(SiMe$_3$)$_2$]

A slurry of KO^{t}Bu (1.200 g, 10.7 mmol) in hexane (40 cm^3) was added to a slurry of Li[CH(SiMe$_3$)$_2$] (1.875 g, 11.3 mmol) also in hexane (40 cm^3) and the reaction mixture stirred for 18 h. The resulting white precipitate was isolated by filtration and washed with hexane (3 x 15 cm^3) and benzene (10 cm^3) and dried under vacuum. This highly pyrophoric white powder was used without further purification. Yield 1.46 g, 77%.

Preparation of K[Cp'Mn(CO)$_2$H]

The method employed for the formation of K[Cp'Mn(CO)$_2$]H followed that reported by Braunschweig and Ganter.[34] A solution of Cp'Mn(CO)$_3$ (9.60 g, 44.0 mmol) and (Ph)$_2$(Me)SiH (5.75 g, 29.0 mmol) in hexane (400 cm^3) was subjected to UV irradiation at -30 °C for 10 h. The reaction mixture was warmed to 0 °C and K[Et$_3$BH] (29.0 cm^3, 1.0 M in THF, 29.0 mmol) added dropwise, and the reaction mixture stirred for a further 1 h. A yellow precipitate formed which was washed with hexane (3 x 10 cm^3) and dried *in vacuo*. This highly pyrophoric yellow powder was used without further purification. Yield 2.30 g, 23%.

Preparation of Dipp$_2$NacNacAlH$_2$

The method employed for the formation of Dipp$_2$NacNacAlH$_2$ followed that reported by Cui *et al*.[35] A solution of Dipp$_2$NacNacH (2.50 g, 6.0 mmol) in hexane (40 cm^3) was added

to a slurry of $H_3Al{\cdot}NMe_3$ (0.56 g, 6.3 mmol) also in hexane (30 cm^3) at room temperature. After stirring for 48 h the reaction mixture was filtered and the filtrate concentrated and cooled to -30 °C affording colourless crystals of $Dipp_2NacNacAlH_2$. Yield 1.81 g, 68%. Spectroscopic data matched those given in the literature.[35]

Preparation of $(CO)_4M(cod)$ (M = Cr, W)

The method employed for the formation of $(CO)_4M(cod)$ (M = Cr, W) followed with minor modifications that reported by Kayran *et al*.[36] cod (4.0 cm^3, 32.6 mmol, M = Cr; 1.0 cm^3, 8.2 mmol, M = W) was added to a slurry of $M(CO)_6$ (0.75 g, 3.4 mmol, M = Cr; 0.20 g, 0.6 mmol, M = W) in hexane (30 cm^3) and subjected to UV irradiation at room temperature until all $M(CO)_6$ had been consumed, as determined by IR spectroscopy (M = Cr , 45 h; M = W, 8 h). The reaction mixture was filtered and the solvent removed *in vacuo* yielding a yellow solid. Extraction with hexane, concentration and cooling to -30 °C afforded yellow crystals of $(CO)_4M(cod)$. Yield M = Cr, 0.40 g, 53.0%; M = W, 0.06 g, 26%. Spectroscopic data matched those given in the literature.[36]

Preparation of $(CO)_4Mo(cod)$

The method employed for the formation of $(CO)_4Mo(cod)$ followed with minor modifications that reported by Kayran *et al*.[36] A slurry of $Mo(CO)_6$ (1.00 g, 3.7 mmol) and cod (2.0 cm^3, 16.3 mmol) in *n*-heptane (40 cm^3) was refluxed for 24 h. After cooling to room temperature the solvent was removed *in vacuo* yielding a brown solid. Cooling a concentrated hexane solution to -30 °C afforded dark yellow crystals of $(CO)_4Mo(cod)$. Yield 0.81 g, 64%. Spectroscopic data matched those given in the literature.[36]

Preparation of $(CO)_5Cr(coe)$

The method employed for the formation of $(CO)_5Cr(coe)$ followed minor modification from that reported by Grevels and Skibbe.[37] A slurry of $Cr(CO)_6$ (0.20 g, 0.9 mmol) and coe (1.0 cm^3, 7.7 mmol) in pentane (25 cm^3) was subjected to UV photolysis at room temperature for 8 h. The resulting yellow solution was used *in situ* assuming quantitative yield.

2.4 References for Chapter II

1. R. J. Errington, *Advanced Practical Inorganic and Metalorganic Chemistry*, Blackie Academic & Professional, London, 1997.
2. R. E. Dodd and P. L. Robinson, *Experimental Inorganic Chemistry. A Guide to Laboratory Practice*, Elsevier Publishing Co.: Amsterdam, 1954.
3. D. Shriver and M. Drezden, *The Manipulation of Air-Sensitive Compounds*, Wiley - Interscience, 1986.
4. A. T. Lubben, J. S. McIndoe and A. S. Weller, *Organometallics*, 2008, **27**, 3303.
5. J. Cosier and A. M. Glazer, *J. Appl. Cryst.*, 1986, **19**, 105.
6. Z. Otwinowski and W. Minor, *Processing of X-Ray Diffraction Data Collected in Oscillation Mode, Methods Enzymol.*, Sweet, Academic Press, 1997.
7. A. Altomare, G. Cascarano, C. Giacovazzo and A. Guagliardi, *J. Appl. Cryst.*, 1993, **26**, 343.
8. L. Palatinus and G. Chapuis, *J. Appl. Cryst.*, 2007, **40**, 786.
9. A. L. Thompson and D. J. Watkin, *J. Appl. Cryst.*, 2011, **44**, 1017.
10. R. I. Cooper, A. L. Thompson and D. J. Watkin, *J. Appl. Cryst.*, 2010, **43**, 1100.
11. G. M. Sheldrick, *Acta Cryst. Section A*, 2008, **64**, 112.
12. G. T. Velde, F. M. Bickelhaupt, E. J. Baerends, C. F. Guerra, S. J. A. Van Gisbergen, J. G. Snijders and T. Ziegler, *J. Comput. Chem.*, 2001, **22**, 931.
13. C. F. Guerra, J. G. Snijders, G. te Velde and E. J. Baerends, *Theor. Chem. Acc.*, 1998, **99**, 391.
14. S. ADF2012, Theoretical Chemistry, Vrije Universiteit, Amsterdam. The Netherlands. http://www.scm.com.
15. A. D. Becke, *Phys. Rev. A*, 1988, **38**, 3098.
16. J. P. Perdew, *Phys. Rev. B*, 1986, **33**, 8822.

17. G. Snijders, P. Vernooijs and E. J. Baerends, *At. Data Nucl. Data Tables*, 1982, **26**, 483.

18. A. Rosa, A. W. Ehlers, E. J. Baerends, J. G. Snijders and G. T. Velde, *J. Phys. Chem.*, 1996, **100**, 5690.

19. S. F. Boys and F. Bernardi, *Mol. Phys.*, 1970, **19**, 553.

20. S. L. Aeilts, M. P. Coles, D. G. Swenson, R. F. Jordan and V. G. Young, *Organometallics*, 1998, **17**, 3265.

21. R. B. King and K. H. Pannell, *Inorg. Chem.*, 1968, **7**, 1510.

22. D. L. Reger, T. D. Wright, C. A. Little, J. J. S. Lamba and M. D. Smith, *Inorg. Chem.*, 2001, **40**, 3810.

23. M. Brookhart, B. Grant and A. F. Volpe, *Organometallics*, 1992, **11**, 3920.

24. M. Findlater, N. J. Hill and A. H. Cowley, *Dalton Trans.*, 2008, 4419.

25. G. X. Jin, C. Jones, P. C. Junk, K. A. Lippert, R. P. Rose and A. Stasch, *New J. Chem.*, 2009, **33**, 64.

26. J. K. Ruff and M. F. Hawthorne, *J. Am. Chem. Soc.*, 1960, **82**, 2141.

27. S. J. Bonyhady, D. Collis, G. Frenking, N. Holzmann, C. Jones and A. Stasch, *Nature Chem.*, 2010, **2**, 865.

28. C. Wang, G. Erker, G. Kehr, K. Wedeking and R. Frohlich, *Organometallics*, 2005, **24**, 4760.

29. T. Munguia, Z. A. Bakir, F. Cervantes-Lee, A. Metta-Magana and K. H. Pannell, *Organometallics*, 2009, **28**, 5777.

30. M. Stender, R. J. Wright, B. E. Eichler, J. Prust, M. M. Olmstead, H. W. Roesky and P. P. Power, *J. Chem. Soc. Dalton Trans.*, 2001, **23**, 3465.

31. M. Stender, B. E. Eichler, N. J. Hardman, P. P. Power, J. Prust, M. Noltemeyer and H. W. Roesky, *Inorg. Chem.*, 2001, **40**, 2794.

32. J. B. Lambert, S. Z. Zhang and S. M. Ciro, *Organometallics*, 1994, **13**, 2430.

33. H. P. Zhu, J. F. Chai, C. He, G. C. Bai, H. W. Roesky, V. Jancik, H. G. Schmidt and M. Noltemeyer, *Organometallics*, 2005, **24**, 380.

34. H. Braunschweig and B. Ganter, *J. Organomet. Chem.*, 1997, **545**, 163.

35. C. Cui, H. W. Roesky, H. J. Hao, H. G. Schmidt and M. Noltemeyer, *Angew. Chem. Int. Ed.*, 2000, **39**, 1815.

36. C. Kayran, F. Kozanoglu, S. Ozkar, S. Saldamli, A. Tekkaya and C. G. Kreiter, *Inorg. Chim. Acta*, 1999, **284**, 229.

37. F. W. Grevels and V. Skibbe, *J. Chem. Soc. Chem. Commun.*, 1984, **11**, 681.

3 Amidinate and Guanidinate Supported Aluminium-Iron Complexes

3.1 Introduction

N,N'-chelating substituents impart both thermodynamic stability and kinetic inertness to metal complexes as a combined result of strong σ-donor properties and the chelate effect. Within this sphere, the amidinate and guanidinate classes of substituent have received much attention in the literature as novel substituents for the stabilisation of low coordinate and/or low oxidation state complexes (Figure 3.1).

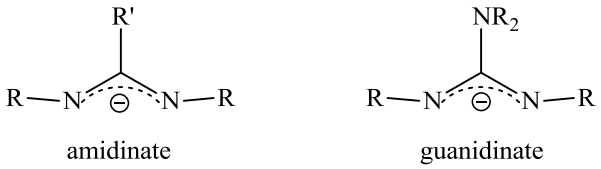

Figure 3.1: *Amidinate and guanidinate substituents*

These types of substituent, particularly those incorporating highly sterically demanding aryl functionalities, have been shown to stabilise a number of low valent and/or low oxidation state compounds from across the Periodic Table, and this chemistry has recently been reviewed in detail.[1,2] The application of highly sterically demanding amidinates and

guanidinates has been pioneered by Jones and co-workers who showed that these substituents could stabilise the formation of N-heterocyclic carbene analogues of gallium, indium and thallium. The N-heterocyclic carbene analogues $Cy_2NC(ArN)_2E$ (E = Ga **3.1** or In **3.2**; Ar = 2,6-di*iso*propylphenyl) have been structurally characterised in which the group 13 element is *N,N'*-chelated forming a four-membered heterocycle and is in the +1 oxidation state (Figure 3.2).

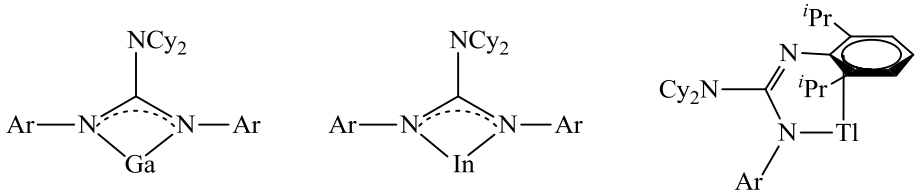

3.1 **3.2** **3.3**

Figure 3.2: *Solid state structures of **3.1-3.3***

However, for E = Tl (**3.3**) a *N,N'*-chelating motif in the solid state is not observed. Rather an interaction with a flanking arene ring occurs, presumably reflecting the size of the thallium(I) centre.[3] The coordination chemistry of the four-membered heterocycles **3.1** and **3.2** has been investigated, revealing that the gallium centre is more nucleophilic than indium.[4,5] Interestingly, the related amidinate complexes $^{t}BuC(ArN)_2E$ are not formed under similar conditions, with either a flanking arene interaction analogous to **3.3** or a dimeric E(II) species being formed instead.[6,7]

In group 14 chemistry, the dimeric germanium(I) species $[RC(ArN)_2Ge]_2$ (where R = ^{t}Bu **3.4** or N^{i}Pr$_2$ **3.5**; Ar = 2,6-di*iso*propylphenyl) were isolated *via* reduction of the corresponding germanium(II) chloride complexes $RC(ArN)_2GeCl$.[8] The geometry and coordination behaviour of these amidinate and guanidinate supported complexes are reminiscent of the more sterically demanding six-membered heterocyclic β-diketiminate

systems, giving an indication of the relative steric and electronic stabilisation these ligands can afford.

The ability to support dimeric low oxidation state species has subsequently been extended to magnesium with the formation of the guanidinate supported magnesium(I) dimer [^{i}Pr$_2$NC(ArN)$_2$Mg]$_2$ (**3.6**), which shows remarkable thermal and kinetic stability.[9] The stability of **3.6** and its comparative ease of preparation has seen it develop into a bespoke and mild reducing agent for organometallic complexes.

There has been much interest in aluminium amidinate and guanidinate substituted species due to the high Lewis acidity of aluminium. Such species have been investigated as precursors for the formation of aluminium cations for Lewis acid catalysed olefin polymerisation chemistry. Jordan and co-workers investigated the effects of ligand substituents on amidinate-supported alkyl aluminium systems of the type MeC(RN)$_2$AlMe$_2$ (R = ^{i}Pr **3.7** or Cy **3.8**), ^{t}BuC(RN)$_2$AlMe$_2$ (R = ^{i}Pr **3.9**, Cy **3.10** or SiMe$_3$ **3.11**) and the related dichloride precursors MeC(^{i}PrN)$_2$AlCl$_2$ (**3.12**) and ^{t}BuC(RN)$_2$AlCl$_2$ (R = ^{i}Pr **3.13**, or SiMe$_3$ **3.14**). Structural characterisation showed **3.7**-**3.14** to be monomeric and to feature a chelating amidinate substituent. Furthermore, these studies revealed that the more sterically demanding ligand substituents pushed forward the flanking R groups, thereby increasing the steric protection of the aluminium centre and favouring a chelating binding motif.[10] The same group carried out similar investigations of the related alkyl aluminium guanidinate systems R$_2$NC(^{i}PrN)$_2$AlMe$_2$ (R = Me **3.15**, Et **3.16**, ^{i}Pr **3.17**) and their dichloride precursors R$_2$NC(^{i}PrN)$_2$AlCl$_2$ (R = Me **3.18**, Et **3.19**, ^{i}Pr **3.20**, SiMe$_3$ **3.21**). Structural characterisation also showed **3.15**-**3.21** to be monomeric with the guanidinate chelating the aluminium centre.[11]

Amidinate precursors of the type R'C(RN)$_2$EX$_2$ (where E = group 13 element; X = halogen) were identified by Aldridge, Jones and co-workers as suitable reagents for the

formation of transition metal-group 13 bonds *via* salt metathesis reactions with transition metal anions. This work led to the structural characterisation of a number of complexes containing transition metal-group 13 bonds, notably, $CpFe(CO)_2[(X)E(NCy)_2C^tBu]$ (X = Cl and E = Al **1.10**, Ga **1.11**; X = Br and E = In **1.12**) (Scheme 3.1).

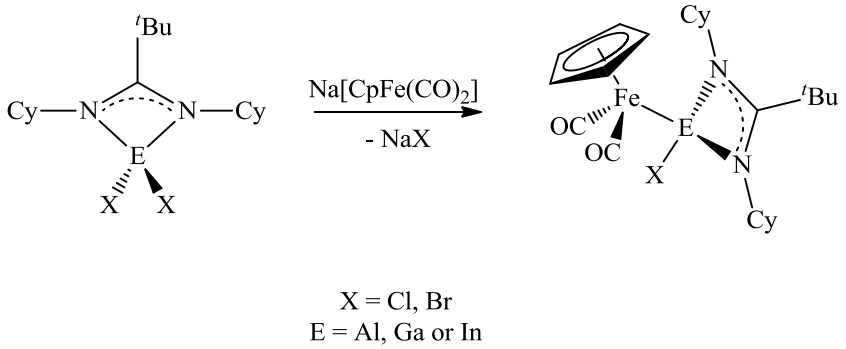

Scheme 3.1: *General synthesis of **1.10-1.12***

The halide abstraction chemistry of **1.10-1.12** was also investigated and the cationic gallium species $[CpFe(CO)_2\{(Et_2O)Ga(NCy)_2C^tBu\}][BAr^f_4]$ (**1.13**) was characterised as the only isolable product of such chemistry.[12]

3.2 Aims of the Present Research

With the success of halide abstraction chemistry for the formation of cationic terminal borylene systems of the type $[CpFe(CO)_2(BNR_2)][BAr^f_4]$ as well as the remarkable increase in stability achieved by the substitution of π-acidic carbonyl ligands for trialkyl phosphines,[13,14] the synthesis of heavier group 13 analogues (*e.g.* featuring aluminium or gallium donors) represents an interesting synthetic challenge. Furthermore, the characterisation of the base stabilised amidinate-substituted gallium cation $[CpFe(CO)_2\{(Et_2O)Ga(NCy)_2C^tBu\}][BAr^f_4]$ (**1.13**) provides encouraging prospects for the

isolation of related aluminium cations through the use of suitably sterically demanding and electron rich guanidinate substituents (Scheme 3.2).

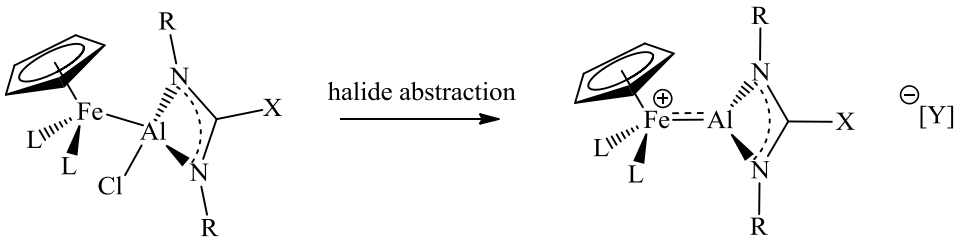

Scheme 3.2: *Halide abstraction to form a cationic three-coordinate aluminium complex*

3.3 Experimental

***Preparation of PhC(CyN)$_2$AlCl$_2$* (I)**

A solution of phenyl lithium (1.92 g, 22.9 mmol) in diethyl ether (20 cm^3) was added slowly at room temperature to a stirred solution of *N*,*N'*-di*cyclo*hexylcarbodiimide (4.72 g, 22.9 mmol) also in diethyl ether (20 cm^3). The reaction mixture was stirred for 3 h and a white precipitate formed. The resulting suspension was cooled to -78 °C and added slowly to a solution of $AlCl_3$ (3.67 g, 27.5 mmol) also in diethyl ether (25 cm^3) at -78 °C. After stirring for 18 h and slowly attaining room temperature the solvent was removed *in vacuo* to yield a white solid. Extraction with hexane (4 x 25 cm^3) yielded a colourless solution which was concentrated and slowly cooled to -30 °C allowing a small amount of oil to form. The supernatant solution was decanted and stored at -30 °C for 48 h affording colourless crystals of **I**. Yield 2.57 g, 30%.

Spectroscopic Data: ^{1}H NMR (C_6D_6, 300 MHz, 298 K): δ 6.89-6.92 (3H, m, Ar*H*), 6.74-6.77 (2H, m, Ar*H*), 2.82-2.92 (2H, m, NC*H*CH$_2$), 0.78-1.70 (20H, m, Cy*H*). ^{13}C{^{1}H} NMR (C_6D_6, 75 MHz, 298 K): δ 178.7 (s, *C*N$_2$), 130.4 (s, Ar*C*), 129.0 (s, Ar*C*), 126.8 (s, Ar*C*), 123.6 (s, Ar*C*), 53.4 (s, NCHCH$_2$), 35.5 (s, Cy*C*), 25.2 (s, Cy*C*), 24.8 (s, Cy*C*). ^{27}Al NMR (C_6D_6, 78 MHz, 298 K): δ 104.

Crystallographic data: $C_{19}H_{27}AlCl_2N_2$, M_r = 381.32, monoclinic, *P* 2$_1$/n, *a* = 9.95849(8), *b* = 9.27693(6), *c* = 22.8557(1) Å, β = 101.6000(7)°, *V* = 2068.37(3) Å^3, *Z* = 4, ρ_c = 1.224 Mg m^{-3}, *T* = 150 K, λ = 1.54180 Å. 22074 reflections collected, 4339 independent [R(int) = 0.020] used in all calculations. R_1 = 0.0346, wR_2 = 0.0949 for observed unique reflections [$I > 2\sigma(I)$] and R_1 = 0.0350, wR_2 = 0.0954 for all unique reflections. Max. and min. residual electron densities 0.37 and -0.35 e Å^{-3}. CCDC reference: 894967.

***Preparation of PhC(^{i}PrN)$_2$AlCl$_2$* (II)**

To a stirred solution of phenyl lithium (0.76 g, 9.1 mmol) in diethyl ether (30 cm^3) was added dropwise at room temperature *N*,*N'*-di*iso*propylcarbodiimide (1.4 cm^3, 9.1 mmol). The reaction mixture was stirred for 2 h then cooled to -78 °C, and added slowly to a solution of $AlCl_3$ (1.45 g, 11.0 mmol) also in diethyl ether (20 cm^3) at -78 °C. After stirring for 18 h and slowly attaining room temperature, the solvent was removed *in vacuo* to yield a white solid. Extraction with hexane (3 x 15 cm^3) yielded a colourless solution which was concentrated and slowly cooled to -30 °C allowing a small amount of oil to form. The supernatant solution was decanted and stored at -30 °C for 48 h affording colourless crystals of **II**. Yield 1.30 g, 47%.

Spectroscopic Data: ^{1}H NMR (C_6D_6, 300 MHz, 298 K): δ 6.89-6.92 (3H, m, Ar*H*), 6.60-6.63 (2H, m, Ar*H*), 3.01 (2H, sept ($^3J_{HH}$ = 5.7 Hz), NC*H*(CH$_3$)$_2$), 0.89 (12H, d ($^3J_{HH}$ = 5.7 Hz), NCH(C*H*$_3$)$_2$). ^{13}C{^{1}H} NMR (C_6D_6, 75 MHz, 298 K): δ 178.5 (s, *C*N$_2$), 130.4 (s, Ar*C*), 129.0 (s, Ar*C*), 127.3 (s, Ar*C*), 126.7 (s, Ar*C*), 46.1 (s, N*C*H(CH$_3$)$_2$), 25.0 (s, NCH(*C*H$_3$)$_2$). ^{27}Al NMR (C_6D_6, 78 MHz, 298 K): δ 105.

Crystallographic data: $C_{13}H_{19}AlCl_2N_2$, M_r = 301.2, monoclinic, *C* 2/c, *a* = 13.4052(3), *b* = 11.0555(2), *c* = 11.9482(2) Å, β = 113.5072(9)^o, *V* = 1623.78(6) Å^3, *Z* = 4, ρ_c = 1.232 Mg m^{-3}, *T* = 150 K, λ = 0.71073 Å. 3610 reflections collected, 1845 independent [R(int) = 0.023] used in all calculations. R_1 = 0.0297, wR_2 = 0.0772 for observed unique reflections [$I > 2\sigma(I)$] and R_1 = 0.0333, wR_2 = 0.0799 for all unique reflections. Max. and min. residual electron densities 0.31 and -0.28 e Å^{-3}. CCDC reference: 894958.

***Preparation of ^{i}Pr$_2$NC(CyN)$_2$AlCl$_2$* (III)**

To a stirred solution of *N*,*N'*-di*cyclo*hexylcarbodiimide (5.19 g, 25.0 mmol) in diethyl ether (30 cm^3) at 0 °C was added slowly a solution of LDA (2.68 g, 25.0 mmol) also in diethyl

ether (25 cm^3). The reaction mixture was stirred for 2 h and a white precipitate formed. The resulting suspension was cooled to -78 °C and added to a solution of $AlCl_3$ (3.61 g, 27.0 mmol) also in diethyl ether (40 cm^3) at -78 °C. After stirring for 18 h and slowly attaining room temperature, the solvent was removed *in vacuo* to yield a white solid. Extraction with toluene (3 x 20 cm^3) yielded a pale yellow solution which was concentrated and subsequently cooled to -30 °C affording colourless crystals of **III**. Yield 6.2 g, 61%.

Spectroscopic Data: ^{1}H NMR (C_6D_6, 300 MHz, 298 K): δ 3.34 (2H, sept ($^3J_{HH}$ = 6.3 Hz), NC*H*$(CH_3)_2$), 3.03 (2H, m, NC*H* of Cy), 1.88-0.98 (20H, m, Cy*H*), 0.93 (12H, d ($^3J_{HH}$ = 6.3 Hz), $CH(CH_3)_2$). $^{13}C\{^1H\}$ NMR (C_6D_6, 75 MHz, 298 K): δ 172.7 (s, *C*N_3), 54.3 (s, N*C*$H(CH_3)_2$), 50.5 (s, N*C*H of Cy), 36.0 (s, Cy*C*), 26.2 (s, Cy*C*), 25.9 (s, Cy*C*), 23.3 (s, $CH(CH_3)_2$). ^{27}Al NMR (C_6D_6, 78 MHz, 298 K): δ 104.

Crystallographic data: $C_{19}H_{36}AlCl_2N_3$, M_r = 404.40, monoclinic, *C*2/c, 1 *a* = 18.7208(8), *b* = 10.1409(4), *c* = 12.0592(6) Å, β = 91.8321(19)°, *V* = 2288.22(18) Å^3, *Z* = 4, ρ_c = 1.174 Mg m^{-3}, *T* = 150 K, λ = 0.71073 Å. 11690 reflections collected, 2587 independent [R(int) = 0.031] used in all calculations. R_1 = 0.0405, wR_2 = 0.1023 for observed unique reflections [$I > 2\sigma(I)$] and R_1 = 0.0507, wR_2 = 0.1077 for all unique reflections. Max. and min. residual electron densities 0.33 and -0.30 e $Å^{-3}$. CCDC reference: 894957

***Preparation of ^{i}Pr$_2$NC(CyN)$_2$Al(Cl)(Me)* (X)**

To a stirred solution of *N*,*N'*-di*cyclo*hexylcarbodiimide (1.86 g, 9.0 mmol) in diethyl ether (15 cm^3) at 0 °C was added slowly a solution of LDA (0.96 g, 9.0 mmol) also in diethyl ether (15 cm^3). The reaction mixture was stirred for 2 h and a white precipitate formed. The resulting suspension was cooled to -78 °C and $MeAlCl_2$ (9.0 cm^3, 1.0 M in hexane, 9.0 mmol) was added dropwise. After stirring for 18 h and slowly attaining room temperature, the solvent was removed *in vacuo* to yield a white solid. Extraction with toluene (3 x 10

cm^3) yielded a colourless solution which was concentrated and subsequently cooled to -30 °C affording colourless crystals of **X**. Yield 1.78 g, 52%.

Spectroscopic Data: ^{1}H NMR (C_6D_6, 300 MHz, 298 K): δ 3.28 (2H, sept, ($^3J_{HH}$ = 6.6 Hz), NC*H*(CH_3)$_2$), 3.08 (2H, m, NC*H* of Cy), 1.93-1.02 (20H, m, Cy*H*), 0.97 (12H, d ($^3J_{HH}$ = 6.6 Hz), -0.06 (3H, s, AlC*H*$_3$). ^{13}C{^{1}H} NMR (C_6D_6, 75 MHz, 298 K): δ 170.9 (s, *C*N_3), 53.5 (s, N*C*H), 49.4 (s, N*C*H), 36.2 (s, Cy*C*), 35.9 (s, Cy*C*), 26.0 (s, Cy*C*), 25.9 (s, Cy*C*), 25.7 (s, Cy*C*), 23.0 (s, NCH_2(*C*H_3)$_2$), -9.1 (br, Al-*C*H_3). ^{27}Al NMR (C_6D_6, 78 MHz, 298 K): δ 128.

Preparation of CpFe(CO)$_2$[(Cl)Al{(N^{i}Pr)$_2$CPh}] **(V)**

To a slurry of Na[CpFe(CO)$_2$] (0.23 g, 1.15 mmol) in diethyl ether (25 cm^3) at -78 °C was added slowly a solution of **I** (0.30 g, 1.00 mmol) also in diethyl ether (25 cm^3) and the reaction mixture stirred for 12 h whilst slowly attaining room temperature. The resulting mixture was filtered, concentrated and subsequently cooled to -30 °C affording colourless crystals of **V**. Yield 0.22 g, 52%.

Spectroscopic Data: ^{1}H NMR (C_6D_6, 300 MHz, 298 K): δ 7.01-6.89 (5H, m, Ar*H*), 4.43 (5H, s, Cp*H*), 3.22 (2H, sept ($^3J_{HH}$ = 6.0 Hz), NC*H*(CH_3)$_2$), 1.23 (6H, d ($^3J_{HH}$ = 6.0), NCH(C*H*$_3$)$_2$), 1.01 (6H, d ($^3J_{HH}$ = 6.0), NCH(C*H*$_3$)$_2$). ^{13}C{^{1}H} NMR (C_6D_6, 75 MHz, 298 K): δ 217.1 (*C*O), 174.8 (*C*N_2), 130.8 (Ar*C*), 130.3 (Ar*C*), 129.6 (Ar*C*), 127.7 (Ar*C*), 82.6 (Cp*C*), 47.1 (N*C*H(CH_3)$_2$), 25.9 (NCH(*C*H_3)$_2$), 25.5 (NCH(*C*H_3)$_2$). ^{27}Al NMR (C_6D_6, 78 MHz, 298 K): δ 167. MS(EI): *m*/*z* 442.0 (M^+) 1 %; accurate mass: calc. 442.0684, meas. 442.0686. IR (CH_2Cl_2 solution, cm^{-1}): 1964, 1899 cm^{-1} (ν_{CO}).

Crystallographic data: $C_{20}H_{24}AlClFeN_2O_2$, M_r = 442.70, monoclinic, *P* 2_1/c, *a* = 9.9088(2), *b* = 12.3092(3), *c* = 17.7168(4) Å, β = 93.0773(10)^o, *V* = 2157.79(8) Å^3, *Z* = 4, ρ_c = 1.363 Mg m^{-3}, *T* = 150 K, λ = 0.71073 Å. 9335 reflections collected, 4907 independent [R(int) = 0.033] which were used in all calculations. R_1 = 0.0458, wR_2 = 0.1224 for observed unique

reflections [$I > 2\sigma(I)$] and R_1 = 0.0675, wR_2 = 0.1365 for all unique reflections. Max. and min. residual electron densities 0.90 and -0.78 e Å^{-3}. CCDC reference: 857132.

***CpM(CO)$_2$[(Cl)Al{(NCy)$_2$CN^{i}Pr$_2$}]* (VI: M = Fe; VIII: M = Ru)**

The two compounds were prepared from **III** in a similar manner, exemplified here for CpFe(CO)$_2$[(Cl)Al{(NCy)$_2$CN^{i}Pr$_2$}]. To a slurry of Na[CpFe(CO)$_2$] (0.28 g, 1.40 mmol) in diethyl ether (30 cm^3) at -78 °C was added slowly to a solution of **III** (0.50 g, 1.32 mmol) also in diethyl ether (35 cm^3), and the reaction mixture stirred for 12 h whilst slowly attaining room temperature. Filtration, concentration and cooling to -30 °C afforded colourless crystals of **VI**. Yield 0.42 g, 58%.

***Spectroscopic Data for* VI:** ^{1}H NMR (C_6D_6, 300 MHz, 298 K): δ 4.46 (5H, s, Cp*H*), 3.31 (4H, m, overlapping NC*H*(CH$_3$)$_2$ and NC*H* of Cy), 1.12-2.16 (20H, m, Cy*H*), 1.08 (12H, d ($^3J_{HH}$ = 6.6 Hz), CH(C*H*$_3$)$_2$). ^{13}C{^{1}H} NMR (C_6D_6, 75 MHz, 298 K): δ 216.9 (*C*O), 170.0 (*C*N$_3$), 82.3 (Cp*C*), 54.4 (N*C*H), 49.5 (N*C*H), 36.7 (Cy*C*), 36.5 (Cy*C*), 26.7 (Cy*C*), 26.6 (Cy*C*), 26.4 (Cy*C*), 23.3 (NCH$_2$(*C*H$_3$)$_2$). ^{27}Al NMR (C_6D_6, 78 MHz, 298 K): δ 163. MS(EI): *m*/*z* 545.3 (M$^+$) 6 %, 489.2 [M-2CO]$^+$ 1 %, 368.3 [M-{CpFe(CO)$_2$}]$^+$ 44 %; accurate mass: calc. 543.2093, meas. 543.2092. IR (CH_2Cl_2 solution, cm^{-1}): 1973, 1912 (ν_{CO}).

***Crystallographic data* VI:** $C_{26}H_{41}AlClFeN_3O_2$, M_r = 545.91, triclinic, *P*-1, *a* = 9.8974(6), *b* = 11.2803(6), *c* = 12.8172(8) Å, α = 81.952(3), β = 83.391(3), γ = 82.656(2)°, *V* = 1398.37(14) Å^3, *Z* = 2, ρ_c = 1.296 Mg m^{-3}, *T* = 150 K, λ = 0.71073 Å. 20032 reflections collected, 6368 independent [R(int) = 0.082] which were used in all calculations. R_1 = 0.0621, wR_2 = 0.1047 for observed unique reflections [$I > 2\sigma(I)$] and R_1 = 0.1082, wR_2 = 0.1224 for all unique reflections. Max. and min. residual electron densities 1.05 and -0.88 e Å^{-3}. CCDC reference: 894959.

***Spectroscopic data for* VIII:** ^{1}H NMR (C_6D_6, 300 MHz, 298 K): δ 4.89 (5H, s, Cp*H*), 3.28 (2H, sept, ($^{3}J_{HH}$ = 6.3 Hz) NC*H*$(CH_3)_2$), 3.23 (2H, m, NC*H* of Cy), 1.14-2.12 (20H, m, Cy*H*), 1.04 (12H, d ($^{3}J_{HH}$ = 6.3 Hz), CH(C*H*$_3)_2$). ^{13}C{^{1}H} NMR (C_6D_6, 75 MHz, 298 K): δ 204.0 (*C*O), 169.5 (*C*N_3), 85.7 (Cp*C*), 53.9 (N*C*H), 49.1 (N*C*H), 36.5 (Cy*C*, 2 overlapping signals), 36.2 (Cy*C*), 26.3 (NCH$_2$(*C*H$_3)_2$), 26.0 (Cy*C*), 22.9 (Cy*C*). ^{27}Al NMR (C_6D_6, 78 MHz, 298 K): δ 154. MS(EI): *m*/*z* 591.2 (M^+) 3 %, 563.2 $[M\text{-}CO]^+$ 3%; accurate mass: calc. 585.1773, meas. 585.1769. IR (CH_2Cl_2 solution, cm^{-1}): 1989, 1927 (ν_{CO}).

***Crystallographic Data for* VIII:** $C_{26}H_{41}AlClRuN_3O_2$, M_r = 591.14, triclinic, *P*-1, *a* = 8.1221(1), *b* = 10.1843(1), *c* = 18.3237(2) Å, α = 94.1715(5), β = 95.1909(5), γ = 110.9440(6)^{o}, *V* = 1400.72(3) Å^3, *Z* = 2, ρ_c = 1.401 Mg m^{-3}, *T* = 150 K, λ = 0.71073 Å. 21533 reflections collected, 6397 independent [R(int) = 0.031] which were used in all calculations. R_1 = 0.0302, wR_2 = 0.0652 for observed unique reflections [$I > 2\sigma(I)$] and R_1 = 0.0366, wR_2 = 0.0720 for all unique reflections. Max. and min. residual electron densities 0.80 and -0.48 e Å^{-3}. CCDC reference: 894961.

***Preparation of CpFe(CO)$_2$[(Cl)Al {(N^{i}Pr)$_2$CN^{i}Pr$_2$}]* (VII)**

To a slurry of Na[CpFe(CO)$_2$] (0.68 g, 3.40 mmol) in diethyl ether (50 cm^3) at -78 °C was added slowly a solution of **3.20** (1.01 g, 3.12 mmol) also in diethyl ether (55 cm^3) and the reaction mixture stirred for 12 h whilst slowly attaining room temperature. The resulting mixture was filtered, concentrated and subsequently cooled to -30 °C affording colourless crystals of **VII**. Yield 0.56 g, 38%.

Spectroscopic Data: ^{1}H NMR (C_6D_6, 300 MHz, 298 K): δ 4.23 (5H, s, Cp*H*), 3.62 (2H, sept ($^{3}J_{HH}$ = 6.6 Hz), NC*H*$(CH_3)_2$), 3.32 (2H, sept ($^{3}J_{HH}$ = 6.6 Hz), NC*H*$(CH_3)_2$), 1.33 (6H, d ($^{3}J_{HH}$ = 6.6 Hz), NCH(C*H*$_3)_2$), 1.15 (6H, d ($^{3}J_{HH}$ = 6.6 Hz), NCH(C*H*$_3)_2$), 1.04 (12H, d ($^{3}J_{HH}$ = 6.6 Hz), NCH(C*H*$_3)_2$). ^{13}C{^{1}H} NMR (C_6D_6, 75 MHz, 298 K): δ 216.8 (*C*O), 169.8

(*C*N_3), 82.0 (Cp*C*), 49.3 N*C*H(CH_3)$_2$), 45.7 (N*C*H(CH_3)$_2$), 25.6 (NCH(*C*H_3)$_2$), 25.4 (NCH(*C*H_3)$_2$), 23.3 (NCH(*C*H_3)$_2$). ^{27}Al NMR (C_6D_6, 78 MHz, 298 K): δ 160. IR (CH_2Cl_2 solution, cm^{-1}): 1973, 1893 (ν_{CO}). Elemental microanalysis: calc. for $C_{20}H_{33}N_3AlClFeO_2$ C 51.55 H 7.14 N 9.02; meas. C 51.41 H 7.02 N 8.93.

Crystallographic Data: $C_{20}H_{33}AlClFeN_3O_2$, M_r = 465.78, triclinic, *P*-1, *a* = 8.7289(1), *b* = 15.4840(2), *c* = 17.7812(3) Å, α = 92.0036(7), β = 92.502(1), γ = 100.7188(6)°, *V* = 2356.82(6) Å^3, *Z* = 4, ρ_c = 1.313 Mg m^{-3}, *T* = 150 K, λ = 0.71073 Å. 34511 reflections collected, 10737 independent [R(int) = 0.053] which were used in all calculations. R_1 = 0.0729, wR_2 = 0.2018 for observed unique reflections [$I > 2\sigma(I)$] and R_1 = 0.0929, wR_2 = 0.2231 for all unique reflections. Max. and min. residual electron densities 1.06 and -0.65 e Å^{-3}. CCDC reference: 894960.

***Preparation of CpFe(CO)$_2$[(Me)Al{(NCy)$_2$CN^{i}Pr$_2$}]* (IX)**

Method A: To a slurry of Na[CpFe(CO)$_2$] (0.38 g, 1.9 mmol) in diethyl ether (35 cm^3) at -78 °C was added slowly a solution of **X** (0.638 g, 1.66 mmol) also in diethyl ether (40 cm^3) and the reaction mixture stirred for 12 h whilst slowly attaining room temperature. The resulting mixture was filtered, concentrated and subsequently cooled to -30 °C affording colourless crystals of **IX**. Yield 0.42 g, 49%.

Method B: Alternatively, to a solution of CpFe(CO)$_2$[(Cl)Al{(NCy)$_2$CN^{i}Pr$_2$}] (0.30 g, 0.66 mmol) in diethyl ether (30 cm^3) at -78 °C was added dropwise MeLi (0.43 cm^3, 1.6 M in diethyl ether, 0.69 mmol). After stirring for 12 h and slowly warming to room temperature, the solvent was removed *in vacuo* to yield an orange solid. Extraction with hexane (3 x 15 cm^3) and subsequent cooling of the concentrated hexane extract yielded colourless crystals of **IX**.

Spectroscopic Data: ^{1}H NMR (C_6D_6, 300 MHz, 298 K): δ 4.37 (5H, s, Cp*H*), 3.30-3.22 (4H, m, overlapping NC*H*), 1.95-1.10 (20H, m, Cy*H*), 1.04 (12H, d ($^{3}J_{HH}$ = 6.3 Hz) CH(C*H*$_3$)$_2$), -0.06 (3H, s, AlC*H*$_3$). ^{13}C{^{1}H} NMR (C_6D_6, 125 MHz, 298 K): δ 218.0 (*C*O), 166.5 (*C*N$_3$), 81.2 (Cp*C*), 53.8 (N*C*H of Cy), 48.7 (br, N*C*H(CH$_3$)$_2$), 36.5 (Cy*C*), 36.4 (Cy*C*), 26.5 (Cy*C*), 26.3 (Cy*C*), 26.1 (s, Cy*C*), 23.0 (NCH$_2$(*C*H$_3$)$_2$), -2.8 (br, Al*C*H$_3$). ^{27}Al NMR (C_6D_6, 78 MHz, 298 K): δ 184. MS(EI): *m*/*z* 525.2 (M^+) 2 %, 348.2 [M-{CpFe(CO)$_2$}]$^+$ 100 %; accurate mass: calc. 523.2647, meas. 523.2640. IR (CH_2Cl_2 solution, cm^{-1}): 1958, 1896 (ν_{CO}).

Crystallographic data: $C_{27}H_{44}AlFeN_3O_2$, M_r = 525.49, triclinic, *P*-1, *a* = 9.9141(2), *b* = 11.3263(2), *c* = 12.8550(2) Å, α = 81.6863(7), β = 83.7688(7), γ = 82.6593(7)°, *V* = 1410.63(4) Å^3, *Z* = 2, ρ_c = 1.237 Mg m^{-3}, *T* = 150 K, λ = 0.71073 Å. 25106 reflections collected, 6408 independent [R(int) = 0.057] which were used in all calculations. R_1 = 0.0480, wR_2 = 0.0937 for observed unique reflections [$I > 2\sigma(I)$] and R_1 = 0.0959, wR_2 = 0.1478 for all unique reflections. Max. and min. residual electron densities 0.91 and -0.83 e Å^{-3}. CCDC reference: 894965.

Preparation of CpFe(CO)$_2$[(I)Al{(NDipp)$_2$CN^{i}Pr$_2$}] **(XI)**

To a slurry of Na[CpFe(CO)$_2$] (0.16 g, 0.81 mmol) in diethyl ether (30 cm^3) at -78 °C was added slowly a solution of **3.22** (0.60 g, 0.81 mmol) also in diethyl ether (40 cm^3) and the reaction mixture stirred for 12 h whilst slowly attaining room temperature. The resulting mixture was filtered, concentrated and subsequently cooled to -30 °C affording colourless crystals of **XI**. Yield 0.20 g, 32%.

Spectroscopic Data: ^{1}H NMR (C_6D_6, 300 MHz, 298 K): δ 7.20-7.13 (6H, m, Ar*H*), 4.43 (2H, sept ($^{3}J_{HH}$ = 6.9 Hz), NC*H*(CH$_3$)$_2$), 4.35 (5H, s, Cp*H*), 4.06 (2H sept ($^{3}J_{HH}$ = 6.9 Hz), C*H*(CH$_3$)$_2$), 3.93 (2H sept ($^{3}J_{HH}$ = 6.6 Hz), C*H*(CH$_3$)$_2$), 1.66 (6H, d ($^{3}J_{HH}$ = 6.6 Hz),

CH(CH_3)$_2$), 1.48 (6H, d ($^3J_{HH}$ = 6.6 Hz), CH(CH_3)$_2$), 1.42 (6H, d ($^3J_{HH}$ = 6.9 Hz), CH(CH_3)$_2$), 1.41 (6H, d ($^3J_{HH}$ = 6.9 Hz), CH(CH_3)$_2$), 0.83 (12H, d, ($^3J_{HH}$ = 6.9 Hz), NCH(CH_3)$_2$). ^{13}C{^{1}H} NMR (C_6D_6, 75 MHz, 298 K): δ 216.8 (s, *C*O), 167.8 (s, *C*N$_3$), 146.8 (s, Ar*C*), 146.0 (s, Ar*C*), 138.6 (s, Ar*C*), 126.7 (s, Ar*C*), 125.5 (s, Ar*C*), 124.5 (s, Ar*C*), 83.9 (s, Cp*C*), 50.7 (s, N*C*H(CH$_3$)$_2$), 31.3 (s, *C*H(CH$_3$)$_2$), 28.6 (s, *C*H(CH$_3$)$_2$), 28.4 (s, CH(*C*H$_3$)$_2$), 27.8 (s, CH(*C*H$_3$)$_2$), 24.9 (s, CH(*C*H$_3$)$_2$), 24.4 (s, CH(*C*H$_3$)$_2$), 23.9 (s, NCH(*C*H$_3$)$_2$). ^{27}Al NMR (C_6D_6, 78 MHz, 298 K): δ 66. MS(EI): *m*/*z* 792.2 (M^+) <1 %, 765 $[M\text{-}CO]^+$ <1 %, 737 $[M\text{-}2CO]^+$ <1 %; accurate mass: calc. $[M\text{-}CO]^+$ 763.2445, meas. 763.2439. IR (CH_2Cl_2 solution, cm^{-1}): 1978, 1920 (ν_{CO}).

Crystallographic data: $C_{38}H_{53}AlFeIN_3O_2$, M_r = 793.59, orthorhombic, *P* b c a, *a* = 18.75650(10), *b* = 19.82660(10), *c* = 20.35820(10) Å, *V* = 7570.76(7) Å^3, *Z* = 8, ρ_c = 1.392 Mg m^{-3}, *T* = 150 K, λ = 0.71073 Å. 102060 reflections collected, 8617 independent [R(int) = 0.030] used in all calculations. R_1 = 0.0325, wR_2 = 0.0693 for observed unique reflections [$I > 2\sigma(I)$] and R_1 = 0.0596, wR_2 = 0.0903 for all unique reflections. Max. and min. residual electron densities 0.79 and -0.95 e Å^{-3}.

3.4 Results and Discussion

3.4.1 Synthetic Chemistry

The synthesis of a number of aluminium aminidate and guanidinate precursors has been achieved through the use of simple salt metathesis chemistry (Scheme 3.3). Addition of a diethyl ether solution of either phenyl lithium or lithium di*iso*propylamide to a simple carbodiimide readily forms the corresponding lithium amidinate or guanidinate. A subsequent salt metathesis reaction with aluminium chloride results in the formation of the respective amidinate or guanidinate aluminium dichloride precursors.

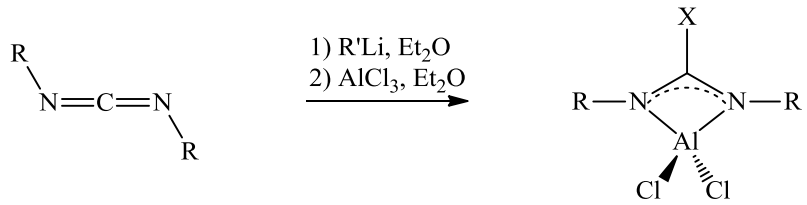

R = Cy, X = Ph (**I**)
R = ^{i}Pr, X = Ph (**II**)
R = Cy, X = $^{i}Pr_2N$ (**III**)

Scheme 3.3: *Synthesis of amidinate and guanidinate aluminium dichloride precursors*

This one-pot synthetic approach enables easy access to the desired aluminium amidinate and guanidinate precursors in yields ranging from 30-65%, depending on the peripheral substituents. The novel precursors **I**-**III** have been characterised by standard spectroscopic and analytical techniques including single crystal X-ray diffraction (Figure 3.2-3.4). All are monomeric in the solid state, feature symmetric binding of the amidinate or guanidinate at the aluminium centre, and show many similarities to the previously reported compound $^{i}Pr_2NC(^{i}PrN)_2AlCl_2$ (**3.20**).

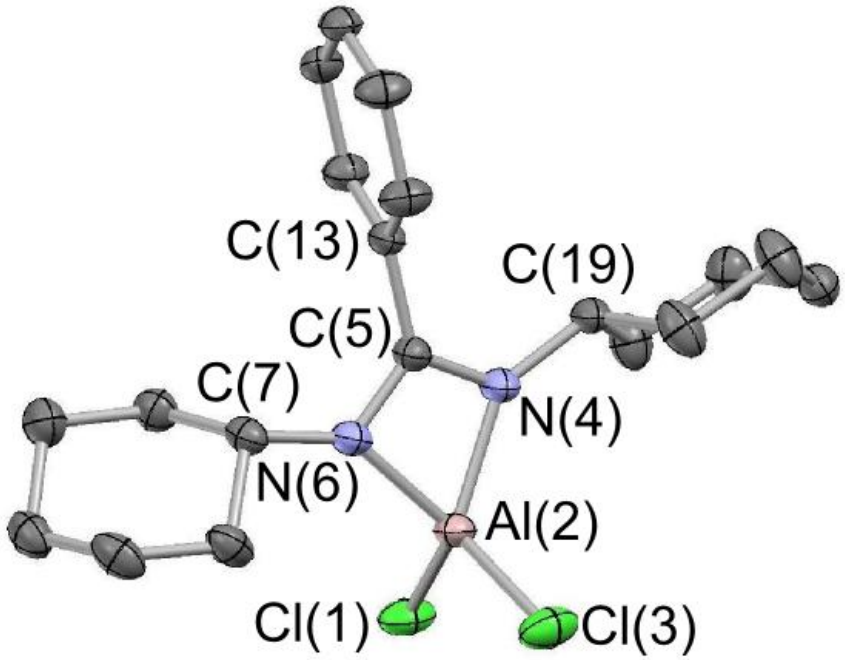

Figure 3.3: *Molecular structure of **I**. Thermal ellipsoids set at the 40% probability level and hydrogen atoms omitted for clarity.* Key bond lengths (Å) and angles (°): Al(2)-N(4) 1.885(2), Al(2)-N(6) 1.886(2), N(4)-C(5) 1.333(2), C(5)-N(6) 1.336(2), C(5)-C(13) 1.488(2), Cl(1)-Al(2) 2.120(1), Al(2)-Cl(3) 2.112(1); N(4)-C(5)-N(6) 110.4(2), N(4)-Al(2)-N(6) 71.09(5), Cl(1)-Al(2)-N(4) 116.69(4), Cl(3)-Al(2)-N(4) 117.79(4), Cl(1)-Al(2)-N(6) 117.94(5), Cl(3)-Al(2)-N(6) 117.10(4), Cl(1)-Al(2)-Cl(3) 111.16(2).

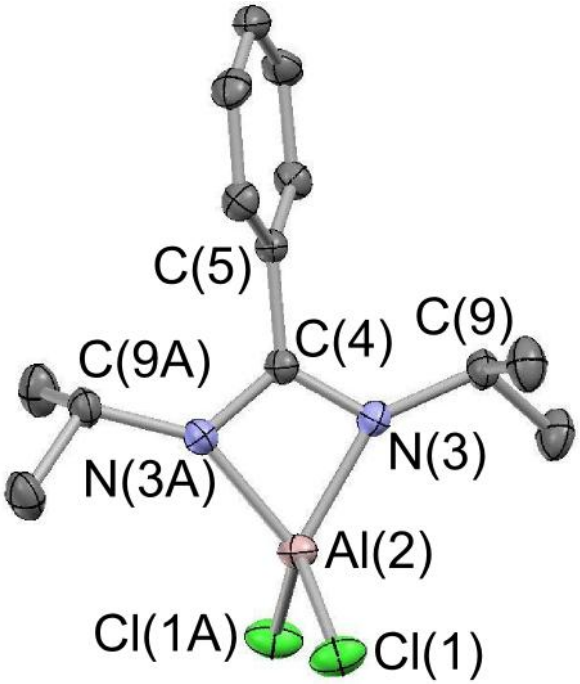

Figure 3.4: *Molecular structure of **II**. Thermal ellipsoids set at the 40% probability level and hydrogen atoms omitted for clarity.* Key bond lengths (Å) and angles (°): Al(2)-N(3) 1.884(2), N(3)-C(4) 1.336(2), C(4)-C(5) 1.485(2), Cl(1)-Al(2) 2.1122(5); N(3)-C(4)-N(3A) 110.5(2), N(3)-Al(2)-N(3A) 71.32(7), Cl(1)-Al(2)-N(3) 117.48(4), Cl(1)-Al(2)-Cl(1A) 111.26(3).

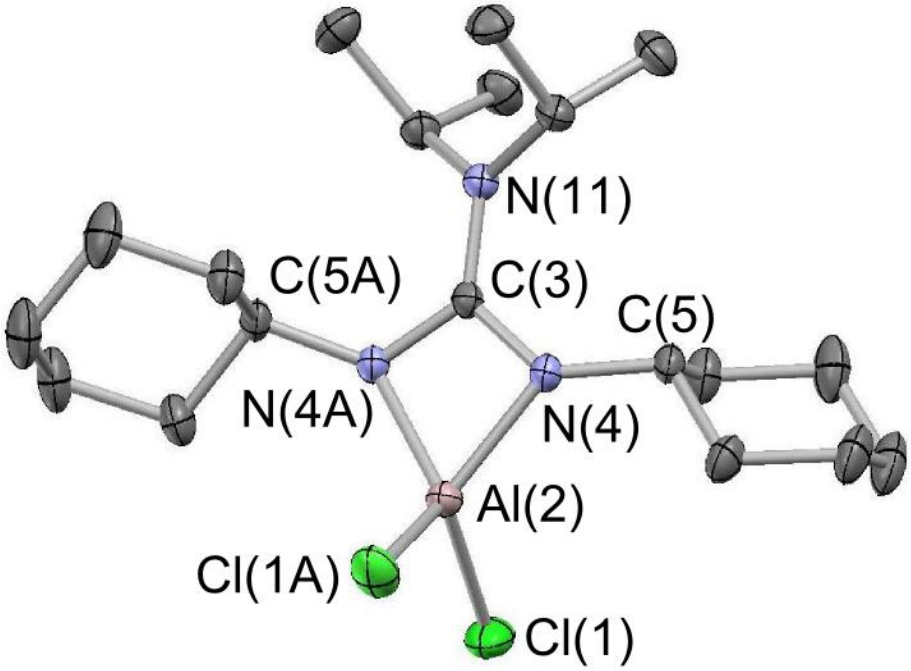

Figure 3.5: *Molecular structure of **III**. Thermal ellipsoids set at the 40% probability level and hydrogen atoms omitted for clarity*. Key bond lengths (Å) and angles (°): Al(2)-N(4) 1.865(2), C(3)-N(4) 1.362(2), C(3)-N(11) 1.356(3), Cl(1)-Al(2) 2.125(1); N(4)-C(3)-N(4A) 108.4(2), N(4)-Al(2)-N(4A) 72.61(8), Cl(1)-Al(2)-N(4) 118.60(5), Cl(1)-Al(2)-Cl(1A) 110.27(4).

Structurally there appears to be significant delocalisation of the negative charge across the N-C-N framework as illustrated by the N-C bond lengths. In **II** and **III** these bonds are crystallographically equivalent, and although not crystallographically equivalent in **I**, are not statistically different. The N-C distances measured for the guanidinate complex **III** (C(3)-N(4) 1.362(2), C(3)-N(11) 1.356(3) Å) show slight elongation in comparison to the amidinate precursor **I** (N(4)-C(5) 1.335(1), C(5)-N(6) 1.333(1) Å). This can be rationalised by the presence of the additional backbone amido substituent bonded to the delocalised framework in the guanidinate substituent. Whilst conjugation of the amido lone pair with the delocalised π-system potentially adds electron density, the amido group, in comparison with alkyl or aryl substituents, is inductively withdrawing. Furthermore, any contribution to bonding from the diamido resonance form available to guanidinate complexes (Figure 3.6) is dependent upon coplanarity of the R_2N and RNCNR functionalities, which is not observed in the solid state for **III**, presumably due to sterics.

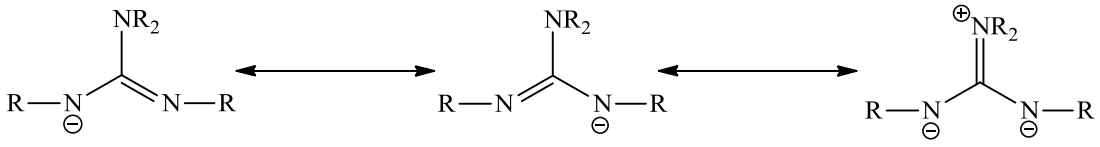

Figure 3.6: *Resonance forms of the guanidinate ligand*

Of particular interest in complexes **I-III** is the N-Al-N angle, as this not only provides information about the steric protection afforded to the aluminium centre but is also a function of the steric interactions between the ligand substituents R and X (Figure 3.7). The amidinate precursors **I** and **II** have N-Al-N angles of 71.09(5)° and 71.32(7) respectively, similar to the related systems $RC(^{i}PrN)_2AlCl_2$ (R = Me **3.12**, 71.16(9)°; R = ^{t}Bu **3.13**, 70.61(1)°) and $^{t}BuC(CyN)_2AlCl_2$ **1.7** 70.96(2)°.[10,12,15] The guanidinate precursor **III** has a marginally wider N-Al-N angle than **I** and **II**, at 72.61(8)°, but one which is similar to those

reported for the related guanidinate precursors $R_2NC(^{i}PrN)_2AlCl_2$ (R = Me **3.18**, 72.7(2)°; R = ^{i}Pr **3.20**, 72.3(2); R = $SiMe_3$ **3.21** 71.4(5)°).[11] The changes in 'bite' angles observed in amidinate and guanidinate systems are rationalised by the steric crowding within the substituent itself (Figure 3.7).

Figure 3.7: *(left) Steric crowding within amidinate and guanidinate substituents; (right) four-membered heterocycle formed upon chelation to aluminium*

The larger the R and X functionalities the greater steric repulsion pushing the R substituents forward, offering greater steric protection of the aluminium centre, as well as causing the nitrogen σ-donor orbitals to point towards the centre of the ligand. This favours the chelating rather than bridging binding motif. In amidinate systems the steric bulk of the X substituent is located directly on the carbon atom bound to the centre of the amidinate, resulting in closer approach of the R and X substituents. In the guanidinate however, steric congestion in the ligand is eased by the nitrogen of the amide acting as a spacer separating the R and X functionalities, giving rise to a slightly larger N-Al-N angle.

Although the structural and electronic properties of the guanidinate and amidinate substituents show notable differences, the similarities observed in the molecular structures of **I**-**III** indicate that these effects are perhaps more subtle than one may at first expect. The solid state structures are maintained in solution: ^{1}H and $^{13}C\{^{1}H\}$ NMR studies show that the symmetric binding and chelation of the aluminium centre is retained.

Precursors **I**-**III**, as well as the previously reported precursor $^{i}Pr_2NC(^{i}PrN)_2AlCl_2$ (**3.20**), readily underwent salt elimination reactions with $Na[CpFe(CO)_2]$ in diethyl ether to give complexes of the type $CpFe(CO)_2[(Cl)Al(NR)_2CX]$ featuring direct iron-aluminium bonds in yields of 38-57% (Scheme 3.4). Reaction of **III** with $Na[CpRu(CO)_2]$ gave the ruthenium analogue $CpRu(CO)_2[(Cl)Al(NCy)_2CN^{i}Pr_2]$ (**VIII**) in a similar fashion.

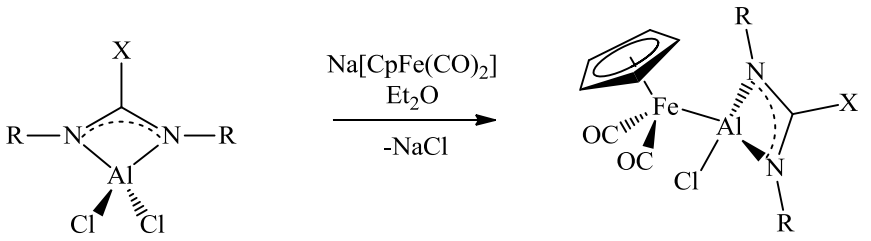

R = Cy, X = Ph (**I**)
R = ^{i}Pr, X = Ph (**II**)
R = Cy, X = N^{i}Pr$_2$ (**III**)
R = ^{i}Pr, X = N^{i}Pr$_2$ (**3.20**)

R = Cy, X = Ph (**IV**)
R = ^{i}Pr, X = Ph (**V**)
R = Cy, X = N^{i}Pr$_2$ (**VI**)
R = ^{i}Pr, X = N^{i}Pr$_2$ (**VII**)

Scheme 3.4: *Salt metathesis reaction of amidinate and guanidinate dichloride precursors with Na[CpFe(CO)$_2$]*

Conveniently these reactions can be monitored *in situ* by ^{27}Al NMR spectroscopy with a downfield shift of *ca*. 60 ppm being found to be diagnostic of metal-aluminium bond formation. Compounds **V**-**VIII** were isolated as colourless crystals after storage of concentrated ethereal solutions of each at -30 °C. These novel compounds were characterised by standard spectroscopic and analytical techniques, as well as by X-ray crystallography (Figures 3.7-3.10).

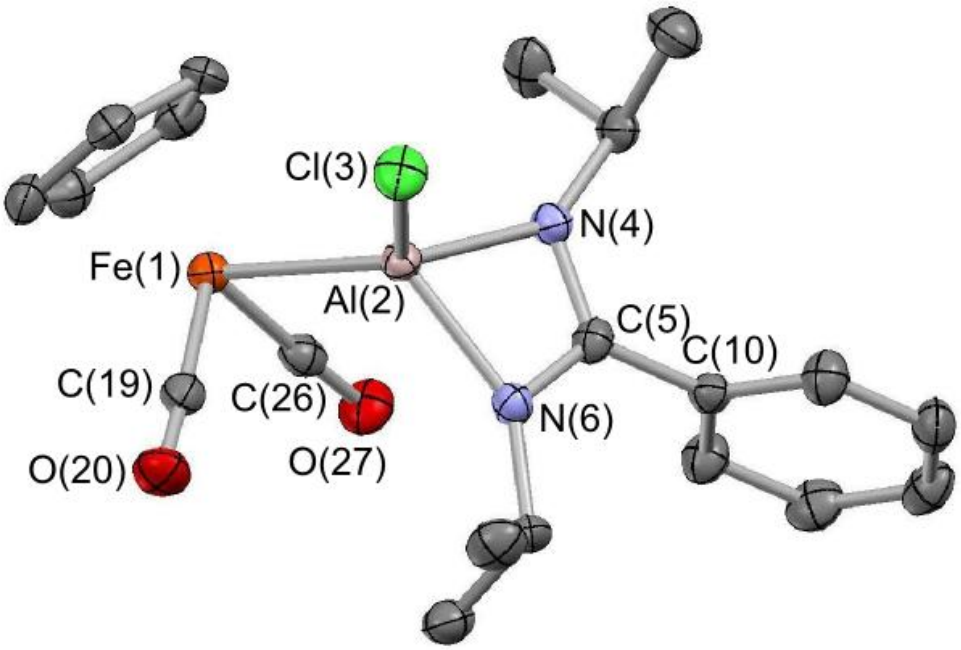

Figure 3.8: *Molecular structure of* ***V****. Thermal ellipsoids set at the 40% probability level and hydrogen atoms omitted for clarity*. Key bond lengths (Å) and angles (°): Fe(1)-Al(2) 2.340(1), Al(2)-Cl(3) 2.157(1), Al(2)-N(4) 1.915(2), Al(2)-N(6) 1.931(2), N(4)-C(5) 1.337(3), C(5)-N(6) 1.340(3); N(4)-Al(2)-N(6) 69.90(9), Cl(3)-Al(2)-N(4) 112.03(7), Cl(3)-Al(2)-N(6) 109.66(7), Fe(1)-Al(2)-N(4) 119.58(7), Fe(1)-Al(2)-N(6) 119.98(7), Fe(1)-Al(2)-Cl(3) 116.95(4), N(4)-C(5)-N(6) 110.7(2).

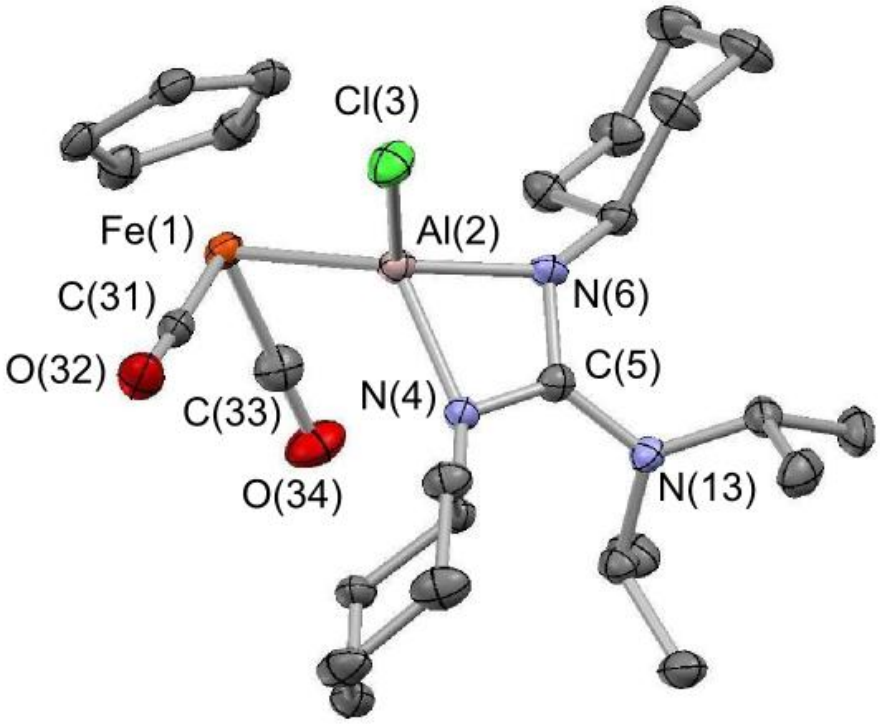

Figure 3.9: *Molecular structure of **VI**. Thermal ellipsoids set at the 40% probability level and hydrogen atoms omitted for clarity*. Key bond lengths (Å) and angles (°): Fe(1)-Al(2) 2.364(2), Al(2)-Cl(3) 2.153(2), Al(2)-N(4) 1.904(3), Al(2)-N(6) 1.919(3), N(4)-C(5) 1.343(4), C(5)-N(6) 1.351(4), C(5)-N(13) 1.386(4); N(4)-Al(2)-N(6) 70.3(1), Cl(3)-Al(2)-N(4) 113.74(9), Cl(3)-Al(2)-N(6) 112.4(1), Fe(1)-Al(2)-N(4) 118.28(9), Fe(1)-Al(2)-N(6) 124.68(9), Fe(1)-Al(2)-Cl(3) 111.59(5), N(4)-C(5)-N(6) 109.5(3).

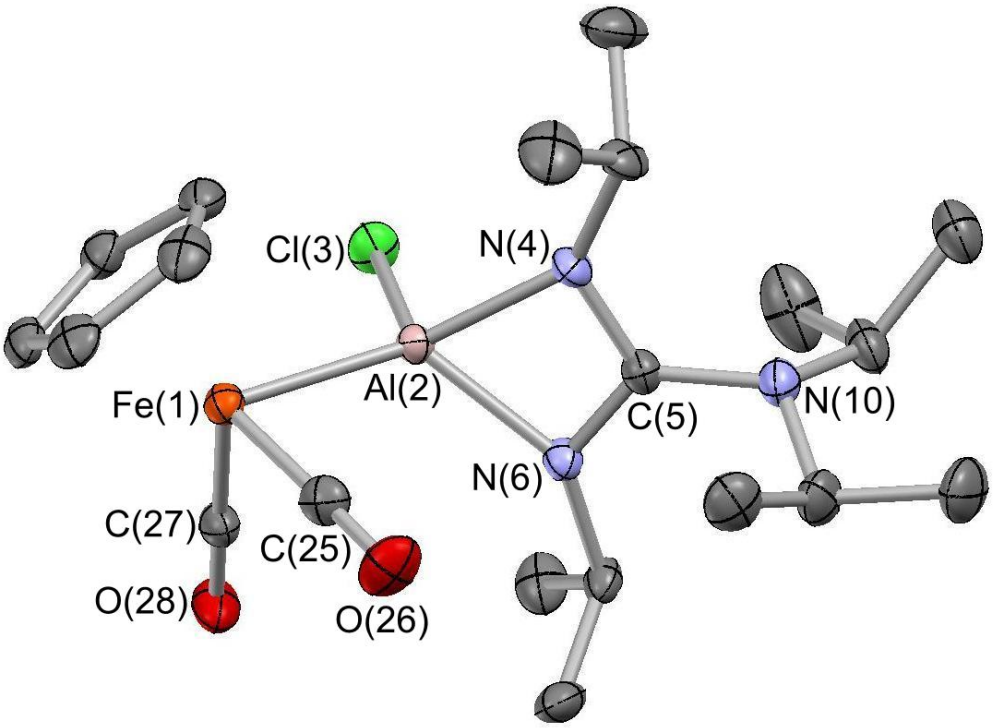

Figure 3.10: *Molecular structure of **VII**. Thermal ellipsoids set at the 40% probability level and hydrogen atoms omitted for clarity*. Key bond lengths (Å) and angles (°) are given for one of the molecules in the asymmetric unit: Fe(1)-Al(2) 2.344(2), Al(2)-Cl(3) 2.167(2), Al(2)-N(4) 1.919(5), Al(2)-N(6) 1.908(5), N(4)-C(5) 1.331(7), C(5)-N(6) 1.323(7), C(5)-N(10) 1.418(7); N(4)-Al(2)-N(6) 69.4(2), Cl(3)-Al(2)-N(4) 108.5(2), Cl(3)-Al(2)-N(6) 108.8(2), Fe(1)-Al(2)-N(4) 126.1(2), Fe(1)-Al(2)-N(6) 123.3(2), Fe(1)-Al(2)-Cl(3) 113.27(8), N(4)-C(5)-N(6) 110.4(5).

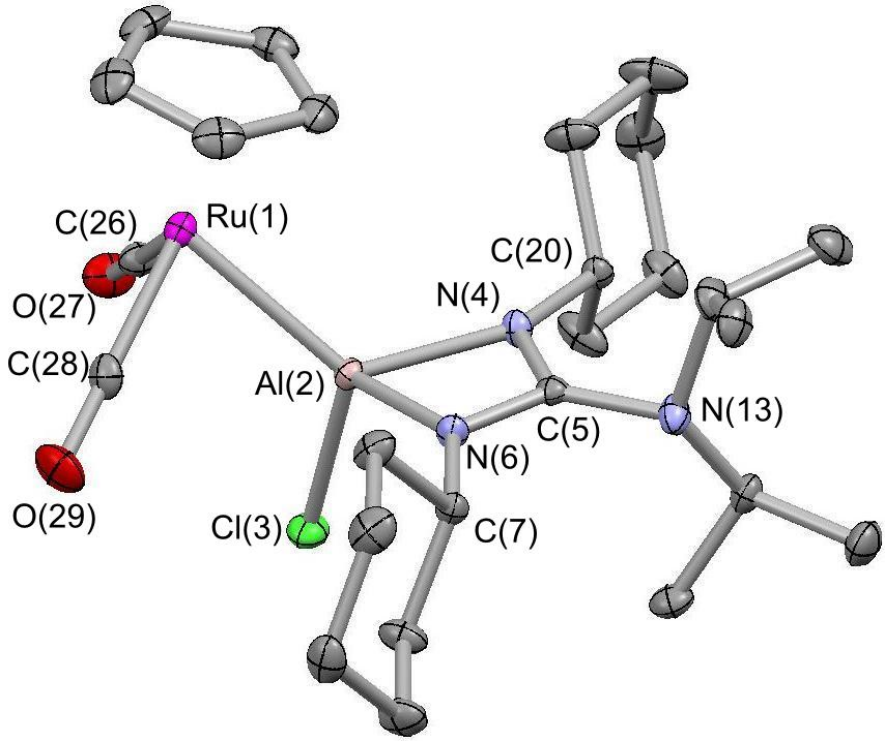

Figure 3.11: *Molecular structure of **VIII**. Thermal ellipsoids set at the 40% probability level and hydrogen atoms omitted for clarity.* Key bond lengths (Å) and angles (°): Ru(1)-Al(2) 2.441(1), Al(2)-Cl(3) 2.164(1), Al(2)-N(4) 1.911(2), Al(2)-N(6) 1.913(2), N(4)-C(5) 1.342(3), C(5)-N(6) 1.328(3), C(5)-N(13) 1.409(3); N(4)-Al(2)-N(6) 69.5(1), Cl(3)-Al(2)-N(4) 107.68(8), Cl(3)-Al(2)-N(6) 107.54(8), Ru(1)-Al(2)-N(4) 124.88(8), Ru(1)-Al(2)-N(6) 121.61(8), Ru(1)-Al(2)-Cl(3) 116.47(4), N(4)-C(5)-N(6) 109.5(2).

The molecular structures of **V**, **VI** and **VIII** each feature a single crystallographically distinct molecule in the asymmetric unit, while **VII** features two essentially identical molecules. In each case a four-coordinate aluminium centre is observed with a geometry that is distorted from tetrahedral to accommodate the constraints imposed by the four-membered heterocycle (N-Al-N 69.90(9)°, 70.3(1)°, 69.4(2)° and 69.5(1)° for **V-VIII** respectively). The aluminium bound chloride substituents in the cases of the iron compounds adopt Cl-Al-Fe-Cp centroid torsion angles that relatively closely approach idealised *syn* conformations (**V** 53.5°, **VI** 58.2° and **VII** 59.0°); by contrast the ruthenium complex **VIII** and the related amidinate complexes $CpFe(CO)_2[(Cl)E(NCy)_2C^tBu]$ (E = Al **1.10** or Ga **1.11**) display torsion angles of 174.0, 176.6 and 177.9° respectively.[12] However, as is the case for related boryl compounds it is likely that a relatively low barrier to rotation around the M-Al bond exists and that the differences observed are within the realms of crystal packing forces.[16] The observed Fe-Al bond lengths (**V** 2.340(1), **VI** 2.364(2) and **VII** 2.344(2) Å) are comparable to the value of 2.370(1) Å reported for **1.10**; the greater Ru-Al distance of **VIII** (2.441(1) Å) is as expected given the greater covalent radius of ruthenium (Δr = 0.14 Å)[17] and the N-Al distances lie within the range of those previously reported.[10-12]

The close similarities between the structures of amidinate and guanidinate derivatives presumably indicate that the contribution from the diamido guanidinate resonance form is minimal. This can be attributed to steric effects, which mean the pendant NR_2 groups in the guanidinate complexes do not lie co-planar with the heterocycle. The carbonyl stretching frequencies observed for **V-VII** are also indicative of relatively subtle differences in the electronic properties of the amidinate and guanidinate substituents (**V** 1964, 1899 cm^{-1}, **VI** 1973, 1912 cm^{-1} and **VII** 1973, 1893 cm^{-1}).

3.4.2 Solution Behaviour of V-VII

Compounds **V**, **VI** and **VII** have been fully characterised by standard spectroscopic and analytical techniques. ^{1}H, ^{13}C and ^{27}Al NMR spectroscopy at room temperature all suggest that the solid state structure is maintained in solution. However, variable temperature ^{27}Al NMR experiments carried out on a fluorobenzene solution of **VI** showed it to undergo a thermally induced, and reversible, change in the coordination environment of the aluminium centre as the sample is cooled. Room temperature spectra show the resonance attributable to the monomeric species present in the solid state at δ_{Al} = 167 ppm, but also a broader resonance at δ_{Al} = 55 ppm. This broader resonance diminishes upon heating the sample but is still visible at 75 °C. On cooling the sample, below room temperature, the resonance at δ_{Al} = 167 ppm begins to decrease in intensity and that at δ_{Al} = 55 ppm increases (Figure 3.12).

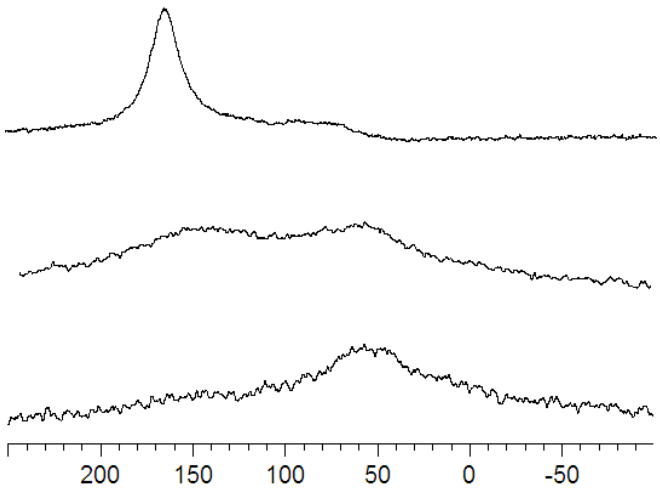

Figure 3.12: *^{27}Al NMR spectra of **VI** at different temperatures; (top) 65 °C, (centre) -20 °C and (bottom) -35 °C*

At -35 °C almost complete conversion to the resonance at δ_{Al} = 55 ppm is observed. Upon warming the sample back to 20 °C the resonance at δ_{Al} = 167 ppm is restored. This change

in coordination environment of aluminium is completely reversible with a single sample able to be cycled multiple times, without any indication of decomposition. As with other quadrupolar nuclei (*e.g.* ^{11}B) the position of the ^{27}Al NMR resonance is known to be highly dependent upon the coordination number of the aluminium centre and less sensitive to the manner of ligand binding.[18] The chemical shifts of the resonances measured using variable temperature ^{27}Al NMR experiments in fluorobenzene suggest that the aluminium centre changes from four-coordinate to five-coordinate upon cooling.[19] The facile formation of five-coordinate aluminium complexes is reported in the literature. Thus, for example, $H_3Al{\cdot}NMe_3$ is monomeric in the gas phase, but the solid state structure is dimeric showing augmented coordination at aluminium.[20] The ability of $H_3Al{\cdot}NMe_3$ to coordinate a second Lewis base forming a five coordinate species has also been demonstrated in the literature.[21,22]

Variable temperature ^{1}H NMR studies were carried out between -35 and 75 °C in fluorobenzene, using a toluene-d_8 insert, to further characterise this process *via* a more informative spectroscopic method. However, only small changes in the chemical shifts of the singlet Cp resonance and the doublet resonance of the N^{i}Pr$_2$ substituent, relative to the toluene-d_8, were observed despite almost quantitative conversion from δ_{Al} = 167 to δ_{Al} = 55 ppm being observed in the ^{27}Al NMR. The small upfield shifts observed in the ^{1}H NMR resonances on cooling (from δ_H = 4.58 to δ_H = 4.50 ppm for the Cp resonance and from δ_H = 1.15 to δ_H = 1.06 ppm for the Me of N^{i}Pr$_2$) suggest that there is little significant rearrangement or redistribution of the ^{1}H NMR active functional groups or ligands within the system. The absence of any new ^{1}H NMR resonances implies that the process being observed on the ^{1}H NMR timescale is a time averaged phenomenon. The absence of suitably diagnostic ^{1}H NMR resonances arises from the specific system employed, which contains no functional groups directly bound to the aluminium centre with ^{1}H NMR

resonances suitable for analysis. A dimerisation equilibrium can tentatively be proposed to rationalise the spectroscopic observations through the thermally induced formation of a chloride bridged dimer (Scheme 3.5) on the basis of a number of chloride bridged dimeric species having been structurally characterised including $[Mes_2AlCl]_2$,[23] $[2,6\text{-}Mes_2C_6H_3AlCl_2]_2$[24] and $[Cp^*AlClMe]_2$.[25]

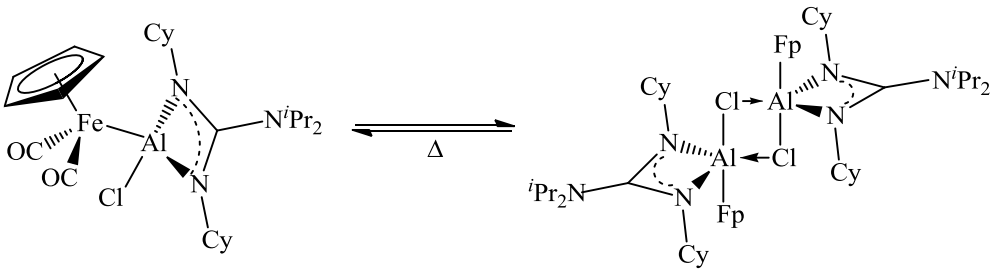

VI Fp = $CpFe(CO)_2$

Scheme 3.5: *Proposed equilibrium for the thermally induced formation of a chloride bridged dimer*

The formation of a chloride bridged dimer relies on dative bond formation from a lone pair of electrons on the chloride to the coordinatively unsaturated aluminium centre. A temperature dependent equilibrium is one possible rationale for the changes observed in the ^{27}Al NMR spectra, with the aluminium centre being four-coordinate in the monomeric species and five-coordinate in the dimeric species. The time averaged signals observed in the ^{1}H NMR reflect the fact that the proton resonances being observed (Cp and N^{i}Pr$_2$ Me) are comparatively removed from the aluminium centre and hence less affected by the increase in coordination number, resulting in a very small difference in the chemical shift observed between the proposed monomer and dimer.

The rate of interconversion between the four-coordinate and five-coordinate species required to observe coalescence in both ^{1}H and ^{27}Al NMR spectra was estimated using the

equation for simple two site exchange $k = (\pi/\sqrt{2})\delta\nu$ (where k = rate of interconversion and $\delta\nu$ = difference between observed four-coordinate and five-coordinate species resonances in Hz). Using the chemical shifts for the four and five-coordinate species obtained from the variable temperature ^{1}H NMR studies, on the ^{1}H NMR timescale an interconversion rate of greater than 60 Hz would result in a time averaged resonance being observed. However, for a time averaged resonance to be observed on the ^{27}Al NMR timescale an interconversion rate of greater than 20,000 Hz would be required, due to the large difference in chemical shift (*ca.* 110 ppm) observed between the proposed monomer and dimer in the ^{27}Al NMR spectrum.

To investigate the thermodynamics of the proposed dimerisation process, a Van't Hoff study was carried out on the variable temperature ^{1}H NMR data from -35 °C (where by ^{27}Al NMR complete conversion to dimer occurs) to 75 °C (where by ^{27}Al NMR almost complete conversion to monomer occurs). To enable the calculation of the equilibrium constant at each temperature (given the difficulties inherent in intergrating ^{27}Al NMR signals) the chemical shifts of the ^{1}H NMR resonances for the Cp and N^{i}Pr$_2$ Me protons at the two extremes (-35 °C and 75 °C) were assumed to be the resonances associated with the dimer and monomer respectively, reflecting the ^{27}Al NMR measurements at these temperatures. Van't Hoff plots derived from both the Cp resonance and the Me resonance were used to determine values of ΔH and ΔS (Figure 3.13 and Figure 3.14).

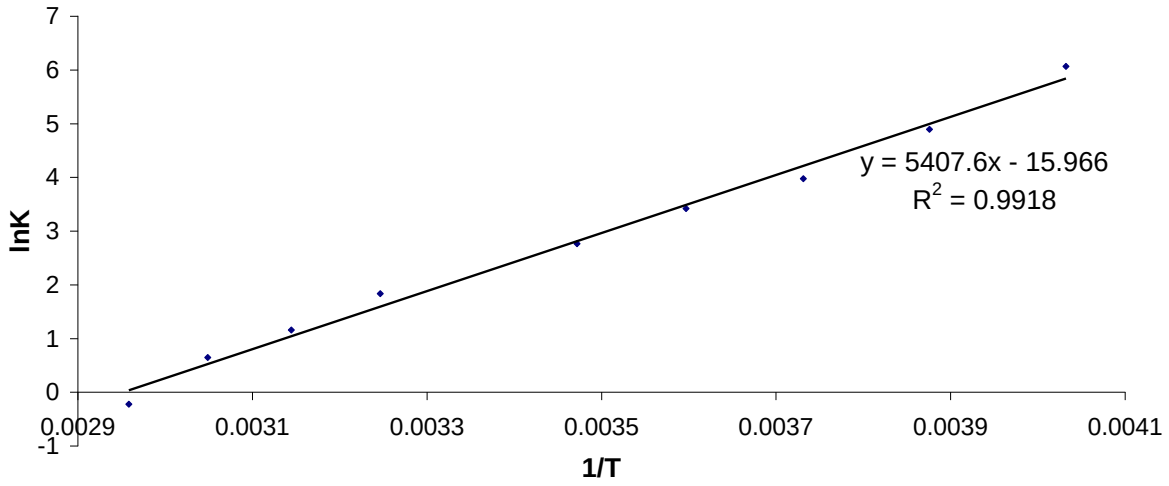

Figure 3.13: *Van't Hoff plot derived from the Cp resonance. ΔH = -45.0 kJ mol^{-1} and ΔS = -133 J mol^{-1} K^{-1} for the reaction 2monomer* ⇌ *dimer*

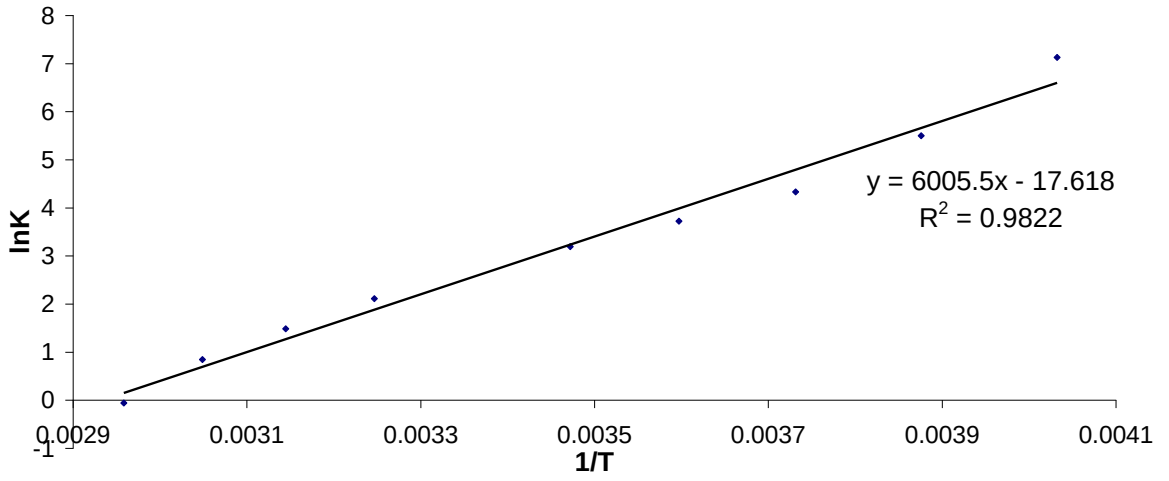

Figure 3.14: *Van't Hoff plot derived from the Me resonance. ΔH = -49.9 kJ mol^{-1} and ΔS = -147 J mol^{-1} K^{-1} 2monomer* ⇌ *dimer*

The values obtained for ΔH and ΔS from both the Van't Hoff plots show reasonable agreement, and the values subsequently quoted in this text are the mean of these results, ΔH = -47.5 kJ mol^{-1} and ΔS = -136 J mol^{-1} K^{-1} (the largest source of error is thought to be the assumption of complete monomer to dimer conversion and is estimated at 10%).

Comparison of these data with literature values for the dimerisation of two molecules of $AlCl_3$ to Al_2Cl_6 show that the process observed in **VI** is less exothermic than the formation of Al_2Cl_6 (ΔH(experimental) = -121 to -127 kJ mol^{-1}; ΔH(calculated) = -133 to -153 kJ mol^{-1} for Al_2Cl_6 formation) which is expected given the greater Lewis acidity of $AlCl_3$. However, entropically the process observed in **VI** is similar to the formation of Al_2Cl_6 (ΔS(experimental) = -154 to -155 J mol^{-1} K^{-1}; ΔS(calculated) = -150 J mol^{-1} K^{-1}).[26]

Crystallisation of **VI** from an ethereal solution at -30 °C yields the four-coordinate monomeric species, verified by X-ray crystallography (Figure 3.9) despite ^{27}Al NMR measurements indicating that the major species in solution at that temperature is five-coordinate. It is likely that crystallisation of the four-coordinate species is more rapid, potentially reflecting relative solubilities, and therefore a 'kinetic' crystallisation occurs yielding **VI**. Hence, methods for the structural characterisation of the five-coordinate system are difficult to conceive.

To assess the viability of chloride binding to the aluminium centre in **VI**, and the effect that this might have on the ^{27}Al NMR spectrum, $[PPh_4]Cl$ was added to a fluorobenzene solution of **VI** (Scheme 3.6).

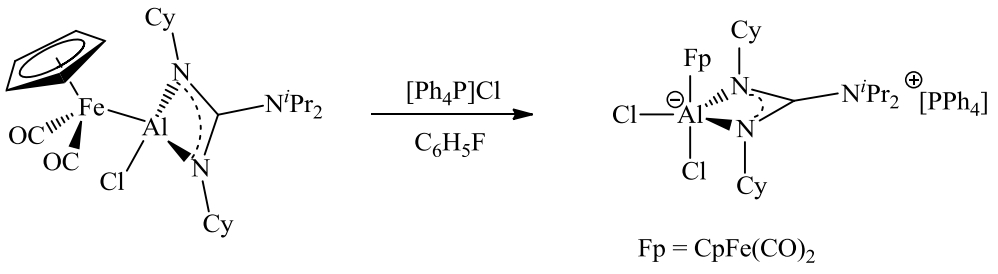

Scheme 3.6: *Reaction of **VI** with [Ph$_4$P]Cl*

Successive addition of aliquots of $[Ph_4P]Cl$ sees the resonance for the four-coordinate species in the ^{27}Al NMR spectrum (δ_{Al} = 167 ppm) diminish and a resonance attributable to

a five-coordinate system (δ_{Al} = 60 ppm) to appear and subsequently increase in intensity. Although the formation of a five-coordinate species on addition of a chloride source does not confirm the presence of a monomer/dimer equilibrium it highlights the fact that the aluminium centre in **VI** remains both Lewis acidic and coordinatively unsaturated. Furthermore, the potential for dative bond formation forming chloride bridged dimers as proposed in Scheme 3.5 serves as a method of trapping a cationic system should it be formed.

3.4.3 Synthesis and spectroscopic study of $CpFe(CO)_2[(Me)Al(NCy)_2CN^iPr_2]$

With the potential for augmented coordination highlighted in the solution studies of $CpFe(CO)_2[(Cl)Al(NCy)_2CN^iPr_2]$ (**VI**) as well as the high bond strength of the aluminium-chloride bond, alternative abstractable substituents were targeted for the formation of a cationic three-coordinate aluminium centre. The abstraction of a methyl anion is well precedented in the literature with a number of reports of methyl anion abstraction from aluminium complexes.[27,28] Although previous reports of methyl anion abstraction from amidinate supported alkyl aluminium precursors have resulted in decomposition, the stabilisation of low valent group 13 cations by transition metals is established in the literature.[29-31] Furthermore, whilst bridging methyl groups are prevalent in aluminium chemistry (*e.g.* $AlMe_3$) the formation of a non-classical three-centre two-electron bond is presumed to be less favourable, requiring much closer contact, than the formation of a simple donor acceptor interaction with a chloride substituent.

In the formation of compounds **V**-**VIII** no evidence of further substitution to form compounds containing Fe-Al-Fe bridged species was observed despite the observation of similar processes for boron based systems, and the more polar nature of the pendant Al-Cl bond (*cf.* B-Cl).[32-34] However, the pendant Al-Cl bond remains reactive towards less bulky

nucleophiles and reaction of **VI** with one equivalent of MeLi yields $CpFe(CO)_2[(Me)Al(NCy)_2CN^iPr_2]$ (**IX**) *via* substitution chemistry. The synthesis of the mixed (chloro)methyl precursor $^iPr_2NC(CyN)_2AlCl(Me)$ (**X**) (Scheme 3.7) and subsequent reaction with $Na[CpFe(CO)_2]$ provides a complementary synthetic route.

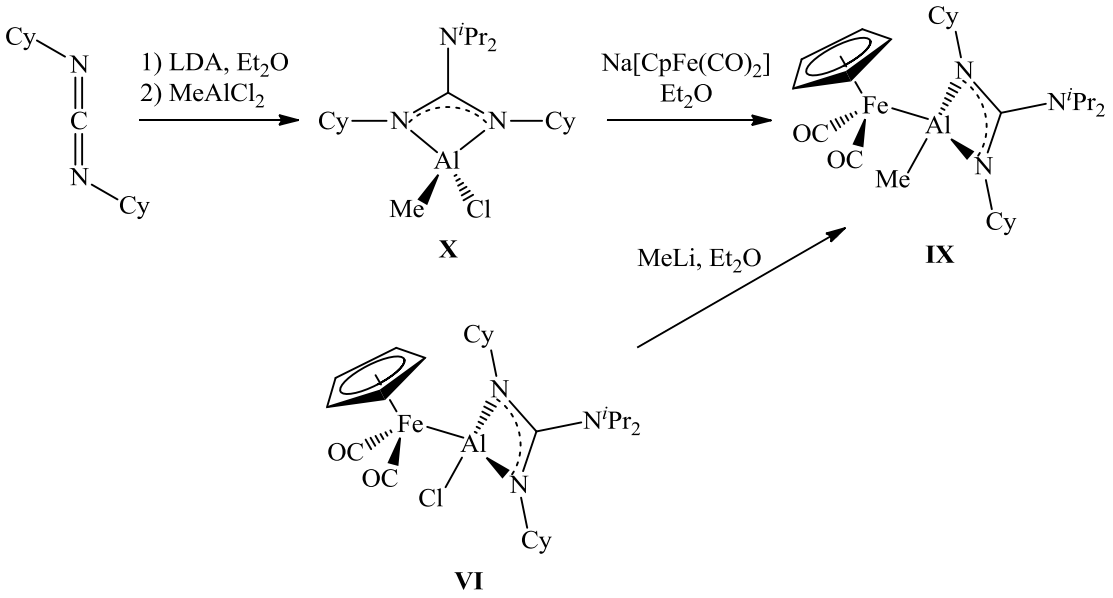

Scheme 3.7: *Complementary syntheses of **IX***

Whilst direct methylation of **VI** with MeLi forms the desired methyl substituted complex, in practice direct synthesis *via* **X** offers increased yields due to the reduced number of synthetic steps. Complex **IX** was isolated as colourless crystals after storage of a concentrated ethereal solution at -30 °C, and was characterised by standard spectroscopic techniques as well as by X-ray crystallography (Figure 3.15).

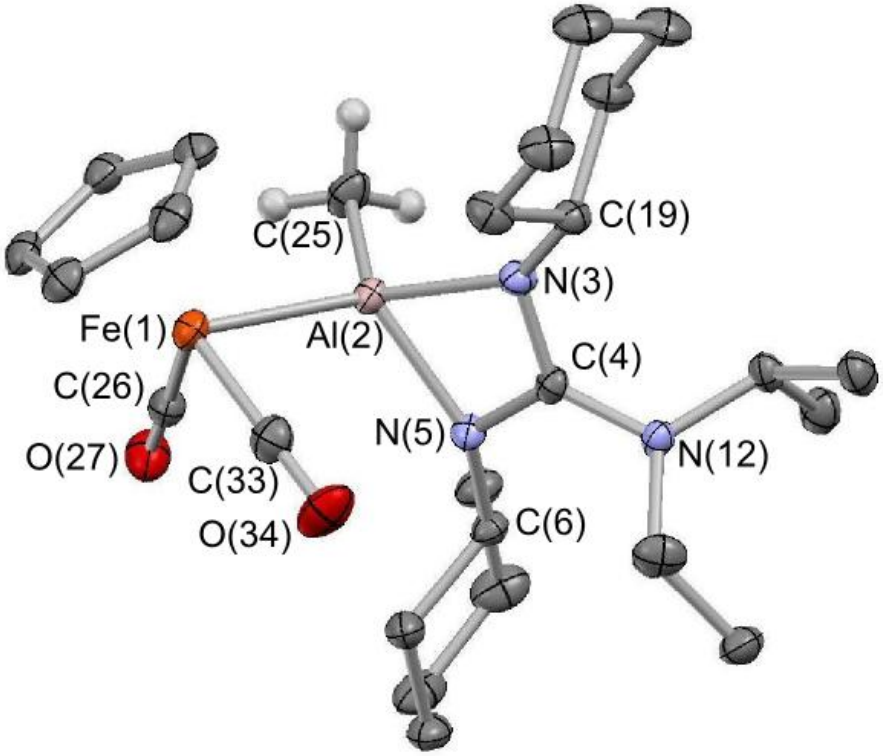

Figure 3.15: *Molecular structure of **IX**. Thermal ellipsoids set at the 40% probability level and hydrogen atoms (except Al-Me) omitted for clarity.* Key bond lengths (Å) and angles (°): Fe(1)-Al(2) 2.411(2), Al(2)-C(25) 1.967(4), Al(2)-N(3) 1.935(3), Al(2)-N(5) 1.930(3), N(3)-C(4) 1.348(5), C(4)-N(5) 1.341(5), C(4)-N(12) 1.386(4); N(3)-Al(2)-N(5) 69.3(2), N(3)-Al(2)-C(25) 115.6(2), N(5)-Al(2)-C(25) 116.3(2), Fe(1)-Al(2)-N(3) 120.8(2), Fe(1)-Al(2)-N(5) 115.3(2), Fe(1)-Al(2)-C(25) 112.9(2), N(3)-C(4)-N(5) 109.7(3).

The molecular structure of **IX** closely resembles that of the chloro analogue **VI**, in which the aluminium centre is also four-coordinate and has distorted tetrahedral geometry. Complex **IX** features longer Fe-Al and N-Al bond lengths than **VI** (*d*(Fe-Al) = 2.411(2) Å for **IX** *cf.* 2.364(2) Å for **VI**; *d*(N-Al) = 1.935(3) and 1.930(3) for **IX** *cf.* 1.904(3) and 1.919(3) Å for **VI**) and such observations are consistent with Bent's rule, implying that there is greater aluminium 3*s*-character in the Al-C bond, than in the corresponding Al-Cl bond, and consequently greater aluminium 3*p*-character in the remaining Fe(1) and N(3)/N(5) bonds to aluminium. A relatively close approach to *syn*-conformation is shown from the C-Al-Fe-Cp centroid torsion angle of 58.1°, almost identical to that of **VI** (58.2°).

The ^{1}H and ^{13}C NMR spectra of **IX** are consistent with the solid state structure being maintained in solution and the protons of the aluminium bound methyl group are observed at δ_H = -0.06 ppm. Comparison of carbonyl stretching frequencies of **VI** and **IX** shows that substituting the chloride substituent for methyl results in a more electron rich complex (*v*(CO) 1958, 1896 cm^{-1} for **IX**, *cf.* *v*(CO) 1973, 1912 cm^{-1} for **VI**).

3.4.4 Halide Abstraction Chemistry

Halide abstraction has proven to be a viable synthetic approach to the formation of a range of cationic group 13 species, most notably for the formation of cationic terminal borylene complexes and a two-coordinate gallium cation.[30,35,36] Compounds **V** and **VI** therefore represent suitable complexes for the formation of three-coordinate aluminium cations stabilised by the {CpFe(CO)$_2$} moiety (Scheme 3.8).

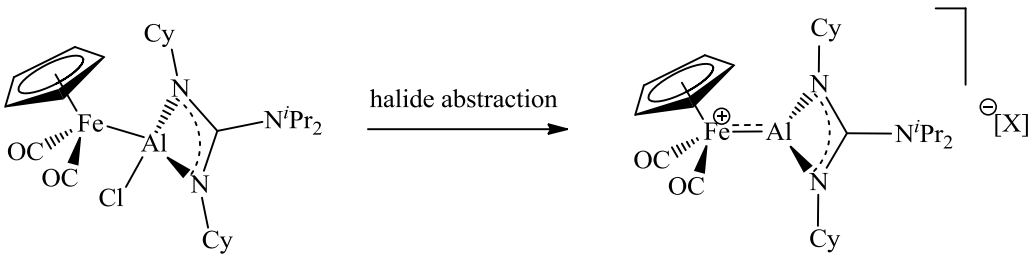

Scheme 3.8: *Proposed halide abstraction to yield a three-coordinate aluminium cation*

Reactions between **V** or **VI** and Na[BAr$^f_4$] at -30 °C in fluorobenzene generate a red solution, which becomes darker and brown upon warming to room temperature. Monitoring the reaction of **V** with Na[BAr$^f_4$] by ^{27}Al NMR spectroscopy showed that upon mixing at -30 °C the ^{27}Al NMR resonance is shifted slightly from that of the precursor δ_{Al} = 160 ppm (*cf.* **V** δ_{Al} = 167 ppm). Upon warming to room temperature a very broad resonance at δ_{Al} = 52 ppm is observed, and after 3 hours at room temperature this is the major signal in the ^{27}Al NMR spectrum, implying a five-coordinate environment for the aluminium centre. The reactivity for **VI** was similar with a very broad resonance ultimately being observed at δ_{Al} = 60 ppm. Formation of a three-coordinate aluminium centre would be expected to result in significant broadening of the resonance, as well as a downfield shift due to reduced valency and the evolution of a cationic complex. However, long scans and wider spectral windows did not show any evidence of the formation of a three-coordinate system. Attempts to isolate the initial product of halide abstraction through low temperature layering of the fluorobenzene reaction mixture with hexane and storage at -30 °C were unsuccessful. After warming samples to room temperature an intractable mixture was observed, with $[CpFe(CO)_2]_2$ the only iron-containing product able to be characterised.

A three-coordinate cationic aluminium system is likely to be highly reactive; the formation of a base stabilised cation represents a less labile synthetic target, and was thought to provide a more tractable and crystalline product (Scheme 3.9).

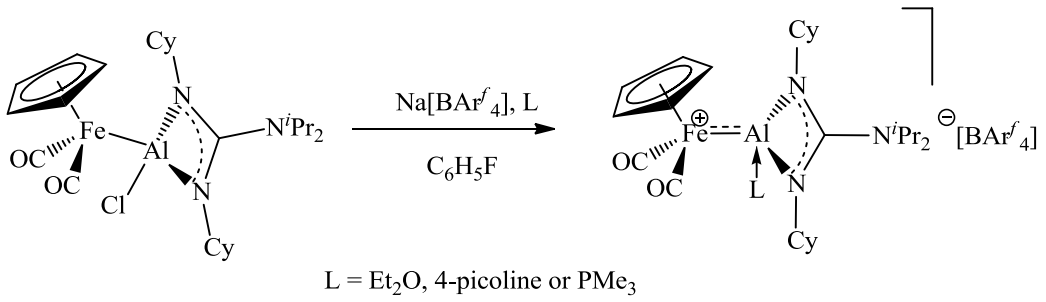

Scheme 3.9: *Proposed formation of a base stabilised cation*

The addition of a fluorobenzene solution of **VI** to a mixture of Na[BAr$^f_4$] and either diethyl ether or 4-picoline yielded similar results to those obtained without the addition of a base. In the case of the more strongly donating 4-picoline the ^{27}Al NMR spectrum ultimately showed a broad resonance at δ_{Al} = 29 ppm, however, the aluminium and iron containing products could not be identified. The amidinate supported compound **V** was also reacted with Na[BAr$^f_4$] in the presence of PMe_3 after which the ^{27}Al NMR spectrum contained a resonance at δ_{Al} = 59 ppm, and in the ^{31}P NMR spectrum resonances for both coordinated and uncoordinated PMe_3 were observed. Identification of the iron and aluminium containing products was unsuccessful.

As alternative approaches to the synthesis of the desired three-coordinate cation both the abstraction and protonation of the methyl substituent of **IX** were investigated (Scheme 3.10)

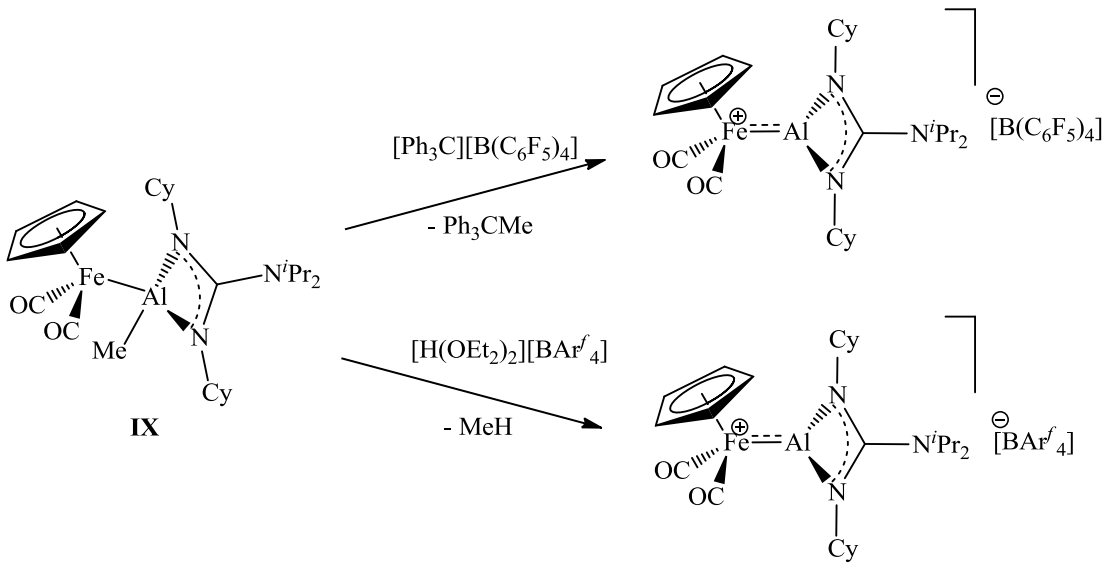

Scheme 3.10: *Synthetic approaches to the formation of a three-coordinate cation from **IX***

These reactions to either abstract a methide anion, using $[Ph_3C][B(C_6F_5)_4]$, or to protonate the methyl group and eliminate methane, using $[H(OEt_2)_2][BAr^f{}_4]$, resulted in similar formations of product mixtures to the halide abstraction experiments. The reactions formed no tractable or isolable products, and the similarity to the observed products of halide abstraction implies the product formed is highly reactive.

The tendency to form complexes with augmented coordination (as outlined in section 3.4.2) makes the formation and isolation of the desired three-coordinate cation very difficult, as it is likely that any cation that is formed will also feature augmented coordination. With this in mind, a more sterically demanding aluminium dihalide precursor was investigated, to offer increased steric protection to the aluminium centre.

3.4.5 Synthesis of $CpFe(CO)_2[(I)Al(NDipp)_2CN^iPr_2]$

The tendency for aluminium compounds to aggregate to coordinatively satisfy the aluminium centre is well established, and the augmented coordination observed in the aforementioned complexes highlights the importance of steric protection for the formation

of low valent aluminium species. The guanidinate substituent offers increased electron donating properties over related amidinates due to the contribution, however small, from the diamido resonance form of the guanidinate. With increased steric protection offered by pendant bulky arene substituents, the formation of compounds featuring a five-coordinate aluminium centre might be suppressed. The highly sterically demanding guanidinate $[^{i}Pr_2NC(DippN)_2]^-$ (Dipp = 2,6-di*iso*propylphenyl) has been shown to stabilise a number of low oxidation state and low valent species.[37-40] This was employed to try to stabilise the aluminium centre and allow access to a three coordinate aluminium cation.

Attempts to prepare $^{i}Pr_2NC(DippN)_2AlCl_2$ *via* an analogous salt metathesis synthetic route to that used for the preparation of **I-III** resulted in exceptionally low yields (<1%) of $^{i}Pr_2NC(DippN)_2AlCl_2$ and the regeneration of large amounts of carbodiimide (Scheme 3.11).

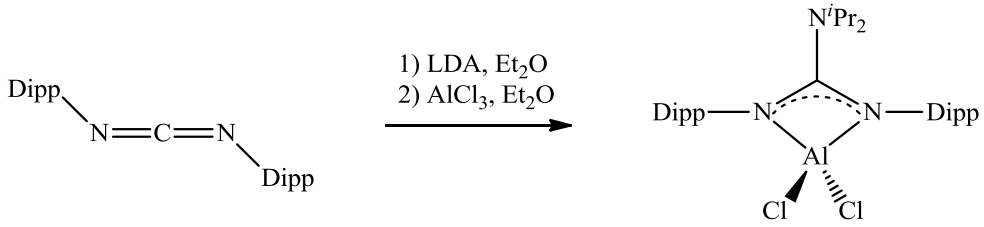

Scheme 3.11: *Salt metathesis for the formation of $^{i}Pr_2NC(DippN)_2AlCl_2$*

Isolation of the free guanidine followed by subsequent lithiation and salt metathesis also resulted in the regeneration of large amounts of carbodiimide, as did the salt metathesis between the potassium salt and aluminium chloride. The cleavage of the C-N$^{i}Pr_2$ bond of this guanidinate has been reported by Jones and co-workers who additionally determined the crystal structure of a zinc complex in which the guanidinate ligand binds asymmetrically. This complex shows an elongated C-N$^{i}Pr_2$ bond which is pre-disposed to form the corresponding zinc amide complex and regenerate the carbodiimide.[41] It is

possible that a similar process takes place during the salt metathesis reaction with aluminium chloride. Subsequent work by Jones and co-workers led to the publication of the iodo analogue $^{i}Pr_2NC(DippN)_2AlI_2$ (**3.22**) *via* an alternative synthetic route (Scheme 3.12).[42]

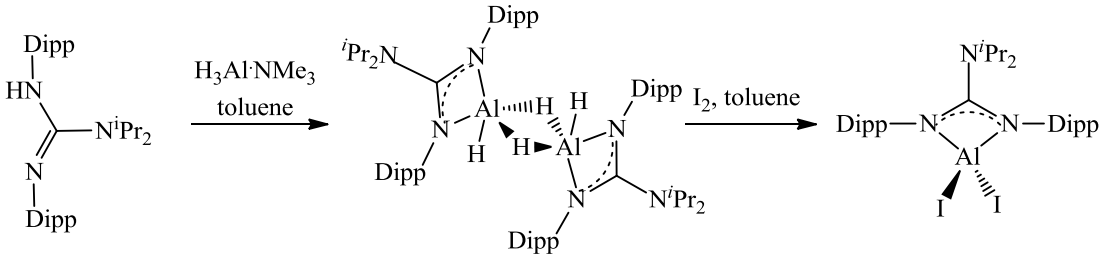

Scheme 3.12: *Preparation of $^{i}Pr_2NC(DippN)_2AlI_2$ (**3.22**)*

This approach negates the requirement for salt metathesis chemistry by using an alane intermediate and provides a convenient synthesis of **3.22**. The precursor **3.22** reacts readily with Na[CpFe(CO)$_2$] in diethyl ether to yield the complex CpFe(CO)$_2$[(I)Al(NDipp)$_2$CN^{i}Pr$_2$] (**XI**), which after storage of a concentrated ethereal solution at -30 °C, was isolated as yellow crystals. Compound **XI** has been fully characterised by standard spectroscopic and analytical techniques as well as by X-ray diffraction (Figure 3.16).

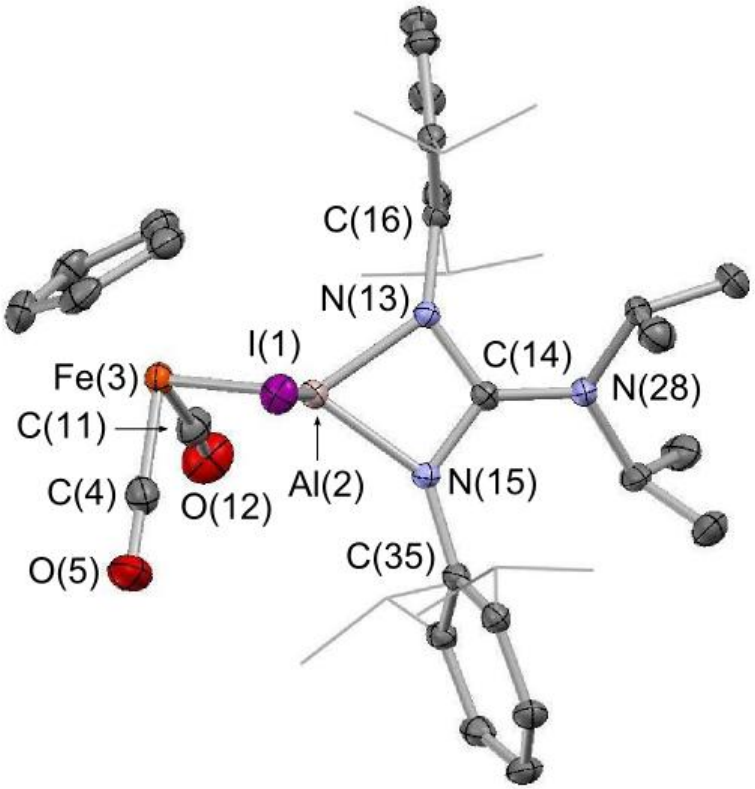

Figure 3.16: *Molecular structure of **XI**. Thermal ellipsoids set at the 40% probability level,* ^{i}*Pr groups of Dipp substituents are shown in wireframe and hydrogen atoms omitted for clarity.* Key bond lengths (Å) and angles (°): Al(2)-Fe(3) 2.374(1), I(1)-Al(2) 2.588(1), Al(2)-N(13) 1.929(2), Al(2)-N(15)) 1.908(2), N(13)-C(14) 1.362(4), C(14)-N(15) 1.369(4), C(14)-N(28) 1.363(4); N(13)-Al(2)-N(15) 69.7(1), I(1)-Al(2)-N(13) 108.85(8), I(1)-Al(2)-N(15) 108.27(8), Fe(3)-Al(2)-N(13) 132.21(8), F(3)-Al(2)-N(15) 126.08(8), I(1)-Al(2)-Fe(3) 106.71(3), N(13)-C(14)-N(15) 106.8(2).

The molecular structure of **XI** closely resembles those of the less bulky chloride substituted complexes **V**-**VII**. Complex **XI**, however, features a longer Fe-Al bond than **V**-**VII** but one which is shorter than that of the methyl substituted species **IX** (*cf.* 2.374(1) Å for **XI** and 2.340(1), 2.364(2), 2.344(2) and 2.411(2) Å for **V**-**VII** and **IX** respectively). N-Al bond lengths are within the range observed in the previously discussed **V**-**IX**. The Al-I bond in **XI** shows slight elongation in comparison to the diiodo-precursor **3.22** (*cf*. 2.588(2) Å for **XI** and 2.517(2) Å for **3.22**).

The reaction of **XI** with the strong Lewis acid $B(C_6F_5)_3$ or $Na[BAr^f_4]$ to generate the three-coordinate cationic species did not proceed cleanly. Monitoring of the reaction with $B(C_6F_5)_3$ by ^{19}F NMR spectroscopy showed no definitive formation of $[IB(C_6F_5)_3]^-$. This potentially can be attributed to sterics, as the iodide ion is perhaps too large to form a strong bond with the bulky Lewis acid $B(C_6F_5)_3$.

3.5 Conclusions and Suggestions for Further Research

The synthesis of half-sandwich iron (and ruthenium) mixed metal complexes with aluminium ligands featuring amidinate and guanidinate substituents has been established. The products have been fully characterised by both standard spectroscopic and analytical techniques as well as by X-ray diffraction. The influence of ligand substituents has been investigated and the amidinate and guanidinate subtitutents have been shown to possess similar properties. Greater structural differences were observed on the substitution of the chloride substituent in the mixed iron-aluminium complex **VI** for a methyl group, providing a more electron rich complex and inducing structural changes that are within the tenets of Bent's rule.

The solution behaviour of the mixed metal guanidinate complexes has been analysed by variable temperature ^{27}Al NMR spectroscopy and the tendency to form

complexes featuring augmented coordination observed. Further work to suppress the formation of five-coordinate species is to be carried out through increasing the steric protection offered to the aluminium centre from both the *N*,*N'*-chelating ligand and from the transition metal. The replacement of π-acidic carbonyl ligands with more strongly σ-donating ligands (*e.g.* trialkyl phosphines) offers not only a more sterically demanding, but also a significantly more electron rich transition metal fragment, thereby reducing the Lewis acidity of the resulting aluminium complex. This forms the basis of the work reported in Chapter IV.

3.6 References for Chapter III

1. F. T. Edelmann, *Adv. Organomet. Chem.*, 2008, **57**, 183.
2. C. Jones, *Coord. Chem. Rev.*, 2010, **254**, 1273.
3. C. Jones, P. C. Junk, J. A. Platts and A. Stasch, *J. Am. Chem. Soc.*, 2006, **128**, 2206.
4. C. Jones, A. Stasch, G. J. Moxey, P. C. Junk and G. B. Deacon, *Eur. J. Inorg. Chem.*, 2009, **24**, 3593.
5. G. J. Moxey, C. Jones, A. Stasch, P. C. Junk, G. B. Deacon, W. D. Woodul and P. R. Drago, *Dalton Trans.*, 2009, **14**, 2630.
6. C. Jones, P. C. Junk, M. Kloth, K. M. Proctor and A. Stasch, *Polyhedron*, 2006, **25**, 1592.
7. C. Jones, P. C. Junk, J. A. Platts, D. Rathmann and A. Stasch, *Dalton Trans.*, 2005, **15**, 2497.
8. S. P. Green, C. Jones, P. C. Junk, K.-A. Lippert and A. Stasch, *Chem. Commun.*, 2006, **38**, 3978.
9. S. P. Green, C. Jones and A. Stasch, *Science*, 2007, **318**, 1754.
10. M. P. Coles, D. C. Swenson, R. F. Jordan and V. G. Young, *Organometallics*, 1997, **16**, 5183.
11. S. L. Aeilts, M. P. Coles, D. G. Swenson, R. F. Jordan and V. G. Young, *Organometallics*, 1998, **17**, 3265.
12. C. Jones, S. Aldridge, T. Gans-Eichler and A. Stasch, *Dalton Trans.*, 2006, **45**, 5357.
13. D. A. Addy, N. Phillips, G. A. Pierce, D. Vidovic, T. Kraemer, D. Mallick, E. D. Jemmis, G. Reid and S. Aldridge, *Organometallics*, 2012, **31**, 1092.
14. D. A. Addy, G. A. Pierce, D. Vidovic, D. Mallick, E. D. Jemmis, J. M. Goicoechea and S. Aldridge, *J. Am. Chem. Soc.*, 2010, **132**, 4586.

15. C. C. Chang, C. S. Hsiung, H. L. Su, B. Srinivas, M. Y. Chiang, G. H. Lee and Y. Wang, *Organometallics*, 1998, **17**, 1595.

16. A. A. Dickinson, D. J. Willock, R. J. Calder and S. Aldridge, *Organometallics*, 2002, **21**, 1146.

17. B. Cordero, V. Gomez, A. E. Platero-Prats, M. Reves, J. Echeverria, E. Cremades, F. Barragan and S. Alvarez, *Dalton Trans.*, 2008, **21**, 2832.

18. R. Benn, A. Rufinska, H. Lehmkuhl, E. Janssen and C. Kruger, *Angew. Chem. Int. Ed.*, 1983, **22**, 779.

19. R. Benn and A. Rufinska, *Angew. Chem. Int. Ed.*, 1986, **25**, 861.

20. J. L. Atwood, F. R. Bennett, F. M. Elms, C. Jones, C. L. Raston and K. D. Robinson, *J. Am. Chem. Soc.*, 1991, **113**, 8183.

21. J. L. Atwood, K. W. Butz, M. G. Gardiner, C. Jones, G. A. Koutsantonis, C. L. Raston and K. D. Robinson, *Inorg. Chem.*, 1993, **32**, 3482.

22. T. D. Humphries, P. Sirsch, A. Decken and G. S. McGrady, *J. Molec. Struct.*, 2009, **923**, 13.

23. M. S. Lalama, J. Kampf, D. G. Dick and J. P. Oliver, *Organometallics*, 1995, **14**, 495.

24. R. J. Wehmschulte, W. J. Grigsby, B. Schiemenz, R. A. Bartlett and P. P. Power, *Inorg. Chem.*, 1996, **35**, 6694.

25. P. R. Schonberg, R. T. Paine and C. F. Campana, *J. Am. Chem. Soc.*, 1979, **101**, 7726.

26. D. W. Chandler and K. E. Johnson, *Inorg. Chem.*, 1999, **38**, 2050.

27. S. Dagorne and D. A. Atwood, *Chem. Rev.*, 2008, **108**, 4037.

28. C. E. Radzewich, I. A. Guzei and R. F. Jordan, *J. Am. Chem. Soc.*, 1999, **121**, 8673.

29. J. A. R. Schmidt and J. Arnold, *Organometallics*, 2002, **21**, 2306.

30. N. R. Bunn, S. Aldridge, D. L. Coombs, A. Rossin, D. J. Willock, C. Jones and L. L. Ooi, *Chem. Commun.*, 2004, **15**,1732.

31. N. R. Bunn, S. Aldridge, D. L. Kays, N. D. Coombs, A. Rossin, D. J. Willock, J. K. Day, C. Jones and L. L. Ooi, *Organometallics*, 2005, **24**, 5891.

32. D. Vidovic and S. Aldridge, *Angew. Chem. Int. Ed.*, 2009, **48**, 3669.

33. D. L. Coombs, S. Aldridge, S. J. Coles and M. B. Hursthouse, *Organometallics*, 2003, **22**, 4213.

34. H. Braunschweig, C. Kollann and U. Englert, *Eur. J. Inorg. Chem.*, 1998, **4**, 465.

35. D. L. Coombs, S. Aldridge, C. Jones and D. J. Willock, *J. Am. Chem. Soc.*, 2003, **125**, 6356.

36. D. L. Kays, J. K. Day, L. L. Ooi and S. Aldridge, *Angew Chem. Int. Ed.*, 2005, **44**, 7457.

37. D. Heitmann, C. Jones, D. P. Mills and A. Stasch, *Dalton Trans.*, 2010, **39**, 1877.

38. C. Jones, D. P. Mills, A. Stasch and W. D. Woodul, *Main Group Chem.*, 2010, **9**, 23.

39. C. Jones, D. P. Mills and A. Stasch, *Dalton Trans.*, 2008, **35**, 4799.

40. C. Jones, R. P. Rose and A. Stasch, *Dalton Trans.*, 2008, **21**, 2871.

41. C. Jones, L. Furness, S. Nembenna, R. P. Rose, S. Aldridge and A. Stasch, *Dalton Trans.*, 2010, **39**, 8788.

42. S. J. Bonyhady, D. Collis, G. Frenking, N. Holzmann, C. Jones and A. Stasch, *Nature Chem.*, 2010, **2**, 865.

4 Synthesis of More Sterically Demanding Iron-Aluminium Complexes

4.1 Introduction

The *N*,*N*′-chelating β-diketiminate (or NacNac) substituent forms a six-membered heterocycle when bound to a metal centre. This offers increased steric protection for the chelated metal centre, in comparison to the related amidinate and guanidinate classes of substituent (Figure 4.1).

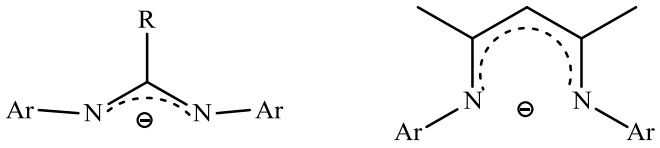

Figure 4.1: *Amidinate/guanidinate substituent (left) and NacNac substituent (right)*

The NacNac substituent has been shown to stabilise a multitude of metal complexes in low oxidation states or valencies from across the Periodic Table and this chemistry has been reviewed in detail.[1] The incorporation of highly sterically demanding aryl groups, for example Mes or Dipp, helps to impart both kinetic inertness and thermodynamic stability to the resulting metal system. In transition metal chemistry the $Dipp_2$NacNac substituent has been employed by Arnold, Bergman and co-workers to stabilise dimethyl niobium and

tantalum complexes of the type ($Dipp_2NacNac$)M($Me)_2$(N^tBu) (where M = Nb **4.1** or Ta **4.2**) as well as the cationic complexes resulting from protonation or abstraction of a methyl group *viz.* [($Dipp_2NacNac$)M(Me)(N^tBu)][$B(C_6F_5)_4$] (where M = Nb **4.3** or Ta **4.4**).[2] Although the $Dipp_2NacNac$ substituent has been utilised in transition metal chemistry, some of the most striking demonstrations of its use come from main group chemistry.

In 2000 Roesky and co-workers reported the formation of the first monomeric aluminium analogue of a *N*-heterocyclic carbene *via* the reduction of $Dipp_2NacNacAlI_2$ (**4.5**) to the Al(I) species $Dipp_2NacNacAl$ (**1.40**) using potassium metal.[3] Although there has been much interest in this area, due to the potential amphoteric nature of aluminium(I) species, the only additional monomeric aluminium analogue of a *N*-heterocyclic carbene remains the related $Dipp_2^{tBu}NacNacAl$ (**1.41**) species reported by Cui and co-workers, also formed by the reduction of the diiodide precursor with potassium metal.[4] The heavier group 13 carbene analogues $Dipp_2NacNacE$ (E = Ga **4.6**, In **4.7** and Tl **4.8**) have also been reported.[5-7]

In related aluminium chemistry, Jordan and co-workers structurally characterised the three-coordinate cationic Al(III) system [$Dipp_2NacNacAlMe$][$B(C_6F_5)_4$] (**4.9**) formed by methide abstraction from the corresponding dimethyl precursor. In the solid state a short Al···F contact with the $[B(C_6F_5)_4]^-$ anion is observed; however, in solution the ^1H NMR spectrum shows the $Dipp_2NacNac$ substituent to be symmetric and the ^{19}F NMR spectrum shows no evidence that the Al···F interaction persists in solution.[8] More recently Fulton and co-workers used a similar approach to structurally characterise the related lead(II) and tin(II) cations [$Dipp_2NacNacE$][X] (E = Pb and X = [$B(C_6F_5)_4$] **4.10**, E = Sn and X = [$MeB(C_6F_5)_3$] **4.11**). The cations **4.10** and **4.11** were formed by the abstraction of chloride or methide anion from the corresponding precursors $Dipp_2NacNacPbCl$ (**4.12**) and $Dipp_2NacNacSnMe$ (**4.13**) respectively.[9]

The $Dipp_2$NacNac substituent has also been utilised in group 2 chemistry to form kinetically inert molecular species. In 2006 Harder and Brettar reported the formation and characterisation of the discrete molecular calcium hydride compound $[(Dipp_2NacNac)Ca(H)(THF)]_2$ (**4.14**).[10] Compound **4.14** is a stable heteroleptic calcium compound that does not undergo redistribution and is soluble in organic solvents. The same group has demonstrated the use of **4.14** to effect ketone reduction and hydrosilylation chemistry as well as the formation of amidoborane complexes, from which further elimination of hydrogen provides insight into the dehydrogenative pathways relevant in amino-borane chemistry.[11,12] Jones and co-workers subsequently reported the related magnesium(I) dimer $[Dipp_2NacNacMg]_2$ (**4.15**) formed from the reduction of the corresponding iodide complex with potassium metal.[13] Compound **4.15**, and the related sterically bulky guanidinate analogue **3.6**, show remarkable stability and as such have found applications as mild and bespoke reducing agents in organometallic chemistry.[14-16]

Although the $Dipp_2$NacNac substituent has been shown to be highly effective in the stabilisation of reactive main group systems, reports of the ligand backbone showing non-innocent behaviour are also present in the literature. Driess and co-workers reported the deprotonation of the backbone methyl substituents in the reaction between $Dipp_2$NacNacLi and $SiBr_4$ (in the presence of TMEDA) resulting in the formation of diamido substituted $(Dipp_2NacNac')SiBr_2$ (**4.16**). Subsequent reduction of **4.16** with potassium graphite yielded the corresponding silylene **4.17** (Scheme 4.1).[17]

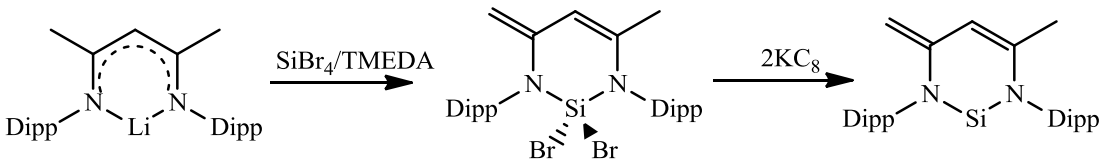

4.16 **4.17**

Scheme 4.1: *In situ deprotonation of the NacNac backbone forming the diamido substituted* ***4.16*** *and subsequent reduction to* ***4.17***

A related boron complex featuring the diamido $Dipp_2$NacNac' ({HC(CMeNDipp)(C(CH_2)NDipp)}$^{2-}$) substituent $Dipp_2$NacNac'BBr (**4.18**) has also been reported, and features a planar three-coordinate boron centre.[18] More recently, Hill and co-workers reported a number of beryllium compounds featuring the $Dipp_2$NacNac substituent. The reduction chemistry of $Dipp_2$NacNacBeCl was investigated, and a further example of non-innocent behaviour of the $Dipp_2$NacNac backbone was observed. This time ligand activation took the form of hydride reduction of the imine functionality, which was structurally characterised in the dinuclear species **4.19** (Figure 4.2).[19] Given that the $Dipp_2$NacNac substituent has been shown to be robust and to stabilise the formation of a number of reactive main group and transition metal systems, it represents a potential substituent for the formation of a cationic three-coordinate aluminium centre bound to a transition metal.

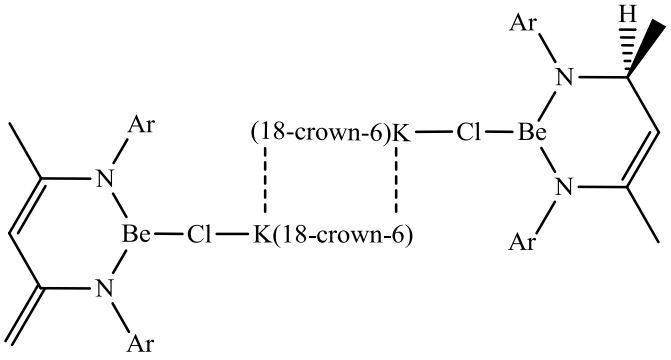

4.19

Figure 4.2: *Structure of **4.19***

4.2 Aims of the present research

The work carried out in this Chapter builds on that of Chapter III, in an attempt to characterise a transition metal bound three-coordinate aluminium cation. Studies of the amidinate and guanidinate complexes in Chapter III highlighted the difficulties in controlling the coordination environment of the aluminium centre, and in the formation of tractable charged species. To address these issues, the work in this Chapter is focused on the formation of more sterically demanding and more electron rich mixed transition metal-aluminium complexes. This was investigated in two approaches: (i) the use of more electron rich and sterically demanding transition metal fragments and (ii) the incorporation of more sterically demanding substituents at aluminium. It was thought that the combination of increased steric protection and reduced Lewis acidity of the aluminium centre are likely to result in the formation of a more easily isolable three-coordinate aluminium cation.

4.3 Experimental

Preparation of Cp*Fe(CO)$_2$[(Cl)Al{(NCy)$_2$CN^{i}Pr$_2$}] **(XII)**

To a slurry of Na[Cp*Fe(CO)$_2$] (0.35 g, 1.3 mmol) in diethyl ether (35 cm^3) at -78 °C was added slowly a solution of **III** (0.47 g, 1.2 mmol) also in diethyl ether (35 cm^3) and the reaction mixture was stirred for 12 h whilst slowly attaining room temperature. The resulting reaction mixture was filtered, concentrated and subsequently cooled to -30 °C affording yellow crystals of **XII**. Yield 0.33 g, 44%.

Spectroscopic data**:** ^{1}H NMR (C_6D_6, 300 MHz, 298 K): δ 3.37 (2H, m, NC*H*CH$_2$), 3.32 (2H, sept J_{HH} = 6.3 Hz), NC*H*(CH$_3$)$_2$), 2.18-1.22 (20H, m, Cy*H*), 1.86 (15H, s, C*H*$_3$ of Cp*), 1.10 (12H, d ($^3J_{HH}$ = 6.3 Hz), NCH(C*H*$_3$)$_2$). ^{13}C{^{1}H} NMR (C_6D_6, 75 MHz, 298 K): δ 218.9 (*C*O), 169.9 (*C*N$_3$), 94.1 (*C* of Cp*), 54.1 (N*C*H of Cy), 49.0 (br, N*C*H(CH$_3$)$_2$), 36.1 (Cy*C*), 35.5 (Cy*C*), 26.5 (Cy*C*), 26.4 (Cy*C*), 26.1 (Cy*C*), 22.9 (br, NCH(*C*H$_3$)$_2$), 10.6 (*C*H$_3$ of Cp*). ^{27}Al NMR (C_6D_6, 78 MHz, 298 K): δ 160. MS(EI): *m*/*z* 615.3 (M$^+$) 13 %, 587.3 [M-CO]$^+$ 1 %, 368.2 [M-{Cp*Fe(CO)$_2$}]$^+$ 24 %; accurate mass: calc. 615.2829, meas. 615.2830. IR (CH_2Cl_2 solution, cm^{-1}) 1951, 1892 cm^{-1} (ν_{CO}). Elemental microanalysis: calc. for $C_{31}H_{51}N_3AlClFeO_2$ C 60.42 H 8.35 N 6.82; meas. C 60.51 H 8.21 N 6.74.

Crystallographic data**:** $C_{31}H_{51}AlClFeN_3O_2$, M_r = 616.05, triclinic, *P*-1, *a* = 10.5121(4), *b* = 11.4183(4), *c* = 14.4923(6) Å, α = 89.0196(18), β = 71.366(2), γ = 80.7037(15)^o, *V* = 1625.6(1) Å^3, *Z* = 2, ρ_c = 1.259 Mg m^{-3}, *T* = 150 K, λ = 0.71073 Å. 21942 reflections collected, 7265 independent [R(int) = 0.020] which were used in all calculations. R_1 = 0.0459, wR_2 = 0.1083 for observed unique reflections [$I > 2\sigma(I)$] and R_1 = 0.0621, wR_2 = 0.1243 for all unique reflections. Max. and min. residual electron densities 0.85 and -0.63 e Å^{-3}. CCDC reference: 894962.

***Preparation of Cp*Fe(CO)$_2$[(Me)Al{(NCy)$_2$CN^{i}Pr$_2$}]* (XIII)**

To a slurry of Na[Cp*Fe(CO)$_2$] (0.28 g, 1.1 mmol) in diethyl ether (45 cm^3) at -78 °C was added slowly a solution of **X** (0.40 g, 1.0 mmol) also in diethyl ether (40 cm^3) and the reaction mixture stirred for 12 h whilst slowly attaining room temperature. The resulting reaction mixture was filtered, concentrated and subsequently cooled to -30 °C affording yellow crystals of **XIII**. Yield 0.30 g, 46%.

***Spectroscopic data*:** ^{1}H NMR (C_6D_6, 300 MHz, 298 K): δ 3.37 (4H, m, overlapping NC*H* and NC*H*(CH$_3$)$_2$), 2.05-1.60 (20H, m, Cy*H*), 1.83 (15H, s, C*H*$_3$ of Cp*), 1.11 (12H, br s, NCH(C*H*$_3$)$_2$), 0.02 (3H, s, AlC*H*$_3$). ^{13}C{^{1}H} NMR (C_6D_6, 125 MHz, 298 K): δ 220.4 (*C*O), 166.3 (*C*N$_3$), 93.0 (*C* of Cp*), 53.9 (N*C*H of Cy), 49.5 (br, N*C*H(CH$_3$)$_2$), 48.0 (br, N*C*H(CH$_3$)$_2$), 36.2 (Cy*C*), 35.9 (Cy*C*), 26.6 (Cy*C*), 26.4 (Cy*C*), 26.2 (Cy*C*), 23.2 (br, NCH(*C*H$_3$)$_2$), 22.9 (br, NCH(*C*H$_3$)$_2$), 10.8 (*C*H$_3$ of Cp*), -3.1 (br, Al*C*H$_3$). ^{27}Al NMR (C_6D_6, 78 MHz, 298 K): δ 181. MS(EI): *m*/*z* 595.3 (M$^+$) 5 %, 348.2 [M-{Cp*Fe(CO)$_2$}]$^+$ 100 %; accurate mass: calc. 593.3421, meas. 593.3422. IR (CH_2Cl_2 solution, cm^{-1}) 1944, 1877 (ν_{CO}).

***Crystallographic data*:** $C_{32}H_{54}AlFeN_3O_2$, M_r = 595.63, triclinic, P-1, *a* = 10.4973(2), *b* = 11.4644(2), *c* = 14.7576(3) Å, α = 86.8923(17)°, β = 70.6133(19)°, γ = 79.5184(17)°, *V* = 1647.31(6) Å^3, *Z* = 2, ρ_c = 1.201 Mg m^{-3}, *T* = 150 K, λ = 1.54180 Å. 33671 reflections collected, 6861 independent [R(int) = 0.0283] used in all calculations. R_1 = 0.0311, wR_2 = 0.0794 for observed unique reflections [$I > 2\sigma(I)$] and R_1 = 0.0319, wR_2 = 0. 0800 for all unique reflections. Max. and min. residual electron densities 0.29 and -0.40 e Å^{-3}. CCDC reference: 894966.

Preparation of $Cp^{Si}Fe(PPh_3)(CO)[(Cl)Al\{(NCy)_2CN^iPr_2\}]$ (XIV)

To a freshly prepared solution of $Na[Cp^{Si}Fe(PPh_3)(CO)]$ (1.6 mmol) in hexane (180 cm^3) at -78 °C was added slowly a solution of **III** (0.87 g, 1.6 mmol) also in hexane (50 cm^3) and the reaction mixture was stirred for 12 h whilst slowly attaining room temperature, and then for a further 48 h at room temperature. A yellow precipitate formed which was isolated by filtration and dried *in vacuo*. Recrystallisation from a dichloromethane/hexane mixture at room temperature yielded yellow crystals of **XIV**. Storage of the hexane filtrate at -20 °C yielded further yellow crystals of **XIV**. Yield 0.32 g, 24%.

***Spectroscopic data*:** ^{1}H NMR (C_6D_6, 300 MHz, 298 K): δ 7.90-7.01 (15H, m, P(C_6H_5)$_3$), 5.71 (1H, s, $Cp^{Si}H$), 4.17 (1H, s, $Cp^{Si}H$), 3.89 (1H, s, $Cp^{Si}H$), 3.76 (1H, s, $Cp^{Si}H$), 3.47 (1H, m, NC*H*), 3.33 (3H, m, NC*H*), 2.24-1.20 (10H, m, Cy*H*), 1.12 (12H, overlapping d ($^3J_{HH}$ = 6.3 Hz) NCH(CH_3)$_2$), 0.43 (9H, s, Si(CH_3)$_3$). ^{13}C{^{1}H} NMR (C_6D_6, 125 MHz, 298 K): δ 221.6 (d, ($^1J_{PC}$ = 25.0 Hz) *CO*), 169.5 (*C*N$_3$), 140.7 (d ($^1J_{PC}$ = 50.0 Hz) Ar*C*), 134.6 (d ($^2J_{PC}$ = 12.5 Hz) Ar*C*), 129.4 (d ($^4J_{PC}$ = 1.9 Hz) Ar*C*), 128.7 (Ar*C*), 93.3 ($Cp^{Si}C$), 91.7 ($Cp^{Si}C$), 83.6 ($Cp^{Si}C$), 83.5 ($Cp^{Si}C$) 75.6 ($Cp^{Si}C$), 55.0 (N*C*H), 54.9 (N*C*H) 49.5 (br N*C*H(CH_3)$_2$), 49.0 (br N*C*H(CH_3)$_2$), 36.6 (Cy*C*), 36.4 (Cy*C*), 36.2 (Cy*C*), 35.8 (Cy*C*), 26.9 (4 x overlapping Cy*C*), 26.4 (Cy*C*), 26.1 (Cy*C*), 23.4 (NCH(*C*H$_3$)$_2$), 23.3 (NCH(*C*H$_3$)$_2$), 0.7 (Si(*C*H$_3$)$_3$ of Cp^{Si}). ^{31}P{^{1}H} NMR (C_6D_6, 121 MHz, 298 K): δ 81.2. ^{27}Al NMR (C_6D_6, 78 MHz, 298 K): δ 181. MS(EI): *m*/*z* 851.3 (M^+) 5 %. IR (CH_2Cl_2 solution, cm^{-1}) 1876 (ν_{CO}).

Crystallographic data: $C_{46}H_{64}AlClFeN_3OPSi$, M_r = 852.37, monoclinic, P21/n, *a* = 19.13688(11), *b* = 12.10825(6), *c* = 21.56418(14) Å, β = 113.3006(7)°, *V* = 4589.20(5) Å^3, *Z* = 4, ρ_c = 1.234 Mg m^{-3}, *T* = 150 K, λ = 1.54180 Å. 100006 reflections collected, 9595 independent [R(int) = 0.024] used in all calculations. R_1 = 0.0382, wR_2 = 0. 0746 for observed unique reflections [$I > 2\sigma(I)$] and R_1 = 0.0371, wR_2 = 0.0745 for all unique reflections. Max. and min. residual electron densities 0.48 and -0.32 e Å^{-3}.

***Preparation of CpFe(CO)$_2$Al[(Cl)Al(Dipp$_2$NacNac)]* (XV)**

To a slurry of Na[CpFe(CO)$_2$] (0.13 g, 0.67 mmol) in diethyl ether (40 cm^3) at -78 °C was added dropwise a solution of Dipp$_2$NacNacAlCl$_2$ (0.32 g, 0.61 mmol) also in diethyl ether (30 cm^3). The reaction mixture was stirred for 24 h whilst slowly attaining room temperature. At this point the ^{27}Al NMR spectrum still showed some starting material so a further addition of Na[CpFe(CO)$_2$] (0.02 g, 0.01 mmol) as a slurry in diethyl ether (10 cm^3) was carried out at room temperature. The reaction mixture was stirred for a further 24 h and then filtered, concentrated and cooled to -30 °C yielding orange crystals of **XV**. Yield 0.08 g, 19%.

***Spectroscopic data*:** ^{1}H NMR (C_6D_6, 300 MHz, 298 K): δ 7.08-7.22 (6H, m, Ar*H*), 5.17 (1H, s, γ-CH), 4.01 (5H, s, Cp*H*), 3.92 (2H, sept ($^3J_{HH}$ = 6.9 Hz), C*H*(CH$_3$)$_2$), 3,47 (2H, sept ($^3J_{HH}$ = 6.6 Hz), C*H*(CH$_3$)$_2$), 1.66 (6H, s, C*H*$_3$ of β-diketiminate), 1.57 (6H, d ($^3J_{HH}$ = 6.6 Hz), CH(C*H*$_3$)$_2$), 1.38 (6H, d ($^3J_{HH}$ = 6.9 Hz), CH(C*H*$_3$)$_2$), 1.20 (6H, d ($^3J_{HH}$ = 6.9 Hz), CH(C*H*$_3$)$_2$), 1.02 (6H, d ($^3J_{HH}$ = 6.6 Hz), CH(C*H*$_3$)$_2$). ^{13}C{^{1}H} NMR (C_6D_6, 75 MHz, 298 K): δ 216.1 (s, *C*O), 170.1 (s, N*C*), 146.3 (s, Ar*C*), 143.0 (s, Ar*C*), 142.9 (s, Ar*C*), 127.6 (s, Ar*C*), 126.0 (s, Ar*C*), 123.7 (s, Ar*C*), 100.2 (γ-*C*H), 81.9 (s, Cp*C*), 30.2 (s, *C*H(CH$_3$)$_2$), 28.1 (s, *C*H(CH$_3$)$_2$), 26.1 (s, CH(*C*H$_3$)$_2$), 25.3 (s, CH(*C*H$_3$)$_2$), 24.9 (s, CH(*C*H$_3$)$_2$), 24.8 (s, CH(*C*H$_3$)$_2$), 24.0 (s, *C*H$_3$ of β-diketiminate). ^{27}Al NMR (C_6D_6, 78 MHz, 298 K): δ 149. IR (CH_2Cl_2 solution, cm^{-1}): 1985, 1928 cm^{-1} (ν_{CO}).

Crystallographic data: $C_{36}H_{46}AlClFeN_2O_2$, M_r = 657.05, triclinic, P-1, a = 10.65290(10), b = 15.6528(2), c = 20.5289(3) Å, ά = 89.6443(5)^o, β = 88.8726(5)^o, γ = 83.9054(5)^o, V = 3403.11(7) Å^3, Z = 4, ρ_c = 1.282 Mg m^{-3}, T = 150 K, λ = 0.71073 Å. 48483 reflections collected, 15462 independent [R(int) = 0.059] used in all calculations. R_1 = 0.0514, wR_2 = 0.1066 for observed unique reflections [$I > 2\sigma(I)$] and R_1 = 0.0862, wR_2 = 0.1380 for all unique reflections. Max. and min. residual electron densities 1.27 and -0.74 e Å^{-3}.

Preparation of Cp*Fe(CO)$_2$[(Cl)Al(Dipp$_2$NacNac)] **(XVI)**

To a slurry of Na[Cp*Fe(CO)$_2$] (0.30 g, 1.1 mmol) in diethyl ether (40 cm^3) at -78 °C was added a solution of Dipp$_2$NacNacAlCl$_2$ (0.46 g, 0.90 mmol) also in diethyl ether (40 cm^3), the reaction mixture was stirred for 12 h whilst slowly attaining room temperature, and subsequently stirred for a further 48 h at room temperature. The resulting mixture was filtered, concentrated and subsequently cooled to -30 °C affording yellow crystals of **XVI**. Yield 0.15 g, 23%.

***Spectroscopic data*:** ^{1}H NMR (C_6D_6, 300 MHz, 298 K): δ 7.24-7.11 (6H, m, Dipp aromatic *H*), 5.10 (1H, γ-C*H*), 3.93 (2H, sept ($^3J_{HH}$ = 6.6 Hz), C*H*(CH$_3$)$_2$), 3.59 (2H, sept ($^3J_{HH}$ = 6.6 Hz), C*H*(CH$_3$)$_2$), 1.59 (6H, s, C*H*$_3$ of β-diketiminate), 1.58 (6H, d ($^3J_{HH}$ = 6.6 Hz), CH(C*H*$_3$)$_2$), 1.44 (6H, d ($^3J_{HH}$ = 6.6 Hz), CH(C*H*$_3$)$_2$), 1.40 (15H, s, C*H*$_3$ of Cp*), 1.24 (6H, d ($^3J_{HH}$ = 6.6 Hz), CH(C*H*$_3$)$_2$), 1.02 (6H, d ($^3J_{HH}$ = 6.6 Hz), CH(C*H*$_3$)$_2$). ^{13}C{^{1}H} NMR (C_6D_6, 125 MHz, 298 K): δ 219.6 (*C*O), 170.0 (N*C*), 146.4 (Ar*C*), 144.4 (Ar*C*), 143.3 (Ar*C*), 127.4 (Ar*C*), 125.8 (Ar*C*), 124.0 (Ar*C*), 99.6 (γ-*C*H), 94.8 (*C* of Cp*), 30.1 (*C*H(CH$_3$)$_2$), 28.2 (*C*H(CH$_3$)$_2$), 26.2 (CH(*C*H$_3$)$_2$), 25.8 (CH(*C*H$_3$)$_2$), 25.4 (CH(*C*H$_3$)$_2$), 25.0 (CH(*C*H$_3$)$_2$), 24.5 (*C*H$_3$ of β-diketiminate), 10.2 (*C*H$_3$ of Cp*). ^{27}Al NMR (C_6D_6, 78 MHz, 298 K): δ 136. MS(EI): *m*/*z* 726.3 (M^+) 2 %, 479.3 [M-{Cp*Fe(CO)$_2$}]$^+$ 100 %; accurate mass: calc. 724.3236, meas. 724.3233. IR (CH_2Cl_2 solution, cm^{-1}) 1964, 1908 (ν_{CO}). Elemental microanalysis: calc. for $C_{41}H_{56}N_2AlFeO_2$ C 67.70 H 7.77 N 3.85; meas. C 67.60 H 7.86 N 3.96.

***Crystallographic data*:** $C_{41}H_{56}AlClFeN_2O_2$, M_r = 727.19, monoclinic, $P2_1/n$, a = 11.2413(1), b = 20.2466(2), c = 17.0845(1) Å, β = 90.4148(4)^o, V = 3888.30(6) Å^3, Z = 4, ρ_c = 1.242 Mg m^{-3}, T = 150 K, λ = 0.71073 Å. 101655 reflections collected, 8860 independent [R(int) = 0.023] which were used in all calculations. R_1 = 0.0449, wR_2 = 0.1276 for observed unique reflections [$I > 2\sigma(I)$] and R_1 = 0.0615, wR_2 = 0.1397 for all

unique reflections. Max. and min. residual electron densities 0.77 and -0.68 e $Å^{-3}$. CCDC reference: 894964.

Procedure for halide abstraction using $[Et_3Si][B(C_6F_5)_4]$, $AlCl_3$, $GaCl_3$ and $B(C_6F_5)_3$

The same method was used for all reactions and is exemplified by the reaction between $[Et_3Si][B(C_6F_5)_4]$ and $Cp^*Fe(CO)_2[(Cl)Al(Dipp_2NacNac)]$. A fluorobenzene solution of $Cp^*Fe(CO)_2[(Cl)Al(Dipp_2NacNac)]$ at -30 °C was transferred *via* cannula to a J Young's NMR tube containing solid $[Et_3Si][B(C_6F_5)_4]$ and a small amount of fluorobenzene also at -30 °C. The NMR tube was subsequently shaken and warmed slowly to room temperature.

***Preparation of {HC(CMeNDipp)(C(CH$_2$)NDipp)}AlCl$_2$Li(OEt$_2$)$_2$* (XVIII)**

To a stirred solution of $Dipp_2NacNacAlCl_2$ (0.51 g, 1.00 mmol) in diethyl ether (50 cm^3) at -78 °C was added dropwise ^{t}BuLi (0.8 cm^3, 1.9 M in pentane, 1.5 mmol). The reaction mixture was allowed to attain room temperature over 12 hours. The reaction mixture was filtered, concentrated and cooled to -30 °C to yield colourless crystals of **XVIII**. Yield 0.25 g, 39%.

***Spectroscopic Data*:** ^{1}H NMR (C_7D_8, 300 MHz, 298 K): δ 7.09-7.21 (6H, m, Ar*H*), 5.31 (1H, s, γ-CH), 3.98 and 4.01 (4H, overlapping sept ($^3J_{HH}$ = 6.9 Hz), C*H*(CH_3)$_2$), 3.85 (1H, s, NCC*H*$_2$), 3.07 (1H, s, NCC*H*$_2$), 2.83 (8H, q ($^3J_{HH}$ = 7.1 Hz), O(C*H*$_2$$CH_3$)$_2$), 1.69 (3H, s, NCC*H*$_3$), 1.51 (6H, d ($^3J_{HH}$ = 6.9 Hz), CH(C*H*$_3$)$_2$), 1.47 (6H, d ($^3J_{HH}$ = 6.9 Hz), CH(C*H*$_3$)$_2$), 1.43 (6H, d ($^3J_{HH}$ = 6.9 Hz), CH(C*H*$_3$)$_2$), 1.30 (6H, d ($^3J_{HH}$ = 6.9 Hz), CH(C*H*$_3$)$_2$), 0.64 (12H, t ($^3J_{HH}$ = 7.1 Hz), O(CH_2C*H*$_3$)$_2$). ^{13}C{^{1}H} NMR (C_7D_8, 75 MHz, 298 K): δ 154.6, 148.8, 148.7, 144.6, 142.0, 141.8, 125.7, 125.6, 124.0, 123.7 (s, N*C* and Ar*C*), 102.4 (s, γ-*C*H), 82.1 (s, NC*C*H$_2$), 65.4 (s, O(*C*H$_2$$CH_3$)$_2$), 28.4 (s, *C*H($CH_3$)$_2$), 28.1 (s, *C*H($CH_3$)$_2$), 27.4

(s, CH(CH$_3$)$_2$), 25.5 (s, CH(CH$_3$)$_2$), 25.4 (s, CH(CH$_3$)$_2$), 24.7 (s, CH(CH$_3$)$_2$), 23.4 (s, NCCH$_3$), 14.2 (s, O(CH$_2$$CH_3$)$_2$). ^{27}Al NMR (C$_7D_8$, 78 MHz, 298 K): δ 100.

Crystallographic data: $C_{37}H_{60}Al_1Cl_2Li_1N_2O_2$, M_r = 669.72, monoclinic, P21/n, a = 13.05030(10), b = 16.81950(10), c = 18.6926(2) Å, β = 101.3483(4)^o, V = 4022.80(6) Å^3, Z = 4, ρ_c = 1.106 Mg m^{-3}, T = 150 K, λ = 0.71073 Å. 65758 reflections collected, 9141 independent [R(int) = 0.027] used in all calculations. R_1 = 0.0526, wR_2 = 0.1280 for observed unique reflections [$I > 2\sigma(I)$] and R_1 = 0.0751, wR_2 = 0.1531 for all unique reflections. Max. and min. residual electron densities 0.67 and -0.43 e Å^{-3}.

Preparation of [{HC(CMeNDipp)(C(CH$_2$)NDipp)}AlCl$_2$][K(18-crown-6] (XIX)

A solution of Dipp$_2$NacNacAlCl$_2$ (0.55 g, 1.06 mmol) in benzene (30 cm^3) was added dropwise to a rapidly stirred suspension of K[CH(SiMe$_3$)$_2$] (0.24 g, 1.2 mmol) also in benzene (10 cm^3) at room temperature. The reaction mixture was stirred for 12 h and then filtered. The filtrate was then added dropwise to a stirred solution of 18-crown-6 (0.28 g, 1.06 mmol) in benzene (15 cm^3), forming a colourless precipitate. After stirring for 2 h, the precipitate was isolated by filtration and washed with hexane (3 x 10 cm^3). Single crystals were grown by recrystallisation of a fraction of the bulk by THF/hexane layering stored at -30 °C. The remainder was shown to be > 95% pure by ^{1}H NMR spectroscopy. Yield 0.75 g, 87%, > 95% pure.

Spectroscopic data: ^{1}H NMR (C$_4$D$_8$O, 300 MHz, 298 K): δ 6.95-7.02 (6H, m, ArH), 4.80 (1H, s, γ-CH), 4.00 (2H, sept ($^3J_{HH}$ = 6.9 Hz), CH(CH$_3$)$_2$), 3.83 (2H, sept ($^3J_{HH}$ = 6.6 Hz) CH(CH$_3$)$_2$), 3.53 (24H s, CH$_2$ of 18-crown-6), 3.05 (1H, d ($^3J_{HH}$ = 1.8 Hz), NCCH_2), 2.30 (1H, d ($^3J_{HH}$ = 1.8 Hz) NCCH_2), 1.42 (3H, s, NCCH_3), 1.22 (6H, d ($^3J_{HH}$ = 6.9 Hz), CH(CH_3)$_2$), 1.21 (6H, d ($^3J_{HH}$ = 6.6 Hz), CH(CH_3)$_2$), 1.19 (6H, d ($^3J_{HH}$ = 6.9 Hz), CH(CH_3)$_2$), 1.17 (6H, d ($^3J_{HH}$ = 6.6 Hz), CH(CH_3)$_2$). ^{13}C{^{1}H} NMR (C$_4$D$_8$O, 75 MHz, 298

K): δ 156.8, 149.2, 149.1, 145.3, 145.1, 144.6, 124.9, 124.8, 123.9, 123.5 (s, N*C* and Ar*C*), 102.9 (s, γ-*C*H), 78.1 (s, NC*C*H_2), 71.3 (s, CH_2 of 18-crown-6), 28.6 (s, *C*H(CH_3)$_2$), 28.4 (s, *C*H(CH_3)$_2$), 27.2 (s, CH(*C*H_3)$_2$), 26.6 (s, CH(*C*H_3)$_2$), 25.7 (s, CH(*C*H_3)$_2$), 25.3 (s, CH(*C*H_3)$_2$), 24.2 (s, NC*C*H_3). ^{27}Al NMR (C_4D_8O, 78 MHz, 298 K): δ 100.

***Crystallographic data*:** $C_{45.90}H_{75.44}AlCl_2KN_2O_6$, M_r = 888.34, monoclinic, P21/c, *a* = 16.22530(10), *b* = 12.24330(10), *c* = 26.6313(2) Å, β = 105.0984(9)^o, *V* = 5107.72(7) Å^3, *Z* = 4, ρ_c = 1.155 Mg m^{-3}, *T* = 150 K, λ = 1.54180 Å. 114679 reflections collected, 10766 independent [R(int) = 0.049] used in all calculations. R_1 = 0.0341, wR_2 = 0.0917 for observed unique reflections [$I > 2\sigma(I)$] and R_1 = 0.0380, wR_2 = 0.0953 for all unique reflections. Max. and min. residual electron densities 0.46 and -0.28 e Å^{-3}.

4.4 Results and Discussion

Salt metathesis reactions between $Na[CpFe(CO)_2]$ and amidinate or guanidinate substituted aluminium precursors (**3.20**, **II**, **III** and **X**) have been shown to result in the ready formation of mixed metal aluminium-iron complexes of the type $CpFe(CO)_2[(X)Al\{(NR)_2CR'\}]$ (where X = Cl, I or Me; R = Cy, ^{i}Pr or Dipp; R' = Ph or N^{i}Pr$_2$). Studies of these complexes in solution identified the formation of species featuring augmented coordination at the aluminium centre. To suppress the increase in coordination number at aluminium and promote the formation of a cationic three-coordinate aluminium complex, the synthesis of more optimal derivatives was investigated *via* two approaches: (i) the use of more sterically demanding and electron rich transition metal fragments and (ii) the use of a more sterically demanding substituent at the aluminium centre.

4.4.1 Reactions with More Sterically Demanding Transition Metal Fragments

The Cp* ligand is more sterically demanding than its Cp counterpart and also forms more electron rich complexes on account of the increased inductive effect from the substitution of protons for methyl groups. The superior electron donating properties of the Cp* ligand can be observed by comparison of the carbonyl stretching frequencies of $[CpFe(CO)_2]_2$ (1997, 1775 cm^{-1}) with those of $[Cp^*Fe(CO)_2]_2$ (1922, 1748 cm^{-1}). In an extension to the established salt metathesis chemistry, the reactions between the aluminium precursors **III** or **X**, and $Na[Cp^*Fe(CO)_2]$ readily yield the corresponding mixed metal complexes $Cp^*Fe(CO)_2[(X)Al(NCy)_2CN^iPr_2]$ (where X = Cl, **XII**, or Me, **XIII**) (Scheme 4.2).

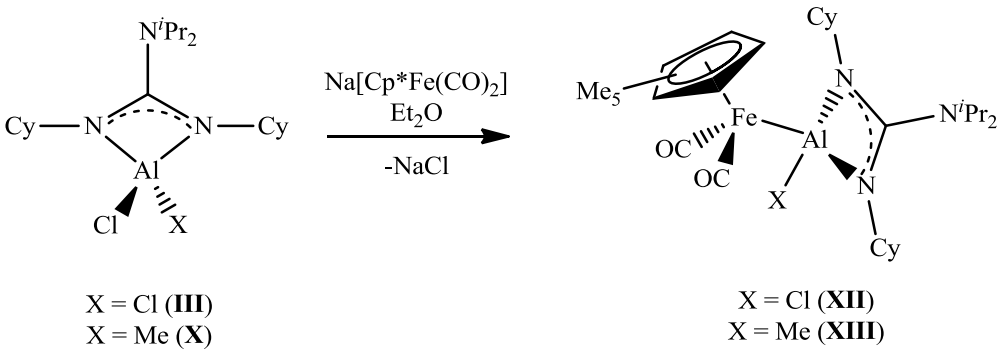

X = Cl (**III**)
X = Me (**X**)

X = Cl (**XII**)
X = Me (**XIII**)

Scheme 4.2: *Reaction between **III** or **X** and Na[Cp*Fe(CO)$_2$]*

Both reactions proceed readily and can be monitored *in situ* by ^{27}Al NMR spectroscopy, with a diagnostic downfield shift of *ca.* 60 ppm being observed upon metal-metal bond formation. Despite the incorporation of the more electron rich Cp* ligand, the ^{27}Al NMR resonances observed for **XII** and **XIII** are almost identical to those of the Cp analogues (**XII** and **XIII** δ_{Al} = 160 and 181 ppm; *cf.* **VI** and **IX** δ_{Al} = 163 and 184 ppm). Complexes **XII** and **XIII** have been characterised by standard spectroscopic and analytical techniques as well as by X-ray crystallography (Figure 4.3 and Figure 4.4).

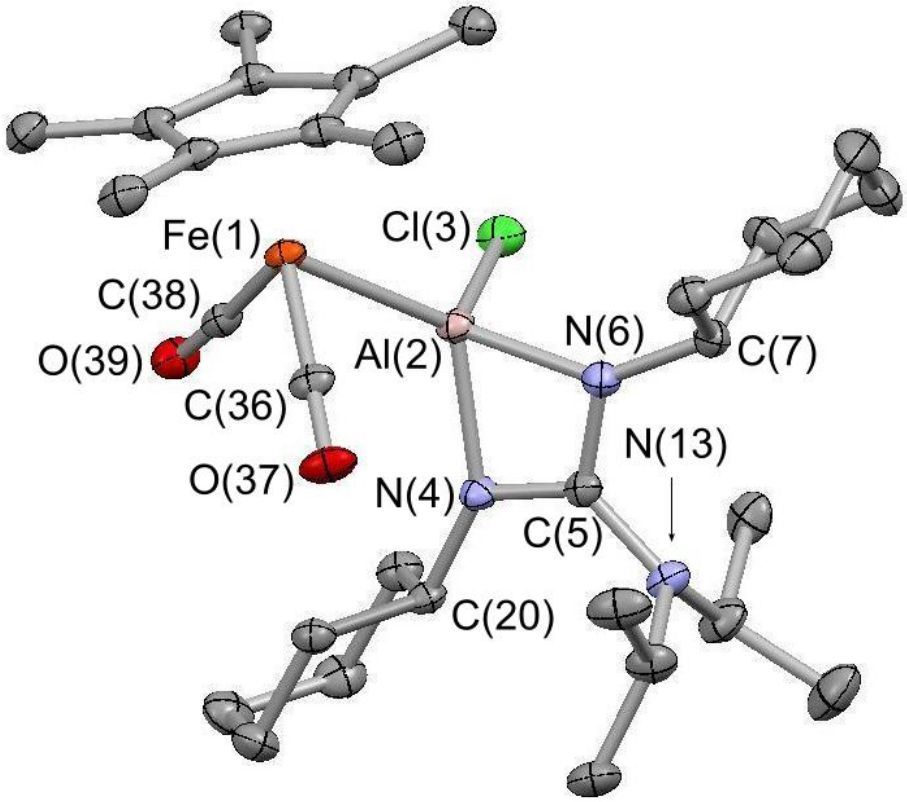

Figure 4.3: *Molecular structure of **XII** Thermal ellipsoids set at the 40% probability level and hydrogen atoms omitted for clarity.* Key bond lengths (Å) and angles (°): Fe(1)-Al(2) 2.357(1), Al(2)-Cl(3) 2.163(2), Al(2)-N(4) 1.926(2), Al(2)-N(6) 1.922(3), N(4)-C(5) 1.328(3), C(5)-N(6) 1.343(3), C(5)-N(13) 1.407(3); N(4)-Al(2)-N(6) 69.15(9), Cl(3)-Al(2)-N(4) 107.36(7), Cl(3)-Al(2)-N(6) 107.63(8), Fe(1)-Al(2)-N(4) 121.09(7), Fe(1)-Al(2)-N(6) 126.67(7), Fe(1)-Al(2)-Cl(3) 115.82(4), N(4)-C(5)-N(6) 109.7(2).

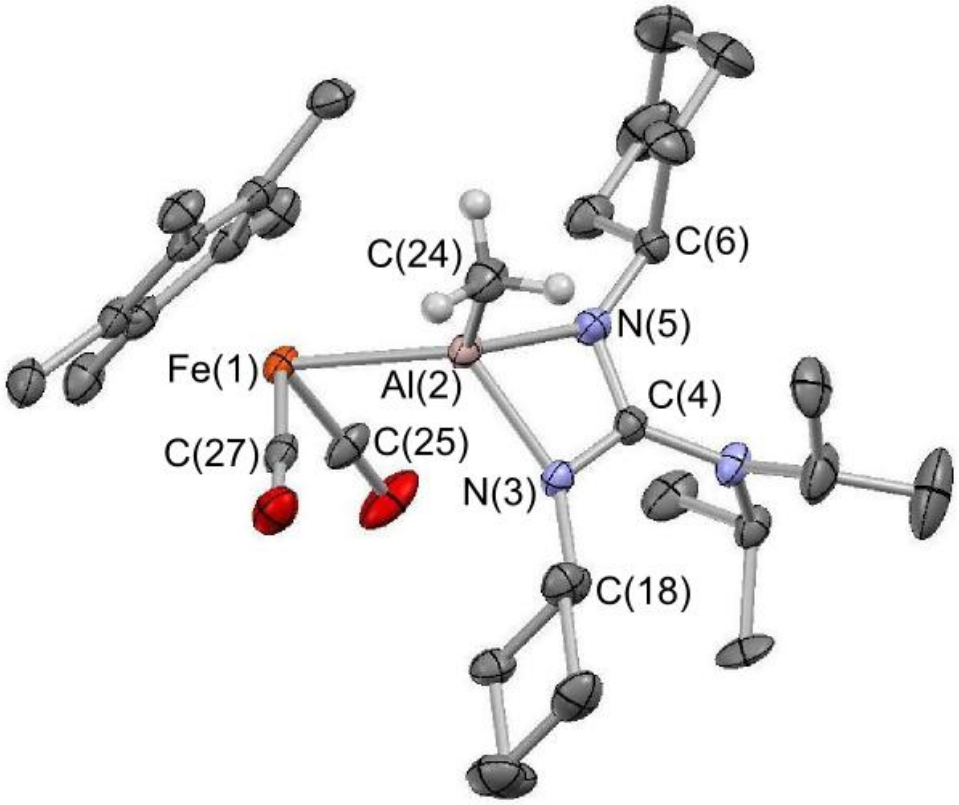

Figure 4.4: *Molecular structure of **XIII** Thermal ellipsoids set at the 40% probability level and hydrogen atoms (except Al-CH_3) omitted for clarity.* Key bond lengths (Å) and angles (°): Fe(1)-Al(2) 2.405(1), Al(2)-C(24) 1.969(2), Al(2)-N(3) 1.945(2), Al(2)-N(5) 1.937(2), N(3)-C(4) 1.333(2), C(4)-N(5) 1.335(2), C(4)-N(100) 1.407(2); N(3)-Al(2)-N(5) 68.51(5), N(3)-Al(2)-C(24) 109.79(6), N(5)-Al(2)-C(24) 110.53(7), Fe(1)-Al(2)-N(3) 117.13(4), Fe(1)-Al(2)-N(5) 122.63(4), Fe(1)-Al(2)-C(24) 118.08(5), N(3)-C(4)-N(5) 110.0(2).

Complexes **XII** and **XIII** both feature a single crystallographically distinct molecule in the asymmetric unit and show many structural similarities with their Cp analogues **VI** and **IX**. In both **XII** and **XIII** a four-coordinate aluminium centre is observed with a geometry that is distorted from tetrahedral to accommodate the constraints imposed by the four-membered heterocycle (N-Al-N 69.15(9) and 68.51(5)° for **XII** and **XIII** respectively). The X-Al-Fe-Cp centroid torsion angles (where X = Cl or Me) both show relatively close approach to idealised *syn* conformations (56.6° for **XII** and 55.7° for **XIII**) although the barrier to rotation around the Fe-Al bond, as in related boryl compounds,[20] is expected to be small such that the observed torsion angles are within the realms of crystal packing forces. The observed Fe-Al bond lengths for both **XII** and **XIII** are similar to their Cp analogues (*d*(Fe-Al) 2.357(1) and 2.405(1) Å for **XII** and **XIII** respectively; *cf.* 2.364(2) and 2.411(2) Å for **VI** and **IX** respectively). Whilst on steric grounds a longer Fe-Al bond length may be expected in the Cp* complexes an alternative bonding description can be considered as a potential rationale for the similar Fe-Al bond lengths in both Cp and Cp* complexes. With the donor/acceptor complex $[CpFe(CO)_2AlPh_3]^-$ (**1.19**) having been previously reported,[21] and the relative electronegativities of Fe and Al (1.83 and 1.61 respectively)[22] **XII** and **XIII** could potentially be considered as a $[Cp^*Fe(CO)_2]^-$ anion coordinated to a $[XAl(NCy)_2CN^iPr_2]^+$ cation as a Lewis acid/base adduct. Under this bonding description a stronger Lewis base (*i.e.* the $[Cp^*Fe(CO)_2]^-$ anion in comparison to $[CpFe(CO)_2]^-$ anion) forms a stronger interaction with the aluminium cation resulting in a shorter Fe-Al bond. The most logical description of the Fe-Al bond, however, is a standard two-centre two-electron bond but a small contribution from this alternative bonding description is conceivable. The orientation of the N^iPr_2 backbone substituent, as in the Cp compounds, shows that the contribution from the diamido guanidinate resonance form is minimal in both **XII** and **XIII**. The carbonyl stretching frequencies for **XII** and **XIII** clearly show these

compounds to be more electron rich than the Cp counterparts (*cf.* 1951, 1892 and 1944, 1877 cm^{-1} for **XII** and **XIII**, respectively; 1973, 1912 and 1958, 1896 cm^{-1} for **VI** and **IX**, respectively).

The structural changes observed on the substitution of the aluminium bound chloride in **XII** for a methyl group in **XIII** are consistent with Bent's rule. A lengthening of the N-Al bond [*d*(N-Al) 1.926(2), 1.922(3) Å for **XII** and 1.945(2), 1.937(2) for **XIII**] and the Fe-Al bond (*d*(Fe-Al) 2.357(1) for **XII** and 2.405(1) for **XIII**) implying that these bonds possess greater aluminium 3*p*-character on account of the greater aluminium 3*s*-character observed in the Al-C bond (*cf.* Al-Cl bond).

^{1}H and ^{13}C NMR studies of **XII** and **XIII** suggest that the solid state structure is maintained at room temperature in solution. Variable temperature ^{27}Al NMR studies were carried out to determine if the formation of a five-coordinate aluminium species is suppressed by the increased steric demands and electron richness of the $\{Cp^*Fe(CO)_2\}$ moiety in comparison to $\{CpFe(CO)_2\}$. However, some evidence for augmented coordination was still observed by ^{27}Al NMR spectroscopy.

The abstraction of chloride from **XII** or methide from **XIII** to yield the corresponding cationic three-coordinate aluminium complexes was investigated using different halide and methide abstraction agents (Scheme 4.3).

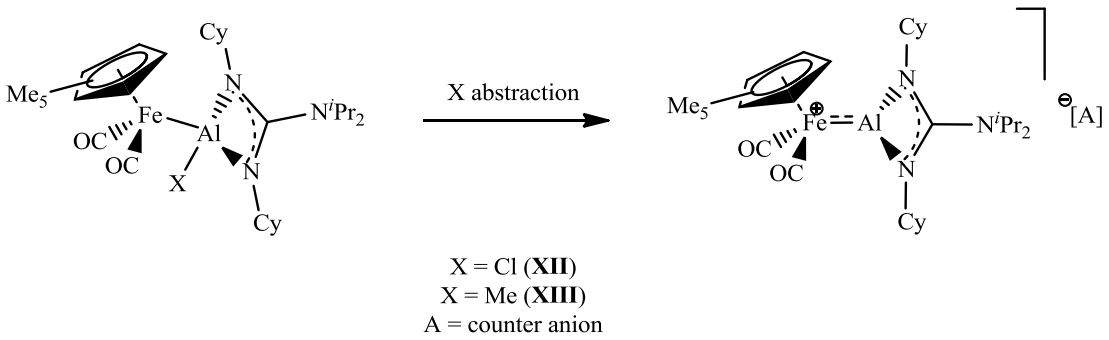

X = Cl (**XII**)
X = Me (**XIII**)
A = counter anion

Scheme 4.3: *Chloride/methide abstraction for the formation of a cationic complex*

Halide abstraction reactions using either $AlCl_3$ or $Na[BAr^f_4]$ yielded inseparable mixtures of products, from which the only identifiable product was $[Cp^*Fe(CO)_2]_2$. This was also observed for the attempted formation of an acetonitrile stabilised cation through halide abstraction with $Na[BAr^f_4]$, in the presence of acetonitrile. Methide abstraction from **XIII** using $B(C_6F_5)_3$ in flurobenzene allowed for spectroscopic characterisation of the anionic product of abstraction $[MeB(C_6F_5)_3]^-$ *via* ^{19}F and ^{11}B NMR spectroscopy. However, with no suitable spectroscopic handle allowing characterisation of the cationic component, and the formation of a number of inseparable products, largely $[Cp^*Fe(CO)_2]_2$, the fate of the cationic component could not be determined.

Despite the increased steric demands and electron-richness provided by the Cp* ligand in **XII** and **XIII** the formation of a stable three-coordinate cation was not definitively established. To further increase the steric demands of the transition metal fragment and make it more electron rich, the incorporation of trialkyl phosphines was investigated. In related boron chemistry the replacement of the π-acidic carbonyl ligands with trialkyl phosphines resulted in the formation of significantly more stable cationic terminal borylene compounds.[23,24] Having identified that the aluminium centre in the mixed metal iron-aluminium complexes remains Lewis acidic, the replacement of CO ligands prior to

forming the aluminium complex is preferable, thereby preventing phosphine coordination to the aluminium centre.

Pannell and co-workers reported the formation of the hexane soluble transition metal nucleophile $Na[Cp^{Si}Fe(CO)(PPh_3)]$ (**4.20**) (where $Cp^{Si} = \eta^5\text{-}C_5H_4SiMe_3$) and the solid state structures of the products formed when **4.20** is quenched with methyl iodide, chlorotimethylsilane and (chloromethyl)pentamethyldisilane ($ClCH_2SiMe_2SiMe_3$) forming $Cp^{Si}Fe(CO)(PPh_3)(Me)$ (**4.21**), $Cp^{Si}Fe(CO)(PPh_3)(SiMe_3)$ (**4.22**) and $Cp^{Si}Fe(CO)(PPh_3)(SiMe_2CH_2SiMe_3)$ (**4.23**) respectively.[25] The transition metal nucleophile **4.20** is formed by deprotonation of the Cp ring in $CpFe(CO)(PPh_3)(SiMe_3)$ by NaN^iPr_2, which is followed by migration of the $SiMe_3$ group to the Cp ring resulting in the formation of **4.20** (Scheme 4.4).

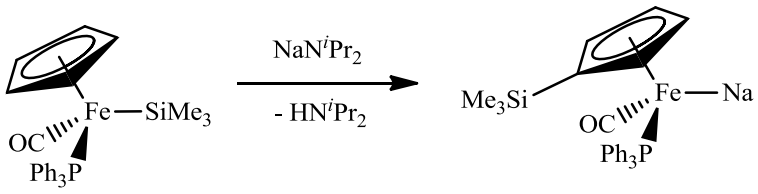

Scheme 4.4: *Formation of $Na[Cp^{Si}Fe(CO)(PPh_3)]$ (**4.20**)*

The reaction between **4.20** and **III** in hexane required an extended reaction time compared to reactions between **III** and the less sterically crowded transition metal anions $Na[CpFe(CO)_2]$ and $Na[Cp^*Fe(CO)_2]$ (Scheme 4.2). A yellow precipitate formed and spectroscopic characterisation identified this as $Cp^{Si}Fe(CO)(PPh_3)[(Cl)Al(NCy)_2CN^iPr_2]$ (**XIV**) (Scheme 4.5).

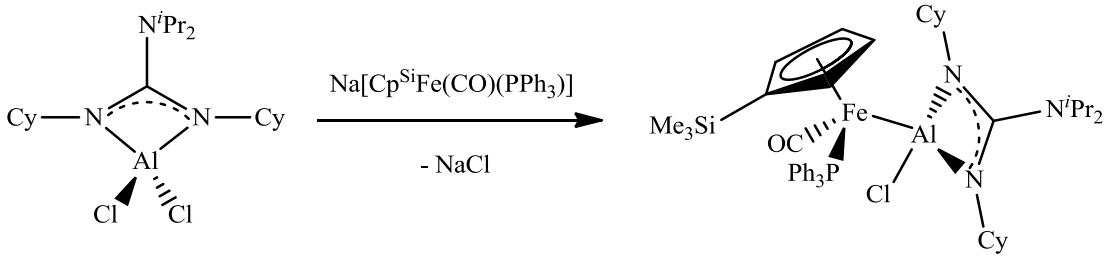

Scheme 4.5: *Reaction between **4.20** and **III***

Recrystallisation of this precipitate from a dichloromethane/hexane mixture yielded **XIV** as yellow crystals. Complex **XIV** has been characterised by standard spectroscopic and analytical techniques including X-ray crystallography (Figure 4.5).

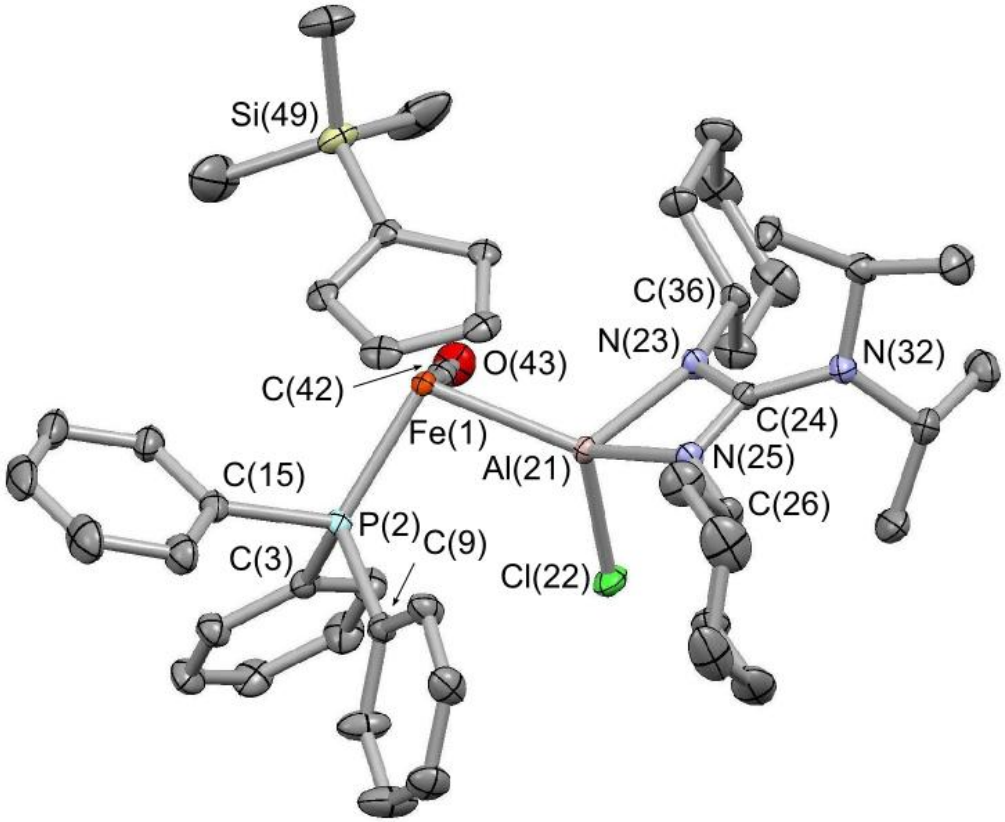

Figure 4.5: *Molecular structure of **XIV** Thermal ellipsoids set at the 40% probability level and hydrogen atoms omitted for clarity.* Key bond lengths (Å) and angles (°): Fe(1)-P(2) 2.197(1), Fe(1)-Al(21) 2.371(1), Al(21)-N(23) 1.943(2), Al(21)-N(25) 1.953(2), N(23)-C(24) 1.333(2), C(24)-N(25) 1.338(2), C(24)-N(32) 1.414(2); N(23)-Al(21)-N(25) 68.56(5), Cl(22)-Al(21)-N(23) 103.76(5), Cl(22)-Al(21)-N(25) 103.43(4), Fe(1)-Al(21)-N(23) 120.06(4), Fe(1)-Al(21)-N(25) 128.51(4), Fe(1)-Al(21)-Cl(22) 120.16(2), N(23)-C(24)-N(25) 110.5(2).

The molecular structure of **XIV** features a single crystallographically distinct molecule in the asymmetric unit and has an Fe-Al bond length of 2.371(1) Å which is longer than that observed in the related non phosphine containing and Cp and Cp* derivatives **VI** and **XII** (*d*(Fe-Al) 2.364 and 2.357 Å respectively). Elongation of the Fe-Al bond is likely due to the increased steric demands imposed by the transition metal fragment, most notably the incorporation of the PPh_3 moiety. This is also likely to contribute to the longer N-Al bond lengths observed in **XIV** (1.943(2) and 1.953(2) Å) compared to those measured in the molecular structures of **VI-IX** and **XI-XIII** (1.904(3)-1.945(2) Å).

The ^{1}H and ^{13}C NMR spectra of **XIV** are consistent with the solid state structure being maintained in solution. Four singlet resonances are observed consistent with formation of the η^5-$C_5H_4SiMe_3$ moiety, and a singlet resonance at δ_H = 0.43 ppm is observed for the $SiMe_3$ substituent. However, the ^{27}Al NMR resonance for **XIV** observed at δ_{Al} = 60 ppm is notably different to that of the related compounds **XII** and **XIII** (δ_{Al} = 160 and 181 ppm respectively), and suggests augmented coordination at the aluminium centre.[26] Whilst a similar resonance was observed at low temperature for **VI**, and the dimerisation equilibrium proposed in that case, this is unlikely in the case of **XIV** given the high steric loading at aluminium. Consequently, it is likely that an intramolecular interaction is the cause of the augmented coordination observed spectroscopically in **XIV**. Of particular interest are the four singlet resonances observed for the Cp^{Si} functionality at δ_H = 5.71, 4.17, 3.89 and 3.76 ppm (Figure 4.6).

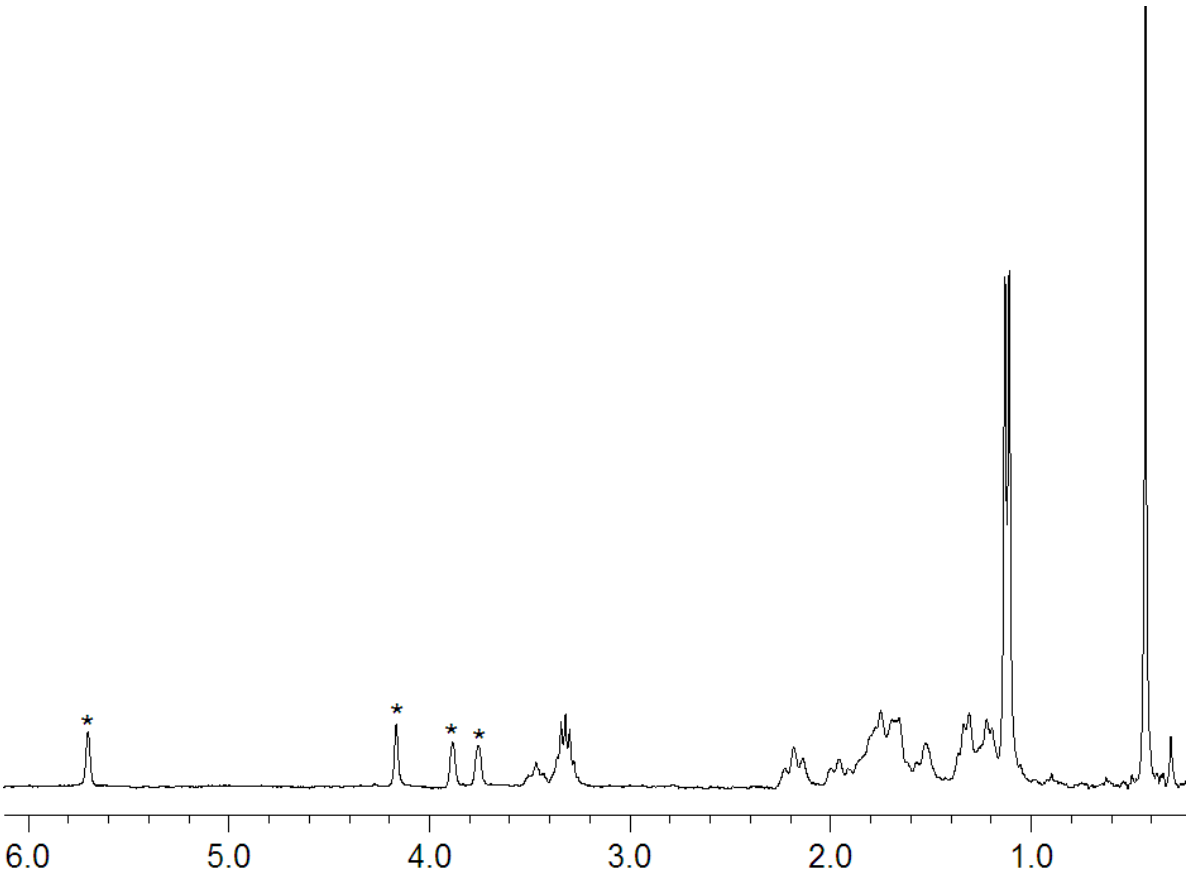

Figure 4.6: *Section of ^{1}H NMR spectrum of **XIV** in C_6D_6; * denotes the Cp^{Si}-H resonances*

Previously reported complexes featuring the [$Cp^{Si}Fe(CO)(PPh_3)$] fragment such as **4.21**-**4.23** contain resonances for the protons of the Cp^{Si} ring which span a *ca.* 1 ppm range (*e.g.* δ_H = 3.8-4.6 for **4.21** and 3.6-4.5 ppm for **4.22** and **4.23**).[25] In **XIV** these resonances span *ca.* 2 ppm range (δ_H = 3.76-5.71 ppm), with the resonance at δ_H = 5.71 ppm shifted over 1 ppm downfield from the other three, possibly as a result of a weak electrostatic interaction with the aluminium centre (Figure 4.7).

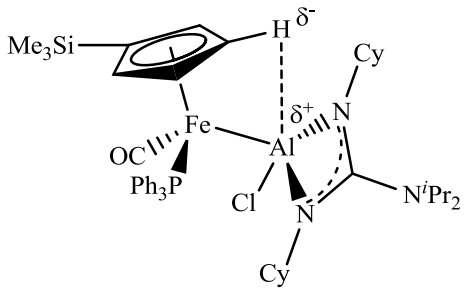

Figure 4.7: *Potential weak electrostatic interaction of the Cp^{Si} substituent with aluminium in **XIV***

The formation of agostic and anagostic interactions is well documented in the literature and has recently been reviewed in detail.[27] Whilst agostic interactions are 3-centre 2-electron interactions resulting in an upfield shift in the ^{1}H NMR, anagostic interactions are largely electrostatic and result in a downfield shift in the ^{1}H NMR of the bound H.[27] In the solid state structure of **XIV** the shortest $Cp^{Si}H\cdots Al$ distance is 2.9 Å, which is comparable to the upper limit of characterised anagostic interactions. The C-H···Al angle of 82° is, however, too acute for this to be classified as an anagostic interaction, which in typical transition metal examples requires a metal based lone pair of electrons. The ^{27}Al NMR resonance observed is largely dictated by the geometry of the aluminium centre, and a weak electrostatic interaction from the $Cp^{Si}H$ may perturb the geometry enough to shift the observed ^{27}Al NMR resonance.

An electrostatic interaction of this type is an alternative rationale for the temperature dependent ^{27}Al NMR resonance observed for **VI**. However, in **VI** it is possible that facile rotation of the Cp ring and the presence of five equivalent Cp hydrogens causes this effect to be averaged out in the ^{1}H NMR spectrum. In **XIV**, however, the chiral nature of the iron centre gives rise to separate resonances for each of the four Cp^{Si}-H protons. Thus, in conjunction with the bulky PPh_3 ligand and $SiMe_3$ functionality on the Cp ring causing the barrier to rotation of the Cp^{Si} ring to increase, the electrostatic interaction may be more

easily observed and identified by the observed downfield shift in the resonance of one Cp^{Si} proton.

Subsequent halide abstraction chemistry with $Na[BAr^{f}_{4}]$ yielded a mixture of products that proved to be inseparable, although a ^{31}P NMR resonance consistent with an Fe-P interaction was retained. Further identification of the products proved unsuccessful. Consequently an alternative system with a more sterically demanding aluminium substituent was investigated.

4.4.2 Increasing the Steric Demands of the Aluminium Substituent

Increasing the size of the heterocycle formed upon coordination of a metal by the *N*,*N*′-chelating ligand from a four-membered ring to a six-membered ring offers greater steric protection of the coordinated metal centre, particularly if bulky aryl groups are incorporated (Figure 4.8).

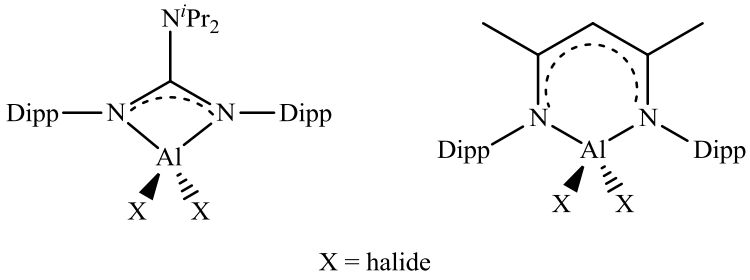

Figure 4.8: *Comparison of the guanidinate (left) and β-diketiminate (right) ligands*

The dichloro precursor $Dipp_2NacNacAlCl_2$ (**4.24**) reported by Roesky, Power and co-workers represents a suitable precursor for salt metathesis reactions with transition metal anions.[28] The reactions between **4.24** and either $Na[CpFe(CO)_2]$ or $Na[Cp^*Fe(CO)_2]$ in diethyl ether afford the corresponding mixed metal compounds

$CpFe(CO)_2[(Cl)Al(Dipp_2NacNac)]$ (**XV**) and $Cp^*Fe(CO)_2[(Cl)Al(Dipp_2NacNac)]$ (**XVI**) (Scheme 4.6). Extended reaction times were required in comparison to the guanidinate and amidinate analogues, due to the high steric demands of the $Dipp_2NacNac$ substituent.

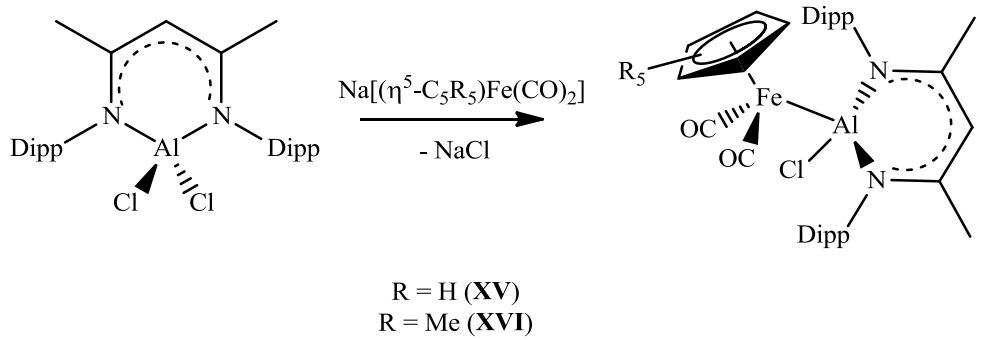

R = H (**XV**)
R = Me (**XVI**)

Scheme 4.6: *Reaction between **4.24** and either $Na[CpFe(CO)_2]$ or $Na[Cp^*Fe(CO)_2]$*

The formation of both **XV** and **XVI** can be monitored *in situ* by ^{27}Al NMR spectroscopy with a downfield shift of *ca.* 40 ppm being diagnostic of metal-metal bond formation. Compounds **XV** and **XVI** were isolated as orange and yellow crystals respectively after storage of concentrated ethereal solutions at -30 °C. Both compounds have been characterised by standard spectroscopic and analytical techniques as well as by X-ray crystallography (Figure 4.9 and Figure 4.10).

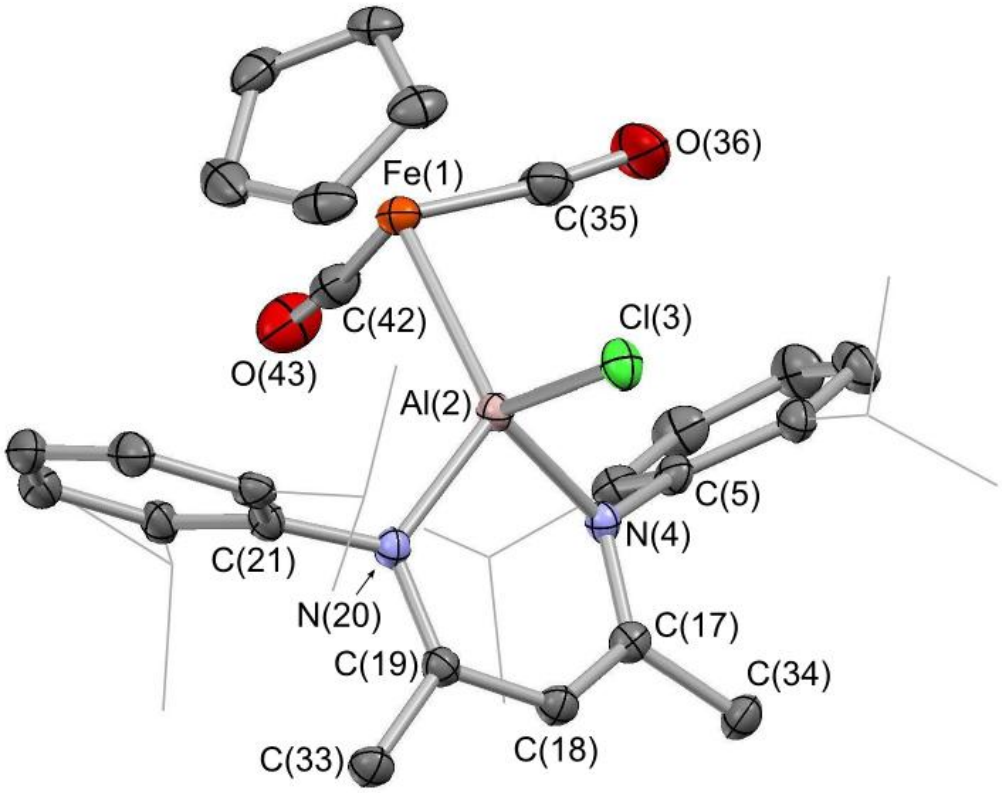

Figure 4.9: *Molecular structure of **XV**. Thermal ellipsoids set at the 40% probability level and hydrogen atoms omitted for clarity.* Key bond lengths (Å) and angles (°): Fe(1)-Al(2) 2.424(1), Al(2)-Cl(3) 2.198(2), Al(2)-N(4) 1.921(3), Al(2)-N(20) 1.936(3); N(4)-Al(2)-N(20) 96.0(1), Cl(3)-Al(2)-N(4) 101.90(8), Cl(3)-Al(2)-N(20) 100.85(9), Fe(1)-Al(2)-N(4) 123.46(8), Fe(1)-Al(2)-N(20) 121.66(8), Fe(1)-Al(2)-Cl(3) 109.28(4).

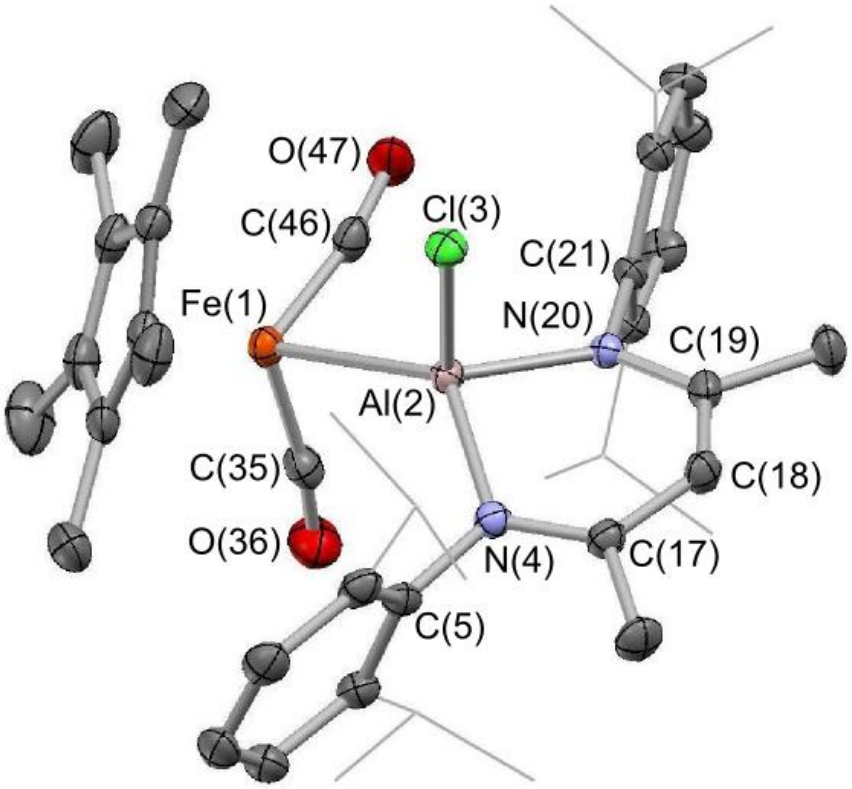

Figure 4.10: *Molecular structure of **XVI**. Thermal ellipsoids set at the 40% probability level and hydrogen atoms omitted for clarity.* Key bond lengths (Å) and angles (°): Fe(1)-Al(2) 2.480(1), Al(2)-Cl(3) 2.199(1), Al(2)-N(4) 1.964(2), Al(2)-N(20) 1.949(2); N(4)-Al(2)-N(20) 94.55(6), Cl(3)-Al(2)-N(4) 98.32(5), Cl(3)-Al(2)-N(20) 101.81(5), Fe(1)-Al(2)-N(4) 127.14(5), Fe(1)-Al(2)-N(20) 120.74(5), Fe(1)-Al(2)-Cl(3) 109.74(3).

The molecular structure of **XV** features two almost identical molecules in the asymmetric unit whilst that of **XVI** only one. In both cases a four-coordinate aluminium centre is observed with a geometry that is further distorted from tetrahedral than that observed in the amidinate or guanidinate substituted complexes. This is most notably manifested in both **XV** and **XVI** by the C(18)···Al(2)···Fe(1) angles of 160.2 and 159.8° respectively, which are significantly closer to linearity than the analogous angle measured for the four-membered heterocycle **XII** (∠C(5)···Al(2)···Fe(1) = 134.0°). This 'flattening' of the geometry at the aluminium centre is likely to be caused by the steric demands imposed by the $Dipp_2$NacNac substituent, a factor which is also responsible for the bending back of the carbonyl ligands at the iron centre (∠Fe-C-O = 173.7(3) and 174.3(3)° for **XV** and 170.7(2) and 169.1(2)° for **XVI**). Furthermore, the increased steric loading at the aluminium centre gives rise to significantly longer Fe-Al bond lengths in **XV** and **XVI** than those measured for the amidinate and guanidinate substituted complexes (2.424(1) and 2.480(1) Å for **XV** and **XVI**; *cf.* 2.340(1)-2.374(1) Å for amidinate/guanidinate complexes). The aluminium bound chloride in both **XV** and **XVI** shows relatively close approach to an idealised *syn* conformation (Cp centroid-Fe-Al-Cl angles of 53.2 and 39.6° respectively) and the Al-Cl bond lengths in both compounds show a slight lengthening in comparison to the precursor **4.24** (2.198(2) and 2.199(1) Å in **XV** and **XVI** respectively; *cf.* 2.134(1) and 2.119(2) Å in **4.24**) which is also likely to be due to the steric loading at the aluminium centre.[28]

Characterisation by ^{1}H and ^{13}C NMR spectroscopy indicates that the solid state structures of **XV** and **XVI** are maintained in solution and ^{27}Al NMR studies do not show evidence of augmented coordination at aluminium. The carbonyl stretching frequencies of **XV** and **XVI** show that substitution of Cp for Cp* results in a *ca.* 20 wavenumber shift (ν_{CO} = 1985, 1928 cm^{-1} **XV**; ν_{CO} = 1964, 1908 cm^{-1} **XVI**) however, both Cp and Cp* compounds contain higher wavenumber carbonyl stretching frequencies than the guanidinate

compounds **VI** and **XII** (ν_{CO} = 1973, 1912 and 1951, 1892 cm^{-1} respectively) implying the $Dipp_2$NacNac substituted complexes are less electron rich.

4.4.3 Halide Abstraction Chemistry

The molecular structures of **XV** and **XVI** both show a 'flattening' of the geometry around the aluminium centre and an elongation of the Al-Cl bond, suggesting that the chloride may be more easily abstracted than in the amidinate and guanidinate complexes. Abstraction of the aluminium bound chloride would yield a three-coordinate cationic complex in which the aluminium centre is expected to be trigonal planar, requiring minimal change in geometry from the molecular structures of **XV** and **XVI** (Scheme 4.7).

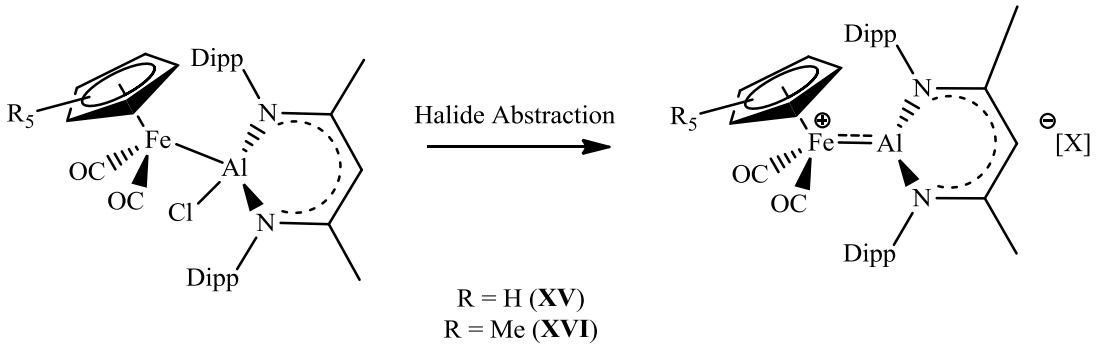

Scheme 4.7: *Halide abstraction from **XV** or **XVI** forming a cationic complex*

A number of halide abstraction reagents are available and initial efforts focused on the use of a strong Lewis acid to remove the chloride. The reaction between **XVI** and the highly Lewis acidic borane $B(C_6F_5)_3$ in flurobenzene did not definitively form the $[ClB(C_6F_5)_3]^-$ anion. Monitoring of the reaction by ^{19}F and ^{11}B NMR spectroscopy identified a small shift in the resonances observed for the $B(C_6F_5)_3$ reagent, but not the characteristic shifts associated with the formation of a four-coordinate borate complex. The very bulky nature

of **XVI** and the steric bulk associated with $B(C_6F_5)_3$ may preclude abstraction. The reaction between **XVI** and $AlCl_3$ under the same conditions resulted in the reformation of the precursor **4.24**, most likely resulting from a redistribution reaction forming $[Cp^*Fe(CO)_2AlCl_2]_n$ as the other product of the reaction (Scheme 4.8).

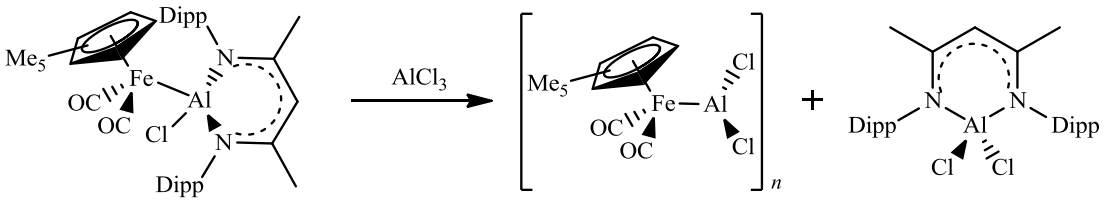

Scheme 4.8: *Redistribution reaction of **XVI** with $AlCl_3$*

The reaction of **XVI** with $GaCl_3$ results in a similar redistribution reaction forming the $[Cp^*Fe(CO)_2GaCl_2]_2$ dimer (**XVII**) also with regeneration of **4.24**. The dimeric gallium chloride complex (**XVII**) was isolated from a fluorobenzene/hexane layering as orange crystals and was characterised by X-ray crystallography (Figure 4.11).

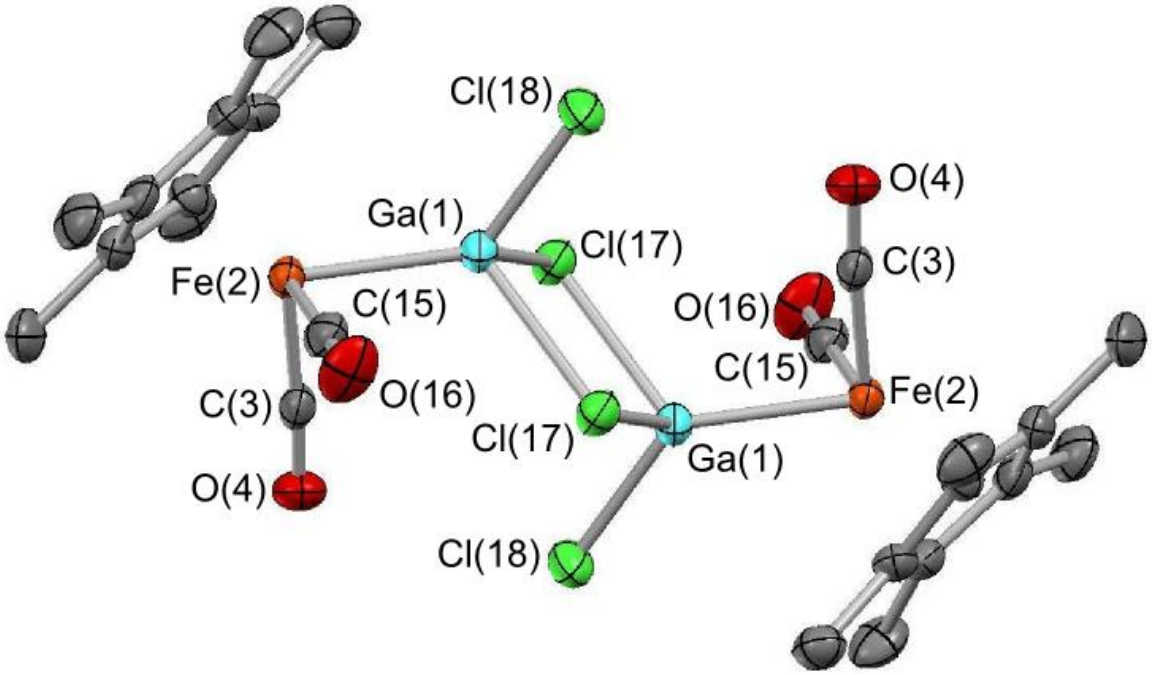

Figure 4.11: *Molecular structure of **XVII**. Thermal ellipsoids set at the 40% probability level, hydrogen atoms omitted for clarity.* Key bond lengths (Å) and angles (°): Ga(1)-Fe(2) 2.230(2), Ga(1)-Cl(17) 2.382(3), Ga(1)-Cl(17') 2.418(3), Ga(1)-Cl(18) 2.203(3); Fe(2)-Ga(1)-Cl(18) 125.2(1), Fe(2)-Ga(1)-Cl(17) 119.78(9), Fe(2)-Ga(1)-Cl(17') 115.51(9), Cl(17)-Ga(1)- Cl(17') 87.21(9), Cl(17)-Ga(1)-Cl(18) 101.2(1).

The molecular structure of **XVII** shows $Cp^*Fe(CO)_2GaCl_2$ to be a dimer featuring terminal and bridging Ga-Cl interactions, and crystallographically identical $Cp^*Fe(CO)_2GaCl_2$ units. The previously reported $[Cp^*Fe(CO)_2GaI_2]_2$ shows many structural similarities with **XVII** and is also dimeric in the solid state.[29] The redistribution, or scrambling, of group 13 halides is well established and it is likely that reforming **4.24** is a favourable and low energy reaction pathway. The redistribution may be prevented by using a salt metathesis based halide abstraction reaction to remove the chloride ligand.

The reaction of **XVI** with $Na[BAr^f_4]$ in fluorobenzene to generate the three coordinate aluminium cation resulted in the formation of a mixture of products by ^{1}H NMR spectroscopy. Within the mixture of products no clear formation of a system with higher symmetry, consistent with cation formation, could be observed and the products of the reaction proved inseparable with $[Cp^*Fe(CO)_2]_2$ being the predominant iron-containing species. The related reaction between **XVI** and $[Et_3Si][B(C_6F_5)_4]$, in flurorobenzene, when monitored by ^{1}H NMR spectroscopy *via* solvent suppression, however, did appear to show the formation of a system with higher symmetry than that observed in **XVI** (Figure 4.12).

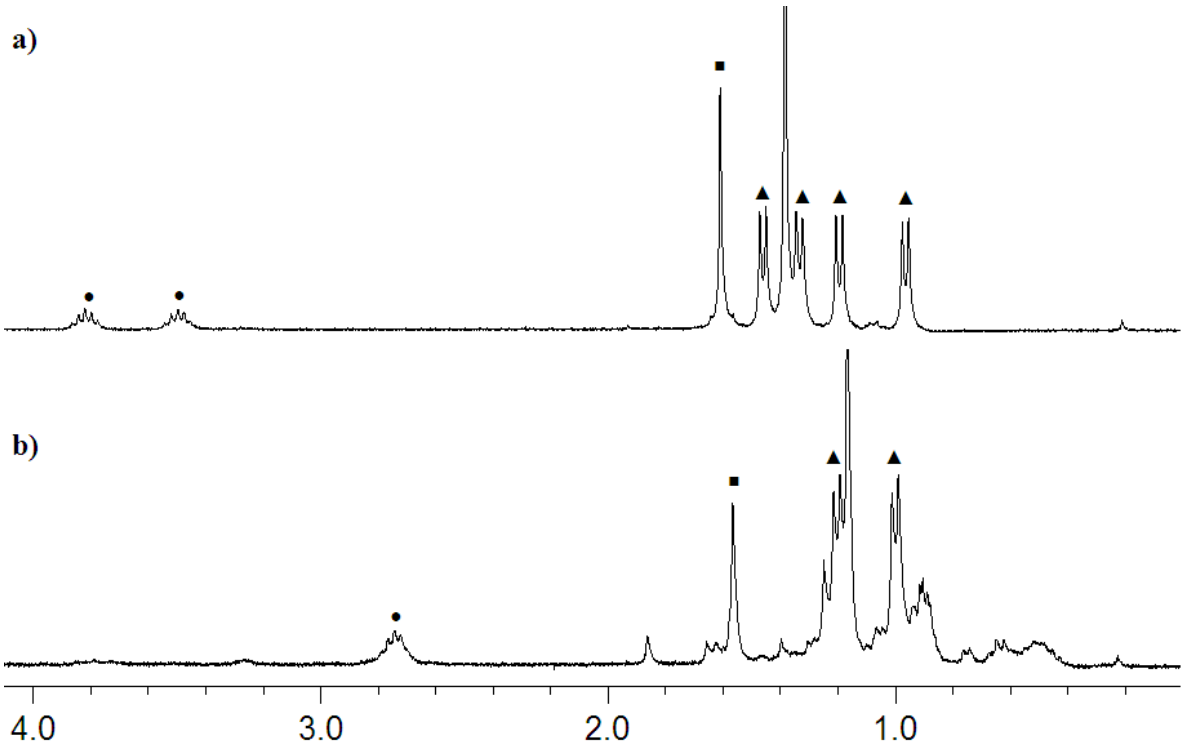

Figure 4.12: *^{1}H NMR spectra (a) **XVI** in fluorobenzene; (b) after reaction with $[Et_3Si][B(C_6F_5)_4]$ in fluorobenzene*

The ^{1}H NMR spectrum of **XVI** in fluorobenzene (Figure 4.12 (a)) clearly shows the $Dipp_2$NacNac substituent is not symmetrical with two methine (●) and four methyl resonances (▲) attributable to the Dipp substituents. After reaction with $[Et_3Si][B(C_6F_5)_4]$ the ^{1}H NMR spectrum (Figure 4.12 (b)) shows a single methine resonance (●) and, although partly obscured by the Et_3SiCl co-product formed appears to show a reduced number of methyl doublets (▲). However, whilst a single resonance is still observed for the Me groups of the the NacNac substituent (■) the spectrum contains two γ-CH resonances suggesting that there are multiple reaction products or that further reactivity occurs. Whilst the reaction with $[Et_3Si][B(C_6F_5)_4]$ clearly leads to the formation of new products the reaction does not progress cleanly and attempts to purify the product through either washing or recrystallisation were unsuccessful. Although many potential pathways for decomposition are possible, in related amidinate chemistry the transfer of a $(C_6F_5)^-$ unit

from $[MeB(C_6F_5)_3]^-$ was observed on cation formation by Schmidt and Arnold, demonstrating the highly reactive nature of three-coordinate aluminium cations.[30]

4.4.4 Reactions Between $Dipp_2$NacNacAl(Cl)(Me) and Transition Metal Anions

The halide abstraction reactions to remove the chloride from **XVI** generated a mixture of products, as the three-coordinate cation is likely to be highly reactive potentially leading to unwanted redistribution reactions. Successful formation of the methyl substituted complexes $CpFe(CO)_2[(Me)Al(NCy)_2CN^iPr_2]$ (**IX**) and $Cp^*Fe(CO)_2[(Me)Al(NCy)_2CN^iPr_2]$ (**XIII**), and subsequent spectroscopic characterisation of the anionic product of methide abstraction $[MeB(C_6F_5)_3]^-$, makes the substitution of the chloride in **XV** and **XVI** for a methyl ligand a logical progression for the formation of a three-coordinate aluminium cation.

The guanidinate complexes **IX** and **XIII** were most efficiently prepared from the salt metathesis reaction between the mixed chloro(methyl)precursor $^iPr_2NC(CyN)_2Al(Cl)(Me)$ (**X**) and the respective transition metal anion. Consequently, the previously reported mixed precursor $Dipp_2$NacNacAl(Cl)Me (**4.25**) was prepared.[31] Reaction between **4.25** and either $Na[CpFe(CO)_2]$ or $Na[Cp^*Fe(CO)_2]$ under the same reaction conditions as used in the preparation of **XV** and **XVI** did not yield the desired mixed iron-aluminium species. Even with extended reaction times, no evidence of metal-metal bond formation was observed by ^{27}Al NMR spectroscopy. Although slower reaction rates were observed in the formation of **XV** and **XVI**, than for the related amidinate and guanidinate systems, the reactions proceeded steadily. The similarity in the steric demands of chloride and methyl substituents implies that the difference between the ready formation of **XV** and **XVI** and the observed lack of reaction with **4.25** is an electronic factor. The replacement of chloride for methyl has been shown to have a significant effect on the

electronic structure of the related mixed metal iron-aluminium complexes **IX** and **XIII**. In **4.24** the aluminium centre is still Lewis acidic enough to react with transition metal nucleophiles, despite the notable steric penalties involved in doing so, whereas the aluminium centre in **4.25** is more electronically satisfied and therefore less Lewis acidic, and accordingly less reactive. Consequently, an alternative synthetic approach is required for the formation of the desired methyl analogues of **XV** and **XVI**.

4.4.5 Dehydrohalogenation chemistry of NacNacAlCl$_2$

The terminal Al-Cl bond of the guanidinate complex CpFe(CO)$_2$[(Cl)Al(NCy)$_2$CN^{i}Pr$_2$] (**VI**) was shown to be reactive toward alkyl lithium reagents, with reaction between **VI** and MeLi resulting in the substitution of the chloride for methyl to form **IX** (Scheme 4.9).

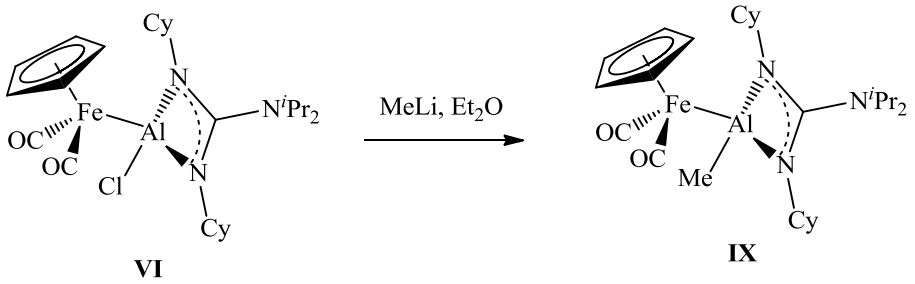

VI **IX**

Scheme 4.9: *Reaction between **VI** and MeLi forming **IX***

The same approach for the Dipp$_2$NacNac substituted complex **XVI** is complicated by the acidity of the protons of the flanking methyl groups. There are examples in the literature where these flanking methyl groups have been deprotonated, turning the Dipp$_2$NacNac substituent into a diamido framework (Dipp$_2$NacNac') (Figure 4.13).[17,18]

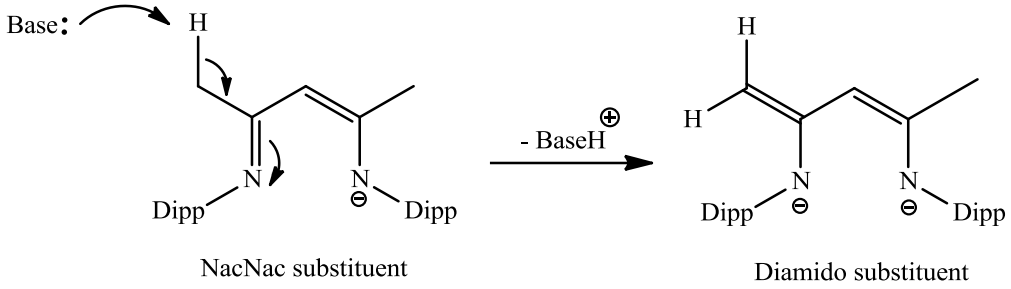

Figure 4.13: *Formation of the Dipp$_2$NacNac' substituent*

The use of the Dipp$_2$NacNac' substituent for the formation of *N*-heterocyclic complexes of main group elements has been pioneered by Driess and co-workers, who reported the formation of a *N*-heterocyclic silylene incorporating the diamido substituent.[17] The silylene (**4.17**) has been shown to activate a number of small molecules, in part due to the reactivity of the Dipp$_2$NacNac' backbone, and this chemistry has been recently reviewed.[32] The same group also structurally characterised the related bromoborane **4.18** (Figure 4.14).[18]

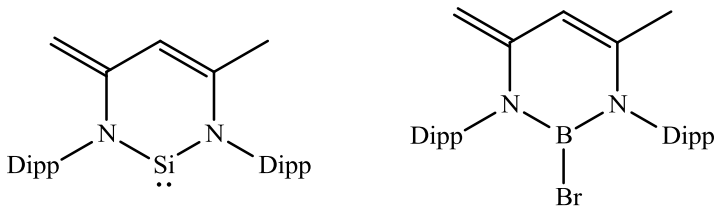

4.17 **4.18**

Figure 4.14: *(left) N-heterocyclic silylene **4.17** and (right) bromoborane **4.18**, featuring the Dipp$_2$NacNac' substituent*

The ability of the Dipp$_2$NacNac substituent to be changed from a monoanionic substituent to a dianionic substituent provides an alternative synthetic approach to the formation of a transition metal bound three-coordinate aluminium cation. Dehydrohalogenation across **4.24** to generate a putative three-coordinate aluminium species, followed by reaction with Na[Cp*Fe(CO)$_2$], would remove the halide abstraction step in the synthesis. Furthermore,

cation formation has been shown by Driess and co-workers through the use of $[H(OEt_2)_2][BAr^f_4]$ to reprotonate the backbone alkene substituent.[33] Thus, for example the following chemistry can be proposed for the synthesis of a cationic three-coordinate aluminium centre bound to a transition metal (Scheme 4.10).

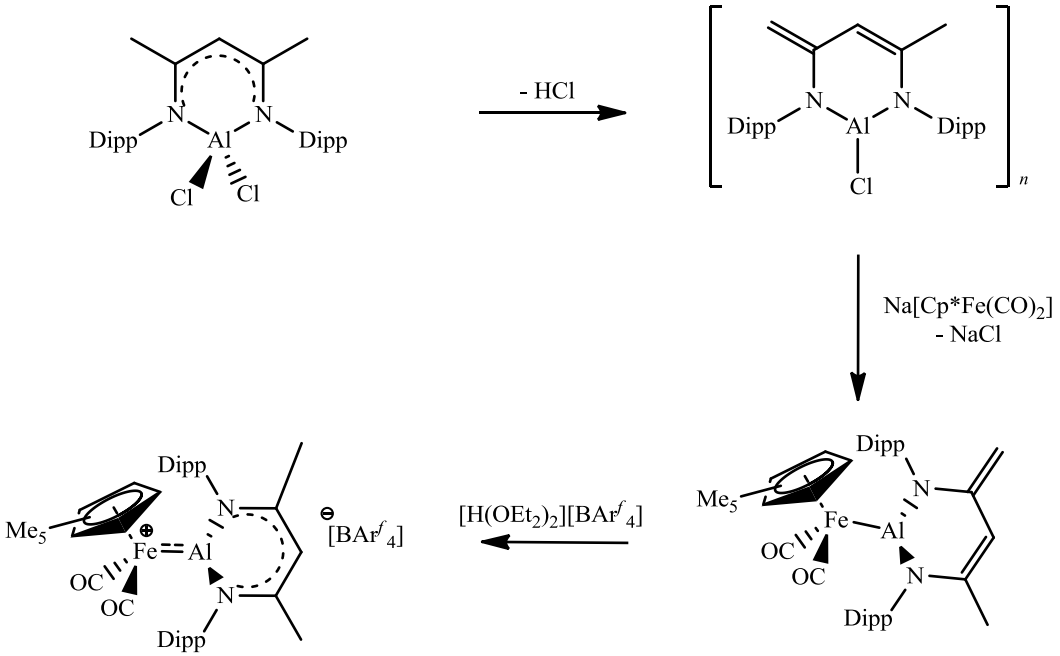

Scheme 4.10: *Dehydrohalogenation synthetic route to formation of a transition metal stabilised three-coordinate aluminium cation*

In order to effect the desired dehydrohalogenation reaction a suitably bulky and non-nucleophilic base is required to first deprotonate the $Dipp_2$NacNac backbone. A number of alkali metal bases were investigated, and the low temperature reaction of **4.24** with ^{t}BuLi in diethyl ether, followed by filtration and crystallisation led to the isolation of the lithium chloride inclusion compound $\{HC(CMeNAr)(C(CH_2)NAr)\}AlCl_2Li(OEt_2)_2$ (**XIX**), which has been characterised by standard spectroscopic and analytical techniques as well as by X-ray crystallography (Figure 4.15).

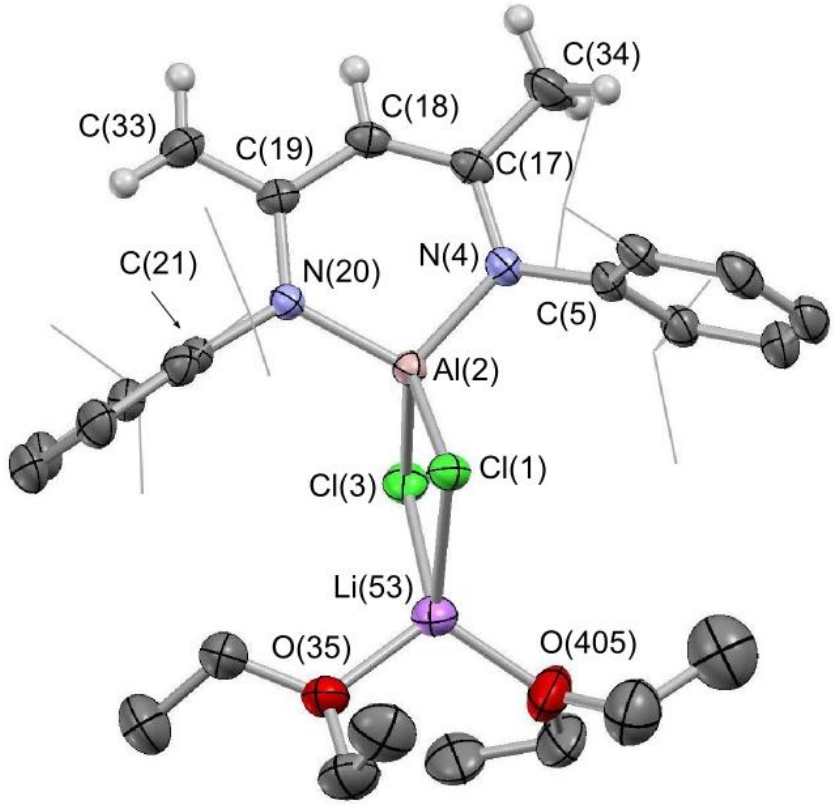

Figure 4.15: *Molecular structure of **XVIII**. Thermal ellipsoids set at the 40% probability level, ^{i}Pr groups of Dipp substituents are shown in wireframe and hydrogen atoms (except NacNac backbone) omitted for clarity.* Key bond lengths (Å) and angles (°): Cl(1)-Al(2) 2.181(1), Al(2)-Cl(3) 2.192(1), Al(2)-N(4) 1.812(2), Al(2)-N(20) 1.815(2), C(19)-C(33)-1.403(3), C(18)-C(19) 1.427(3), C(17)-C(18) 1.390(3), C(17)-C(34) 1.450(3), Cl(1)-Li(53) 2.422(4), Cl(3)-Li(53) 2.459(5), O(35)-Li(53) 1.912(5), Li(53)-O(405) 1.850(6); N(4)-Al(2)-N(20) 104.86(8), Cl(1)-Al(2)-N(4) 111.02(6), Cl(3) -Al(2)-N(4) 116.35(6), Cl(1)-Al(2)-N(20) 116.47(6), Cl(3)-Al(2)-N(20) 110.86(6), Cl(1)-Al(2)-Cl(3) 97.74(3), Cl(1)-Li(53)-Cl(3) 84.9(2), Cl(1)-Li(53)-O(35) 103.6(2), Cl(1)-Li(53)-O(405) 120.3(3), Cl(3)-Li(53)-O(35) 122.8(2), Cl(3)-Li(53)-O(405) 110.5(3), O(35)-Li(53)-O(405) 112.5(3).

The molecular structure of **XVIII** contains a single molecule in the asymmetric unit and features a four-coordinate aluminium centre in a distorted tetrahedral geometry. The C_3N_2 fragment of the heterocycle in **XVIII** is essentially planar and the aluminium centre sits above this plane by 0.261 Å, *i.e.* less significantly than in the precursor **4.24** (0.525 Å).[28] Complex **XVIII** also features shorter N-Al bond lengths (1.812(2) and 1.815(2) Å) and longer Al-Cl bond lengths (2.181(1) and 2.192(1) Å) than **4.24** (N-Al 1.8843(9) and 1.8663(9) Å; Al-Cl 2.1344(4) and 2.1185(4) Å).[28] The reduced N-Al bond lengths observed in **XVIII** are likely to be associated with the increase in planarity, along with the change in formal charge at the aluminium centre from neutral in **4.24** to formally anionic in **XVIII** with a coordinated lithium counter-ion. The exocyclic C-C bonds of **XVIII** show clear single and double bond character (C(17)-C(34) 1.450(3) and C(19)-C(33) 1.403(3) Å), closely resembling those reported for $Dipp_2$NacNac'BBr (**4.18**) (*d*(C-C) 1.444(9) and 1.401(9) Å), but show less differentiation than those reported in $Dipp_2$NacNac'$SiBr_2$ (**4.16**) (*d*(C-C) 1.504(2) and 1.343(2) Å).[17,18] The endocyclic single and double bonds of **XVIII** are clearly identifiable (C(18)-C(19) 1.427(3) and C(17)-C(18) 1.390(3) Å) and are similar to those reported in **4.18** (*d*(C-C) 1.427(9) and 1.379(9) Å) but are also less distinct than in **4.16** (*d*(C-C) 1.461(2) and 1.345(2) Å).[17,18] The differentiation of single and double C-C bonds is likely to be dependent not only on the complex itself but the extent of crystallographic disorder across the $Dipp_2$NacNac' backbone observed.

Characterisation by ^{1}H and ^{13}C NMR spectroscopy, in toluene- d_8 indicates that the solid state structure of **XVIII** is maintained in solution with diagnostic alkenyl resonances observed at δ_H = 3.07 and 3.85 ppm. The reduction in symmetry is confirmed by four resonances attributable to the ^{i}Pr methyl groups, overlapping methine resonances for the Dipp substituents are also observed. In the ^{27}Al NMR spectrum **XVIII** is characterised by a sharp resonance at δ_{Al} = 100 ppm, which is identical in shift to that of **4.24**. This essentially

unchanged ^{27}Al NMR shift further supports the notion that the position of the ^{27}Al NMR resonance is largely dependent upon the coordination number observed at aluminium, and less on the specific type or arrangement of ligands coordinated to the aluminium centre. Whilst stable in diethyl ether, allowing crystallisation, **XVIII** is unstable in aromatic solvents (*e.g.* benzene and toluene) with samples decomposing over the course of 12 hours to a number of products.

The reactivity of **XVIII** is defined by the reduced Lewis acidity of the aluminium centre, presumably resulting from its formal negative charge. Consequently, **XVIII** does not react with the transition metal anions Na[CpFe(CO)$_2$] or Na[Cp*Fe(CO)$_2$] in ethereal, aromatic or hydrocarbon solvents, even over extended reaction times. To determine the ease of protonation of the Dipp$_2$NacNac' backbone the acid [H(OEt$_2$)$_2$][BAr$^f_4$] was added to a benzene- d_6 solution of **XVIII** (Scheme 4.11).

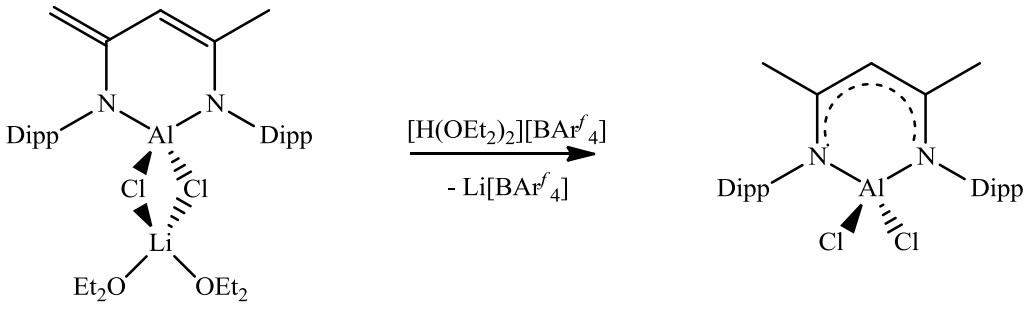

Scheme 4.11: *Reaction of* **XVIII** *with [H(OEt$_2$)$_2$][BAr$^f_4$]*

The reaction between **XVIII** and [H(OEt$_2$)$_2$][BAr$^f_4$] proceeds readily and complete conversion to **4.24** is observed by ^{1}H NMR spectroscopy. This is accompanied by the formation of a Li[BAr$^f_4$] clathrate allowing easy separation of the products and the free diethyl ether can be removed under vacuum.

Complex **XVIII** can be considered a LiCl inclusion compound, where the highly Lewis acidic aluminium centre coordinates LiCl. This type of complex is more commonly

associated with lanthanides, where lithium bases are often avoided due to their propensity to form 'ate' complexes. The use of potassium bases often prevents the formation of such complexes as potassium is less readily included in the complex. To promote the formation of a three coordinate aluminium centre and the dehydrohalogenation of **4.24**, the bulky alkyl potassium reagent K[CH(SiMe$_3$)$_2$] (**4.26**) was used (Scheme 4.12).

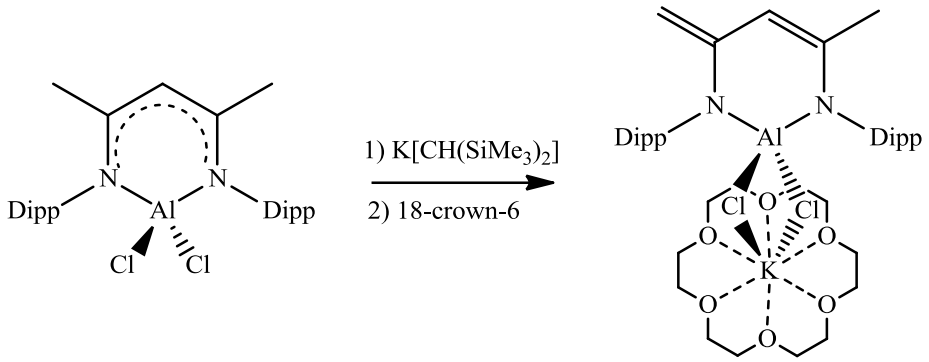

Scheme 4.12: *Reactivity between **4.24** and **4.26**. Followed by addition of 18-crown-6.*

The reaction between **4.24** and **4.26** in benzene proceeds very cleanly, and can be monitored by ^{1}H NMR spectroscopy. The expected alkenyl resonances were observed and a reduction in symmetry across the Dipp$_2$NacNac substituent is observed for the ^{i}Pr functionalities of the Dipp groups. The product of this reaction proved highly reactive and multiple attempts to grow single crystals suitable for X-ray crystallography were unsuccessful. The compound was shown to be spectroscopically pure by ^{1}H and ^{13}C NMR spectroscopy, although a ^{27}Al NMR resonance could not be identified. Subsequent reactions with the transition metal anions Na[CpFe(CO)$_2$] and Na[Cp*Fe(CO)$_2$] proved unsuccessful. The addition of the benzene filtrate from the reaction between **4.24** and **4.26** to a solution of 18-crown-6 in benzene led to the immediate formation of a white precipitate that was insoluble in aromatic, hydrocarbon and diethyl ether solvents. ^{1}H NMR spectroscopy of a sample in THF-d_8 showed that the compound had retained the alkenyl resonances and

reduced symmetry attributable to the $Dipp_2$NacNac' backbone and also contained 18-crown-6. Single crystals were grown from a THF/hexane layering at -30 °C and the solid state structure of **XIX** determined by X-ray crystallography (Figure 4.16).

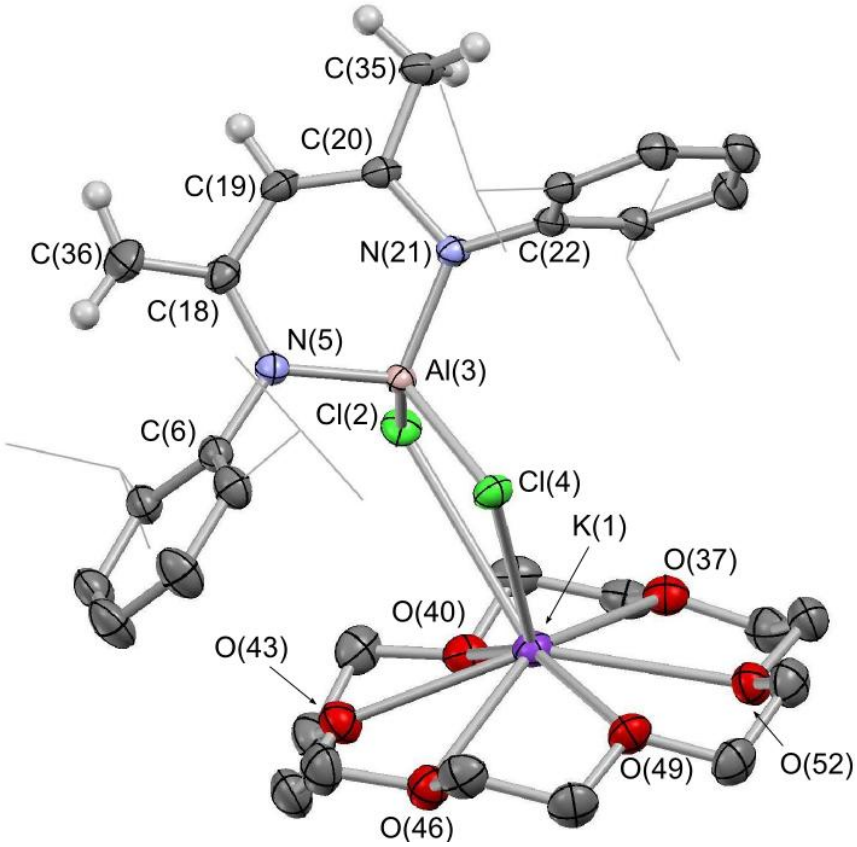

Figure 4.16: *Molecular structure of **XIX**. Thermal ellipsoids set at the 40% probability level, ^{i}Pr groups of Dipp substituents are shown in wireframe and hydrogen atoms (except NacNac backbone) omitted for clarity.* Key bond lengths (Å) and angles (°): Cl(2)-Al(3) 2.1651(5), Al(3)-Cl(4) 2.1593(5), Al(3)-N(5) 1.830(2), Al(3)-N(21) 1.829(1), C(18)-C(36) 1.355(2), C(18)-C(19) 1.462(2), C(19)-C(20) 1.354(2), C(20)-C(35) 1.501(2); N(5)-Al(3)-N(21) 103.63(5), Cl(2)-Al(3)-N(5) 112.90(4), Cl(4)-Al(3)-N(5) 113.45(4), Cl(2)-Al(3)-N(21) 112.04(4), Cl(4)-Al(3)-N(21) 111.76(4), Cl(2)-Al(3)-Cl(4) 103.36(2).

The molecular structure of **XIX** contains a single molecule in the asymmetric unit and features a four-coordinate aluminium centre with distorted tetrahedral geometry. The C_3N_2 fragment of the heterocycle in **XIX** is close to planar and the aluminium centre sits above this plane by 0.563 Å, which is a greater deviation from planarity observed in both **XVIII** and the precursor **4.24** (0.261 and 0.525 Å respectively).[28] Complex **XIX** also features longer N-Al bond lengths than **XVIII** (*cf.* 1.830(2) and 1.829(1) Å for **XIX**; 1.812(2) and 1.815(2) Å for **XVIII**) and shorter Al-Cl bond lengths than **XVIII** (*cf.* 2.1651(2) and 2.1593(5) for **XIX**; 2.181(1) and 2.192(1) Å for **XVIII**). The addition of 18-crown-6 to sequester the potassium results in long K···Cl contact distances of 3.29 and 3.43 Å, as the alkali metal is stabilised by the crown ether and therefore less closely associated with the aluminate anion component of **XIX**. The greater degree of charge separation is likely to result in differing bond lengths around the aluminium centre being observed, as **XIX** is closer to being a separated ion pair than **XVIII**. Consequently, the association of the $[K(18\text{-crown-6})]^+$ cation to the aluminate anion is likely to be weak in the solid state, and in THF solution it is possible that a separated ion pair exists, solvated by THF. The exocyclic C-C bonds of **XIX** show greater distinction between the double and single bonds than **XVIII** (*cf.* C(36)-C(18) 1.355(2) and C(20)-C(35) 1.501 Å for **XIX**; C(33)-C(19) 1.403(2) and C(17)-C(34) 1.450(3) for **XVIII**), and this is also observed for the endocyclic C-C bonds (C(18)-C(19) 1.462 and C(19)-C(20) 1.354 Å for **XIX**; C(19)-C(18) 1.427(3) and C(18)-C(17) 1.390 Å for **XVIII**).

Characterisation by ^{1}H, ^{13}C and ^{27}Al NMR spectroscopy, in THF- d_8, indicates that the solid state structure of **XIX** is maintained in solution. The ^{1}H NMR spectrum of **XIX** shows the expected alkenyl resonances (δ_H = 2.30 and 3.05 ppm), as well as four methyl and two methine resonance attributable to the Dipp substituents consistent with the reduced

symmetry of the $Dipp_2$NacNac' backbone. In the ^{27}Al NMR spectrum a resonance at δ_{Al} = 100 ppm is observed almost identical to that of both **XVIII** and **4.24**.

The isolation and characterisation of **XIX** provides insight into the product formed in the initial reaction between **4.24** and **4.26**, as the elimination of potassium chloride clearly does not take place. Deprotonation of the $Dipp_2$NacNac backbone occurs and the potassium is included within the compound, probably stabilised by an arene interaction from the flanking Dipp groups or through the coordination of a benzene solvent molecule. The inclusion and stabilisation of potassium within the $Dipp_2$NacNac framework has been reported by Hill and co-workers who obtained preliminary structural data on a dinuclear beryllium compound featuring unusual hydride reduction of the imido substituent. The dinuclear species formed (**4.27**) (Figure 4.17) features the potassium stabilised by a flanking arene interaction from the Dipp substituents of each $Dipp_2$NacNac ligand. Subsequent addition of 18-crown-6 led to the isolation and full structural characterisation of the dimeric crown ether complex **4.19**.[19]

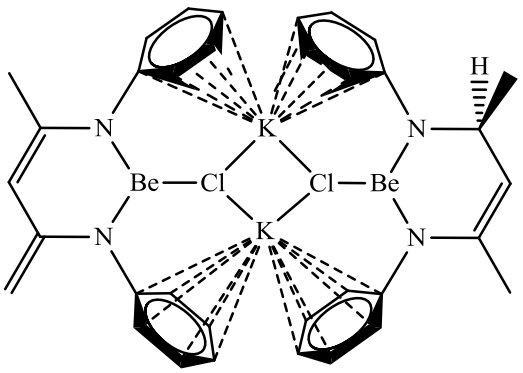

4.27

Figure 4.17: *Structure of **4.27** (^{i}Pr groups of Dipp substituents omitted for clarity)*[19]

The structural characterisation of **XIX** shows that, like **XVIII**, the aluminium centre remains four-coordinate and consequently, is more electronically satisfied than in **4.24**, on

account of being formally an aluminate anion, resulting in the observed lack of reactivity with transition metal anions. Furthermore, the formation of **XIX** clearly shows the challenges associated with the generation of a three-coordinate aluminium species by the elimination of chloride, demonstrating the Lewis acidic and chlorophilic nature of aluminium complexes.

4.5 Conclusions and Further Work

The synthesis of mixed iron-aluminium complexes featuring the more sterically demanding and electron rich [Cp*Fe(CO)$_2$] and [Cp^{Si}Fe(CO)(PPh$_3$)] fragments have been structurally characterised, with guanidinate substituents at the aluminium centre. The related [CpFe(CO)$_2$] and [Cp*Fe(CO)$_2$] aluminium complexes featuring the Dipp$_2$NacNac substituent have also been characterised. The increased steric demands of the Dipp$_2$NacNac ligand were demonstrated by extended reaction times being required for metal-metal bond formation, and the solid state structures show significant distortion on account of the steric loading at aluminium. The halide abstraction chemistry of **XVI** was investigated and the facile nature of ligand redistribution reactions with other group 13 halide abstraction agents identified.

The dehydrohalogenation chemistry of **4.24** has been investigated and the difficulty in facilitating chloride elimination from aluminium identified with the characterisation of both lithium and potassium chloride inclusion complexes. Furthermore, the reactivity of these ‘ate’ complexes was investigated and shown to be dominated by the reduced electrophilicity of the aluminium centre in comparison to **4.24**.

Further work to try to dehydrohalogenate the mixed iron-aluminium complexes **XV** and **XVI** may allow the formation of the desired three-coordinate aluminium centre, however, the difficulty in elimination of both LiCl and KCl has already been observed. The

abstraction of a methyl group has been shown to be more readily achieved and further efforts to replace the chloride substituent for a methyl group, if successful, would leave a precursor with greater chance of successful characterisation of the desired three-coordinate aluminium cation.

4.6 References

1. L. Bourget-Merle, M. F. Lappert and J. R. Severn, *Chem. Rev.*, 2002, **102**, 3031.
2. N. C. Tomson, J. Arnold and R. G. Bergman, *Dalton Trans.*, 2011, **40**, 7718.
3. C. M. Cui, H. W. Roesky, H. G. Schmidt, M. Noltemeyer, H. J. Hao and F. Cimpoesu, *Angew. Chem. Int. Ed.*, 2000, **39**, 4274.
4. X. Li, X. Cheng, H. Song and C. Cui, *Organometallics*, 2007, **26**, 1039.
5. M. S. Hill, P. B. Hitchcock and R. Pongtavornpinyo, *Dalton Trans.*, 2005, **2**, 273.
6. M. S. Hill and P. B. Hitchcock, *Chem. Commun.*, 2004, **16**,1818.
7. N. J. Hardman, B. E. Eichler and P. P. Power, *Chem. Commun.*, 2000, **20**,1991
8. C. E. Radzewich, I. A. Guzei and R. F. Jordan, *J. Am. Chem. Soc.*, 1999, **121**, 8673.
9. M. J. Taylor, A. J. Saunders, M. P. Coles and J. R. Fulton, *Organometallics*, 2011, **30**, 1334.
10. S. Harder and J. Brettar, *Angew. Chem. Int. Ed.*, 2006, **45**, 3474.
11. J. Spielmann, G. Jansen, H. Bandmann and S. Harder, *Angew. Chem. Int. Ed.*, 2008, **47**, 6290.
12. J. Spielmann and S. Harder, *Eur. J. Inorg. Chem.*, 2008, **9**,1480.
13. S. P. Green, C. Jones and A. Stasch, *Science*, 2007, **318**, 1754.
14. S. J. Bonyhady, D. Collis, G. Frenking, N. Holzmann, C. Jones and A. Stasch, *Nature Chem.*, 2010, **2**, 865.
15. C. Jones, L. McDyre, D. M. Murphy and A. Stasch, *Chem. Commun.*, 2010, **46**, 1511.
16. S. J. Bonyhady, S. P. Green, C. Jones, S. Nembenna and A. Stasch, *Angew. Chem. Int. Ed.*, 2009, **48**, 2973.
17. M. Driess, S. Yao, M. Brym, C. van Wuellen and D. Lentz, *J. Am. Chem. Soc.*, 2006, **128**, 9628.

18. C. I. Someya, S. Inoue, C. Praesang, E. Irran and M. Driess, *Chem. Commun.*, 2011, **47**, 6599.

19. M. Arrowsmith, M. S. Hill, G. Kociok-Koehn, D. J. MacDougall, M. F. Mahon and I. Mallov, *Inorg. Chem.*, 2012, **51**, 13408.

20. A. A. Dickinson, D. J. Willock, R. J. Calder and S. Aldridge, *Organometallics*, 2002, **21**, 1146.

21. J. M. Burlitch, M. E. Leonowicz, R. B. Petersen and R. E. Hughes, *Inorg. Chem.*, 1979, **18**, 1097.

22. A. L. Allred, *J. Inorg. Nucl. Chem.*, 1961, **17**, 215.

23. D. A. Addy, N. Phillips, G. A. Pierce, D. Vidovic, T. Kraemer, D. Mallick, E. D. Jemmis, G. Reid and S. Aldridge, *Organometallics*, 2012, **31**, 1092.

24. D. A. Addy, G. A. Pierce, D. Vidovic, D. Mallick, E. D. Jemmis, J. M. Goicoechea and S. Aldridge, *J. Am. Chem. Soc.*, 2010, **132**, 4586.

25. T. Munguia, Z. A. Bakir, F. Cervantes-Lee, A. Metta-Magana and K. H. Pannell, *Organometallics*, 2009, **28**, 5777.

26. R. Benn and A. Rufinska, *Angew. Chem. Int. Ed.*, 1986, **25**, 861.

27. M. Brookhart, M. L. H. Green and G. Parkin, *Proc. Nat. Acad. Sci. U. S. A.*, 2007, **104**, 6908.

28. M. Stender, B. E. Eichler, N. J. Hardman, P. P. Power, J. Prust, M. Noltemeyer and H. W. Roesky, *Inorg. Chem.*, 2001, **40**, 2794.

29. N. R. Bunn, S. Aldridge, D. L. Kays, N. D. Coombs, J. K. Day, L. L. Ooi, S. J. Coles and M. B. Hursthouse, *Organometallics*, 2005, **24**, 5879.

30. J. A. R. Schmidt and J. Arnold, *Organometallics*, 2002, **21**, 2306.

31. H. P. Zhu, J. F. Chai, C. He, G. C. Bai, H. W. Roesky, V. Jancik, H. G. Schmidt and M. Noltemeyer, *Organometallics*, 2005, **24**, 380.

32. S. Yao, Y. Xiong and M. Driess, *Organometallics*, 2011, **30**, 1748.

33. M. Driess, S. Yao, M. Brym and C. van Wuellen, *Angew. Chem. Int. Ed.*, 2006, **45**, 6730.

5 Coordination of Al-H Bonds to Transition Metal Centres

5.1 Introduction

The formation of complexes featuring coordinated E-H bonds (where E = B, Si) is well established, and the nature of such three-centre two-electron interactions has been the subject of a plethora of recent studies.[1-3] Characterisation of σ-complexes allows the fundamental properties of E-H bond activation to be studied since such systems can be considered as an arrested state along the E-H oxidative addition pathway. Insight into the properties and principles controlling the position of an E-H σ-complex along this pathway relate directly to potentially rate determining steps in catalytic hydroboration and hydrosilylation transformations.

Despite the libraries of borane and silane σ-complexes in the literature, reports of σ-alane complexes are notably rare. Unsupported σ-alane complexes featuring transition metal fragments that allow direct comparison with classical borane and silane complexes remain essentially unknown. In 1990 Pörschke and co-workers characterised the first unsupported σ-alane complex formed by reaction of the quinuclidine adduct of dimethylalane (quin·$AlMe_2H$) with the nickel(0) complex Ni(cdt) (**1.139**); the resulting σ-complex (quin·$AlMe_2H$)Ni(cdt) (**1.140**) was structurally characterised (Scheme 5.1).

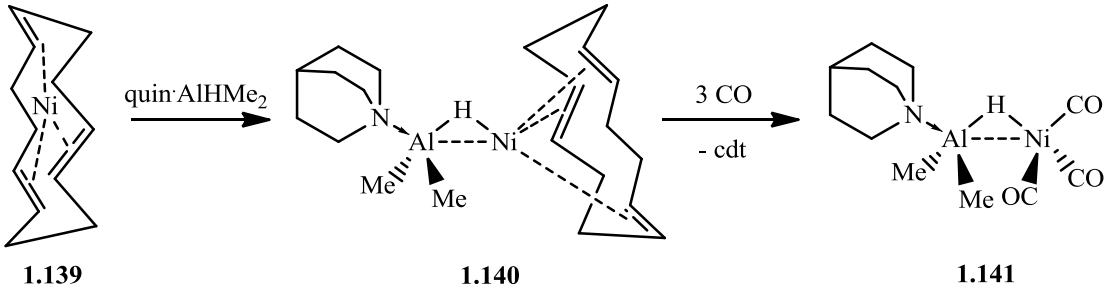

1.139 **1.140** **1.141**

Scheme 5.1: *Formation of **1.140** and subsequent reaction with three equivalents of CO forming **1.141***

Remarkably, this Al-H-Ni interaction is maintained on exposure to three equivalents of CO, resulting in the formation of the corresponding tricarbonyl complex (quin·$AlMe_2H$)$Ni(CO)_3$ (**1.141**).[4] Fischer and co-workers subsequently reported σ-alane complexes resulting from C-H bond activation occurring at low-valent intermediates in reactions between the aluminium(I) species AlCp* and transition metal complexes. Thus, for example, the reaction between $Ni(AlCp^*)_3$ and Cp*Al in benzene results in the activation of a C-H bond generating an aluminium(III) centre in the product $(Cp^*Al)_3Ni\{HAlPh(\eta^2\text{-}C_5Me_5)\}$ (**1.144**) which also features an unsupported Ni-H-Al interaction.[5] The same group subsequently reported the reaction between (η^6-toluene)Fe(η^4-1,3-butadiene) (**1.145**) and AlCp* which results in the intramolecular C-H activation of methyl groups of the Cp* ligand and the formation of **1.146** and **1.147** featuring both aluminium(I) and aluminium(III) ligands (Scheme 5.2).[6]

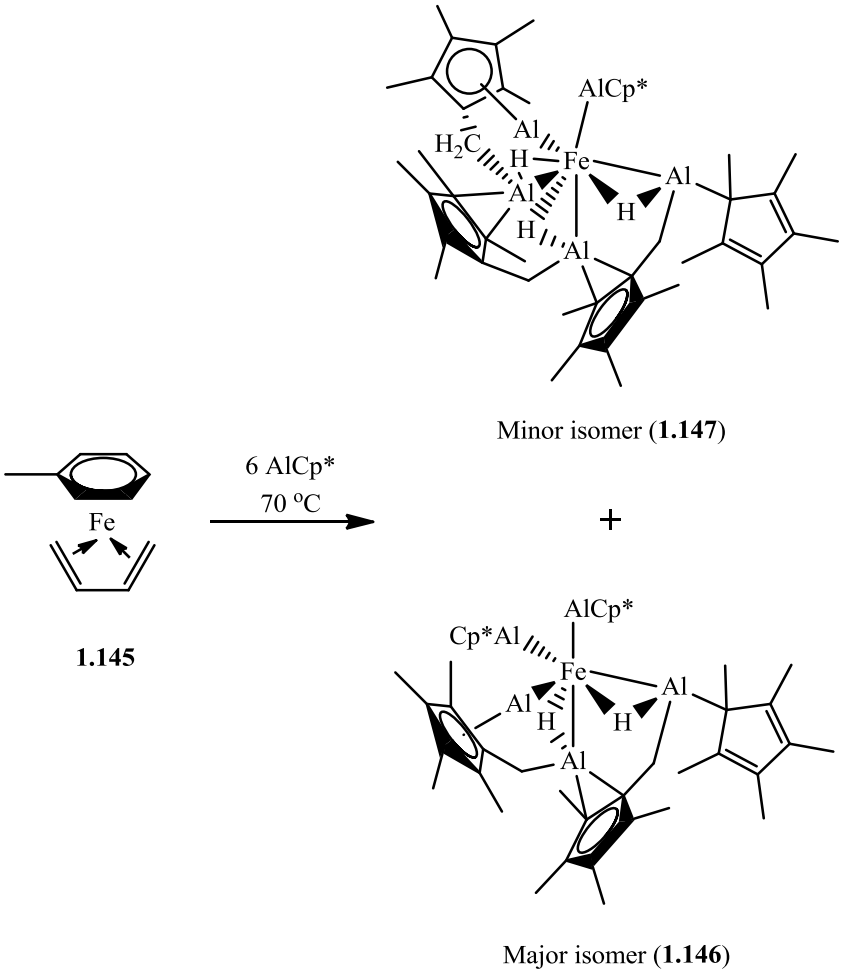

Scheme 5.2: *Reaction between **1.145** and AlCp**

In contrast to the formation of σ-alane complexes, for which general synthetic approaches have yet to be defined, there are several methods established in the literature for the formation of σ-borane complexes. Hartwig and co-workers reported photolytic preparation through direct coordination of the B-H bond to the *in situ* formed {Cp'Mn(CO)$_2$} for complexes featuring HBCat (**1.118**), and HBPin (**1.119**) (Scheme 5.3). In addition, salt metathesis reactions between the transition metal anion K[Cp'Mn(CO)$_2$H] and a chloroborane could also be used to access these complexes. However, due to the dimeric nature of HBCy$_2$, the complex Cp'Mn(CO)$_2$(HBCy$_2$) (**1.120**) can be formed only *via* the salt metathesis route.[1]

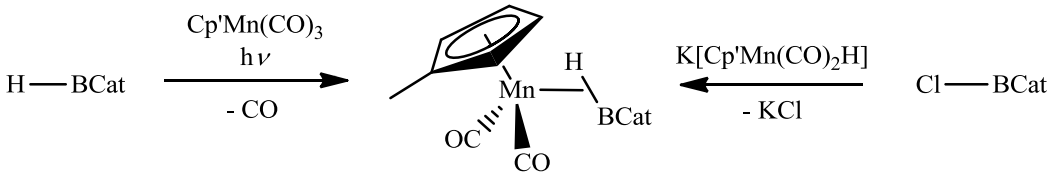

1.118

Scheme 5.3: *Photolytic and salt metathesis routes to* ***1.118***

The groups of Shimoi and Braunschweig have both employed photolytic generation of a 16-electron species in the synthesis of the four-coordinate $L{\cdot}BH_3$ complexes $M(CO)_5(\kappa^1\text{-}H_3B{\cdot}L)$ (where M = Cr and L = NMe_3 **1.88**, PMe_3 **1.89**, PPh_3 **1.90**, IMe **1.91**; where M = W and L = NMe_3 **1.92**, PMe_3 **1.93**, PPh_3 **1.94**, IMe **1.95**) and $CpMn(CO)_2(\kappa^1\text{-}H_3B{\cdot}L)$ (L = NMe_3 **1.96**, PMe_3 **1.97**, IMe **1.98**).[7-9] The displacement of labile dihydrogen ligands has also been demonstrated for the formation of σ-borane complexes by Sabo-Etienne and co-workers, who characterised the κ^2-complex $(Cy_3P)_2(H)_2Ru(\kappa^2\text{-}H_2BMes)$ (**1.120**) as the product from the reaction between $Ru(H_2)_2(H)_2(PCy_3)_2$ (**1.72**) and $(H_2BMes)_n$.[10] With these precedented approaches to the formation of σ-borane complexes in mind, the development of related methods for the formation of σ-alane complexes represents a logical extension to the families of σ-complexes in the literature.

5.2 Aims of the Present Work

The work in Chapters III and IV focused on the formation of a cationic three-coordinate aluminium centre bound to a transition metal in order to gain entry, *via* FLP chemistry, into a catalytic cycle for the reduction of small molecules (*e.g.* CO) (Figure 5.1). However, the formation of σ-alane complexes provides an alternative entry point into the catalytic cycle (Figure 5.1).

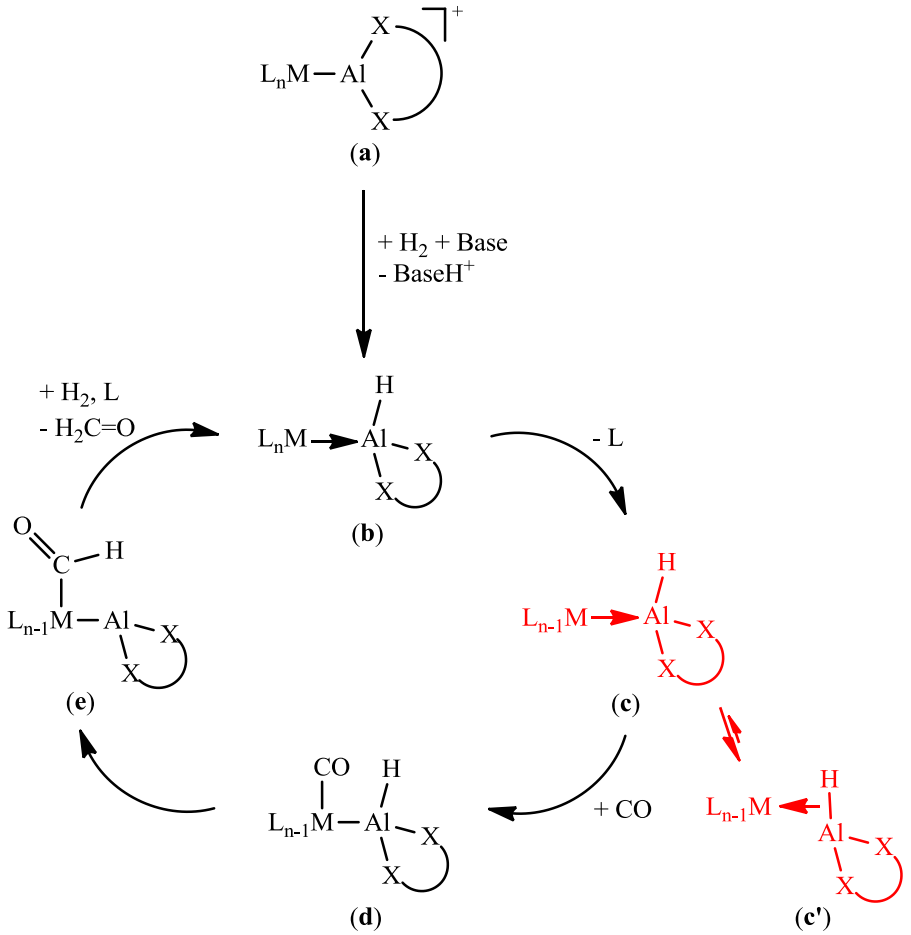

Figure 5.1: *Idealised catalytic cycle for reduction of small molecules from a σ-alane complex*

The 16-electron transition metal species (**c**) represents an isomeric form of the σ-complex (**c'**), in which coordination of the two electrons from the Al-H σ-bond forms an 18-electron transition metal complex. From the formation of a complex similar to (**c'**) the potential for hydride transfer chemistry from coordinated Al-H bonds to transition metal fragments can then be investigated (Figure 5.1). Due to the comparatively sparse reports of σ-alane complexes in the literature, the work reported in this Chapter is focused on the formation of stable σ-alane complexes, thereby permitting their structure, bonding and reactivity to be investigated. This is of interest not only from the potential applications in catalytic

chemistry, but also from a fundamental interest in structure and bonding, and for comparison to archetypal dihydrogen, borane and silane σ-complexes.

5.3 Experimental

***Preparation of Cp'Mn(CO)$_2$[HAl(Cl)(N^{i}Pr)$_2$CPh]* (XX)**

To a slurry of K[Cp'Mn(CO)$_2$H] (0.40 g, 1.8 mmol) in diethyl ether (30 cm^3) at -78 °C was added slowly a solution of PhC(^{i}PrN)$_2$AlCl$_2$ (0.50 g, 1.7 mmol) also in diethyl ether (25 cm^3). After stirring for 18 h and slowly attaining room temperature, the solvent was removed *in vacuo* to yield an orange solid. Extraction with hexane (3 x 10 cm^3) and subsequent cooling of the concentrated hexane extract yielded pale yellow crystals of **XX**. Yield 0.13 g, 17%.

Spectroscopic data: ^{1}H NMR (300 MHz, C_6D_6, 298 K): δ 6.99-7.08 (5H, m, Ar*H*), 4.33 (2H, m, Cp'*H*), 4.26 (2H, m, Cp'*H*), 3.26 (2H, sept ($^3J_{HH}$ = 6.3 Hz), NC*H*(CH$_3$)$_2$), 1.68 (3H, s, C*H*$_3$ of Cp'), 1.19 (6H, d ($^3J_{HH}$ = 6.3 Hz), NCH(C*H*$_3$)$_2$), 1.08 (d, 6H, ($^3J_{HH}$ = 6.3 Hz), NCH(C*H*$_3$)$_2$), -13.93 (1H, s, Al-*H*-Mn). ^{13}C{^{1}H} NMR (126 MHz, C_6D_6, 298 K): δ 228.7 (*C*O), 174.3 (*C*N$_2$), 130.2 (Ar*C*), 129.7 (Ar*C*), 128.9 (Ar*C*), 127.9 (Ar*C*), 101.0 (Cp'*C*), 81.9 (Cp'*C*), 80.5 (Cp'*C*), 46.4 (N*C*H(CH$_3$)$_2$), 25.1 (4 x degenerate NCH(*C*H$_3$)$_2$), 13.5 (CH$_3$ of Cp'). ^{27}Al NMR (78 MHz, C_6D_6, 298 K): δ 152. IR (hexane solution, cm^{-1}): 1974, 1899 (ν_{CO}).

Crystallographic data: $C_{21}H_{27}AlClMnN_2O_2$, M_r = 456.82, triclinic, *P*-1, *a* = 9.9819(2), *b* = 10.0605(2), *c* = 12.3107(3) Å, α = 83.621(1), β = 69.174(1), γ = 76.672(1)^o, *V* = 1123.8(1) Å^3, *Z* = 2, ρ_c = 1.350 Mg m^{-3}, *T* = 150 K, λ = 0.71073 Å. 8684 reflections collected, 5039 independent [R(int) = 0.037] used in all calculations. R_1 = 0.0346, wR_2 = 0.0798 for observed unique reflections [$I > 2\sigma(I)$] and R_1 = 0.0525, wR_2 = 0.0872 for all unique reflections. Max. and min. residual electron densities 0.26 and -0.38 e Å^{-3}. CSD reference: 857128.

***Preparation of {PhC(^{i}PrN)$_2$}$_2$AlH* (XXI)**

To a solution of $H_3Al{\cdot}NMe_3$ (0.60 g, 6.8 mmol) in toluene (45 cm^3) at -78 °C was added a solution of PhC(^{i}PrN)(^{i}PrNH) (1.39 g, 6.8 mmol) also in toluene (55 cm^3) and effervescence observed. The reaction mixture was stirred for 18 h whilst slowly attaining room temperature and then filtered. Storage of the concentrated filtrate at -30 °C yielded colourless crystals of **XXI**. Yield 1.12 g, 38%.

Spectroscopic data: ^{1}H NMR (500 MHz, C_6D_6, 298 K): δ 7.28 (10H, overlapping m, Ar*H*), 5.00 (1H, br, Al*H*), 3.53 (4H, sept ($^3J_{HH}$ = 6.9 Hz), C*H*(CH$_3$)$_2$), 1.45 (24H, d ($^3J_{HH}$ = 6.9 Hz), CH(C*H*$_3$)$_2$). ^{13}C{^{1}H} NMR (126 MHz, C_6D_6, 298 K): δ 174.5 (N_2C), 128.3 (Ar*C*), 128.2 (Ar*C*), 128.0 (Ar*C*), 127.9 (Ar*C*), 46.7 (*C*H(CH$_3$)$_2$), 25.3 (CH(*C*H$_3$)$_2$). ^{27}Al NMR (78 MHz, C_6D_6, 298 K): δ 59. MS(EI) *m/z* 433 $(M\text{-}H)^+$ 98%; accurate mass: calc. 433.2903, meas. 433.2906.

Crystallographic data: $C_{26}H_{38}AlN_4$, M_r = 433.60, monoclinic, *P* 2$_1$/n, *a* = 11.25060(10), *b* = 16.7969(2), *c* = 14.2359(2) Å, β = 92.1192(4), *V* = 2688.39(5) Å^3, *Z* = 4, ρ_c = 1.071 Mg m^{-3}, *T* = 150 K, λ = 0.71073 Å. 12003 reflections collected, 6113 independent [R(int) = 0.037] used in all calculations. R_1 = 0.0818, wR_2 = 0.2277 for observed unique reflections [$I > 2\sigma(I)$] and R_1 = 0.0951, wR_2 = 0.2366 for all unique reflections. Max. and min. residual electron densities 1.60 and -0.45 e Å^{-3}.

***Preparation of (OC)$_5$W[κ^1-H$_2$Al(NDipp)$_2$CN^{i}Pr$_2$]* (XXII)**

A solution in hexane (120 cm^3) containing $W(CO)_6$ (0.50 g, 1.4 mmol) and [^{i}Pr$_2$NC(DippN)$_2$AlH$_2$]$_2$ (0.70 g, 0.7 mmol) was subjected to UV photolysis for 100 min. The resulting yellow solution was filtered and the solvent removed *in vacuo* to yield a pale yellow solid. Extraction with pentane (3 x 10 cm^3) followed by concentration and storage at -30 °C yielded pale yellow crystals of **XXII**. Yield 0.06 g, 8%.

Spectroscopic data: ^{1}H NMR (300 MHz, C_6D_6, 298 K): δ 7.09 (2H, m, Ar*H*), 7.07 (2H, m, Ar*H*), 7.04 (2H, m, Ar*H*), 6.80 (1H, br, Al*H*), 3.97 (2H, sept ($^{3}J_{HH}$= 7.5 Hz), NC*H*$(CH_3)_2$), 3.65 (4H, overlapping sept, ($^{3}J_{HH}$ = 6.5, 7.0 Hz), C*H*$(CH_3)_2$), 1.49 (6H, d ($^{3}J_{HH}$= 6.5 Hz), CH(C*H*$_3)_2$), 1.38 (6H, d ($^{3}J_{HH}$ = 7.0 Hz), CH(C*H*$_3)_2$), 1.29 (6H, d ($^{3}J_{HH}$ = 7.0 Hz), CH(C*H*$_3)_2$), 1.27 (6H, d ($^{3}J_{HH}$= 6.5 Hz), CH(C*H*$_3)_2$), 0.72 (12H, d ($^{3}J_{HH}$ = 7.5 Hz), NCH(C*H*$_3)_2$), -7.11 (1H, d ($^{2}J_{HH}$= 20.0 Hz), Al-*H*-W). ^{13}C{^{1}H} NMR (126 MHz, C_6D_6, 298 K): δ 199.1 (*C*O, $^{1}J_{WC}$= 137.8 Hz), 195.7 (*C*O, $^{1}J_{WC}$= 125.8 Hz), 167.3 (*C*N_3), 145.3 (N*C*Ar), 138.4 (Ar*C*), 128.7 (Ar*C*), 127.0 (Ar*C*), 124.8 (Ar*C*), 124.7 (Ar*C*), 50.7 (N*C*H$(CH_3)_2$), 28.7 (*C*H$(CH_3)_2$), 29.0 (*C*H$(CH_3)_2$), 27.5 (CH(*C*$H_3)_2$), 28.1 (CH(*C*$H_3)_2$), 23.7 (overlapping CH(*C*$H_3)_2$), 23.6 (NCH(*C*$H_3)_2$). ^{27}Al NMR (78 MHz, C_6D_6, 298 K): δ 55. IR (hexane solution, cm^{-1}): 1983 (s, CO), 1951 (m, CO), 1585 (m, Al-H). Elemental microanalysis: calc. for $C_{36}H_{50}N_3AlO_5W$ C 52.99, H 6.18, N 5.15; meas. C 52.86, H 6.03, N 5.12.

Crystallographic data: $C_{36}H_{50}N_3AlO_5W$, M_r = 815.64, monoclinic, *P* $2_1/n$, *a* = 10.6432(1), *b* = 19.5995(2), *c* = 18.6008(2) Å, β = 98.423(1)°, *V* = 3838.3(1) Å^3, *Z* = 4, ρ_c = 1.411 Mg m^{-3}, *T* = 150 K, λ = 1.54180 Å. 22161 reflections collected, 7994 independent [R(int) = 0.045] used in all calculations. R_1 = 0.0273, wR_2 = 0.0424 for observed unique reflections [$I > 2\sigma(I)$] and R_1 = 0.0286, wR_2 = 0.0426 for all unique reflections. Max. and min. residual electron densities 1.01 and -1.11 e Å^{-3}. CSD reference: 857130.

Preparation of Cp'Mn(CO)$_2$[κ^1-H$_2$Al(Dipp$_2$NacNac)] **(XXIV)**

A solution in toluene (100 cm^3) containing Cp'Mn$(CO)_3$ (0.10 cm^3, 0.70 mmol) and Dipp$_2$NacNacAlH_2 (0.31 g, 0.70 mmol) was subjected to UV photolysis for 165 min. The resulting red solution was filtered, concentrated and cooled to -30 °C yielding yellow crystals of **XXIV**. Yield 0.06 g, 13%.

Spectroscopic data: ^{1}H NMR (300 MHz, C_6D_6, 298 K): δ 7.12-7.13 (6H, m, Ar*H*), 5.75 (1H, s, Al*H*), 4.95 (1H, s, γ-CH), 3.67 (2H, m, Cp'*H*), 3.58 (2H, m, Cp'*H*), 3.45 (2H, sept ($^{3}J_{HH}$ = 6.6 Hz), C*H*$(CH_3)_2$), 3.39 (2H, sept ($^{3}J_{HH}$ = 6.9 Hz), C*H*$(CH_3)_2$), 1.56 (3H, s, C*H*$_3$ of Cp'), 1.54 (6H, s, C*H*$_3$ of β-diketiminate), 1.51 (6H, d ($^{3}J_{HH}$ = 6.9 Hz), CH(C*H*$_3)_2$), 1.47 (6H, d ($^{3}J_{HH}$ = 6.6 Hz), CH(C*H*$_3)_2$), 1.15 (6H, d ($^{3}J_{HH}$ = 6.6 Hz), CH(C*H*$_3)_2$), 1.10 (6H, d ($^{3}J_{HH}$ = 6.9 Hz), CH(C*H*$_3)_2$), -15.42 (1H, s, Al-*H*-Mn). ^{13}C{^{1}H} NMR (126 MHz, C_6D_6, 298 K): δ 229.9 (*C*O), 170.4 (N*C*), 145.5 (Ar*C*), 142.8 (Ar*C*), 141.8 (Ar*C*), 127.5 (Ar*C*), 125.3 (Ar*C*), 124.2 (Ar*C*), 98.1 (Cp'*C*), 97.7 (γ-*C*H), 80.7 (Cp'*C*), 80.4 (Cp'*C*), 29.4 (*C*H$(CH_3)_2$), 28.4 (*C*H$(CH_3)_2$), 25.6 (*C*H$_3$ of β-diketiminate), 24.7 (CH(*C*H$_3)_2$), 24.6 (CH(*C*H$_3)_2$), 24.3 (CH(*C*H$_3)_2$), 23.8 (CH(*C*H$_3)_2$), 13.2 (*C*H$_3$ of Cp'). ^{27}Al NMR (78 MHz, C_6D_6, 298 K): δ 58. IR (CH_2Cl_2 solution, cm^{-1}): 1948 (s, CO) 1879 (s, CO). Elemental microanalysis: calc. for $C_{37}H_{50}AlMnN_2O_2$ C 69.78, H 7.92, N 4.40; meas. C 69.62, H 7.72, N 4.51. ***Crystallographic data***: $C_{37}H_{50}AlMnN_2O_2$, M_r = 636.30, monoclinic, P 2_1/n, a = 10.1264(1), b = 20.4974(3), c = 16.7518(2) Å, β = 103.6045(6)°, V = 3379.53(7) Å^3, Z = 4, ρ_c = 1.251 Mg m^{-3}, T = 150 K, λ = 0.71073 Å. 57790 reflections collected, 7686 independent [R(int) = 0.102] used in all calculations. R_1 = 0.0722, wR_2 = 0.0821 for observed unique reflections [$I > 2\sigma(I)$] and R_1 = 0.0390, wR_2 = 0.0607 for all unique reflections. Max. and min. residual electron densities 0.54 and -0.57 e Å^{-3}. CSD reference: 857129.

Preparation of (OC)$_4$Cr[κ^2-H$_2$Al(Dipp$_2$NacNac)] **(XXV)**

Method A: A J. Young's NMR tube was charged with a toluene-d_8 solution (1 cm^3) of Dipp$_2$NacNacAlH$_2$ (0.020 g, 0.04 mmol) and $Cr(CO)_6$ (0.008 g, 0.04 mmol) and subjected to UV photolysis for 90 min. During the reaction pale yellow crystals consisting of **XXV** (89%) and the κ^1-cocrystallite (11%) were formed. Yield 0.010 g, 49%.

Method B: A solution of $Cr(cod)(CO)_4$ (0.020 g, 0.07 mmol) in toluene (10 cm^3) was added slowly to a solution of $Dipp_2NacNacAlH_2$ (0.098 g, 0.22 mmol) also in toluene (15 cm^3) at room temperature and the reaction mixture stirred for 16 h. Over the course of the reaction a yellow precipitate formed which was isolated by filtration and the solvent removed *in vacuo* yielding a yellow powder. This was recrystallised from dichloromethane/hexane layering at -30 °C yielding crystals consisting solely of **XXV**. Yield 0.034 g, 75%.

Spectroscopic Data: ^{1}H NMR (300 MHz, CD_2Cl_2, 298 K): δ 7.42-7.11 (6H, m, Ar*H*), 5.56 (1H, s, γ-C*H*), 2.92 (4H, sept ($^3J_{HH}$ = 6.9 Hz), C*H*$(CH_3)_2$), 1.89 (6H, s, CH_3 of β-diketiminate), 1.31 (12H, d ($^3J_{HH}$ = 6.9 Hz), CH(CH_3)$_2$), 1.24 (12H, d ($^3J_{HH}$ = 6.9 Hz), CH(CH_3)$_2$), -10.48 (2H, s, Al-*H*-Cr). ^{13}C{^{1}H} NMR (75 MHz, CD_2Cl_2, 298 K): δ 228.9 (*C*O), 217.9 (*C*O), 174.0 (N*C*), 143.8 (Ar*C*), 137.2 (Ar*C*), 129.3 (Ar*C*), 125.5 (Ar*C*), 100.8 (γ-*C*H), 29.1 (*C*H$(CH_3)_2$), 24.8 (CH(*C*H_3)$_2$), 24.3 (CH(*C*H_3)$_2$), 24.1 (*C*H_3 of β-diketiminate). ^{27}Al NMR (78 MHz, CD_2Cl_2, 298 K): δ 50. IR (CH_2Cl_2 solution, cm^{-1}): 1980 (m, CO), 1938 (s, CO), 1872 (m, CO), 1868 (m, CO). MS(EI): *m/z* 610.2 (M^+) 10%.

Crystallographic Data from Method A: $(0.89)C_{33}H_{43}AlCrN_2O_4$, $(0.11)C_{34}H_{43}AlCrN_2O_5$, M_r = 613.89, orthorhombic, *P*nma, a = 17.5944(2), b = 21.1678(3), c = 9.0575(1) Å, V = 3380.1(1) $Å^3$, Z = 4, ρ_c = 1.206 Mg m^{-3}, T = 150 K, λ = 0.71073 Å. 7354 reflections collected, 3951 independent [R(int) = 0.019] used in all calculations. R_1 = 0.0456, wR_2 = 0.1025 for observed unique reflections [$I > 2\sigma(I)$] and R_1 = 0.0569, wR_2 = 0.1103 for all unique reflections. Max. and min. residual electron densities 0.66 and -0.58 e $Å^{-3}$. CSD reference: 857131.

Crystallographic Data from Method B: $C_{33}H_{43}AlCrN_2O_4$, M_r = 610.69, orthorhombic, *P*nma, a = 17.5623(2), b = 21.1664(2), c = 9.0431(1) Å, V = 3361.6(1) $Å^3$, Z = 4, ρ_c = 1.207 Mg m^{-3}, T = 150 K, λ = 0.71073 Å. 47317 reflections collected, 3624 independent [R(int) =

0.029] used in all calculations. R_1 = 0.0322, wR_2 = 0.0885 for observed unique reflections [$I > 2\sigma(I)$] and R_1 = 0.0340, wR_2 = 0.0885 for all unique reflections. Max. and min. residual electron densities 0.49 and -0.58 e Å^{-3}.

Preparation of (OC)$_4$Mo[κ^2-H$_2$Al(Dipp$_2$NacNac)] **(XXVI)**

Method A: A J. Young's NMR tube was charged with a toluene-d_8 solution (1 cm^3) of Dipp$_2$NacNacAlH$_2$ (0.020 g, 0.04 mmol) and Mo(CO)$_6$ (0.012 g, 0.04 mmol) and subjected to UV photolysis for 90 min. During the reaction pale yellow crystals formed which were recrystallised from dichloromethane/hexane layering at -30 °C. X-ray analysis showed the crystals to consist of **XXVI** (91%) and the κ^1-cocrystallite (9%). Yield 0.007 g, 31%.

Method B: A J. Young's NMR tube was charged with a solution of Mo(cod)(CO)$_4$ (0.010 g, 0.03 mmol) and Dipp$_2$NacNacAlH$_2$ (0.040, 0.09 mmol) in benzene-d_6 (1 cm^3). After sonication for 72 h all of the Mo(cod)(CO)$_4$ had been consumed, as determined by ^{1}H NMR spectroscopy, and the solvent was removed *in vacuo* to yield a yellow solid. Recrystallisation from dichloromethane/hexane layering at -30 °C yielded pale yellow crystals suitable for X-ray crystallography. X-ray analysis showed the crystals to consist of **XXVI** (91%) and the κ^1-cocrystallite (9%). Yield 0.018 g, 60% (Although quantitative by ^{1}H NMR spectroscopy).

Spectroscopic Data: ^{1}H NMR (300 MHz, CD_2Cl_2, 298 K): δ 7.26-7.12 (6H, m, Ar*H*), 5.44 (1H, s, γ-C*H*), 2.83 (4H, sept ($^3J_{HH}$ = 6.6 Hz), C*H*(CH$_3$)$_2$), 1.79 (6H, s, C*H*$_3$ of β-diketiminate), 1.18 (12H, d ($^3J_{HH}$ = 6.6 Hz), CH(C*H*$_3$)$_2$), 1.11 (12H, d ($^3J_{HH}$ = 6.6 Hz), CH(C*H*$_3$)$_2$), -6.85 (2H, s, Al-*H*-Mo). ^{13}C{^{1}H} NMR (75 MHz, CD_2Cl_2, 298 K): δ 217.7 (*C*O), 205.6 (*C*O), 172.9 (N*C*), 142.8 (Ar*C*), 128.1 (Ar*C*), 124.5 (Ar*C*), 123.6 (Ar*C*), 99.4 (γ-*C*H), 27.9 (*C*H(CH$_3$)$_2$), 23.7 (CH(*C*H$_3$)$_2$), 23.4 (CH(*C*H$_3$)$_2$), 22.9 (*C*H$_3$ of β-

diketiminate). ^{27}Al NMR (78 MHz, CD_2Cl_2, 298 K): δ 50. IR (CH_2Cl_2 solution, cm^{-1}): 1981 (s, CO), 1941 (m, CO), 1873 (br, CO).

Crystallographic Data from Method A: $(0.91)C_{33}H_{43}AlMoN_2O_4$, $(0.09)C_{34}H_{43}AlMoN_2O_5$, M_r = 657.02, orthorhombic, *P*nma, a = 17.6692(4), b = 21.941(4), c = 9.1498(2) Å, V = 3442.6(1) Å^3, Z = 4, ρ_c = 1.268 Mg m^{-3}, T = 150 K, λ = 0.71073 Å. 40344 reflections collected, 3971 independent [R(int) = 0.073] used in all calculations. R_1 = 0.0669, wR_2 = 0.1800 for observed unique reflections [$I > 2\sigma(I)$] and R_1 = 0.1079, wR_2 = 0.1931 for all unique reflections. Max. and min. residual electron densities 1.65 and -1.41 e Å^{-3}.

Preparation of $(OC)_4W[\kappa^2$-$H_2Al(Dipp_2NacNac)]$ **(XXVII)**

A J. Young's NMR tube was charged with a solution of W(cod)$(CO)_4$ (0.030 g, 0.07 mmol) and $Dipp_2NacNacAlH_2$ (0.080, 0.18 mmol) in benzene-d_6 (1 cm^3) and heated at 70 °C for 5 h. Slow cooling of the reaction mixture to room temperature resulted in the formation of yellow crystals of **XXVII**. Yield 0.031 g, 42%.

Spectroscopic Data: ^{1}H NMR (300 MHz, CD_2Cl_2, 298 K): δ 7.26-7.13 (6H, m, Ar*H*), 5.50 (1H, s, γ-C*H*), 2.81 (4H, sept ($^3J_{HH}$ = 6.6 Hz), C*H*$(CH_3)_2$), 1.81 (6H, s, C*H*$_3$ of β-diketiminate), 1.18 (12H, d ($^3J_{HH}$ = 6.6 Hz), CH(C*H*$_3)_2$), 1.12 (12H, d ($^3J_{HH}$ = 6.6 Hz), CH(C*H*$_3)_2$), -7.71 (2H, s, Al-*H*-W). ^{13}C{^{1}H} NMR (75 MHz, CD_2Cl_2, 298 K): δ 208.2 (*C*O), 198.3 (*C*O), 174.1 (N*C*), 143.4 (Ar*C*), 136.5 (Ar*C*), 129.0 (Ar*C*), 125.2 (Ar*C*), 100.6 (γ-*C*H), 28.7 (*C*H$(CH_3)_2$), 24.4 (CH(*C*H$_3)_2$), 24.2 (CH(*C*H$_3)_2$), 23.8 (*C*H$_3$ of β-diketiminate). ^{27}Al NMR (78 MHz, CD_2Cl_2, 298 K): δ 58. IR (CH_2Cl_2 solution, cm^{-1}): 1976 (s, CO), 1935 (m, CO), 1883 (s, CO), 1853 (m, CO).

Crystallographic Data: $C_{33}H_{43}AlN_2O_4W$, M_r = 742.55, orthorhombic, *P*nma, a = 17.5825(1), b = 21.2770(1), c = 9.1293(3) Å, V = 3415.3(1) Å^3, Z = 4, ρ_c = 1.444 Mg m^{-3}, T = 150 K, λ = 0.71073 Å. 57194 reflections collected, 4004 independent [R(int) = 0.013]

used in all calculations. R_1 = 0.0240, wR_2 = 0.0639 for observed unique reflections [$I > 2\sigma(I)$] and R_1 = 0.0332, wR_2 = 0.0723 for all unique reflections. Max. and min. residual electron densities 0.55 and -1.35 e Å^{-3}.

Preparation of (OC)$_5$Cr[κ^1-H$_2$Al(Dipp$_2$NacNac)] **(XXVIII)**

A solution of Cr(coe)(CO)$_5$ (0.27 g, 0.91 mmol) in pentane (30 cm^3) was added to a solution of Dipp$_2$NacNacAlH$_2$ (0.40 g, 0.90 mmol) also in pentane (30 cm^3) and the reaction mixture stirred in the dark for 90 min. During the reaction **XXVIII** was formed as a yellow precipitate which was isolated by filtration and dried *in vacuo* yielding a pale yellow powder. Yield 0.30 g, 52%. Samples of **XXVIII** in CD_2Cl_2 decomposed over the course of several hours forming **XXV** as the major product.

Spectroscopic data: ^{1}H NMR (300 MHz, CD_2Cl_2, 298 K): δ 7.24-7.40 (6H, m, Ar*H*), 5.37 (1H, s, γ-CH), 3.18 (2H, sept ($^3J_{HH}$ = 6.6 Hz), C*H*(CH$_3$)$_2$), 3.17 (2H, sept ($^3J_{HH}$ = 6.6 Hz), C*H*(CH$_3$)$_2$), 1.83 (6H, s, C*H*$_3$ of β-diketiminate), 1.42 (6H, d ($^3J_{HH}$ = 6.6 Hz), CH(C*H*$_3$)$_2$), 1.34 (6H, d ($^3J_{HH}$ = 6.6 Hz), CH(C*H*$_3$)$_2$), 1.31 (6H, d ($^3J_{HH}$ = 6.6 Hz), CH(C*H*$_3$)$_2$), 1.18 (6H, d ($^3J_{HH}$ = 6.6 Hz), CH(C*H*$_3$)$_2$), -11.50 (1H, s, Al-*H*-Cr).

5.4 Results and Discussion

5.4.1 Synthesis of κ^1-Coordinated Al-H σ-Complexes

The primary synthetic procedures for the formation of σ-borane and σ-silane complexes feature either salt metathesis or E-H bond coordination (E = B or Si) at an (*in situ* generated) unsaturated transition metal fragment. In work described in Chapter III, *N*,*N'*-donor stabilised aluminium dihalides **I-III** have been shown to be reactive towards the $Na[CpFe(CO)_2]$ and $Na[Cp^*Fe(CO)_2]$ transition metal anions, forming the mixed iron-aluminium complexes **V-VIII** (Scheme 5.4). The related reaction between **I** and the hydrido transition metal reagent $K[Cp'Mn(CO)_2H]$ (**5.1**) forms the manganese complex $Cp'Mn(CO)_2[HAl(Cl)(N^iPr)_2CPh]$ (**XX**) (Scheme 5.4) *via* salt metathesis.

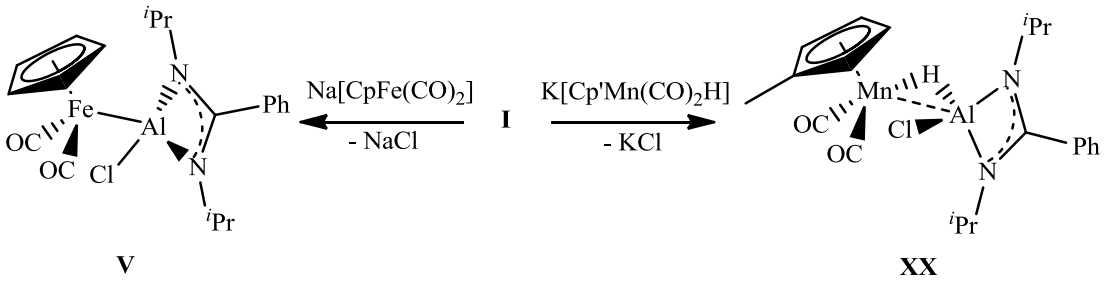

V **XX**

Scheme 5.4: *Salt metathesis reactions for the preparation of **IV** and **XX***

As in the case of the related non-hydride containing complex **V**, the reaction can be monitored *in situ* by ^{27}Al NMR spectroscopy with a downfield shift of *ca.* 50 ppm being observed on formation of **XX**. Complex **XX** was isolated as pale yellow crystals after storage of a concentrated hexane solution at -30 °C and has been characterised by standard spectroscopic and analytical techniques as well as by X-ray diffraction (Figure 5.2).

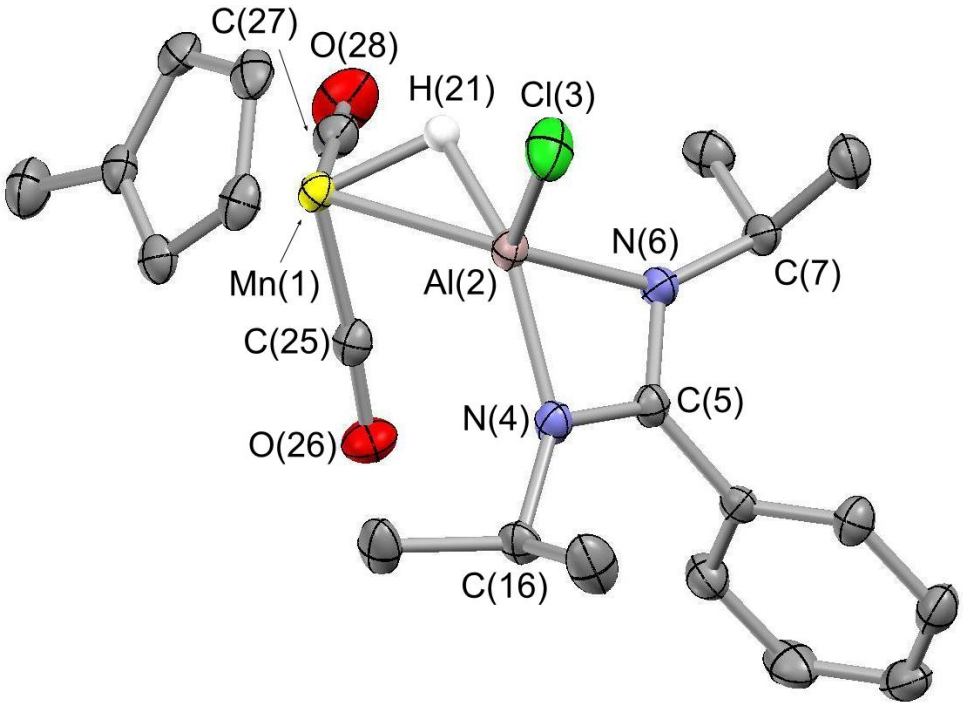

Figure 5.2: *Molecular structure of **XX**. Thermal ellipsoids set at the 40% probability level, hydrogen atoms (except metal bound H's) omitted for clarity.* Key bond lengths (Å) and angles (°): Mn(1)···Al(2) 2.446(1), Mn(1)-H(21) 1.56(3), Al(2)-H(21) 1.72(3), Al(2)-Cl(3) 2.156(1), Al(2)-N(4) 1.923(2), Al(2)-N(6) 1.906(2), N(4)-C(5) 1.329(3), C(5)-N(6) 1.331(3); Mn(1)-H(21)-Al(2) 97(1), Mn(1)-Al(2)-Cl(3) 116.32(3), Mn(1)-Al(2)-N(4) 119.93(6), Mn(1)-Al(2)-N(6) 121.66(7), Cl(3)-Al(2)-N(4) 109.42(7), Cl(3)-Al(2)-N(6) 111.21(7), N(4)-Al(2)-H(21) 151.7(8), N(6)-Al(2)-H(21) 103.4(8), N(4)-Al(2)-N(6) 69.66(8), N(4)-C(5)-N(6) 110.6(2).

XX crystallises with a single crystallographically distinct molecule in the asymmetric unit and features the aluminium centre in a pseudo trigonal bipyramidal geometry, in a manner that closely resembles related silane complexes, with due allowances being made for the four-membered heterocycle and the Mn-H linkage.[2,3,11] The trigonal bipyramidal geometry of the aluminium centre is demonstrated by the sum of the angles subtended at aluminium by the Mn-Al, Al-Cl and Al-N(6) vectors (349.1°), and the H(21)-Al(2)-N(4) angle (151.7(8)°). The presence of the Mn-H-Al linkage can be inferred crystallographically with the location of H(21) being apparent in the Fourier difference map. Comparison of the molecular structures of **XX** and the related complex $CpFe(CO)_2[(Cl)Al(N^iPr)_2CPh]$ **V** identifies a significantly longer M-Al bond in **XX** (2.446(1) Å *cf.* 2.340(1) Å for **V**), even accounting for the difference in covalent radii (Δr = 0.07 Å).[12] Moreover, the (O)C-M-Al angles in **XX** (76.0(1) and 115.7(1)°) show significant disparity compared to those of **V** (80.7(1) and 82.1(1)°) and both of these observations are consistent with the incorporation of a hydride ligand within the coordination sphere of the manganese atom. The presence of the Mn-H-Al linkage was also confirmed by ^{1}H NMR spectroscopy in benzene-d_6 solution, with a resonance at δ_H = -13.93 ppm being indicative of a bridging hydride ligand. Compound **XX** can be thus classed as a chloride substituted σ-alane complex.

In an attempt to obtain a σ-alane complex without a chloride substituent, the substitution chemistry of **XX** was investigated; however, simple exchange reactions with silanes proved unsuccessful and more reactive hydride sources such as $LiAlH_4$ and $K[Et_3BH]$ led to decomposition. The difficulty in accessing mixed (chloro)alane precursors of the type XAl(Cl)(H) (where X = monoanionic bidentate substituent), and their tendency to undergo substituent redistribution reactions, meant that salt metathesis chemistry was not a viable approach to non-halide systems. Thus, synthetic approaches targeted instead the coordination of isolable alane molecules to unsaturated transition metal fragments. Initial

attempts to prepare the dihydroalane analogue of **I**, *i.e.* PhC(^{i}PrN)$_2$AlH$_2$, highlighted the requirement for the use of sterically demanding substituents at aluminium. Thus, the reactions between the amidine PhC(^{i}PrN)(^{i}PrNH) and $H_3Al{\cdot}NMe_3$ and between the amidine hydrochloride salt and $LiAlH_4$ yielded the *bis(*amidinate) compound [(PhC(^{i}PrN)$_2$]$_2$AlH (**XXI**), despite 1:1 reaction stoichiometries being employed in both reactions. As a result, the previously reported (and more sterically demanding) guanidinate supported alane [{^{i}Pr$_2$NC(DippN)$_2$}Al(H)(μ-H)]$_2$ (**5.2**) was employed.[13]

In the presence of **5.2**, *in situ* photolytic generation of the 16-electron [W(CO)$_5$] fragment in hexane resulted in the formation of the σ-alane complex (OC)$_5$W[κ^1-H$_2$Al(NDipp)$_2$CN^{i}Pr$_2$] (**XXII**) (Scheme 5.5).

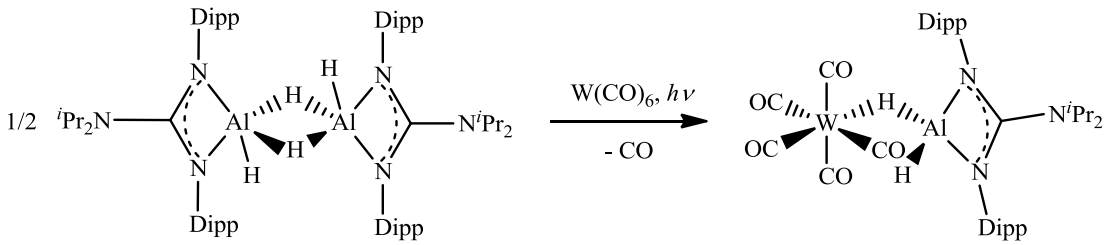

Scheme 5.5: *Photolytic preparation of (OC)$_5$W[κ^1-H$_2$Al(NDipp)$_2$CN^{i}Pr$_2$] (**XXII**)*

Isolation of **XXII** was achieved through the fractional crystallisation of a pentane solution at -30 °C and **XXII** has been characterised by standard spectroscopic and analytical techniques as well as by X-ray diffraction (Figure 5.3).

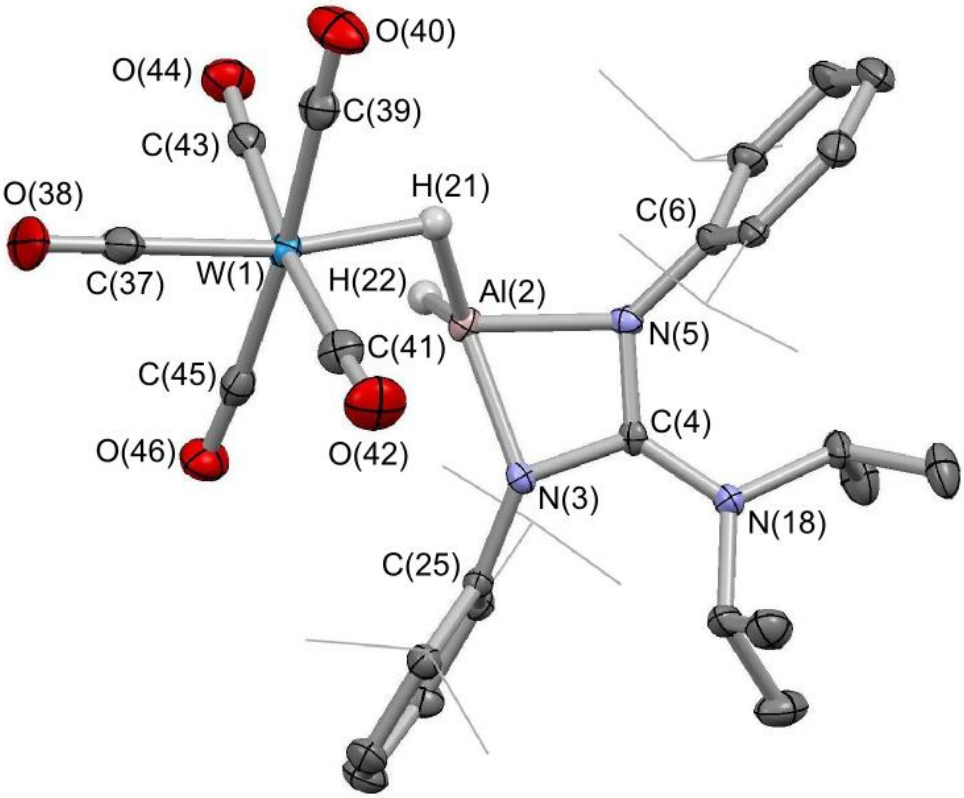

Figure 5.3: *Molecular structure of **XXII**. Thermal ellipsoids set at the 40% probability level, ^{i}Pr groups of Dipp substituents are shown in wireframe and hydrogen atoms (except metal bound H's) omitted for clarity.* Key bond lengths (Å) and angles (°): W(1)···Al(2) 2.841(1), W(1)-H(21) 1.80(3), W(1)-C(37) 2.014(3), W(1)-C(39) 2.055(3), W(1)-C(41) 2.062(3), W(1)-C(43) 2.052(3), W(1)-C(45) 2.024(3), Al(2)-H(21) 1.67(3), Al(2)-H(22) 1.68(3), Al(2)-N(3) 1.913(2), Al(2)-N(5) 1.892(2), N(3)-C(4) 1.387(3), C(4)-N(5) 1.356(3), C(4)-N(18) 1.344(3); W(1)-H(21)-Al(2) 102(2), W(1)-Al(2)-H(22) 36(2), H(21)-Al(2)-H(22) 123(2), W(1)-Al(2)-N(3) 118.47(7), W(1)-Al(2)-N(5) 131.71(7), N(3)-Al(2)-N(5) 70.45(9), N(3)-C(4)-N(5) 106.2(2).

The molecular structure of **XXII** consists of a single crystallographically distinct molecule in the asymmetric unit and features the aluminium centre in a pseudo trigonal bipyramidal geometry in a manner similar to **XX**, with due allowances made for the four-membered heterocycle and a long Al···W interaction. The trigonal bipyramidal geometry is demonstrated by the sum of the angles subtended at aluminium by the N(3)-Al(2), Al(2)-H(22) and Al(2)-H(21) vectors (359.2°) and the N(5)-Al(2)-W(1) angle is 131.71(7)°. The geometry of the aluminium centre of **XXII** closely resembles that of the gallium centre in the related σ-gallane complex $(OC)_5W[\kappa^1\text{-}H_3Ga\cdot quin]$ (**1.148**) (Figure 5.4).[14]

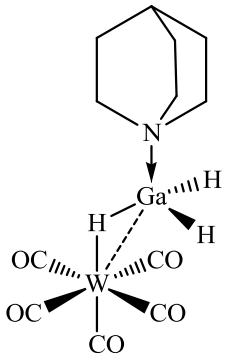

1.148

Figure 5.4: *Structural formula of **1.148***

In **1.148** the gallium atom features a pseudo trigonal bipyramidal geometry in which the hydride ligands form the trigonal plane and the related angles N-Ga-W 118.3(1)° and W-H-Ga 125(4)° are observed.[14] The position of the hydride atoms in **XXII** could be inferred crystallographically, and both H(21) and H(22) were located in the Fourier difference map. Moreover, in the ^{1}H NMR spectrum both terminal and bridging resonances could be identified (δ_H = 6.80 and -7.11, respectively), with the terminal Al-H being definitively assigned through $^1H\{^{27}Al\}$ experiments. The W-H-Al resonance, however, is readily identified as a doublet ($^2J_{HH}$ = 20 Hz) without the need for decoupling experiments.

Interestingly the exchange of terminal and bridging hydrides is slow on the NMR timescale with distinct resonances being observed for both even upon heating the sample to 75 °C. This is also the case for the σ-gallane complex **1.148**, although ready fluxional exchange is observed in the related four-coordinate borane κ^1-complexes $(OC)_5W(\kappa^1\text{-}H_3B{\cdot}L)$ (L = NMe_3, PMe_3, PPh_3 or IMe **1.92-1.95** respectively), even at low temperatures.[8,9,15,16] The ^{1}H NMR spectrum of the guanidinate backbone in **XXII** further supports the asymmetric κ^1-mode of coordination, as four resonances attributable to the methyl groups and two attributable to the methine groups of the Dipp substituents are observed, clearly demonstrating the reduction of symmetry from **5.2**. Analysis of the IR spectrum of **XXII** shows that pseudo C_{4v} geometry of the tungsten centre is maintained in solution and two distinct ν(CO) bands observed at 1983 and 1951 cm^{-1}, the latter with a clear shoulder. This is consistent with the IR spectra for previously reported $(OC)_5WL$ complexes, for which $2A_1$ + E IR active bands are predicted.[17] The substitution of a CO ligand for the Al-H bond results in a red shift in the observed carbonyl stretching frequencies due to the replacement of a σ-donor and good π-acceptor CO ligand with the poorer π-acceptor alane ligand. Attempts to dehydrogenate **XXII** to form a formal tungsten-aluminium double bond proved unsuccessful resulting ultimately in complex decomposition. No evidence was obtained for the substitution of a second carbonyl ligand, forming the corresponding κ^2-complex, and under prolonged photolysis the decomposition product $[^iPr_2NC(DippNH)_2][(OC)_5W\text{-}H\text{-}W(CO)_5]$ (**XXIII**) was identified both spectroscopically and by X-ray diffraction.

With the importance of steric shielding at the aluminium centre having been clearly identified, the coordination chemistry of the highly sterically demanding monomeric species $Dipp_2NacNacAlH_2$ (**5.3**) was also investigated.[18] The enhanced steric protection of the aluminium centre offered by the $Dipp_2NacNac$ substituent was identified in Chapter IV,

and it is further illustrated by the monomeric nature of **5.3** (in comparison to the dimeric guanidinate complex **5.2**, for example). Superficially, the monomeric nature of **5.3** might be thought likely to facilitate coordination of the Al-H bond to an *in situ* generated 16-electron transition metal fragment. Accordingly **5.3** readily reacts with $Cp'Mn(CO)_3$ under photolytic conditions in toluene or benzene to form $Cp'Mn(CO)_2[\kappa^1\text{-}H_2AlDipp_2NacNac]$ (**XXIV**) (Scheme 5.6).

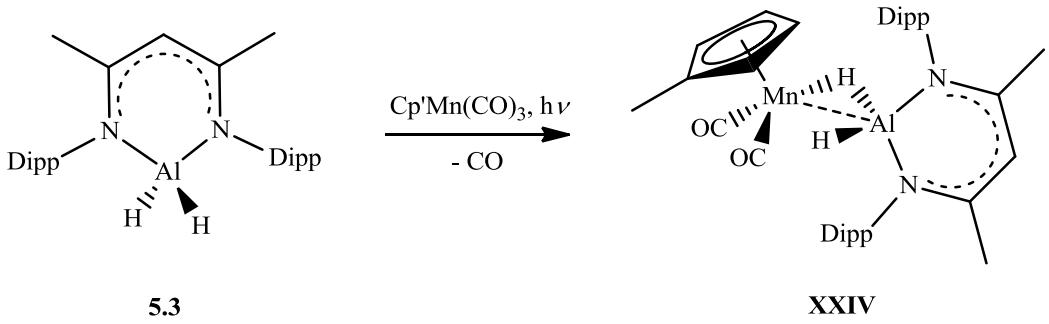

5.3 **XXIV**

Scheme 5.6: *Reaction of **5.3** with $Cp'Mn(CO)_3$ under photolytic conditions*

XXIV was isolated as yellow single crystals after slow cooling of a concentrated toluene solution to -30 °C. Characterisation of **XXIV** was carried out by standard spectroscopic and analytical techniques as well as by X-ray diffraction (Figure 5.5).

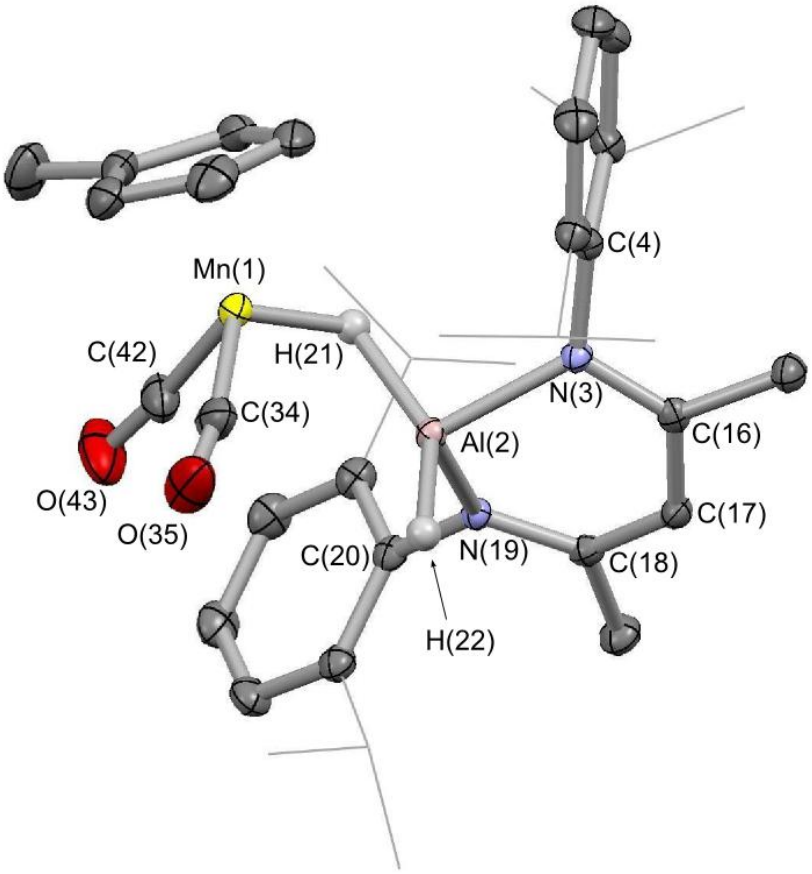

Figure 5.5: *Molecular structure of **XXIV**. Thermal ellipsoids set at the 40% probability level, ^{i}Pr groups of Dipp substituents are shown in wireframe and hydrogen atoms (except metal bound H's) omitted for clarity.* Key bond lengths (Å) and angles (°): Mn(1)···Al(2) 2.654(1), Mn(1)-H(21) 1.56(3), Al(2)-H(21) 1.70(3), Al(2)-H(22) 1.59(2), Al(2)-N(3) 1.910(2), Al(2)-N(19) 1.925(2); Mn(1)-H(21)-Al(2) 109(2), Mn(1)-Al(2)-H(22) 109.5(9), H(21)-Al(2)-H(22) 143(1), Mn(1)-Al(2)-N(3) 119.53(8), Mn(1)-Al(2)-N(19) 119.11(8), N(3)-Al(2)-H(21) 100(1), N(3)-Al(2)-H(22) 106(1), N(19)-Al(2)-H(21) 96(1), N(19)-Al(2)-H(22) 105(2) N(3)-Al(2)-N(19) 95.19(9).

The molecular structure of **XXIV** contains a single molecule in the asymmetric unit and features the aluminium centre in a distorted trigonal bipyramidal geometry, with due allowances being made for the six-membered heterocycle. The trigonal bipyramidal geometry is demonstrated by the sum of the angles subtended at aluminium by the Mn-Al, Al-N(3) and Al-N(19) vectors (333.8°) and the H(21)-Al-(2)-H(22) angle is 143(1)°. Interestingly the aluminium centre sits out of the plane created by the C_3N_2 backbone of the heterocycle by *ca*. 0.75 Å, whereas in the free alane precursor **5.3** the aluminium centre is coplanar with the heterocycle.[19] Presumably coordination to the [Cp'Mn$(CO)_2$] fragment results in an increase in steric demands within the heterocycle causing this deviation from planarity.

The increased steric demands imposed by the $Dipp_2$NacNac substituent result in a greater Mn···Al separation in **XXIV** (2.654(1) Å) than that observed in the less sterically encumbered (chloro)alane complex **XX** (2.446(1) Å) as well as a greater Mn-H-Al bond angle (109(2) *cf.* 97(1)° for **XX**). The positions of the hydride atoms of **XXIV** could be inferred crystallographically and H(21) and H(22) were located in the Fourier difference map. Moreover, spectroscopic analysis of **XXIV** identified a suitably high-field resonance consistent with the presence of a Mn-H-Al bridging interaction at δ_H = -15.42 ppm, with the corresponding terminal Al-H resonance being located at δ_H = 5.75 ppm. The identification of both terminal and bridging hydride resonances shows that, as with **XXII**, the exchange between bridging and terminal hydrides is slow on the NMR timescale. Even upon heating to 75 °C no evidence of fluxionality was observed. Furthermore, four methyl resonances and two methine resonances attributable to the Dipp substituents were observed which is consistent with a reduction in symmetry of the $Dipp_2$NacNac substituent backbone. This further supports the idea of a single Mn-H-Al interaction in solution and slow exchange of bridging and terminal hydrides. Attempts to induce dehydrogenation of **XXIV** through

prolonged heating or the use of the hydrogen acceptor tbe (3,3-dimethyl-1-butene) proved unsuccessful.

The carbonyl stretching frequencies observed for **XX** (1974 and 1899 cm^{-1}) and **XXIV** (1948 and 1879 cm^{-1}) both show a red shift in comparison to the $Cp'Mn(CO)_3$ precursor, consistent with the substitution of a good π acceptor ligand with a poorer π acceptor. In the case of **XXIV** the observed stretching frequencies are comparable to those reported in four-coordinate borane complexes, in which the borane acts predominantly as a σ-donor (1947-1919, 1858-1820 cm^{-1} for four-coordinate boranes).[7,16] Those observed for **XX**, however, are more closely comparable to those reported for three-coordinate boranes (1995-1967 and 1937-1901 cm^{-1}) for which π acceptor properties are known to be structurally relevant.[1] To further investigate the bonding in these systems and the possibility of manganese to alane back-donation in **XX**, Density Functional Theory (DFT) calculations were carried out on these κ^1-complexes.

5.4.2 DFT Calculations on κ^1-Coordinated Al-H Complexes

DFT calculations were carried out by Dr Joshua Bates, from the Aldridge group, on the κ^1-complexes **XXII** and **XXIV** to corroborate hydrogen positions, as a means to compare the intrinsic thermodynamics of alane binding with other σ-complexes, and with a view to probing issues of back-bonding. Calculations show excellent agreement with the X-ray structural data and estimate ligand binding energies to be comparable to, or slightly greater than dihydrogen, but significantly less than those for CO at both transition metal fragments (D_o = 22.9, 14.3, 36.2 kcal mol^{-1} for alane, H_2 and CO complexes of $[W(CO)_5]$; and 26.9, 25.6, 54.2 kcal mol^{-1} for the corresponding $[Cp'Mn(CO)_2]$ complexes). From the calculated binding energies it is clear that each ligand (alane, H_2 and CO) binds more strongly to the more electron rich $[Cp'Mn(CO)_2]$ fragment, however, the increase in binding energy is

smallest for the alane and greatest for CO. These findings are consistent with a comparatively minor role of π-back-bonding in alane coordination, in comparison with H_2 and CO. This is supported by the X-ray structural data obtained which clearly shows primarily 'end-on' coordination of the Al-H bond in both **XXII** and **XXIV**, as well as minimal Al-H bond activation, consistent with the Al-H bond acting predominantly as a σ-donor.

By contrast, the X-ray structure of **XX** features a more 'side-on' coordination of the Al-H bond than **XXII** and **XXIV**. This is demonstrated by a reduced Mn···Al distance (2.446(1) Å for **XX** and 2.654(1) Å for **XXIV**) and by a markedly tighter Mn-H-Al angle (97(1)° for **XX** and 109(2)° for **XXIV**). In addition, carbonyl stretching frequencies comparable with those of three-coordinate boranes, and the torsional alignment of the Al-H bond in **XX** indicate a different Al-H binding interaction to that observed in **XXIV**. The alignment of the Al-H bond in **XX** is approaching perpendicular to the Cp centroid-Mn vector, demonstrated by the Cp centroid-Mn-Al-H torsion angle of 105.1°. This orientation allows for overlap between the HOMO of the [Cp'Mn(CO)$_2$] fragment and an orbital of Al-H σ*-character (Figure 5.6).

Figure 5.6: *(left) HOMO of the [Cp'Mn(CO)$_2$] fragment, (right) orientation of the Al-H bond in **XX***

For comparison, the analogous torsion angle in Cp'Mn(CO)$_2${(H)Si(F)Ph$_2$} is 111.3° and in Cp'Mn(CO)$_2${(H)BCat} 89.1°.[1,11] It is conceivable that the more 'side-on' binding of the

alane in **XX** can be attributed to the reduced steric demands associated with the amidinate ligand, and/or (by analogy with silanes) to the presence of an electron withdrawing group at aluminium lowering the energy of the Al-H σ* orbital, thereby leading to greater back-bonding.

With statistically equivalent Mn-H bond lengths (1.56(3) Å) being observed in both **XX** and **XXIV** it is likely that, as observed in silane complexes of the [Cp'Mn(CO)$_2$] fragment, an asymmetric oxidative addition process occurs. Consequently, the Mn-H interaction forms early and is comparatively insensitive to progression along the oxidative addition pathway. The extent of oxidative addition is more accurately reflected in the observed Mn-Al distance and corresponding Mn-H-Al angle, with the process of oxidative addition reflected as a 'pivoting' of the alane ligand about this bridging hydrogen atom.[1,3,11]

The model systems CpMn(CO)$_2$[H(Cl)Al(NMe)$_2$CMe] (**XXa**) and CpMn(CO)$_2$[κ^1-H$_2$Al(NMeCMe)$_2$CH] (**XXIVa**) (Figure 5.7) both show a very soft potential energy surface for the 'pivoting' of the alane ligand around the bridging hydrogen atom.

XXa **XXIVa**

Figure 5.7: *Structures of the model systems **XXa** and **XXIVa***

For **XXa** changes in the Mn-H-Al angle from 80-110° result in a net energetic penalty of *ca.* 3 kcal mol^{-1}, compared to the lowest energy geometry. This small energetic penalty is a result of two conflicting parameters, the instantaneous interaction energy and the ligand

preparation energy. As the Mn-H-Al angle becomes tighter, and the Mn···Al contact closer, the instantaneous interaction energy increases, presumably due to better orbital overlap between the [$CpMn(CO)_2$] and [$H(Cl)Al(NMe)_2CMe$] fragments. However, as this angle tightens the preparation energy required to transform the ground state geometries of the [$CpMn(CO)_2$] and [$H(Cl)Al(NMe)_2CMe$] fragments into the increasingly distorted fragments in the complex increases, thereby all-but cancelling out the greater instantaneous interaction energy (Figure 5.8).

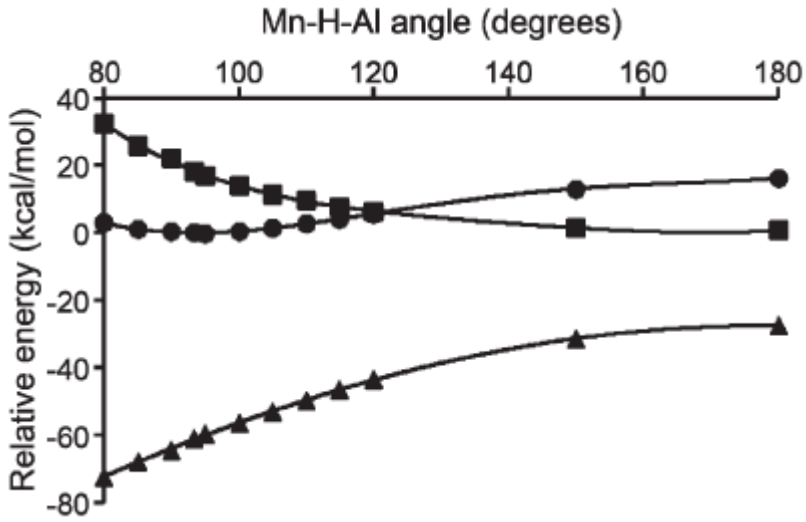

Figure 5.8: *Results from varying Mn-H-Al angle in **XXa**; (●) total energy relative to ground state, (▲) instantaneous interaction energy between the [$CpMn(CO)_2$] and [$H(Cl)Al(NMe)_2CMe$] fragments, (■) fragment preparation energy*

For the alane fragment a significant contribution to the preparation energy is associated with lengthening the Al-H bond. Opposing contributions from instantaneous interaction and ligand preparation energies are also observed for **XXIVa**, resulting in a similarly soft potential energy surface.

Fragment orbital analysis of **XXa** as a function of Mn-H-Al angle shows that the greater instantaneous interaction energy as the Mn-H-Al angle tightens is attributable to increases in both the donor component from the alane, and the back-bonding component to the alane. Thus, at a Mn-H-Al angle of 180° orbital interactions involving population of the LUMO of the [$CpMn(CO)_2$] fragment (alane σ-donation) account for 17.7 kcal mol^{-1} with back-bonding into the LUMO or LUMO + 1 of the [$H(Cl)Al(NMe)_2CMe$] fragment being essentially negligible. In contrast, at the energetic minimum, σ-donation from the alane contributes 36.5 kcal mol^{-1} and π back-donation 12.8 kcal mol^{-1}, close to a quarter of the total interaction energy (Figure 5.9).

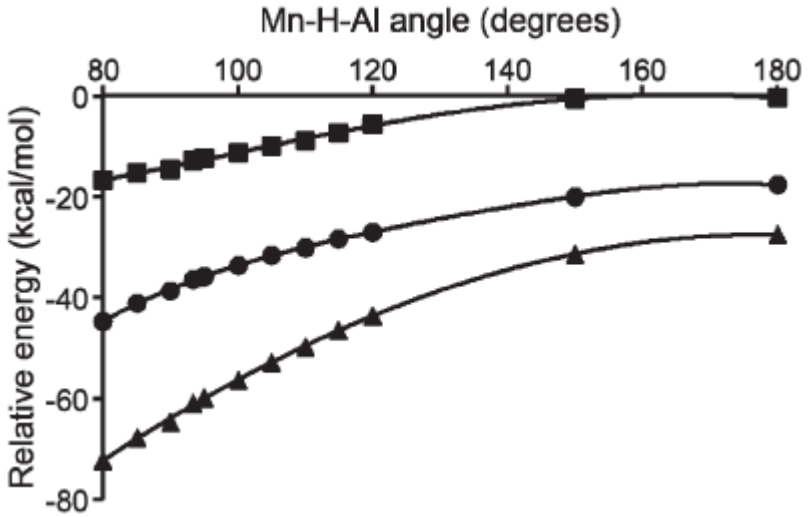

Figure 5.9: *Results from varying Mn-H-Al angle in **XXa**; (▲) instantaneous interaction energy, (●) energy associated with interactions involving the LUMO of the [$CpMn(CO)_2$] fragment, (■) energy associated with interactions involving population of the LUMO and LUMO + 1 of the [$H(Cl)Al(NMe)_2CMe$] fragment*

Comparison of the model amidinate and NacNac systems (**XXa** and **XXIVa** respectively) shows, perhaps unexpectedly, that the ligand preparation energies for both the

[$CpMn(CO)_2$] and corresponding alane fragment are actually very similar for both systems. However, for any given Mn-H-Al angle the instantaneous interaction energy is always greater for the amidinate supported alane, as shown by the calculated binding energies at the lowest energy geometry for the model systems **XXa** and **XXIVa** of 41.7 and 33.2 kcal mol^{-1} respectively. Fragment orbital analysis of the NacNac model system **XXVa** reveals that the reduced instantaneous interaction energy between the [$CpMn(CO)_2$] and [$H_2Al(NMeCMe)_2CH$] fragments is a result of weaker σ-donating properties of the alane, and that the contribution from back-bonding to the complex is similarly dependent upon Mn-H-Al angle.

Overall, quantum chemical calculations imply that the extent of back-bonding observed in the differing amidinate and NacNac systems is dependent upon the Mn-H-Al angle. Calculations on the replacement of the electron withdrawing Cl ligand of **XXa** for hydride result in very subtle effects. Moreover, the energetic penalties associated with 'pivoting' the alane ligand around the hydrogen of the Mn-H-Al linkage are small, and within the realms of crystal packing forces. As such it is possible the crystal environment rather than steric/electronic properties of the ligand determines the subtleties of ligand binding.

5.4.3 Synthesis of κ^2-Coordinated Al-H σ-Complexes by Photolysis

The photolytic preparation and subsequent characterisation of the κ^1-alane complexes **XXII** and **XXIV** incorporating the [$W(CO)_5$] and [$Cp'Mn(CO)_2$] transition metal fragments allows comparison of the structure and bonding of σ-alane complexes to the libraries of borane and silane complexes. To further investigate the coordination chemistry of the monomeric alane fragment $Dipp_2NacNacAlH_2$ (**5.3**) the reaction between **5.3** and $Cr(CO)_6$

under photolytic conditions was carried with the aim of forming an analogue of the κ^1 tungsten complex **XXII** (Scheme 5.7).

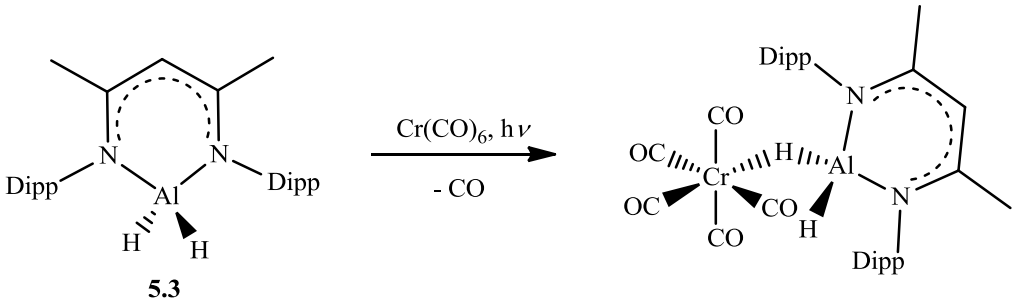

Scheme 5.7: Proposed reaction of $Cr(CO)_6$ and **5.3** under photolytic conditions

Photolysis of an equimolar solution of $Cr(CO)_6$ and **5.3** in toluene-d_8 led to the rapid formation of a yellow solution, the ^{1}H NMR spectrum of which showed a resonance attributable to the formation of a Cr-H-Al linkage. As the reaction progressed yellow crystals began to form and the resonance attributable to the Cr-H-Al linkage began to decrease. Analysis of the yellow crystals identified the major product of the reaction to be $(CO)_4Cr[\kappa^2\text{-}H_2AlDipp_2NacNac]$ (**XXV**) which has been characterised by standard spectroscopic and analytical techniques as well as by X-ray diffraction (Figure 5.10).

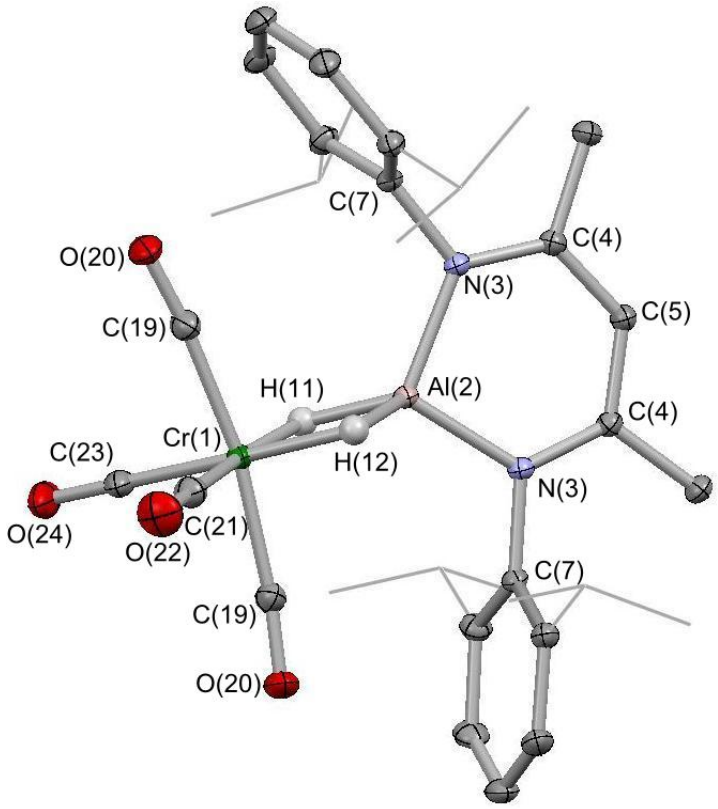

Figure 5.10: *Molecular structure of **XXV**. Thermal ellipsoids set at the 40% probability level, ^{i}Pr groups of Dipp substituents are shown in wireframe, hydrogen atoms (except metal bound H's) and minor component omitted for clarity.* Key bond lengths (Å) and angles (°): Cr(1)···Al(2) 2.420(1), Cr(1)-H(11) 1.64, Cr(1)-H(12) 1.69, Cr(1)-C(19) 1.892(2), Cr(1)-C(21) 1.834(3), Cr(1)-C(23) 1.846(3), Al(2)-H(11) 1.51, Al(2)-H(12) 1.65, Al(2)-N(3) 1.856(1); Cr(1)-H(11)-Al(2) 100, Cr(1)-H(12)-Al(2) 93, H(11)-Cr(1)-H(12) 81, H(11)-Al(2)-H(12) 86, N(3)-Al(2)-N(3) 98.93(8), Cr(1)-C(19)-O(20) 173.4(3).

The molecular structure of **XXV** features half a molecule in the asymmetric unit with the plane formed by the Cr-H-Al linkages and the CO ligands *trans* to the alane representing a crystallographic mirror plane. Crystallographic studies confirmed the major (89%) component of the crystal features a κ^2-alane ligand bound to a $[Cr(CO)_4]$ unit, with the minor (11%) co-crystallite featuring a κ^1-alane ligand bound to $[Cr(CO)_5]$. The κ^2-binding motif is reflected by a linear C(5)···Al(2)···Cr(1) unit 179.5(1)° and essentially equivalent Cr-H-Al linkages. The Cr···Al distance observed in **XXV** (2.420(1) Å) is notably shorter than the W···Al distance measured in **XXII** (2.841(1) Å), even allowing for the differing covalent radii of chromium and tungsten (Δr = 0.23 Å).[12] From the molecular structure of **XXV**, assessment of the σ-donor properties of the Al-H bond and CO can be made from the respective *trans* Cr-C bond lengths (*d*(Cr-C) 1.834(3) and 1.846(3) Å *trans* to alane and 1.892(2) Å *trans* to CO) being consistent with the Al-H bond being a weaker π-acceptor and σ-donor than CO. The hydride positions of **XXV** could be inferred crystallographically and H(11) and H(12) were located in the Fourier difference map. The ^{1}H NMR spectrum of **XXV** contains a high field resonance consistent with the presence of the Cr-H-Al linkage (δ_H = -10.48); the presence of two methyl resonances and a single methine resonance attributable to the Dipp substituents, is also indicative of symmetry being maintained across the $Dipp_2$NacNac substituent. Both of these observations further support the presence of a κ^2-binding motif and confirm that this is maintained in solution. Analysis of the IR spectrum of **XXV** shows the chromium centre possesses pseudo-C_{2v} symmetry giving rise to four stretching frequencies (1980, 1938, 1872 and 1868 cm^{-1}), all of which are red shifted from those of the parent $Cr(CO)_6$.

Two factors might be considered in order to rationalise the formation of an unprecedented κ^2-complex, given that the related guanidinate and $Dipp_2$NacNac supported σ-alane complexes (**XXII** and **XXIV** respectively) feature κ^1-coordination: (i) ease of the

loss of a second CO ligand and (ii) the steric demands of the supporting ligand. The formation of **XXIV** from the photolytic reaction between $Cp'Mn(CO)_3$ and **5.3** features a substantially more electron rich transition metal fragment, for which progressive CO loss becomes more difficult. Substitution of CO forming **XXIV** makes the transition metal fragment more electron rich than the $Cp'Mn(CO)_3$ precursor, on account of substitution of a good π acceptor, CO ligand, for the alane which is a poor π acceptor. This is shown by the red-shifted IR stretching frequencies of **XXIV**, a result of increased π-back-bonding to the remaining CO ligands. This presumably disfavours the formation of a κ^2-complex from the $Cp'Mn(CO)_3$ precursor, and whilst examples of complexes of the type $Cp'Mn(CO)L_2$ have been characterised,[20,21] the formation of $Cp'MnL_3$ complexes, through this synthetic approach, has not been demonstrated in the literature. Consequently, the formation of the κ^1-complex **XXIV** can be rationalised by the greater electron richness of the $Cp'Mn(CO)_3$ precursor. By contrast, for the comparatively electron poor $M(CO)_6$ systems (M = Cr, Mo or W) successive loss of CO is less challenging, with a number of complexes of the type $(OC)_4ML_2$ having been characterised. Consequently, whilst the formation of the κ^1-complex **XXII** may partially be attributed to the greater back-bonding associated with tungsten carbonyl fragments over their chromium counterparts, it is likely that the high steric demands of the $Dipp_2$NacNac substituent also play a role in the substitution of the second CO ligand, resulting in the formation of the κ^2-complex **XXV**. The greater steric demands of the $Dipp_2$NacNac substituent, in comparison to the guanidinate, result in the closer approach of the Dipp substituents to the $[M(CO)_5]$ fragment and elimination of a second equivalent of CO, forming **XXV**, eases the steric congestion observed at the metal centre. Although the κ^2-binding motif is unprecedented for σ-alane complexes a number of κ^2-complexes of related neutral silanes and boranes are reported in the literature.[10,22-28]

In a similar fashion, the reaction between $Mo(CO)_6$ and **5.3** in toluene-d_8 under photolytic conditions formed yellow crystals during the course of the reaction. Recrystallisation from a dichloromethane/hexane layering at -30 °C yielded crystals suitable for X-ray diffraction. Crystallographic studies showed that the major (91%) component of the crystals was $(OC)_4Mo[\kappa^2\text{-}H_2AlDipp_2NacNac]$ (**XXVI**) and the minor (9%) component $(OC)_5Mo[\kappa^1\text{-}H_2AlDipp_2NacNac]$ (Figure 5.11).

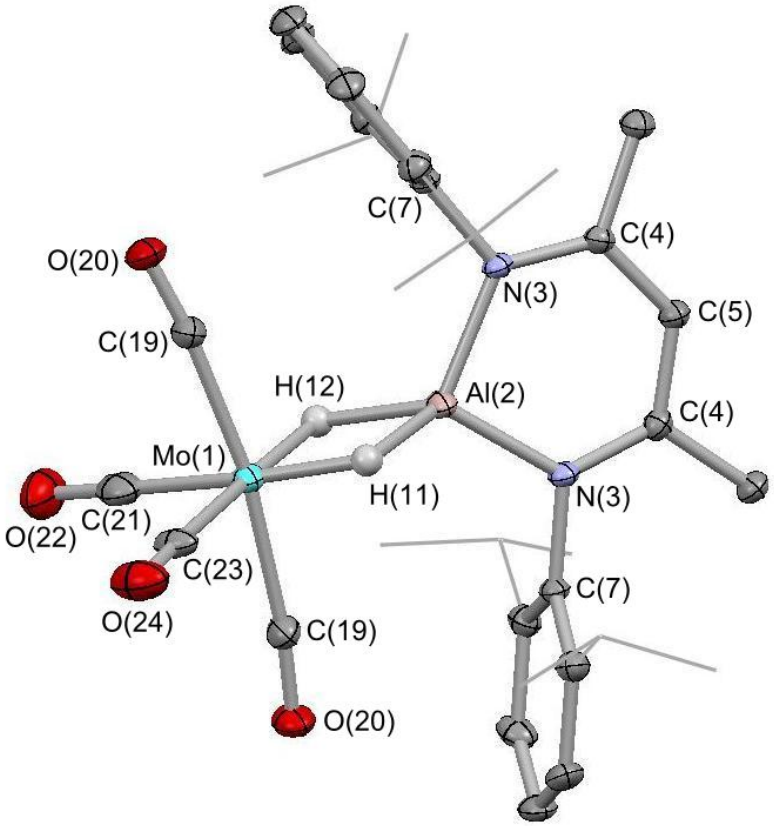

Figure 5.11: *Molecular structure of **XXVI**. Thermal ellipsoids set at the 40% probability level, ^{i}Pr groups of Dipp substituents are shown in wireframe, hydrogen atoms (except metal bound H's) and minor component omitted for clarity.* Key bond lengths (Å) and angles (°): Mo(1)···Al(2) 2.585(2), Mo(1)-H(11) 1.65, Mo(1)-H(12) 1.70, Mo(1)-C(19) 2.037(5), Mo(1)-C(21) 1.943(8), Mo(1)-C(23) 1.963(6), Al(2)-H(11) 1.65, Al(2)-H(12) 1.76, Al(2)-N(3) 1.853(3); Mo(1)-H(11)-Al(2) 103, Mo(1)-H(12)-Al(2) 97, H(11)-Mo(1)-H(12) 81, H(11)-Al(2)-H(12) 79, N(3)-Al(2)-N(3) 99.2(2), Mo(1)-C(19)-O(20) 173.8(4).

The molecular structure of **XXVI** consists of half a molecule in the asymmetric unit with the plane formed from by the Mo-H-Al linkages and the CO ligands *trans* to the alane representing a crystallographic mirror plane. The κ^2-binding motif is reflected by a linear C(5)···Al(2)···Mo(1) unit 179.4(1)° and essentially equivalent Mo-H-Al linkages. The Mo···Al distance of 2.585(2) Å is greater than the Cr···Al distance observed in **XXV** as expected from the difference in covalent radii (Δr = 0.15 Å).[12] The hydride positions of the Mo-H-Al linkage could be inferred crystallographically and H(11) and H(12) were located in the Fourier difference map. Furthermore, spectroscopic characterisation of **XXVI** identified a resonance at suitably high field for the Mo-H-Al linkage in the ^{1}H NMR spectrum, δ_H = -6.85 ppm. Symmetry across the $Dipp_2$NacNac substituent was further supported by the observation of two methyl resonances and a single methine resonance attributable to the Dipp substituents.

Given the successful formation of the chromium and molybdenum κ^2-complexes **XXV** and **XXVI**, the reaction between **5.3** and $W(CO)_6$ under photolytic conditions was investigated. Conversion of **5.3** to the κ^2-complex was minimal, and with extended reaction times decomposition to the previously characterised $[(OC)_5W\text{-}H\text{-}W(CO)_5]^-$ anion was observed. Despite the characterisation of a number of complexes of the type $(OC)_4WL_2$, the greater radial extent and elevated energy of the 5*d*-orbitals of tungsten, in comparison to the 3*d* and 4*d* of chromium and molybdenum respectively, gives rise to increased π-back-bonding making the substitution of the CO ligands more difficult in tungsten. In order to isolate the tungsten analogue an alternative synthetic approach was required, and labile sources of the $[W(CO)_4]$ fragment were investigated.

5.4.4 Synthesis of κ^2-Coordinated Al-H σ-Complexes *via* Labile Ligand Displacement

The photolytic preparation of the chromium and molybdenum κ^2-complexes **XXV** and **XXVI** has set the precedent for the *bis*(Al-H) binding motif. Quantum chemical calculations of the binding energies for the related κ^1-complexes **XXII** and **XXIV** act as a guide to the thermodynamics of Al-H bond coordination. With preliminary calculations suggesting that the displacement of ligands such as acetonitrile was unlikely,* the displacement of *bis*-alkene complexes by the Al-H bond was investigated through the reaction between $(OC)_4Cr(cod)$ (**5.4**) and **5.3** (Scheme 5.8).

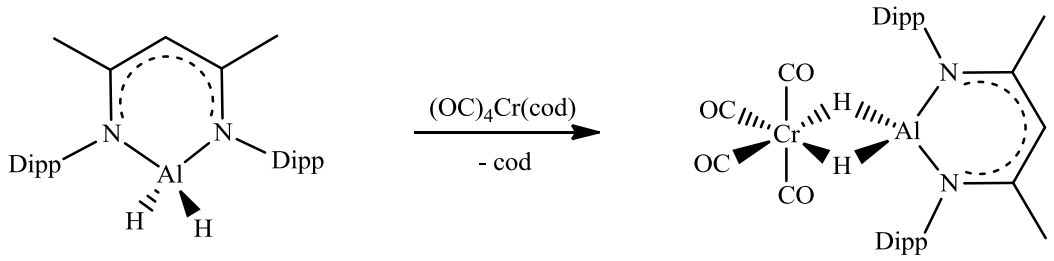

5.3 **XXV**

Scheme 5.8: *Proposed reactivity between $(OC)_4Cr(cod)$ (**5.4**) and **5.3***

The reaction between **5.4** and three equivalents of **5.3**, results in the formation of **XXV**, as indicated by ^1H NMR spectroscopy, with a resonance at δ_H = -10.48 ppm diagnostic of the Cr-H-Al linkage being observed, as well as resonances attributable to free *cyclo*octadiene. Three equivalents of **5.3** were used to drive any potential equilibrium between alane coordination and alkene coordination to favour the desired alane coordination. Single crystals were obtained from a dichloromethane/hexane layering at -30 °C and X-ray diffraction studies confirmed that the crystals contained solely the desired κ^2-complex **XXV**, with none of the κ^1-co-crystallite being observed.

*Preliminary binding energies calculated:
$(MeCN)W(CO)_5$: -26.4 kcal mol^{-1} and for $Cp'Mn(CO)_2(MeCN)$: -30.7 kcal mol^{-1}.

In the related reaction between $(CO)_4Mo(cod)$ (**5.5**) and three equivalents of **5.3** the displacement of the cod ligand was slower, due to the increased metal to ligand back-bonding making the cod more difficult to displace. However, with extended reaction times full displacement of the cod ligand was observed by ^1H NMR spectroscopy. Single crystals were obtained from a dichloromethane/hexane layering at -30 °C and X-ray diffraction studies identified the major component of the crystal to be the κ^2-complex **XXVI**. Unlike chromium, the κ^1-co-crystallite was still observed in close to identical relative percentages to those found from the formation of **XXVI** photolytically, despite preforming the $[Mo(CO)_4]$ fragment. This is possibly due to the requirement for longer reaction times which allows for alternative reaction pathways involving CO exchange. As attempts to form the analogous tungsten analogue through photolytic chemistry proved unsuccessful, the reaction between three equivalents of **5.3** and $(OC)_4W(cod)$ (**5.6**) was carried out to see if the cod displacement route developed for chromium and molybdenum would form the desired tungsten complex (Scheme 5.9).

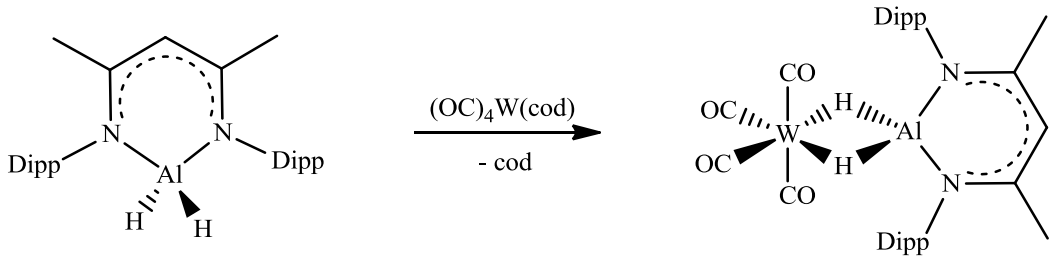

5.3 **XXVII**

Scheme 5.9: *Proposed reactivity between **5.3** and $(OC)_4W(cod)$ (**5.6**)*

Due to the increased π-back-donation from the tungsten centre to the cod ligand, complete displacement of the alkene required warming of the reaction mixture to 70 °C. The reaction was monitored by the formation of resonances attributable to free cod, and once complete consumption of the starting material was confirmed, slow cooling of the reaction mixture

yielded yellow crystals of $(OC)_4W[\kappa^2\text{-}H_2AlDipp_2NacNac]$ (**XXVII**) which were suitable for X-ray diffraction (Figure 5.12).

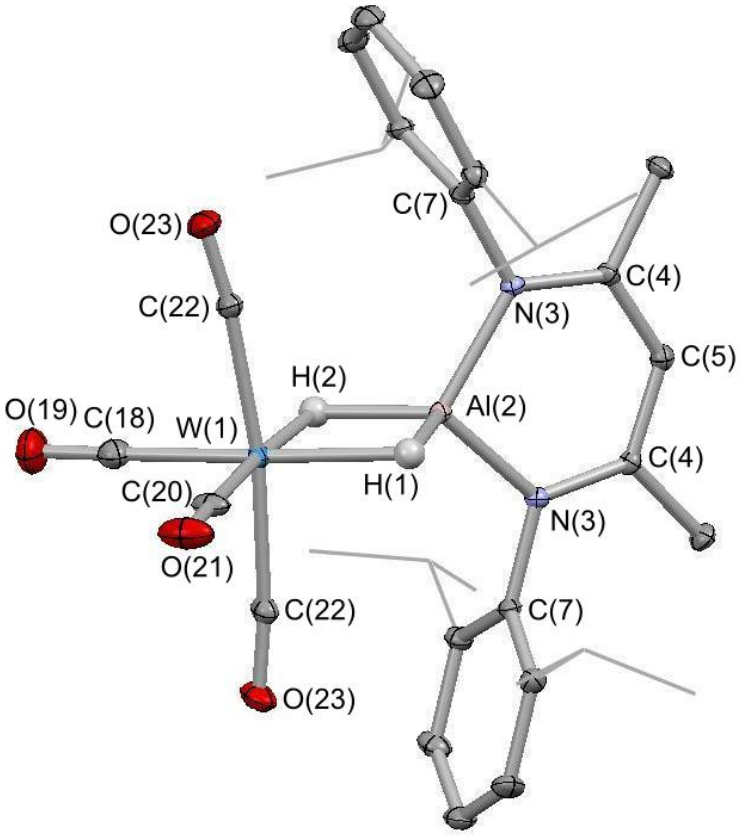

Figure 5.12: *Molecular structure of **XXVII**. Thermal ellipsoids set at the 40% probability level, ^{i}Pr groups of Dipp substituents are shown in wireframe and hydrogen atoms (except metal bound H's) omitted for clarity.* Key bond lengths (Å) and angles (°): W(1)···Al(2) 2.554(1), W(1)-H(1) 2.0, W(1)-H(2) 1.8, W(1)-C(18) 1.992(5), W(1)-C(20) 1.978(5), W(1)-C(22) 2.038(3), H(1)-Al(2) 1.7, Al(2)-H(2) 1.70, Al(2)-N(3) 1.853(2); W(1)-H(1)-Al(2) 87, W(1)-H(2)-Al(2) 93, H(1)-W(1)-H(2) 83, H(1)-Al(2)-H(2) 97, N(3)-Al(2)-N(3) 99.6(2), W(1)-C(22)-O(23) 173.6(3).

The molecular structure of **XXVII** is very similar to the chromium and molybdenum analogues and consists of half a molecule in the asymmetric unit with the plane formed from by the W-H-Al linkages and the CO ligands *trans* to the alane representing a crystallographic mirror plane. The κ^2-binding motif is reflected by a linear C(5)···Al(2)···W(1) unit 179.2(1)° and essentially equivalent W-H-Al linkages. The W···Al distance of 2.554(1) Å is slightly shorter than the Mo···Al distance observed in **XXVI** (2.585(2) Å) which is presumably attributable to a tighter binding of the bridging hydrides as a result of the more radially extended 5*d*-orbitals. The hydride positions of the W-H-Al linkage could be inferred crystallographically and H(1) and H(2) were located in the Fourier difference map. Additionally they were identified spectroscopically in the ^{1}H NMR spectrum at δ_H = -7.71 ppm. The symmetry across the $Dipp_2$NacNac substituent is maintained with two methyl resonances and a single methine attributable to the Dipp substituents being observed, which is consistent with a κ^2-binding motif.

5.4.5 Synthesis and Reactivity of $(OC)_5Cr[\kappa^1\text{-}H_2AlDipp_2NacNac]$

The characterisation of the κ^1-co-crystallite in the photolytic reaction between $Cr(CO)_6$ and **5.3**, suggests that $(OC)_5Cr[\kappa^1\text{-}H_2AlDipp_2NacNac]$ (**XXVIII**) is a viable entity in its own right, and a potential intermediate in the photolytic synthesis of **XXV**. With the ease of alkene displacement having been demonstrated for the preparation of **XXV**-**XXVII**, the thermal reactivity between a *mono*-alkene chromium complex and **5.3** was investigated in order to try to isolate **XXVIII**, and prevent further reactivity on to **XXV**. $(OC)_5Cr(coe)$ (**5.7**) is stable enough to be prepared *in situ* at room temperature, can be generated free from the corresponding *bis*(alkene) complex, and is therefore a suitable precursor for the preparation of **XXVIII**.

The reaction between a pentane solution of freshly prepared **5.7** and three equivalents of **5.3** also in pentane, readily forms a yellow precipitate of **XXVIII** which was isolated by filtration and dried *in vacuo* (Scheme 5.10).

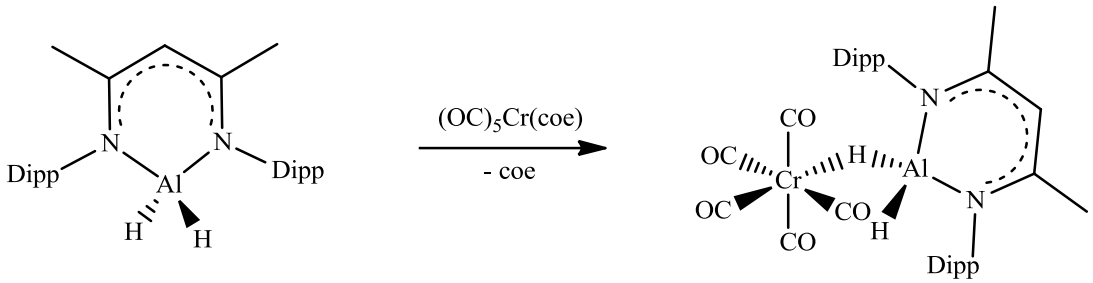

5.3 **XXVIII**

Scheme 5.10: *Reaction between $(OC)_5Cr(coe)$(**5.7**) and **5.3***

Characterisation of the yellow precipitate by ^{1}H NMR spectroscopy confirmed the formation of the κ^1-complex **XXVIII**, with four methyl and two methine resonances attributable to the Dipp substituents, consistent with reduction in symmetry of the $Dipp_2$NacNac substituent. Furthermore, a hydride resonance at δ_H = -11.50 ppm integrating to a single hydrogen is diagnostic of the formation of a Cr-H-Al linkage (*cf.* δ_H = -10.48 ppm for **XXV**). Consistent with observations made of the κ^1-complexes **XXII** and **XXIV**, the ^{1}H NMR spectrum of **XXVIII** shows slow exchange between terminal and bridging hydrogen atoms on the NMR timescale, giving rise to the observed reduction in symmetry.

The preparation of **XXVIII** is carried out in pentane providing immediate precipitation of the product allowing the isolation of **XXVIII** without decomposition. In solution, however, **XXVIII** readily reacts at room temperature forming **XXV** with concomitant loss of CO, even without photolysis (Scheme 5.11).

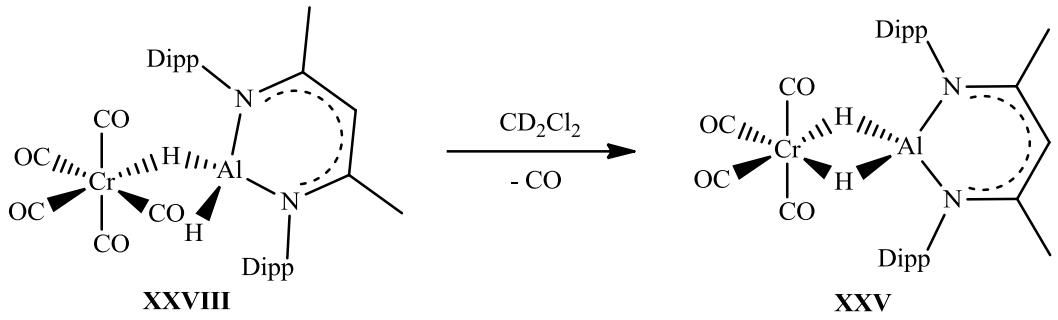

Scheme 5.11: *Conversion of **XXVIII** to **XXV** in solution*

The conversion of **XXVIII** to **XXV** can be monitored by ^{1}H NMR spectroscopy by the progressive decrease in intensity observed for the hydride resonance of **XXVIII** at δ_H = -11.50 ppm, and appearance and progressive increase in intensity of the hydride resonance attributable to **XXV** at δ_H = -10.48 ppm over a period of twelve hours. Through monitoring the increase in the intensity of the hydride resonance attributable to **XXV**, the change in concentration of **XXV** as a function of time was determined at four different temperatures. The concentration against time data for the formation of **XXV** fits with a first order reaction over two half lives. Due to the nature of the experiment reactions were carried out in a sealed system allowing CO to build up in the system. This is likely to retard the evolution of CO and potentially prevent full conversion of **XXVIII** to **XXV**, and as a result the kinetic data was fitted over two half lives. Concentration data at very short reaction times were omitted due to the large inherent error associated with the measurement of very low intensity NMR resonances (full kinetic data available on Appendix CD). The activation parameters for the conversion of **XXVIII** to **XXV** were obtained from an Eyring plot (Figure 5.13) and $\Delta H^{\ddagger}$ and $\Delta S^{\ddagger}$ calculated to be 79.5 kJ mol^{-1} and -58 J K^{-1} mol^{-1} respectively.

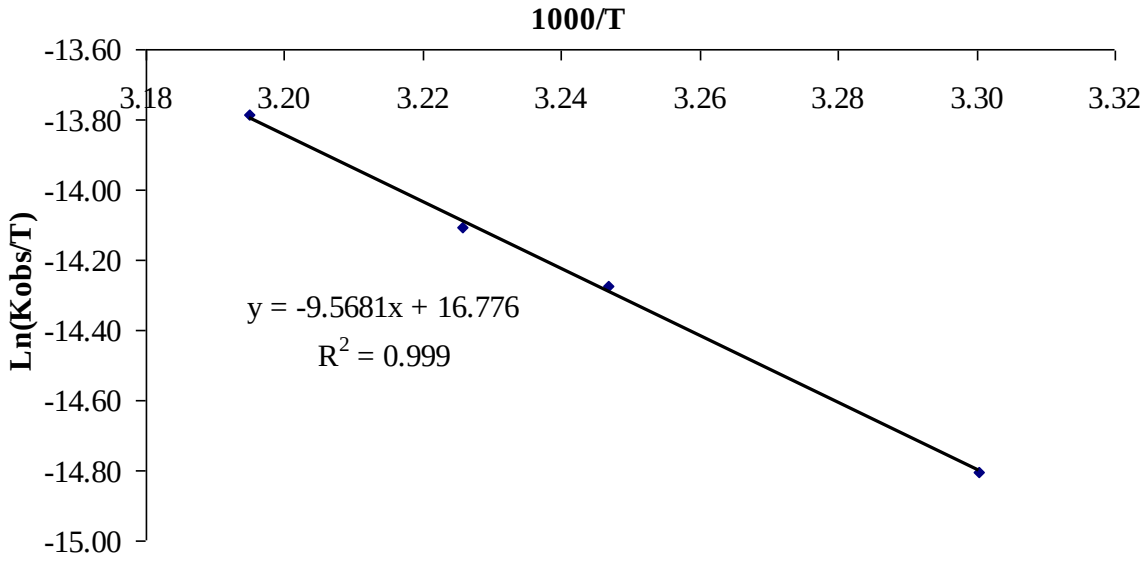

Figure 5.13: *Eyring plot for the conversion of **XXVIII** to **XXV***

The activation parameters show close similarity to those reported for chelate ring closing reactions of related κ^1-diimine complexes of the type $(\kappa^1\text{-L-L})M(CO)_5$ to $(\kappa^2\text{-L-L})M(CO)_4$ complexes (where M = Cr, Mo or W).[29] The negative value calculated for the entropy of activation suggests the mechanism for the conversion of **XXVIII** to **XXV** goes through an associative transition state, in which the rate determining step involves significant Cr-H bond formation generating a seven-coordinate transition state. Subsequent loss of CO from the transition state affords **XXV**. The large positive enthalpy of activation implies that the Cr-H-Al linkage formed in **XXV** is weaker than the Cr-C bond that is broken, which would be as expected given the known strength of M-CO bonds.

5.5 Conclusions and Suggestions for Further Work

A number of κ^1-alane complexes have been characterised featuring the *N,N'*-chelating amidinate, guanidinate and $Dipp_2$NacNac substituents. The extension of salt metathesis

methodology for the formation of Al-H-M interactions has been demonstrated through the use of the hydride containing transition metal anion K[Cp'Mn(CO)$_2$H]. The κ^1-coordination of Al-H bonds to classical transition metal fragments allows comparison of the Al-H-M interaction to the libraries of silane and borane σ-complexes characterised in the literature. Unlike related borane complexes exchange of the terminal and bridging hydrogen atoms is slow on the NMR timescale. The bonding within these complexes has been investigated through quantum chemical calculations, which finds the Al-H bond to have a predominantly σ-donor role.

The characterisation of κ^2-alane complexes from both photolytic and ligand displacement methodologies represents an unprecedented binding motif for the alane ligand. Furthermore, the structural characterisation of complexes of the type (OC)$_4$M[κ^2-H$_2$AlDipp$_2$NacNac] allow for comparison of the binding of CO and the Al-H bond, which is consistent with the Al-H bond being a weaker σ-donor and weaker π-acceptor than CO.

Dehydrogenation of the complexes to afford a direct M-Al bond is an area that represents considerable interest for future work, due to the current relevance of reversible hydrogen uptake. However, with no signs of facile dehydrogenation this may require particularly forcing conditions. Other topics for future work include the potential to form cationic complexes through hydride abstraction, as well the investigation of other supporting ligand frameworks and the reactivity of alane complexes with transition metal hydride complexes. Work towards the formation of a three-coordinate σ-alane complex to allow comparison to borane complexes, and entry into the proposed catalytic cycle for the reduction of small molecules represents a challenging area of further work.

5.6 References for Chapter V

1. S. Schlecht and J. F. Hartwig, *J. Am. Chem. Soc.*, 2000, **122**, 9435.
2. U. Schubert, *Adv. Organomet. Chem.*, 1990, **30**, 151.
3. G. S. McGrady, P. Sirsch, N. P. Chatterton, A. Ostermann, C. Gatti, S. Altmannshofer, V. Herz, G. Eickerling and W. Scherer, *Inorg. Chem.*, 2009, **48**, 1588.
4. K. R. Porschke, W. Kleimann, Y. H. Tsay, C. Kruger and G. Wilke, *Chem. Ber.*, 1990, **123**, 1267.
5. T. Steinke, C. Gemel, M. Cokoja, M. Winter and R. A. Fischer, *Angew. Chem. Int. Ed.*, 2004, **43**, 2299.
6. T. Steinke, M. Cokoja, C. Gemel, A. Kempter, A. Krapp, G. Frenking, U. Zenneck and R. A. Fischer, *Angew. Chem. Int. Ed.*, 2005, **44**, 2943.
7. Y. Kawano, K. Yamaguchi, S. Miyake, T. Kakizawa and M. Shimoi, *Chem. Eur. J.*, 2007, **13**, 6920.
8. T. Kakizawa, Y. Kawano and M. Shimoi, *Organometallics*, 2001, **20**, 3211.
9. P. Bissinger, H. Braunschweig, T. Kupfer and K. Radacki, *Organometallics*, 2010, **29**, 3987.
10. G. Alcaraz, E. Clot, U. Helmstedt, L. Vendier and S. Sabo-Etienne, *J. Am. Chem. Soc.*, 2007, **129**, 8704.
11. W. Scherer, G. Eickerling, M. Tafipolsky, G. S. McGrady, P. Sirsch and N. P. Chatterton, *Chem. Commun.*, 2006, **48**, 2986.
12. B. Cordero, V. Gomez, A. E. Platero-Prats, M. Reves, J. Echeverria, E. Cremades, F. Barragan and S. Alvarez, *Dalton Trans.*, 2008, **21**, 2832.
13. S. J. Bonyhady, D. Collis, G. Frenking, N. Holzmann, C. Jones and A. Stasch, *Nature Chem.*, 2010, **2**, 865.

14. K. Ueno, T. Yamaguchi, K. Uchiyama and H. Ogino, *Organometallics*, 2002, **21**, 2347.

15. Y. Kawano, M. Hashiva and M. Shimoi, *Organometallics*, 2006, **25**, 4420.

16. M. Shimoi, S. Nagai, M. Ichikawa, Y. Kawano, K. Katoh, M. Uruichi and H. Ogino, *J. Am. Chem. Soc.*, 1999, **121**, 11704.

17. R. E. Dessy and L. Wieczorek, *J. Am. Chem. Soc.*, 1969, **91**, 4964.

18. C. Cui, H. W. Roesky, H. J. Hao, H. G. Schmidt and M. Noltemeyer, *Angew. Chem. Int. Ed.*, 2000, **39**, 1815.

19. B. Twamley, N. J. Hardman and P. P. Power, *Acta Cryst. Sec. E.*, 2001, **57**, 227.

20. D. W. Lee and J. G. Morse, Phosphorus Sulfur and Silicon and the Related Elements, 1995, 106, 211-225.

21. J. A. T. Lin, A. C. Yeh, Y. C. Chou, T. Y. R. Tsai and Y. S. Wen, *J. Organomet. Chem.*, 1995, **486**, 147.

22. M. C. Lipke and T. D. Tilley, *J. Am. Chem. Soc.*, 2011, **133**, 16374.

23. C. M. Thomas and J. C. Peters, *Angew. Chem. Int. Ed.*, 2006, **45**, 776.

24. C. J. Stevens, R. Dallanegra, A. B. Chaplin, A. S. Weller, S. A. Macgregor, B. Ward, D. McKay, G. Alcaraz and S. Sabo-Etienne, *Chem. Eur. J.*, 2011, **17**, 3011.

25. G. Alcaraz, A. B. Chaplin, C. J. Stevens, E. Clot, L. Vendier, A. S. Weller and S. Sabo-Etienne, *Organometallics*, 2010, **29**, 5591.

26. C. Y. Tang, N. Phillips, J. I. Bates, A. L. Thompson, M. J. Gutmann and S. Aldridge, *Chemical Communications*, 2012, **48**, 11999.

27. C. Y. Tang, A. L. Thompson and S. Aldridge, *Angew. Chem. Int. Ed.*, 2010, **49**, 921.

28. K. D. Hesp, F. O. Kannemann, M. A. Rankin, R. McDonald, M. J. Ferguson and M. Stradiotto, *Inorg. Chem.*, 2011, **50**, 2431.

29. M. J. Schadt and A. J. Lees, *Inorg. Chem.*, 1986, **25**, 672.

Appendix I

List of Publications

Salt Metathesis for the Synthesis of M-Al and M-H-Al Bonds
I.M. Riddlestone, J. Urbano, N. Phillips, M.J. Kelly, D. Vidovic, J.I. Bates, R. Taylor and S. Aldridge, *Dalton Trans.*, 2013, **42**, 249. DOI: 10.1039/c2dt31974h.

σ-Alane Complexes of Chromium, Tungsten and Manganese
I.M. Riddlestone, S. Edmonds, P. Kaufman, J. Urbano, J.I. Bates, M.J. Kelly, A.L. Thompson, R. Taylor and S. Aldridge, *J. Am Chem. Soc.*, 2012, **134**, 2551. DOI: 10.1021/ja21198921

Coordinative Trapping of the Boron Beta-diketiminato System [B(NMesCMe)$_2$CH] via Templated Metal Synthesis
E. Firinci, J.I. Bates, I.M. Riddlestone, N. Phillips and S. Aldridge, *Chem. Commun.*, **49**, 1509. DOI: 10.1039/c3cc38073d

Sterically Encumbered Iridium bis(N-heterocyclic carbene) Complexes: Air Stable 14-electron Cations and Facile Degenerate C-H Activation
N. Phillips, J. Rowles, M.J. Kelly, I. Riddlestone, N.H. Rees, A. Dervisi, I.A. Fallis and S. Aldridge, *Organometallics*, 2012, **31**, 8075. DOI: 10.1021/om301060h

Extending the Chain: Synthetic, Structural and Reaction Chemistry of a BN Allenylidene Analogue
J. Niemeyer, D.A. Addy, I. Riddlestone, M. Kelly, A. Thompson, D. Vidovic and S. Aldridge, *Angew. Chem. Int. Ed.*, 2011, **50**, 8908. DOI: 10.1002/anie.201103757

Borane to Boryl Hydride to Borylene Dihydride: Explicit Demonstration of Boron-to-Metal α-Hydride Migration in Aminoborane Activation
M. O'Neill, D.A. Addy, I. Riddlestone, M.J. Kelly, N. Phillips and S. Aldridge, *J. Am. Chem. Soc.*, **133**, 11500. DOI: 10.1021/ja2050748